DEVELOPMENT OF REDUCED GRAPHENE OXIDE/POLYMER NANOCOMPOSITES FOR OPTICAL LIMITING, OPTICAL ACTUATION AND ELECTRICAL APPLICATIONS

Thesis submitted to

Cochin University of Science and Technology

in partial fulfilment of the requirements

for the award of the degree of

Doctor of Philosophy

under the Faculty of Technology

by

Muralidharan M. N.

Department of Polymer Science and Rubber Technology

Cochin University of Science and Technology

Kochi- 682 022, Kerala, India

August 2017

Development of Reduced Graphene Oxide/Polymer Nanocomposites for Optical Limiting, Optical Actuation and Electrical Applications

Ph.D. Thesis

Author

Muralidharan M. N.
Research Scholar
Department of Polymer Science and Rubber Technology
Cochin University of Science and Technology
Kochi- 682 022, Kerala, India.
E-mail: mnmuralidharan@gmail.com

Supervising Teachers

Guide

Dr. Thomas Kurian
Professor
Department of Polymer Science and
Rubber Technology
Cochin University of Science and
Technology (CUSAT)
Kochi- 682 022, Kerala, India.
E-mail: drtkurian@gmail.com

Co-guide

Dr. P. Radhakrishnan
Professor (Rtd.)
International School of Photonics
Cochin University of Science and
Technology (CUSAT)
Kochi- 682 022, Kerala, India.
E-mail: padmanabhan.radhak@gmail.com

Department of Polymer Science and Rubber Technology
Cochin University of Science and Technology
Kochi- 682 022, Kerala, India

August 2017

Dr. Thomas Kurian
Professor
Department of Polymer Science and
Rubber Technology
Cochin University of Science and
Technology (CUSAT)
Kochi- 682 022, Kerala, India.
E-mail: drtkurian@gmail.com

Dr. P. Radhakrishnan
Professor (Rtd.)
International School of Photonics
Cochin University of Science and
Technology (CUSAT)
Kochi- 682 022, Kerala, India.
E-mail: padmanabhan.radhak@gmail.com

Date: ....

Certificate

This is to certify that the thesis entitled **"Development of Reduced Graphene Oxide/Polymer Nanocomposites for Optical Limiting, Optical Actuation and Electrical Applications"**, which is being submitted by Mr. Muralidharan M. N., in partial fulfillment of the requirements of the degree of Doctor of Philosophy, to Cochin University of Science and Technology (CUSAT), Kochi, Kerala, India, is a record of the bonafide research work carried out by him under our joint guidance and supervision.

Mr. Muralidharan has worked on the research problem in the Department of Polymer Science and Rubber Technology of CUSAT. All the relevant corrections and modifications suggested by the audience during the pre-synopsis seminar and recommended by the Doctoral Committee of the candidate have been incorporated in the thesis. In our opinion, the thesis fulfills all the requirements according to the regulations. The results embodied in this thesis have not been submitted for the award of any other degree or diploma.

Dr. Thomas Kurian
(Supervising Guide)

Dr. P. Radhakrishnan
(Co-Guide)

Declaration

I hereby declare that the thesis entitled, **"Development of Reduced Graphene Oxide/Polymer Nanocomposites for Optical Limiting, Optical Actuation and Electrical Applications"**, is the original work carried out by me under the joint guidance and supervision of Dr. Thomas Kurian, Professor, Department of Polymer Science and Rubber Technology, Cochin University of Science and Technology, Kochi-682 022, and Dr. P. Radhakrishnan, Professor (Rtd.), International School of Photonics, Cochin University of Science and Technology, Kochi-682 022. No part of this thesis has been presented for any other degree from any other institution.

Kochi-22   **Muralidharan M. N.**
05-08-2017

Acknowledgements

I take this opportunity to express my deep sense of gratitude to my supervisors Dr. Thomas Kurian, Professor, Department of Polymer Science and Rubber Technology, Cochin University of Science and Technology (CUSAT) and Dr. P. Radhakrishnan, Professor, International School of Photonics (ISP), CUSAT for their generous help and inspiring guidance throughout the tenure of my research. I owe them much more than what can be literally expressed.

I am extremely grateful to Dr. A. Seema, Scientist, C-MET, Thrissur for her valuable suggestions and guidance throughout my work. She has really been an inspiration and role model in my professional life.

I express my sincere gratitude to Prof. Honey John, Head, Department of Polymer Science and Rubber Technology (PSRT), CUSAT and the teachers at PSRT including Prof. K. E. George, Prof. Rani Joseph, Prof. Eby Thachil, Prof. Philip Kurian, Prof. Sunil K. Narayanankutty, Dr. Jayalatha Gopalakrishnan, Dr. C. P. Reghunathan Nair, Dr. Sailaja, Dr. Jinu Jacob George, Dr. Prsanth and Dr. Jyothishkumar for their whole hearted support and constructive criticism throughout my research tenure.

I am also grateful to all the teachers at ISP including Prof. Mujeeb, Prof. V. P. N. Namboori, Prof. Kailasnath, Prof. Sheenu Thomas and Prof. Pramod Gopinath for their personal support and valuable suggestions. The help rendered by Dr. Mathew S., at ISP is gratefully acknowledged. My work would not have completed without his support and help. The support and personal affection of all my friends at ISP are fondly remembered.

I am grateful to Dr. N. Raghu, Director, C-MET, Thrissur and former Directors of C-MET, Thrissur Dr. K. R. Dayas and Dr. V. Kumar for extending their whole hearted support to carry out my research work. I am also thankful to Dr. N. R. Munirathnam, Director General, C-MET and Dr. D. P. Amalnerker, former Executive Director, C-MET for giving permission to carry out my research work as a part time research scholar. I am also indebted to all the Scientists, Technical Staff,

||||| **Preface** |||||

The development of graphene/polymer nanocomposites has opened up a new and interesting area in materials science in recent years. These nanocomposite materials show great improvement in properties that cannot be achieved using conventional composites or virgin polymers. The extent of the improvement is related directly to the degree of dispersion of the nanofillers in the polymer matrix. The most important aspect of these nanocomposites is that all these improvements are obtained at a very low filler loading in the polymer matrix. Graphene based fillers have been used in polymer nanocomposites and hold potential for a variety of technological applications.

Graphene has many advantages in terms of properties, cost and purity over carbon nanotubes and similar filler materials. However, the low dispersibility of graphene is the major challenge for many applications of polymer/graphene composites. Chemical functionalization of graphene has been the most common method employed by many researchers to overcome this challenge. However, chemical functionalization can deteriorate many other important properties. The use of reduced graphene oxide (RGO) instead of pure graphene is now accepted as a better alternative to overcome the dispersibility issues. In RGO, the residual functional groups left out after the reduction of graphene oxide can help in uniform dispersion throughout the polymer matrix.

The successful development of RGO/polymer nanocomposites mainly depends on the type of polymer selected and method of preparation of RGO. A simple and cost effective methodology for the preparation of the composite is also equally important for wide spread deployment of the material for practical applications. When the elasticity is of particular importance for an application, the difficulty in rubber processing always accompanies the system. However, thermoplastic elastomers provide the

ease of processing of plastics with the elasticity of a rubber. This work emphasizes on the development of a simple and cost effective method for the preparation of RGO nanocomposite systems with both plastic and elastomeric polymers for various applications.

Even though one can find tremendous applications for graphene/polymer composites, this work mainly focuses on development of RGO/polymer composites for optical limiting, optical actuation and electrical applications.

The thesis is divided in to eight chapters. **Chapter 1** gives a general introduction about graphene, its properties and applications with special reference to graphene/polymer nanocomposites. In addition to giving an overview of various applications of graphene/polymer nanocomposites, the scope and objectives of the present work are also included. In **Chapter 2**, a detailed description of the materials used and methods employed for the study is given. **Chapter 3** deals with the preparation and characterisation of graphene oxide and reduced graphene oxide. Graphene oxide is prepared through chemical route with a modified synthesis protocol. The reduction of graphene oxide is carried out through both chemical and thermal methods. Results of the detailed characterisation of the synthesised materials are discussed.

Chapter 4 of the thesis discusses the development of RGO/polymer composites and their characterisation. This chapter is divided into two parts. Part A discusses about *in situ* reduced graphene oxide/poly(vinyl alcohol) (PVA) nanocomposites and Part B deals with thermally reduced graphene oxide/thermoplastic polyurethane (TPU) nanocomposites. The uniform dispersion of RGO into the polymer matrices helped to achieve significant improvement in the thermal, mechanical, electrical and optical properties of the composites which can find many potential applications. **Chapter 5** describes the nonlinear optical absorption (NLA) and optical limiting properties of the composites. Part A of this chapter deals with NLA and optical limiting studies on RGO/PVA nanocomposites and Part B

discusses that of RGO/TPU nanocomposites. Both the systems exhibited excellent optical limiting characteristics. The NLA and optical limiting characteristics were found to increase with increasing RGO content. The retention of optical limiting properties of RGO even when incorporated to a polymer matrix enables to develop a practical solid state optical limiter. In **Chapter 6**, the optically triggered actuation in RGO/polymer nanocomposites is studied. An Infrared (IR) light source is used as the stimulus to remotely actuate the composite actuators. In Part A of the chapter, RGO/PVA based photomechanical actuators are studied in detail. The effect of filler loading and the effect of an applied pre-strain on the actuator properties are studied. Under IR irradiation, RGO/PVA nanocomposites exhibited contraction and the contraction increased with increasing RGO content. Similarly, in Part B, the photomechanical stress and strain achievable for RGO/TPU nanocomposites under IR illumination is studied. With an applied pre-strain the composites exhibited contraction in length. Photomechanical strain as high as 50% was obtained for this system. These results motivates the deployment of optically triggered actuators in applications such as biomedical devices. In **Chapter 7**, the studies on the electrical properties of the RGO/PVA and RGO/TPU composites are discussed in Part A and Part B respectively. The improvement in electrical conductivity with low filler loading can help to find many potential applications in electrical and allied industries.

Chapter 8 presents the conclusion of the work and describes the future outlook in this direction.

Abstract

Polymer nanocomposites have attracted enormous interest of scientific community in the last few decades for various technological applications. In this work, reduced graphene oxide (RGO)/polymer nanocomposites were developed by simple solvent casting process. Reduced graphene oxide/poly(vinyl alcohol) (PVA) nanocomposites were prepared by the *in situ* reduction of graphene oxide in PVA solution. Thermally reduced graphene oxide was used in the preparation of RGO/thermoplastic polyurethane (TPU) nanocomposites. The thermal and mechanical properties of RGO/PVA and RGO/TPU nanocomposites improved with the incorporation of RGO in the polymer matrix. The nonlinear optical absorption and optical limiting properties of the nanocomposites were studied. It was found that the RGO/polymer nanocomposites of the present study exhibited excellent optical limiting characteristics. The optical actuation properties of the nanocomposites were studied with infrared light as the stimulus. The photomechanical strain and stress observed in the case of the nanocomposite optical actuators established their suitability for remote controlled actuator applications. The electrical characteristics of RGO/PVA and RGO/TPU nanocomposites improved with the incorporation of RGO. The reduced graphene oxide/polymer nanocomposites can be used for many potential applications such as antistatic coatings, thermal sensors, resettable fuses and inrush current limiters.

Key words: Graphene, Nanocomposites, Reduced Graphene Oxide, Poly(vinyl alcohol), Thermoplastic polyurethane, Optical limiting, Optical actuators, Photomechanical response, Electrical conductivity

<p style="text-align:center">**||||| Contents |||||**</p>

Chapter 4
DEVELOPMENT OF REDUCED GRAPHENE OXIDE/POLYMER NANOCOMPOSITES

Part A

PREPARATION AND CHARACTERIZATION OF *IN SITU* REDUCED GRAPHENE OXIDE/POLY(VINYL ALCOHOL) NANOCOMPOSITES

Chapter **6**

OPTICAL ACTUATORS USING REDUCED GRAPHENE OXIDE/POLYMER NANOCOMPOSITES .... 181 - 207

Part A

OPTICAL ACTUATION OF *IN SITU* REDUCED GRAPHENE OXIDE/POLY(VINYL ALCOHOL) NANOCOMPOSITES

Part B

THERMALLY REDUCED GRAPHENE OXIDE/THERMOPLASTIC POLYURETHANE NANOCOMPOSITES AS PHOTOMECHANICAL ACTUATORS

Chapter **7**

REDUCED GRAPHENE OXIDE/POLYMER NANOCOMPOSITES FOR ELECTRICAL APPLICATIONS....... 209 - 231

List of Abbreviations and Symbols

AC	Alternating Current
AFM	Atomic Force Microscopy
BET	Brunauer-Emmett-Teller
CNT	Carbon nanotube
CVD	Chemical Vapour Deposition
DC	Direct Current
DMF	N, N – Dimethyl formamide
DSC	Differential Scanning Calorimetry
DTA	Differntial Thermal Analysis
EDS	Energy Dispersive Spectroscopy
EMI	Electromagnetic Interference
ESA	Excited State Absorption
FTIR	Fourier Transform Infrared
GIC	Graphite Intercalation Compound
GO	Graphene Oxide
HRGO	Hydrazine Reduced Graphene Oxide
HRTEM	High Resolution Transmission Electron Microscopy
I_0	Intensity at focus
IR	Infrared
I-V	Current – Voltage
L_{eff}	Effective length
NLA	Nonlinear Optical Absorption
NLO	Nonlinear Optical
NMP	N-methyl -2-pyrrolidone
PVA	Poly(vinyl alcohol)
PVDF	Poly(vinylidene difluoride)
RGO	Reduced Graphene Oxide
RSA	Reverse Saturable Absorption
SA	Saturable Absorption
SAED	Selected Area Electron Diffraction

SEM	Scanning Electron Microscopy
SMPU	Shape Memory Polyurethane
tanδ	Dielectric loss
TEM	Transmission Electron Microscopy
T_g	Glass transition temperature
TGA	Thermogravimetric Analysis
T_m	Melting temperature
TPA	Two Photon Absorption
TPU	Thermoplastic polyurethane
TRGO	Thermally Reduced Graphene Oxide
UTM	Universal Testing Machine
UV	Ultraviolet
XRD	X-Ray Diffraction
Z	Position of sample with respect to focus of lens
ϕ	Activation energy
ρ	Resistivity
σ	Conductivity
ω	Angular frequency
α	Linear absorption coeffcient
β	Nonlinear absorption coefficient
ϵ'	Real part of dielectric permitivitty
ϵ''	Imaginary part of dielectric permitivitty
$\chi^{(3)}$	Third order nonlinear susceptibility
χ_c	Degree of Crystallisation

.....ജരര.....

Chapter 1

GENERAL INTRODUCTION

The rapid growth in the field of nanotechnology and the use of nanomaterials for commercial applications has accelerated the development of novel materials and systems in this field. The last decade has witnessed the growth of Graphene, a new addition to the nanomaterial family, as an omnipresent material in every facet of science and technology. This chapter presents an effort to understand graphene, its properties and applications. The various members of the graphene family and how they can be combined with polymers for the development of high performance materials are also discussed.

1.1   Graphene – the wonder material

In the recent past, materials with two-dimensional (2D) crystalline nature have been identified and analyzed worldwide with great enthusiasm. Graphene is one of the most widely investigated materials in this category

Part of this chapter is accepted for publication as a book chapter entitled "Polymer-Graphene Composites: Electronic Applications" in "Encyclopedia of Polymeric Applications", Taylor & Francis Group, USA, 2017 (In Press)

Development of Reduced Graphene Oxide/Polymer Nanocomposites for Optical Limiting, Optical Actuation and Electrical Applications

1

due to both academic curiosity and the promising potential applications of the material [1]. Graphene is an allotrope of carbon, with one-atom thick planar sheets of sp^2 hybridised carbon atoms densely packed in a honeycomb crystal lattice. In graphene, the carbon-carbon bond length is about 0.142 nm. Graphene can be considered as the mother of all graphitic forms including zero dimensional fullerenes, one-dimensional carbon nanotubes and three-dimensional graphite (figure 1.1) [2]. Even though graphene was theoretically predicted long back, till last decade it was unable to physically isolate it from graphite. In 2010, the Nobel Prize in Physics was awarded to two scientists, Andre K. Geim and Konstantin S. Novoselov, for their ground breaking experiments regarding graphene. They have succeeded in producing, isolating, identifying and characterizing graphene.
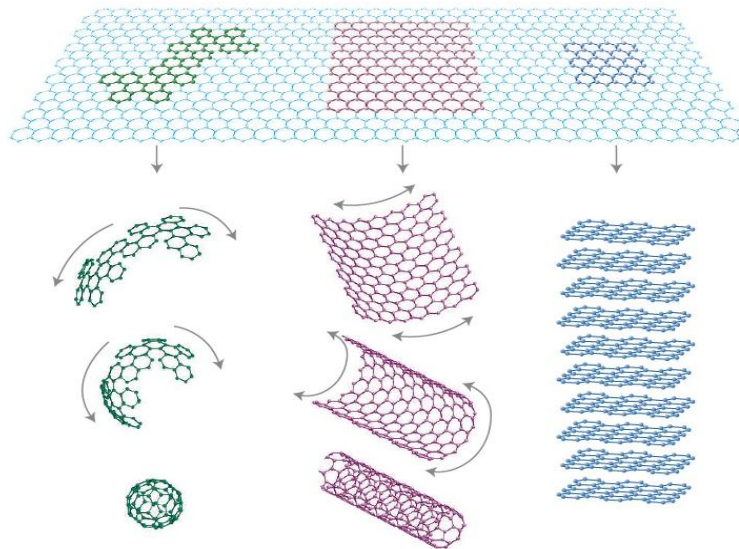
Figure 1.1: Graphene is a 2D building material for carbon materials of all other dimensionalities. It can be wrapped up into 0D bucky balls, rolled into 1D nanotube or stacked into 3D graphite [2].

Around 225 years ago, Lavoisier listed ''Carbone'' in his book ''Traite Elementaire de Chimie'' as one of the newly identified chemical elements. He had identified the versatility of carbon and shown that it was the elementary component of both diamond and graphite [3]. Since then, there have been continuous efforts to find out more allotropes of carbon and researchers became more passionate about studying the properties of this element which can adopt many structures ranging from diamond and graphite (3D) to graphene (2D), nanotubes (1D) or fullerenes (0D).

In the early days, physicists believed that the independent existence of a stable two-dimensional plane was not possible. The theory of graphene was first explored by P. R. Wallace in 1947 during his efforts in understanding the electronic properties of more complex, 3D graphite [4]. In 1962, Hanns-Peter Boehm, in his descriptions about single-layer carbon foils, coined the term Graphene as a combination of graphite and the suffix -ene [5, 6]. However, the wonder material of the present era was emerged only in the year 2004, when Andre Geim, Konstantin Novoselov and their collaborators from the University of Manchester (UK), and the Institute for Microelectronics Technology in Chernogolovka (Russia), presented their results on graphene structures in Science magazine. Later in 2010, they were awarded Noble Prize for this outstanding contribution. They used a simple but effective mechanical exfoliation method for extracting thin layers of graphite from a graphite crystal with Scotch tape and then transferred these layers to a silicon substrate [7]. Once the technology was developed, a large number of other groups started conducting experiments to further improve the quality and quantity of the product. This resulted in phenomenal growth

in graphene research including production of graphene layers on substrates, functionalizing graphene and exploring the various applications of graphene.

The impressive properties shown by single and few layer graphene sheets encouraged the rapid adoption of graphene as a material of interest for a variety of applications. These unique properties keep the material always a step ahead compared to other similar materials such as carbon nanotubes, graphite, indium tin oxides etc. Various research groups are still trying to identify and exploit these properties for more advanced applications. Some of these unique properties are discussed in the following sections.

1.2 Properties of Graphene

1.2.1 Physical properties

Graphene is a highly stable odorless solid material with grayish or shining black color. The material has got a very high specific surface area with a theoretical value of 2675 m^2/g. Graphene has a unique structure with one-atom thick planar sheets of sp^2 hybridised carbon atoms densely packed in a honeycomb crystal lattice [8]. The carbon atoms in the plane are bonded by σ -bonds with a bond length of 0.142 nm. These bonds are extremely strong and give a rigid backbone to the graphene. The p – orbitals perpendicular to the graphene plane, will not participate in the σ – bonds, and can bind covalently with neighboring atoms there by forming a half filled π – band responsible for the electron conduction in the graphene plane. In other words the graphene structure can be described as two identical sub lattices A and B, superimposed on each other (figure 1.2).
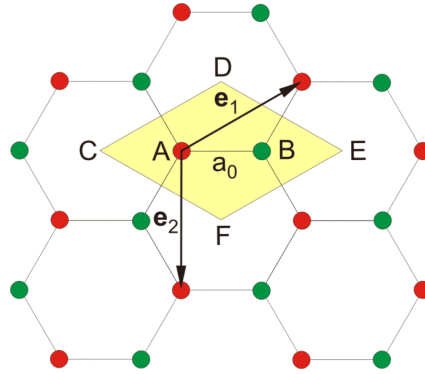
Figure 1.2: Crystallographic structure of graphene. Atoms from different sub lattices (A & B) are marked by different colors.

CDEF represents the unit cell. e_1 and e_2 are elementary translation vectors. a_0 is the distance between two nearest atoms which is 0.142 nm.

1.2.2 Electronic and electrical properties

One of the most interesting aspects of the graphene is its highly unusual nature of charge carriers, which behave as mass less relativistic particles (Dirac fermions) [9]. Graphene has an ambipolar electric field effect at room temperature; that is charge carriers can be tuned between electrons and holes by applying a required gate voltage. Another important electronic property of graphene is the Quantum Hall effect (QHE), due to which the electrons, confined to a plane and subjected to high magnetic fields, execute only prescribed quantum trajectories.

1.2.3 Optical properties

Single layer graphene is almost transparent over a broad wavelength range. It absorbs only 2.3% of incident light. It was reported that there is a linear increase in the absorption of light with the addition of number of graphene layers [8].

Development of Reduced Graphene Oxide/Polymer Nanocomposites for Optical Limiting, Optical Actuation and Electrical Applications

5

1.2.4 Mechanical properties

Graphene is considered to be one of the strongest materials ever measured. Measurements have shown that graphene has a breaking strength 200 times greater than steel, bulk strength of 130 GPa and Young's modulus of 0.5 TPa. These high values make graphene very strong and rigid [10].

1.2.5 Thermal properties

In electronic components and devices, the huge amount of heat generated during the device operation needs to be dissipated to improve the performance and reliability of the devices. Hence the thermal management is one of the key factors in electronics and graphene finds a lot of applications in this field due to its unique thermal properties. Graphene exhibits a negative coefficient of thermal expansion and is found to be strongly dependent on temperature. At room temperature the value of temperature coefficient is found to be $(-8.0 \pm 0.7) \times 10^{-6}$ K^{-1} [11]. Thermal conductivity in the range ~$(4.84 \pm 0.44) \times 10^3$ to $(5.30 \pm 0.48) \times 10^3$ W/m.K is reported for single layer pure defect free graphene at room temperature [12]. Compared to graphene, the thermal conductivity of graphite is about 5 times smaller (1000 W/m.K).

1.3 Methods for synthesis

The cost effective preparation of high quality graphene materials on the desired scale is essential for many applications. Graphene can be produced by several methods [13-18]. However, most of these existing methods vary greatly in terms of time spent, required facilities, and most

importantly the cost associated with the production. The table 1.1 compares different methods for the production of graphene.

Table 1.1: Comparison of different methods for the production of Graphene

Method	Ref	Cost / Quality	No. Of layers	Yield	Nature of produced graphene	Precursor
Mechanical exfoliation	[13]	Low/High	Single & multiple	Low	Pristine	Graphite
Chemical reduction of GO	[14]	Low/Low	Single & multiple	High	Chemically modified	Graphite oxide
Liquid phase exfoliation	[15]	Low/High	Single & multiple	Low	Pristine	Graphite
Epitaxial growth	[16]	High/High	Single & multiple	Low	Pristine	SiC
Chemical Vapour Deposition	[17]	High/High	Single & multiple	Low	Pristine	Hydro-carbons
From CNT	[18]	High/Low	Single & multiple	High	Chemically modified	MWCNT

The preparation of conducting nanocomposites using graphene highly depends on the exfoliation of the graphite down to single graphene sheet in the matrices. This can be attained to a great extent by exfoliation technique. The main disadvantage of exfoliation technique is that the yield is very low. Mainly there are two types of exfoliation techniques: (1) mechanical exfoliation and (2) exfoliation of graphite in solvents.

Mechanical exfoliation was one of the first methods to produce graphene. Andre Geim and Konstantin Novoselov adopted this method to isolate graphene for the first time in 2004. Even though chemical oxidation of graphite and subsequent exfoliation can yield large amount of graphene oxide, the extensive chemical treatment can induce structural defects and this may affect the electronic structure of graphene. The advantage of mechanical exfoliation is that it can be used to produce 'high quality' graphene. Hence mechanical exfoliation technique is desirable for producing graphene without affecting its electronic structure. Scotch-tape method which is a form of mechanical exfoliation uses a piece of tape to which a sample of graphite is pasted. By peeling off the tape, we can isolate the top layers of graphite to obtain graphene. Generally, a chunk of graphitic material is stuck to the tape and the tape is doubled back on itself and pressed against the graphitic material. By unpeeling the tape, the material is separated into two pieces. This process is repeated several times, each time cleaving the material thinner until eventually single-layer regions remain stuck to the tape. The tape is then pressed against an oxidized silicon wafer. The backside of the tape is rubbed for several minutes with soft plastic tongs to transfer the graphene to the oxide before slowly removing the tape [13].

Solution phase exfoliation of graphite in certain organic solvents is another method to yield high quality mono-layer graphene. This is typically done by exposure of graphite powders in organic solvents such as N, N-dimethyl formamide (DMF) or N-methyl-2-pyrrolidone (NMP) for a very long time to high intensity ultrasound, thereby achieving the exfoliation. The degree or extent of exfoliation is determined by various parameters like ultrasonic solvent, sonication power and sonication time.

Other important methods of graphene synthesis are substrate based methods. The major advantage of substrate-based methods is their high compatibility with the current semiconductor technology. But the graphene produced based on these usually consists of several layers and the overall quality depends highly on the type of substrate materials used. The high cost of production is another challenge associated with these methods. Chemical vapour deposition (CVD) and epitaxial growth are the two major substrate based methods for graphene synthesis.

CVD is an attractive approach for the production of graphene due to its capability of producing large area deposition. Moreover there are no intense mechanical and/or chemical treatments. In CVD method, a wafer with a thin transition metal film plays the role of catalyst. This substrate is placed in a heated furnace and is attached to a gas delivery system, which will flow a gaseous carbon source downstream to the wafer. It is believed that carbon is then adsorbed and absorbed into the metal surface at high temperatures. Once it is allowed to cool, the same will be precipitated on the substrate. In order to achieve large-area continuous single-layer graphene growth, we have tune various parameters like reaction time, flow rate of carbon-containing precursors, flow rate of inert and reducing gases, temperature of the flow-cell, heating and cooling rates and the thickness of the metal layer.

Epitaxial growth of a material refers to the formation of a crystal on top of a crystalline substrate that exhibits a similar structure. Silicon carbide (SiC), also known as Moissanite or Carborundum, was first reported in 1885. When SiC substrate is heated under ultra high vacuum,

silicon atoms sublimate from the substrate. The removal of Si leaves surface carbon atoms to rearrange into graphene layers. The thickness of graphene layers depends on the annealing time and temperature. It is possible to obtain few layer graphene with few minutes annealing of the SiC surface at temperature around 1200 °C. The technique of epitaxial growth has been an attractive approach especially for semiconductor industry because the products are obtained on SiC substrates and requires no transfer before processing devices.

1.3.1 Synthesis of graphene by chemical route

1.3.1.1 Preparation of graphite oxide

Chemical conversion of graphite to graphene oxide has emerged to be one of the most viable routes to obtain graphene in considerable quantities [19]. Graphite oxide is a product from oxidation of graphite, and maintains the original layered structure of graphite. Due to the existence of large number of hydroxyl, carboxyl, carbonyl and epoxy functional groups attached onto the basal and edge planes, graphite oxide is strongly hydrophilic in nature. The graphite oxide platelets differ from "pristine" graphene, by the fact that graphene has superb electrical conductivity compared to the insulating nature of graphite oxide sheets. Due to the strong hydrophilic nature of graphite oxide, it gets easily exfoliated in water yielding a dispersion consisting mostly of single layer sheets (graphene oxide).

Graphite oxide can be synthesized from graphite flakes using different methods like Brodie, Staudenmaier, or Hummers' method or some variation of these methods. All these methods involve oxidation of

graphite using some oxidizing agents like concentrated sulphuric acid, nitric acid, potassium chlorate (KClO$_3$), and potassium permanganate. The major chemical methods for the synthesis of graphite oxide are Brodie's method (potassium chlorate (KClO$_3$) and fuming nitric acid (HNO$_3$) as oxidants), Staudenmaier's method (KClO$_3$, HNO$_3$ and H$_2$SO$_4$ as oxidants and Hummers' method (potassium permanganate (KMnO$_4$) and concentrated sulphuric acid (H$_2$SO$_4$) as oxidants. Presently, the most widely used methods are Hummer's method and its modifications.

Once graphite oxide is prepared, rather than retaining a stacked structure of graphite oxide, it will be better to exfoliate the same into monolayer or few-layered stacks. The exfoliated graphite oxide is called graphene oxide. There are different mechanical or thermal methods available for the exfoliation technique. Most commonly sonicating graphite oxide in water is used for the exfoliation. It is necessary to get better dispersibility of graphene oxide in solvent for further processing. The factors like extend of surface functionalization imparted on the surface during oxidation and selection of solvent are of greater importance to get better dispersibility.

1.3.1.2 Reduction of graphene oxide

Both graphite oxide and graphene oxides are electrically insulating materials due to their disrupted sp^2 bonding networks. Since the electrical conductivity can be recovered by restoring the π-network, reduction of graphene oxide is considered to be the most important reactions of graphene oxide [19].

When colloidally dispersed, a variety of chemical means may be used to reduce graphene oxide. Chemical reduction of exfoliated graphene oxide has been performed with several reducing agents including hydrazine, hydrohalic acid, sodium borohydride ($NaBH_4$) etc. Hydrazine hydrate, unlike other strong reducing agents, does not react with water and was found to be the best one for obtaining graphene from graphene oxide. During the reduction process, the brown coloured dispersion of graphene oxide in water turned black and the reduced sheets aggregated and precipitated. The reduced graphene oxide became less hydrophilic due to the removal of oxygen atoms and thus precipitated.

Thermal reduction is another approach to reduce graphene oxide to reduced graphene oxide. This technique utilizes the heat treatment to remove the oxide functional groups from graphene oxide surfaces. The exfoliation happens when the decomposition rate of the epoxy and hydroxyl sites of graphite oxide exceeded the diffusion rate of the evolved gases, thus yielding pressures that exceeded the Vander Waals forces holding the graphene sheets together. Figure 1.3 illustrates the conversion of graphite to graphene through chemical route.
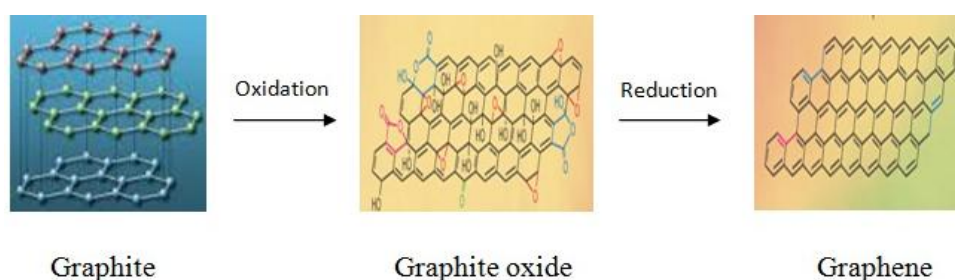
Figure 1.3: Chemical synthesis of graphene

1.4 Applications of graphene

Graphene and the members of graphene family including graphene oxide, reduced graphene oxide, graphene ribbons, etc. cater to almost all the field of technological applications. The wide range of applications include sensors, actuators, transparent conducting layers in displays and solar cells, supercapacitors, transistors, drug delivery systems, nano antennas, optoelectronic and nanophotonic devices and so on.

Another most outstanding application is to use graphene as filler into a polymer matrix thereby forming polymer nanocomposites. Graphene is one of the strongest and stiffest known materials and is also very light weight. Hence graphene as filler imparts improvement to the composite properties such as increased strength, increased conductivity, and increased thermal stability. There are various methods for the incorporation of graphene into the composite. Graphene based composites find applications in a large number of fields, including actuators, sorbent/filter/medical applications, lightweight high-strength structural components, electrically and/or thermally conducting nanocomposites.

1.5 Polymer nanocomposites using graphene or reduced graphene oxide

The development of a nano level dispersion of graphene particles in a polymer matrix has opened a new and interesting area in materials science in recent years. These nanocomposite materials show great improvement in properties that cannot be achieved using conventional composites or virgin polymers. The extent of the improvement is related directly to the degree of dispersion of the nanofillers in the polymer matrix. The most important

aspect of these nanocomposites is that all these improvements are obtained at a very low filler loading in the polymer matrix. Graphene based fillers have been used in polymer nanocomposites and hold potential for a variety of possible applications [20-24]. GO and other graphite derivatives such as graphite intercalation compounds (GICs) can be used as precursors for the large scale production of graphene [25]. Polymer matrix composites with graphene-based filler include polystyrene (PS), polymethyl methacrylate (PMMA), polypropylene (PP), polyester, polyurethane (PU), etc. To achieve large property enhancements in their nanocomposites, layered materials such as GO are exfoliated and well dispersed in the polymer matrix. Rapid heating, as well as ultrasonication of GO are used to produce highly-exfoliated platelets for Nanocomposites. Themally-expanded GO ('TEGO') is reduced and can be use to make electrically conductive composites [26]. These fillers can be dispersed into polymers using techniques such as solution mixing, melt mixing, or in situ polymerization; of these methods, in situ polymerization might offer superior dispersion of this filler. The incorporation of graphene materials as fillers show great improvements in properties such as elastic modulus, tensile strength, electrical conductivity, and thermal stability. Moreover, these improvements are often observed at low loadings of filler evidently due to the large interfacial area and high aspect ratio of these materials, requiring small amounts of filler to achieve percolation.

1.5.1 Properties of polymer nanocomposites using graphene or reduced graphene oxide

Exfoliated carbon sheets obtained from graphene oxide (GO) via either chemical reduction or thermal reduction can be dispersed in polymers to modify their physical properties.

1.5.1.1 Electrical Conductivity

The most surprising property of graphene is its very high electrical conductivity. When used as fillers with insulating polymer matrix, conductive graphene may greatly enhance the electrical conductivity of the composites [21, 23, 27-29]. Various factors influence the electrical conductivity and the percolation threshold of the composites. These factors include the aggregation of filler, the presence of functional groups on graphene sheets, concentration of fillers, aspect ratio of the graphene sheets, inter-sheet junction, distribution in the matrix, wrinkles and folds, processing methods, etc. The pristine graphene has the highest conductivity, however difficulty in producing a large amount by mechanical exfoliation limits its use and compels to rely on chemically reduced graphene oxide and thermally reduced graphene oxide.

1.5.1.2 Thermal Conductivity

Superior thermal transport properties of graphene dispersion have potential for thermal management in miniaturized electronic devices, for thermal pastes, and for heat-actuated, shape-memory polymers. It has been reported that 2-D, platelet-like GNP can improve thermal conductivity more effectively than 1-D, rodlike CNT. However, unlike the exponential increase in electrical conductivity, thermal conductivity enhancement by the carbon nanofillers is not as dramatic, even lower than expected from effective medium theory. This is partly due to smaller contrast in thermal conductivity between polymers and graphitic carbons compared to the contrast in electrical conductivity. Moreover, since thermal energy is transferred mainly in the form of lattice vibration (phonons), poor coupling

Development of Reduced Graphene Oxide/Polymer Nanocomposites for Optical Limiting,
Optical Actuation and Electrical Applications

15

in vibration modes at the filler-polymer and filler-filler interfaces will impart significant thermal resistance [30].

1.5.1.3 Mechanical Properties.

Higher mechanical properties (elastic modulus and tensile strength) of graphene sheets have attracted the attention of researchers. The polymer reinforced with graphene has been employed to explore intrinsic strength (125 GPa) and elastic modulus (1.1 TPa) of nanosheets to bulk polymer composites. Similar to other composites, the mechanical properties are dependent on the reinforcement phase concentration and distribution in the host matrix, interface bonding, and reinforcement phase aspect ratio, etc. Although the pristine graphene has the highest theoretical strength, the presence of functional groups on the GO surfaces has the additional benefits of its high level of dispersion in polar solvents and water. The improved GO/polymer interaction facilitates high molecular level dispersion and enhanced interfacial interaction, leading to high mechanical properties [21]. The interaction of graphene and polymer at the interface of effective load transfer has been extensively investigated. The tailoring of mechanical properties by a covalent and non-covalent bond configuration between the matrix and sheets reinforcement can provide exceptional features. The responsible Van der Waals forces and hydrogen-bond interactions were reported for improved mechanical properties. While modulus increase with graphene dispersion is evident for all polymers, it is more pronounced for elastomeric matrices. This is due to greater stiffness contrast between reinforcement and matrix.

1.5.1.4 Thermal Stability

Improved thermal stability of host polymers is another benefit expected from graphene-based reinforcements. Decomposition of graphene composites is substantially slower than neat polymers, which is attributed to restricted chain mobility of polymers near the graphene surface. During combustion, inflammable anisotropic nanoparticles form a jammed network of char layers that retards transport of the decomposition products. This suggests application of graphene/ polymer nanocomposites for flame retardation [31, 32].

1.5.2 Preparation methods of polymer/ graphene nanocomposites

The mechanism for the interaction in polymer/graphene nanocomposites depends on the polarity, molecular weight, hydrophobicity, reactive groups, etc., Solution blending, melt mixing, and in situ polymerization are the three common synthesis methods of the polymer matrix composites.

1.5.2.1 Solution blending

Solution blending is the most common technique to fabricate polymer-based composites provided the polymer is readily soluble in common aqueous and organic solvents, such as water, acetone, DMF, chloroform, dichloromethane (DCM) and toluene. Graphene or modified graphene can be dispersed easily in a suitable solvent, such as water, acetone, chloroform, tetrahydrofuran (THF), DMF or toluene, owing to the weak forces that stack the layers together. To homogenize the dispersion of graphene sheets, ultrasonic power can be used. Long time exposure to high power ultrasonication can induce defects in graphene sheets which are detrimental to the composite properties. During the blending, the polymer coats the surface of the individual sheet and interconnects each sheet after the solvents

are removed. Solution blending of GO and RGO sheets tend to agglomerate during slow solvent evaporation, resulting in inhomogeneous distribution of sheets in polymer matrix. The distribution can be controlled by controlling the evaporation time using spin coating or drop casting. Various polymer composites such as graphene–PVA, GO–PVA, graphene–polyvinyl chloride (PVC), PVA–GO layer by layer assembly, PVDF-thermally reduced graphene, etc. have been prepared using this technique [33-37].

1.5.2.2 Melt mixing

In the melt mixing method, no solvent is required and graphite or graphene or modified graphene is mixed with the polymer matrix in the molten state. A thermoplastic polymer is mixed mechanically with graphite or graphene or modified graphene at elevated temperatures using conventional methods, such as extrusion and injection moulding. The polymer chains are then intercalated or exfoliated to form nanocomposites. This is a popular method for preparing thermoplastic nanocomposites. Polymers, which are unsuitable for adsorption or insitu polymerization, can be processed using this technique. A wide range of polymer nanocomposites, such as Polypropylene/Exfoliated graphite (EG), high density polyethylene (HDPE)/EG, etc., have been prepared using this method. In addition, the restacking process is a newly imposed approach in which nanocomposites are obtained via a transformation of the host material into a colloidal system and precipitation in the presence of the polymer [21]. This method differs from other methods because a previously formed host layered crystal is not used. These Nanocomposites show interesting microstructural phase changes as well as enhanced thermal stability relative to both parent phases [21, 38].

1.5.2.3 In situ interactive polymerization

This fabrication technique starts with the dispersion of GO or RGO in monomer followed by the polymerization of the monomers. Graphene or modified graphene is first swollen within the liquid monomer. A suitable initiator is then diffused and polymerization is initiated either by heat or radiation. A variety of polymer nanocomposites have been prepared using this method including graphene/polyurethane, graphene/nylon-6, graphene oxide/polypropylene, chemically modified graphene/PMMA, etc. [39 - 41].

1.5.3 Applications of polymer/graphene or RGO nanocomposites

Graphene–polymer nanocomposites have found applications in various electronic and photonic devices including actuators, sensors, capacitors, fuel cells, etc. The following sections will elaborate on the major applications of polymer–graphene composites and recent developments in each field.

1.5.3.1 Actuator applications

'Actuator' is a term generally used to represent materials or devices which can undergo a mechanical deformation when excited with an appropriate external stimulus [43]. In the recent past, graphene-polymer composite actuators have attracted considerable attention of researchers because of their unique advantages such as low cost, ease of processing, large displacements obtained and their resemblance to the properties of human muscles. These features make them the most promising candidates for many applications including artificial muscles and robotics. Graphene-polymer composite actuators are considered as one of the most versatile

actuator systems since they can be triggered by electrical, optical, thermal or chemical stimulus.

The electrically triggered polymer actuators can basically follow two different mechanisms: either by utilizing Maxwell's stress, which is generated as a result of the electrostatic attraction between the two electrodes, or by pure electrostrictive effect [44]. However, there can be another class of polymer actuators in which the large mechanical deformation is caused due to the movement of charge by ions at low voltages as in the case of ionic polymer - metal composites [45]. There have been several reports during the last few years to develop electromechanical actuators with excellent actuator performance by combining the unique properties of graphene with different polymer systems. Unlike the conventional polymer based electromechanical actuators, graphene-polymer composite actuators follow different mechanisms in different systems depending on the materials and the design of the actuators. This makes them the most versatile actuator materials for various practical applications.

In a study by Chen et al. using poly(methylmethacrylate) functionalized graphene – polyurethane (MG–PU) composite actuators, it was found that the introduction of functionalised graphene into PU matrix significantly improved the electric field induced strain behaviour when compared to pure PU films. There was an increase in the electric field induced strain from 17.6% for pure PU to about 32.8% for 1.5 wt% MG–PU composite film which is almost two times than that of pure film [46].

Graphene can undergo contraction on heating due to its negative temperature coefficient of thermal expansion. This unique property was

utilized by Zhu et al. for designing a bimorph actuator using graphene–epoxy hybrid system [47]. The graphene-on-organic film actuator was developed as a cantilever in which graphene acted both as the conducting layer and heating layer. Upon applying electric power, the graphene was directly heated and the epoxy was warmed up by diffused heating. Due to the mismatch in thermal expansion of graphene and epoxy, the cantilever exhibited a deflection towards the graphene coated side. The device exhibited high actuation behaviour at very low power. For instance, the cantilever tip showed a deflection of 1 μm with an input voltage as low as 1 V within 0.02 seconds and returned back to its original position within 0.1 second. They have also reported that the flapping and bending motion of the actuators can be controlled by changing the frequency and duration of applied voltage. They have demonstrated the working of this graphene-on-organic film actuator in the form of a dragon fly wing as illustrated in figure 1.4.
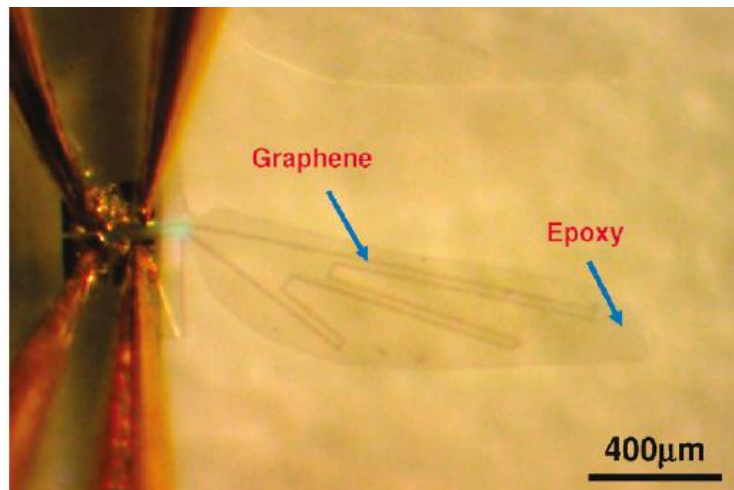
Figure 1.4: Graphene-on-organic film which is in the form of a dragonfly wing [47]

A similar bimorph actuator based on a bi-layer of graphene and polydiacetylene (PDA) was reported by Liang et al. [48]. The actuator generated large actuation motion under low electric current in response to both dc and ac signals. For example, for a bimorph of size 10 mm length by 2.7 mm width, at a very low dc current of 20 mA (current density of 0.74 A/mm^2), a displacement as large as 1.8 mm and a curvature of 0.37 cm^{-1} were obtained. Similarly, an actuation stress as high as 160 MPa/g was obtained under an applied dc of only 0.29 A/mm^2. Under ac signal, this actuator displayed reversible swing behaviour. Moreover, it was also demonstrated that a strong resonance can be generated when the frequency and the value of applied ac and the state of the actuators reach an appropriate value. This interesting actuation behaviour was explained based on two mechanisms. The electric field-induced deformation is considered as the dominant one, and the thermal induced expansion of PDA was proposed as the second mechanism contributing to this high actuation performance.

Recently, the electroactive performance of graphene loaded cellulose composite actuators was reported by Sen et al. [49]. The films of microcrystalline cellulose (MCC) loaded with graphene nanoplatelets were prepared by solvent casting method. An ionic liquid, 1-butyl-3-methylimidazolium chloride (BMCl), was used as the solvent. The composite films were converted in to actuator strips by forming electrodes using gold leaf. The incorporation of graphene enhanced the conductivity and mechanical properties of the composite. The actuator performance was measured at 3 to 7 V. The study reported that the graphene loading reduced the actuation speed but enhanced the ability to operate at higher excitation

voltages. Moreover, an increase of 267% in the maximum displacement at an excitation voltage of 3V was achieved with the addition of graphene. This clearly indicates that the loading of graphene nanoplatelets resulted in better electroactive performance of the cellulose based-composite actuator.

Electro-active actuators based on graphene reinforced Nafion composite electrolytes were developed and their actuation performances were investigated by Jung et al. [50]. In addition to the enhanced mechanical properties imparted by graphene loading, the proton conductivity was drastically improved on incorporation of graphene. The displacement obtained for graphene loaded Nafion at 0.5 V was twice that of recast Nafion. When the exciting voltage was increased to 1.5 V, the increase in displacement for the composite was three times. This displacement was higher than that for single-walled carbon nanotube reinforced ionic polymer metal composites (IPMCs) reported earlier. The bending deformations and blocking force obtained for graphene-Nafion composites is much higher than that of recast Nafion-based IPMC actuators. The efficiency analysis confirmed that the electromechanical efficiency of the graphene-Nafion composite actuators is almost twice than that of recast Nafion. In a similar Nafion based actuator system, instead of incorporating graphene in to the Nafion matrix, graphene-polyanilene composite was used as the electrolyte [51]. Maximum conductivity was obtained for films with aniline and 90% graphene. A tip displacement of 8.1 mm was obtained for 6.8V.

Polymer nanocomposite based optical actuator is one of the fast developing fields in the contemporary research. The unique features like

Development of Reduced Graphene Oxide/Polymer Nanocomposites for Optical Limiting, Optical Actuation and Electrical Applications

23

wireless actuation and remote controllability make them one of the prime focuses of actuator research. Optically triggered actuators are potentially important in biomedical field where any stimulus other than electricity is more preferred to drive the actuators. Basically, an optically triggered actuator consists of an 'energy transfer unit' which absorbs the light energy and 'molecular switch unit' where the mechanical deformation takes place. In a polymer composite based optical actuator, the filler act as the 'energy transfer unit' and the polymer matrix itself act as the 'molecular switch unit'. Due to the excellent infrared (IR) absorption characteristics of graphene, there have been considerable interest to utilize graphene − polymer composite actuators which can work under IR light as the stimulus.

The optical actuation performance of graphene-polymer composite depends mainly on the quality of graphene, the type of polymer system used, and the interaction between the polymer and graphene. In a graphene-polymer composite actuator, the homogeneous dispersion of graphene is one of the important aspects to be ensured for good optical actuation behaviour. The homogeneity of graphene dispersion was achieved by many researchers using functionalisation techniques.

The IR triggered actuation in Graphene–polydimethylsiloxane (PDMS) systems showed less photomechanical stress and strain. For example, 2 wt% graphene nanoplatelet-PDMS system exhibited a change in stress of only less than 40kPa [52]. Even with single layer graphene (1 wt%) the photomechanical stress of the PDMS system was <50kPa [53]. However, graphene–PDMS systems exhibited excellent reversibility. Seema et al. reported a Thermally reduced graphene oxide (TRGO)-PDMS

system with a higher photomechanical stress of 133.44 kPa [54]. Even though the strain obtained was only 7.17%, the actuation behaviour was 100% reversible.

Similarly, graphene/styrene-isoprene-styrene (SIS) copolymer composite was studied as an optical actuator [55]. The maximum photomechanical stress and strain obtained were 28.34 kPa and 3.1% respectively. However, the on –off cycle of the actuator exhibited a marching behaviour due to creep deformation which became less prominent after a few on-off cycles.

Graphene-polymer composite actuators which can be driven by solvents, pH, chemicals etc. can find a wide range of applications particularly in the biomedical field. A solvent driven actuator was developed by Deng et al. by pattering few layer graphene (FLG) on an epoxy based photoresist polymer (SU-8) [56]. The FLG/SU-8 bilayer can fold when immersed in water due to de-solvation of SU-8 or can unfold when immersed in acetone due to re-solvation of SU-8. Even after solvation and de-solvation, the graphene layer is held intact. This also puts up an opportunity to integrate graphene based sensors on solvent driven self folding polymer actuators.

1.5.3.2 Flexible Electronics

In recent years there has been intensive research on flexible and stretchable electronics especially in the field of wearable electronic devices, stretchable circuits, flexible batteries, membrane keyboards, biomedical sensors and artificial tissues. One of the critical parameter to realize flexible electronics is to retain the high conductivity under mechanical deformations. Polymer composites have the advantages of

being able to be folded, stretched, and deformed into the required shape. Flexible conducting composites are prepared by loading conductive fillers such as metal powders, CNT, conductive carbon black etc. into polymers. Graphene with its high conductivity and flexibility is a good filler material for flexible conducting composites

Chen et al. reported graphene foams (GF)/PDMS composites for flexible, and stretchable electronics. [57] They have synthesized three-dimensional graphene foam by template-directed chemical vapour deposition. Interconnected flexible network of graphene in the GF will act as the fast transport channel of charge carriers for high electrical conductivity. GF was used as filler in PDMS and it is found that even at low filler concentration (0.5wt% of GF) the composites show a very high electrical conductivity of ~10 S cm^{-1}

Wong et al. have developed a process to fabricate highly conductive and flexible graphene areogel/PDMS composites. [58] Graphene aerogel was prepared by spontaneous reduction process and due to porous nature of this aerogel the incorporation of PDMS into the graphene framework was easier. Graphene aerogel/PDMS composite showed a high conductivity of 95 S/m at small filler loading of 0.8wt%. The flexibility of the composites were studied by electromechanical tests and achieved good retention in conductivity (of about 80%) under various bending conditions

1.5.3.3 Sensor applications

In the recent past, graphene/polymer nanocomposites have emerged as the most promising materials for cost effective sensors having excellent sensitivity and selectivity with fast and reliable sensing techniques. The

unique electrical, thermal and optical properties of graphene when combined with the light weight, good processability and excellent mechanical properties of polymers offers a new class of materials capable of fulfilling the stringent requirements for a wide variety of sensors. Graphene – polymer nanocomposites have attracted enormous interest mainly due to the fact that, exceptionally high performing composites can be prepared by the use of extremely small quantities of the filler due to their nano-level dispersion in the polymer matrix.

Basically, 'sensors' detect the changes in any of its physical properties and convert it in to a measurable signal. Based on the changes in their optical, electrical, chemical, electrochemical and mechanical properties, graphene – polymer nanocomposites can be used as biosensors, chemical sensors, gas/vapour sensors, strain sensors etc. The following sections will elaborate on some of the common types of sensors using graphene – polymer nanocomposites.

1.5.3.3.1 Biosensors

Graphene – polymer composite biosensors based on the fluorescence, chemiluminescence and colorimetric detection systems have been extensively studied by many researchers. [59- 62] Generally, the term "graphene" in the literature is used to mention a wide range of graphene-like structures which differ in their chemical structures, their level of oxidation, number of layers, size and shape due to different methods of synthesis. In optical sensing applications, graphene oxide (GO) and reduced graphene oxide (RGO) are better preferred among the different types of graphene-like systems. The fluorescence quenching efficiency of

Development of Reduced Graphene Oxide/Polymer Nanocomposites for Optical Limiting, Optical Actuation and Electrical Applications

27

GO and RGO can be exploited for fluorescence based optical sensors. [59, 60, 63] In the fluorescence based optical sensors, researchers have demonstrated two types of sensors: "Signal-On" sensors and the "Signal-off" sensors. In the case of signal-on sensors, when an analyte is introduced to the system, it reacts with the fluorescent label and separates it from the GO (which is the fluorescent quencher) and hence the fluorescence intensity increases. The increase in fluorescence intensity can be directly correlated with the concentration of the analyte. In the case of signal-off sensors, the fluorescent labels are not completely absorbed by the GO. But when the analyte is added, they quench the fluorescence by the absorption by GO. However, signal-off sensors have lower sensitivity than signal-on sensors. GO can also quench the chemiluminescence and colour and hence can be used in optical sensors based on chemiluminescence and colour also. [60]

1.5.3.3.2 Chemical Sensors

A fluorescence based chemical sensor for detecting 2,4,6-trinitrotoluene (TNT) in aqueous solution was developed by Zhang et al. by combining GO with a conjugated polymer [64]. A hybrid organic–inorganic fluorescent system was prepared by the insitu polymerisation of poly(p-phenylenevinylene) (PPV) within mesoporous silica nanoparticles (MSNs). The surface of PPV-MSN was functionalized with GO to obtain the hybrid material (GO–PPV–MSN). The GO–PPV–MSN exhibited strong fluorescence in aqueous solution. The sensor was designed by encapsulating the polymer in the channels of the mesoporous nanoparticle so that the polymer does not involve in direct interaction with GO to avoid fluorescence quenching. In the presence of the target molecule (TNT), the

amino groups on the hybrid fluorescent material formed a complex by binding with the TNT molecules present in the solution. Through the fluorescence resonance energy transfer (FRET) mechanism, this complex strongly suppressed the fluorescence emission of the hybrid GO–PPV–MSN. In addition to increasing the water solubility, the incorporation of GO also improved the detection sensitivity.

A sensor for the determination of para-nitrophenol (4-NP) was developed based on graphene quantum dots (GQDs) coated with a polymer [65]. A polymer coating on the GQDs were formed by sol-gel polymerization of 3-aminopropyl triethoxy silane (APTES) monomer with tetra ethoxy silane (TEOS) as a crosslinker. When interacted with 4-NP, the fluorescence of the polymer coated GQDs was efficiently quenched. This fluorescence based chemical sensor showed fast response, good specificity and lower detection limit.

Huamin et al developed a polymer–graphene composite sensor based on chemiluminescence mechanism for the detection of sulfamethoxazole (SMZ). They used chitosan–graphene oxide-molecular imprinted polymer (CG-MIP) as a recognition element [66].

Trimethoprim (TMP) is a widely used antibacterial drug for the treatment of urinary, intestinal and respiratory infections. An electrochemical sensor for detecting TMP was developed recently by the electropolymerization of pyrrole on a graphene oxide-modified glassy carbon electrode [67]. In this system, the polymer can act both as the template of the recognition element and as a transducer of the signal. Graphene oxide (GO) can act as the site for the analyte. Due to the presence of oxygen containing functional groups

in GO, it can ensure strong interaction with TMP through hydrogen bonding. This improves the sensitivity towards TMP detection which is measured as a significant increase in the peak current response during square wave voltammetry measurements. In a similar work, polypyrrole (PPy) – reduced graphene oxide (RGO) – Au nanoparticle composite was used as a sensor for the detection of levofloxacin (LEV), another antibacterial agent [68]. Here, the metal nanoparticles enable to ensure higher electrode surface which in turn can significantly increases the analyte signal. The selectivity of the PPy–RGO/AuNP modified electrode towards LEV was also studied in the presence of some interfering substances like chlorotetracycline, oxytetracycline, prulifloxacin and norfloxacin. It was found that the sensors exhibited excellent selectivity towards LEV and the other species do not mask the LEV response. In another work demonstrated by Liu et al. a sensor was developed to detect chlorotetracycline, an antibiotic, using poly(o-phenylenediamine) (POPDA) and RGO composite [69]. The special recognition of the analyte by POPDA and the response amplification by RGO were combined to achieve a sensor with high sensitivity. A similar POPDA-RGO-metal nanoparticle system was also used for the sensing of cefotaxime (CEF) [70]. A glassy carbon electrode was coated with RGO having COOH groups at the edges (RGO–COOH). Then, gold nano particles and porous platinum nanoparticles dispersed in an ionic liquid was coated on the modified electrode. Then the OPDA was electroploymerized on the electrode in the presence of CEF by cyclic voltammetry. As seen in the earlier cases, here also RGO–COOH and the metal particles increase current signal where as polymer plays the recognition role.

1.5.3.3.3 Strain sensors

Strain sensors basically measure a local deformation due to an applied strain. Strain sensors mainly find application in damage detection, structural health monitoring and structural and fatigue studies of materials. The outstanding electrical properties of graphene have made it the most promising material for the development of strain sensors. In general, graphene based strain sensors can work mainly based on three mechanisms: (1) based on structure deformation of graphene, (2) based on over connected graphene sheets and finally (3) based on tunnelling effect of neighbouring graphene sheets.

The structural deformation of graphene due to an applied strain can induce attractive changes to its electronic band structure and electrical properties. There have been a lot of theoretical calculations to find out the effect of different types of strain on graphene. Experimentally, strain sensors based on the structural deformation of graphene has already been demonstrated by many researchers. A CVD grown graphene, transferred on a flexible polydimethysiloxane (PDMS) substrate, showed a guage factor of ~151 [71]. When strain was applied, initially, the resistance was decreased, which was due to the relaxation of pre-existing wrinkles on the graphene sheet. With further increase in strain resulted in increase in resistance due to distortion of hexagonal honey comb crystal structure of graphene. Even though these sensors have high sensitivity, the large strains can cause unrecoverable structural deformation which limits their practical application. Efforts were made by researchers to overcome this limitation by forming rippled graphene layers on pre-strained PDMS [72]. The

graphene layer was deposited on a pre-strained PDMS and when the strain of the PDMS was released, the graphene layer above the PDMS formed a rippled structure. The resistance of this sensor was found to linearly decrease with increasing strain. The resistance changed from 5.9 kΩ to 3.6 kΩ when the strain was increased from 0 % to 20 % till the graphene layer was completely flat.

Strain sensors based on the strain induced changes in whole conductive network are the most common type of graphene based strain sensors. The conductivity between the neighbouring graphene flakes is dependent on the overlap area and the contact resistance. When a compressive strain or tension strain is applied, the overlap area can become large or small which will result in a significant change in resistance. Li et al used graphene woven fabrics (GWF) on PDMS as a highly sensitive strain sensor [73]. When a strain is applied GWF undergoes significant changes in their polycrystalline structures. Overlapped area between the graphene flakes changed in width when they were stretched. The change of electrical network of GWF resulted in an increase in resistance. A gauge factor of ~10^3 under 2 to 6 % strain and a gauge factor of ~10^6 at higher strains were obtained. The cracks formed during stretching were recovered when the stress was removed due to the elastic nature of underlying PDMS which brought back the broken pieces of graphene to complete the conducting network.

Another kind of graphene based strain sensors basically work on the principle of tunnelling effect between neighbouring graphene flakes. Generally, the distance between two graphene sheets determines the mode

of conduction of current. In a graphene-polymer composite, current can flow due to the tunnelling effect from one isolated graphene sheet to another. It can be predicted that the change in resistance is exponential with the distance [74]. Thus the tunnelling effect can be used to develop strain sensors with higher gauge factor. A strain sensor was developed using a reduced graphite oxide– polyvinylidenefluoride (PVDF) composite film [75]. A gauge factor of 12.1 was reported for a 2.2 wt.% RGO-PVDF film. The change of resistance with strain is explained as a result of the loss of conductive interconnections or tunnelling effect between neighbouring graphene flakes and the change in conductivity from deformed graphene.

1.5.3.3.4 Gas/Vapour Sensors

The most common gas/vapour sensor based on graphene is the chemiresistor type where the significant change in electrical resistance in response to adsorbed gas/vapour molecules is used as the sensing modality. Generally, the sensitivity and selectivity of graphene-based gas/vapour sensors can be improved by making graphene-conducting polymer composites. There have been a lot of researches to develop gas/vapour sensors by combining graphene or its derivatives with conducting polymers. An ammonia gas sensor was developed by Wu et al. using HCl-doped graphene-PANI (polyaniline) composite through an insitu chemical oxidation polymerization [76]. During the composite preparation, the π electron cloud of graphene overlap with that of PANI and forms an extended π–π conjugation system. This promotes the charge interaction with NH_3 gas molecule. This helps to achieve an improved sensing performance for graphene-PANI sensor when compared to pure PANI at the same NH_3 gas

concentration. Moreover, the homogeneous dispersion of graphene increases the surface area of graphene-PANI composite thereby enhancing the sensitivity of graphene/PANI sensors for NH_3 gas.

A similar kind of NH_3 gas sensor was also reported by Jang et al. [77]. A nanocomposite of reduced graphene oxide (rGO) and polypyrrole (PPy) was prepared using in situ polymerization method. The composite was used to fabricate a NH_3 gas sensor with high sensitivity and fast response time. The effective electron charge transfer between rGO/PPy and NH_3 resulted in an improved response for NH_3 gas. Excellent reproducibility was exhibited by the PPy/rGO composite-based gas sensor during the recovery process at lower temperature of 373 K.

In a similar work, Hu et al. [78] has also reported an ammonia gas sensors based on rGO and pyrrole. The sensor exhibited excellent responsive sensitivity and selectivity to ammonia (NH_3) gas. A resistance change as high as 2.4 % and response time as fast as 1.4 s was obtained for an NH_3 concentration as low as 1 ppb. Graphene oxide (GO) conducting polymer hydrogels were prepared by Shi et al. [79]. Among the various hydrogels prepared, high sensitivity towards ammonia gas was shown by GO/PPy composite hydrogels. It showed an increase of 40 % resistance within 600s when exposed to to 800 ppm of NH_3 gas. This was almost 7 % higher than for pure PPy. The ultra thin layers on the graphene sheets helps more NH_3 molecules to access the PPy surface which could be the reason for high performance of this sensor.

A hydrogen gas sensor was developed by Al-Mashat et al. based on a graphene/PANi nanocomposite [80]. Chemically synthesized graphene was

mixed with aniline monomer and polymerized using ammonium persulfate. The rapid reaction results in the nucleation growth of PANi into uniform nanofibers on the surface of graphene. The gas sensing properties of the graphene/PANi sensor were tested using 1 % concentration of H_2 gas and compared with sensors using PANi nanofiber alone and sensors with graphene alone. The normalized resistance (R/R_0) of graphene/PANi composite was found to be much higher (16.7 %) than that of PANi-based sensor (9.83 %) and graphene alone based sensor (0.83 %) due to the higher porosity of the graphene/PANi composite.

Reduced graphene oxide (rGO)-polyionic liquid (PIL) complex and rGO-PIL/PEDOT composites were prepared by a few researchers for sensor applications [81]. When compared to pristine rGO sensor, these new rGO-PIL and rGO-PIL/PEDOT-based sensors can detect VOCs with enhanced sensitivity and selectivity. They were capable of detecting VOCs including methanol, ethanol, acetone, methyl acetate, dimethylsulfide and toluene even at very low volatile organic content (VOC) concentrations in the range of several ppm. The sensors were having rapid response (within 3 s). The electro-sorption behavior was studied using the Langmuir-Henry-Clustering (LHC) model which can be used to evaluate the amount of analyte and to identify the diffusion regimes taking place in the transducer. Based on the shape of the electro-sorption curves, it was deduced that the diffusion is exponential for the rGO-PIL/PEDOT sensor exposed to methanol, suggesting a clustering regime of diffusion.

In an another work by the same group, they prepared hybrid thin films of rGO and PEDOT using a vapour phase polymerization of PEDOT

onto rGO platelets. These hybrid thin films were used in a chemiresistor based sensor to detect trace levels of different VOCs [82]. For the preparation of rGO/PEDOT hybrids, rGO platelets were first decorated with ferric (Fe^{3+}) ions which will help to initiate the polymerization of EDOT to form PEDOT on rGO surface. PIL molecules were used to bridge rGO with PEDOT to from the hybrid. During fabrication of the sensor, initially, GO dispersion with Fe^{3+} ions and PIL was spin coated on to the electrode and subsequently GO was reduced to rGO. The deposited film was then exposed to EDOT vapors to form the composite film of rGO:PIL/PEDOT. These chemiresistor based sensors exhibited excellent sensitivity towards different VOCs even in ppm level due to the synergistic effect of rGO–PEDOT hybrid sensing material. The high surface to volume ratio of the graphene material along with high electron mobility enables high sensitivity and low noise sensing of VOCs where as PEDOT acts as an absorbent layer and it concentrates the analyte molecules on to the surface of the graphene composite. The VOC molecules act as dopants to the graphene material which can significantly affect the electron/hole transport and the carrier mobility which in turn results in a sensitive change in the resistance. VOC vapors can also induce conformational changes in PEDOT chains or doping which can also result in a change in resistance. Thus in the rGO–PEDOT hybrid films, both act as active sensing component and the synergistic contribution of both helps to achieve high sensitivity and fast response. The effect of incorporation of magnetic nanoparticles (Fe_3O_4) in to this system was also studied by the same researchers. In the Fe_3O_4-rGO/PIL-PEDOT composites, PILs served as ionic stabilizers and/or counter ions of conducting polymers. This multi-

component hybrid material system based sensor was capable of detecting both polar (ethanol, methanol, acetone, water) and non-polar (chloroform, styrene, dichlorobenzene, toluene) VOCs. The sensors exhibited high sensitivity even at very low concentrations of ppm or sub-ppm level.

A chemiresistor based vapour sensor was developed using GO/polypyrene (GO/PPr) composite films by Shi et al. [83]. A combination of PPr and GO resulted in a sensing active material with improved mechanical properties and a continuous and porous morphology with an uninterrupted conducting phase. These vapor sensors exhibited a fast, linear and reversible response to toluene. They gave a high normalized sensitivity of 9.87×10^{-4} ppm^{-1} for toluene vapors. This high sensing ability of the GO/PPr composite film was due to the high interaction of the PPr layer on rGO sheets with toluene vapor.

Other than the resistance based VOC sensors, colorimetric-based VOC sensors were also realised with graphene – polymer composites. For example, Wang et al. reported a VOC sensor based on stacked composite films of PDA and graphene [84]. PDA is π-conjugated polymer which can undergo intense chromatic change (blue to red) in response to various stimuli including temperature, solvent, mechanical stress and ligand–receptor interactions. However, due to low sensitivity, PDA sensors show many limitations in practical device applications. When graphene was combined with PDA, the graphene layer provided an efficient and transparent support to PDA and increased the absorbing area of gaseous molecules which helped to enhance the colorimetric signal of PDA. This colorimetric sensor exhibited excellent sensitivity towards various VOCs

including tetrahydrofuran, chloroform, methanol, and dimethylformamide even at very low concentrations of ~0.01 %. A logarithmic relationship was observed between the chromatic response and the VOC concentration in the range of ~0.01–10 %. At relatively high concentrations, the colour change caused by the VOCs was even detectable by the naked eye.

1.5.3.4 Electrical applications

In the modern electronic era, with the rapid development of highly integrated electronic components, there is a growing concern due to the generation of severe electromagnetic radiation which can harmfully affect the performance of high precision electronic components as well as the living environment of human beings. In this context, electromagnetic interference (EMI) shielding materials have great demand in commercial, military and scientific electronic devices and communication systems. EMI shielding is a process of achieving a certain level of attenuation of electromagnetic radiation using a suitably designed shield. Compared to conventional metal based EMI shielding materials, the use of conducting polymer composites for EMI shielding has multiple advantages like lightweight, corrosion resistance, flexibility and ease of processing. The major factors that decide the EMI shielding effectiveness (SE) of a composite material are the intrinsic conductivity, dielectric constant and aspect ratio of the conductive filler material. Graphene, with large aspect ratio and high conductivity is considered as one of the most suitable filler material in polymer composites for EMI shielding applications.

Very high SE values have been achieved by many researchers with graphene as the filler material. A light weight, flexible graphene/PDMS foam

composite was developed for EMI shielding applications by Chen et al. [85]. The composite material exhibited outstanding shield effectiveness as high as 30 dB in the 30 MHz–1.5 GHz frequency range and 20 dB in the X-band frequency range. The density of the material was as low as 0.06 g/cm^3 and thus its specific shielding effectiveness can attain 500 dB cm^3/g which surpasses the best values for metals and carbon-based composite materials. Due to high flexibility, no obvious degradation in performance was observed even after bending 10000 times to a radius of ~2.5 mm. This light weight flexible EMI shielding material can find potential applications in aerospace and next generation flexible electronics.

Another flexible and lightweight composite EMI shielding material using graphene nanosheet (GN)/waterborne polyurethane (WPU) composites were reported by Hsiao et al. [86]. Covalently modified GN with aminoethyl methacrylate (AEMA-GNs) was used as the filler material in WPU. Due to the high compatibility of AEMA-GNs with WPU matrix, homogeneously dispersed composites were obtained. 5 vol. % AEMA-GN loaded WPU composites exhibited electrical conductivity of 43.64 S/m and EMI shielding effectiveness of 38 dB over the frequency of 8.2–12.4 GHz.

Zhang et al. developed graphene-PMMA nanocomposites for EMI shielding applications [87]. These nanocomposites at a filler loading of 1.8 vol % exhibited a high conductivity of 3.11 S/m, and an EMI shielding efficiency of 13 to 19 dB in the frequencies range of 8 to 12 GHz. The EMI shielding efficiency was mainly attributed to the absorption rather than the reflection. In another report by Liang et al. graphene/epoxy composites with a low percolation threshold of 0.52 vol.% was studied as a EMI shielding

material [88]. The highest SE obtained for the composites containing 15 wt% (8.8 vol.%) functionalised graphene was 21 dB in the X-band.

The EMI shielding efficiency of functionalized grapheme (f-G)-poly(vinylidene fluoride) (PVDF) nanocomposites were studied by Eswaraiah et al. [89]. For a 5wt% f-G loading, an EMI shielding effectiveness of ~ 20 dB was obtained in X-band region and ~18 dB in broadband (1–8GHz) region. The reflectivity (R), transmissivity (T) and absorptivity (A) were 0.78, 0.01, and 0.21 respectively. The reflectivity was found to increase from10 to 80% with an increase in mass fraction of f-G from 1 to 5 wt%. The predominant mechanism for EMI shielding in these composites was reflection rather than absorption.

1.5.3.5 Shape memory applications

Shape memory polymers or polymer composites are materials which can "memorize" a permanent shape and can be "fixed" in to a certain temporary shape under appropriate conditions. Later, when a trigger (e.g., heat or light) is applied, the temporary shape is transformed to the memorized permanent shape [90]. Shape memory polymers, in general, possess at least two different "phases". The first one is the stable network which is responsible to retain the original shape and the second phase is influenced by the external trigger to form the deformed shape.

The incorporation of conducting fillers in to the shape memory polymer is one of the most widely adopted methods to develop smarter shape memory materials. The unique electrical, thermal, and mechanical properties of graphene have made it the most attractive filler material for shape memory polymers. In addition to imparting mechanical strength,

due to the high thermal conductivity of graphene, it can uniformly heat the shape memory polymer composite which results in faster response and better shape recoverability. Many researchers have already succeeded in improving the shape memory effect by incorporating graphene to the polymer matrix. For example, the addition of a meagre 0.1 wt% of high-quality graphene in polyurethane (PU) enabled to achieve a shape recovery of 1.8 MPa cm^{-3} [91]. They have used highly crystallized few layer graphene with large geometrical dimensions. The improved properties were also influenced by the effective stress transfer from graphene to PU. In a similar work, Han and Chun [92] utilized functionalized graphene/PU nanocomposites for shape memory applications. For a functionalised graphene loading as low as 0.5%, the composites exhibited a shape fixity of 98% and shape recovery ratio of 94% after 4 cycles thermomechanical cycle tests. The covalent bonding between the functionalised graphene sheets and the NCO terminated PU helped to achieve uniform dispersion and thereby improved shape memory properties. A composite with triple stage shape memory performance was demonstrated by combining chemically modified graphene oxide with an interpenetrating polymer network of polyurethane with two different molecular weights [93].

The shape memory effect of graphene oxide (GO) incorporated shape memory polyurethane (SMPU) nanofibers were studied by thermal cyclic tests [94]. The SMPU/GO nanofibrous mats exhibited better shape memory effect and lower thermal shrinkage when compared with pristine SMPU nanofibrous mats. With a GO loading of 4.0 wt%, a very low thermal shrinkage ratio 4.7 $\pm$ 0.3%, and a very high average fixation ratio and recovery ratio of 92.1% and 96.5% were obtained, respectively. The GO

cross-linked SMPU molecular chains are not free to shrink and hence can be stabilized much more quickly for reaching the final structure which results in high fixation and recovery ratio.

In a similar study, the correlation between the temperature dependent shape memory effect and the cross linking density in GO/polyurethane nano composites was established by Ponnamma et al. [95]. As the filler concentration was varied, the crosslinking density was also varied which in turn affected the shape memory properties. A concept of quantifying shape memory in terms of physical crosslinks and filler–polymer entanglements of the PU/GO nanocomposite system was introduced by the researchers in this work.

The shape memory properties of reduced graphene oxide paper (RGOP)/epoxy composite was studied by electrical resistive heating [96]. The excellent heat conductive property of RGOP helped to serve as a conductive layer to transmit heat to the polymer. The shape recovery speed was found to increase with increasing applied voltage. The recoverability of the composite was approximately 100% taking only 5 s under 6 V. It was found that the shape recovery rate of the composite can be controlled by programming the synergistic effect between the mass ratio and the applied voltage.

A high temperature shape memory material was demonstrated with graphene-polyimide nanocomposite by Yoonessi et al. [97]. Amine functionalised graphene was grafted with imide moieties. Nanocomposite films were prepared by solvent casting method. The nanocomposites exhibited shape memory behaviour with a triggering temperature of 230°C.

The shape recovery rate was found to improve with incorporation of graphene.

Graphene–polymer composites have emerged as one of the most promising materials that can revolutionize the field of electronics and optoelectronics. In this chapter, we have briefly introduced various methods of preparation of graphene–polymer composites and their applications in various fields. A broad range of applications, including actuators, sensors, EMI shielding and shape memory applications have been reviewed in detail. It is well established that the use of graphene–polymer composites can enhance the performance of many devices when compared to conventional materials due to the combination of the unique electrical, optical and thermal properties of graphene and the structural and functional properties of polymers. The sensitivity and selectivity of most of the sensors were improved with the use of graphene–polymer composites as the active sensing material. Similarly, in actuators, they could yield higher displacements and force compared to conventional polymer based actuators. Moreover, they showed better controllability and tunability. They have also proved their efficiency as an EMI shielding material for many practical device applications. The actuation and shape memory effect shown by graphene – polymer composites in response various stimuli makes them the most appropriate material for robotic and artificial muscle applications. Even though graphene – polymer composites have proved their capability for high performance device applications, the production of graphene – polymer composite based devices in commercial level is still at a growing stage. This can be geared up only with more efforts for the low cost production of high quality graphene. However, graphene – polymer

composites proclaims themselves as the next generation material for high performance devices with their extra ordinary properties.

1.5.3.6 Optical limiting applications

Optical limiting is a mechanism by which certain materials, which are transparent to light at low intensities, restrict the transmission of light above a threshold input intensity. Graphene, GO and RGO were found to exhibit high nonlinear optical absorption which makes them suitable as good optical limiters. Most of the studies were based on dispersions in liquid. However, for practical device applications, these need to be used as solid materials and dispersion of graphene or GO or RGO in solid matrix is very important. There have been a few studies on the nonlinear optical properties of RGO in various solid matrices including glass and polymers. The nonlinear optical properties of covalently functionalized GO in silica gel glasses were studied by Tao et al. [98]. They have observed that the nonlinear optical response of functionalised GO was better in silica gel glass than in deionized water. Similarly RGO with porphyrin incorporated in polymers were studied as optical limiters by a few researchers [99]. There have been a few reports on the optical limiting properties of graphene/polymer composites also. However, in order to avoid the dispersibility issues of graphene, functionalization was required in most of the cases [100,101].

1.6   Scope of the work

Even though there have been a lot of research carried out worldwide in the field of graphene/polymer nanocomposites, the uniform dispersion of pure graphene in polymer matrix is still a problem for many

applications. Moreover, the production of high quality graphene through methods like CVD or epitaxial growth is neither simple nor cost effective. For many applications, especially as graphene/polymer composites, such electronic quality graphene is not required and not suitable. In this context, graphene-like materials like reduced graphene oxide (RGO) will be a good alternative and research in this direction is rapidly progressing.

The successful development of RGO/polymer nanocomposites mainly depends on the type of polymer selected and method of preparation of RGO. A simple and cost effective methodology for the preparation of the composite is also equally important for wide spread deployment of the material for practical applications. Instead of methods involving high-end machineries and processing equipments, a solution based system will be more attractive due to its ease of operation. However, the selection of solvent is also a major concern since it should not harm the environment. Aqueous based polymers like polyvinyl alcohol can make the system more eco friendly since water can be used as the solvent thereby avoiding the possibility of any type of environmental issues. Moreover these types of polymer composites, which are biocompatible, can find a lot of applications in bio medical field. However, water soluble polymers have their own disadvantages also and cannot be used everywhere. In such cases, a polymer soluble in less hazardous polar solvents can be a better choice for solution processing. When the elasticity is of particular importance for an application, the difficulty in rubber processing always accompanies the system. However, thermoplastic elastomers provide the ease of processing of plastics with the elasticity of a rubber. Thermoplastic polyurethanes are good choice for rubbery materials which can be processed through simple

methods like solution casting. Hence there is an impending demand for the development of a simple and cost effective method for the preparation of RGO nanocomposite systems with both plastic and elastomeric polymers for various applications.

Even though many applications for graphene/polymer composites have been discussed in this chapter, there is still scope to explore many unexploited areas. With the advancement in optoelectronics and photonic devices, the use of powerful lasers has become inevitable in the present information era. However, protection from powerful lasers has also emerged as a major challenge. Hence the importance of optical limiting materials and devices, which can protect sensors and human eyes beyond a threshold light intensity, has steadily increased. Even though there have been lot of research on optical limiting materials, for practical device applications a single material or limiting mechanism may not be sufficient to meet all the stringent application requirements. Moreover, most of the studies on optical limiting materials were using liquid dispersions where as in real practice, we require a solid material for device fabrication. Hence the development of RGO/polymer nanocomposites for optical limiting applications will have lasting impact from device perspective.

In the case of actuators, electrically triggered actuators hold the major share of the actuator industry. However, for systems where stimulus other than electricity is preferred, optical actuators are the most suited devices. However, there have been comparatively less research in this direction. The actuator behaviour of the graphene/polymer actuators mainly depend on the type of polymer system. By judiciously choosing the

appropriate polymer system, we can cater to many applications especially in biomedical devices. Hence the development of RGO/polymer systems for optically triggered actuators will be a noteworthy attempt.

The electrical properties of RGO/polymer composites are of great interest for many potential applications including EMI shielding, conductive pathways in wearable devices, supercapacitors, etc. However, for applications such as antistatic coatings, composites systems which can be directly coated on to substrate will be more preferred. Finding out various possible electrical applications for RGO/polymer composites can help to make flexible, light weight and low cost appliances in all facets of life.

1.7 Objectives of the work

The main objective of this work is to develop reduced graphene oxide/polymer nanocomposites suitable for optical limiting, optical actuation and electrical applications. The objectives include:

- Synthesis of graphene oxide from natural graphite flakes through a modified synthesis protocol using chemical oxidation method.

- Synthesis of reduced graphene oxide (RGO) using chemical and thermal reduction methods.

- Preparation of RGO/polymer nanocomposites using *in situ* chemical reduction of graphene oxide in poly(vinyl alcohol) systems and with thermally reduced graphene oxide in thermoplastic polyurethane system.

- Characterization of RGO/polymer nanocomposites for their thermal, mechanical, optical and morphological characteristics.

- Study of nonlinear optical absorption in RGO/polymer composites and the demonstration of RGO/polymer nanocomposites as optical limiters.

- Study of photomechanical actuation in RGO/polymer composites and demonstration of RGO/polymer nanocomposites as optical actuators.

- Studies on the electrical properties of RGO/polymer nanocomposites suitable for various applications.

References

[1] Rao, C. N. R., Biswas, K., Subrahmanyam, K. S., & Govindaraj, A. (2009). Graphene, the new nanocarbon. *Journal of Materials Chemistry*, *19*(17), 2457-2469.

[2] Geim, A. K., & Novoselov, K. S. (2007). The rise of graphene. *Nature materials*, *6*(3), 183-191.

[3] Lavoisier AL. (1789) Traite Elementaire de Chimie. Paris

[4] Wallace, P. R. (1947). The band theory of graphite. *Physical Review*, *71*(9), 622.

[5] Boehm, H. P., Clauss, A., Fischer, G. O., & Hofmann, U. (1962). Das adsorptionsverhalten sehr dünner kohlenstoff-folien. *Zeitschrift für anorganische und allgemeine Chemie*, *316*(3-4), 119-127.

[6] Boehm, H. P., Setton, R., & Stumpp, E. (1994). Nomenclature and terminology of graphite intercalation compounds (IUPAC Recommendations 1994). *Pure and Applied Chemistry*, *66*(9), 1893-1901.

[7]   Novoselov, K. S., Geim, A. K., Morozov, S. V., Jiang, D., Zhang, Y., Dubonos, S. V., ... & Firsov, A. A. (2004). Electric field effect in atomically thin carbon films. *science*, *306*(5696), 666-669.

[8]   Allen, M. J., Tung, V. C., & Kaner, R. B. (2009). Honeycomb carbon: a review of graphene. *Chemical reviews*, *110*(1), 132-145.

[9]   Neto, A. C., Guinea, F., Peres, N. M., Novoselov, K. S., & Geim, A. K. (2009). The electronic properties of graphene. *Reviews of modern physics*, *81*(1), 109.

[10]   Lee, C., Wei, X., Kysar, J. W., & Hone, J. (2008). Measurement of the elastic properties and intrinsic strength of monolayer graphene. *science*, *321*(5887), 385-388.

[11]   Yoon, D., Son, Y. W., & Cheong, H. (2011). Negative thermal expansion coefficient of graphene measured by Raman spectroscopy. *Nano letters*, *11*(8), 3227-3231.

[12]   Balandin, A. A., Ghosh, S., Bao, W., Calizo, I., Teweldebrhan, D., Miao, F., & Lau, C. N. (2008). Superior thermal conductivity of single-layer graphene. *Nano letters*, *8*(3), 902-907.

[13]   Geim, A. K., & Kim, P. (2008). Carbon wonderland. *Scientific American*, *298*(4), 90-97.

[14]   Dreyer, D. R., Park, S., Bielawski, C. W., & Ruoff, R. S. (2010). The chemistry of graphene oxide. *Chemical Society Reviews*, *39*(1), 228-240.

[15]   Stankovich, S., Dikin, D. A., Piner, R. D., Kohlhaas, K. A., Kleinhammes, A., Jia, Y., & Ruoff, R. S. (2007). Synthesis of graphene-based nanosheets via chemical reduction of exfoliated graphite oxide. *carbon*, *45*(7), 1558-1565.

[16]   Emtsev, K. V., Speck, F., Seyller, T., Ley, L., & Riley, J. D. (2008). Interaction, growth, and ordering of epitaxial graphene on SiC {0001} surfaces: A comparative photoelectron spectroscopy study. *Physical Review B*, *77*(15), 155303.

[17] Batzill, M. (2012). The surface science of graphene: Metal interfaces, CVD synthesis, nanoribbons, chemical modifications, and defects. *Surface Science Reports*, *67*(3), 83-115.

[18] Lim, J., Maiti, U. N., Kim, N. Y., Narayan, R., Lee, W. J., Choi, D. S., ... & Kim, H. (2016). Dopant-specific unzipping of carbon nanotubes for intact crystalline graphene nanostructures. *Nature communications*, *7*, 10364.

[19] Galande, C., Gao, W., Mathkar, A., Dattelbaum, A. M., Narayanan, T. N., Mohite, A. D.,…& Ajayan, P. M. (2014). Science and engineering of graphene oxide. *Particle & Particle Systems Characterization*, *31*(6), 619-638.

[20] Pei, S., & Cheng, H. M. (2012). The reduction of graphene oxide. *Carbon*, *50*(9), 3210-3228.

[21] Kuilla, T., Bhadra, S., Yao, D., Kim, N. H., Bose, S., & Lee, J. H. (2010). Recent advances in graphene based polymer composites. *Progress in polymer science*, *35*(11), 1350-1375.

[22] Tao, C. A., Zou, X., Hu, Z., Liu, H., & Wang, J. (2016). Chemically functionalized graphene/polymer nanocomposites as light heating platform. *Polymer Composites*, *37*(5), 1350-1358.

[23] Wang, M., Duan, X., Xu, Y., & Duan, X. (2016). Functional three-dimensional graphene/polymer composites.

[24] Sun, Y., & Shi, G. (2013). Graphene/polymer composites for energy applications. *Journal of Polymer Science Part B: Polymer Physics*, *51*(4), 231-253.

[25] Li, Y., & Chopra, N. (2015). Progress in large-scale production of graphene. Part 1: chemical methods. *Jom*, *67*(1), 34-43.

[26] Potts, J. R., Shankar, O., Murali, S., Du, L., & Ruoff, R. S. (2013). Latex and two-roll mill processing of thermally-exfoliated graphite oxide/ natural rubber nanocomposites. *Composites Science and Technology*, *74*, 166-172.

[27] Brennan, B., Spencer, S. J., Belsey, N. A., Faris, T., Cronin, H., Silva, S. R. P., ... & Pollard, A. J. (2017). Structural, chemical and electrical characterisation of conductive graphene-polymer composite films. *Applied Surface Science*, *403*, 403-412.

[28] Kumar, P., Kumar, A., Cho, K. Y., Das, T. K., & Sudarsan, V. (2017). An asymmetric electrically conducting self-aligned graphene/polymer composite thin film for efficient electromagnetic interference shielding. *AIP Advances*, *7*(1), 015103.

[29] Kumar, P., Yu, S., Shahzad, F., Hong, S. M., Kim, Y. H., & Koo, C. M. (2016). Ultrahigh electrically and thermally conductive self-aligned graphene/polymer composites using large-area reduced graphene oxides. *Carbon*, *101*, 120-128.

[30] Kim, H., Abdala, A. A., & Macosko, C. W. (2010). Graphene/polymer nanocomposites. *Macromolecules*, *43*(16), 6515-6530.

[31] Kashiwagi, T.. Fangming Du, Jack F. Douglas, Karen I. Winey, Richard H. Harris Jr, John R. Shields (2005) *Nanoparticle Networks Reduce the Flammability of Polymer Nanocomposites, Departmental Papers (MSE), Department of Materials Science & Engineering, University of Pennsylvania.*

[32] Chiang, C. L., & Yang, J. M. (2016). Flame retardance and thermal stability of polymer/graphene nanosheet oxide composites. *Novel Fire Retardant Polymers and Composite Materials*, 295.

[33] Liang, J., Huang, Y., Zhang, L., Wang, Y., Ma, Y., Guo, T., & Chen, Y. (2009). Molecular-level dispersion of graphene into poly (vinyl alcohol) and effective reinforcement of their nanocomposites. *Advanced Functional Materials*, *19*(14), 2297-2302.

[34] Xu, Y., Hong, W., Bai, H., Li, C., & Shi, G. (2009). Strong and ductile poly (vinyl alcohol)/graphene oxide composite films with a layered structure. *Carbon*, *47*(15), 3538-3543.

[35] Vadukumpully, S., Paul, J., Mahanta, N., & Valiyaveettil, S. (2011). Flexible conductive graphene/poly (vinyl chloride) composite thin films with high mechanical strength and thermal stability. *Carbon*, *49*(1), 198-205.

[36] Zhao, X., Zhang, Q., Hao, Y., Li, Y., Fang, Y., & Chen, D. (2010). Alternate multilayer films of poly (vinyl alcohol) and exfoliated graphene oxide fabricated via a facial layer-by-layer assembly. *Macromolecules*, *43*(22), 9411-9416.

[37] Yu, J., Huang, X., Wu, C., & Jiang, P. (2011). Permittivity, thermal conductivity and thermal stability of poly (vinylidene fluoride)/graphene nanocomposites. *IEEE Transactions on Dielectrics and Electrical Insulation*, *18*(2).

[38] Potts, J. R., Dreyer, D. R., Bielawski, C. W., & Ruoff, R. S. (2011). Graphene-based polymer nanocomposites. *Polymer*, *52*(1), 5-25.

[39] Wang, X., Hu, Y., Song, L., Yang, H., Xing, W., & Lu, H. (2011). In situ polymerization of graphene nanosheets and polyurethane with enhanced mechanical and thermal properties. *Journal of materials Chemistry*, *21*(12), 4222-4227.

[40] Xu, Z., & Gao, C. (2010). In situ polymerization approach to graphene-reinforced nylon-6 composites. *Macromolecules*, *43*(16), 6716-6723.

[41] Huang, Y., Qin, Y., Zhou, Y., Niu, H., Yu, Z. Z., & Dong, J. Y. (2010). Polypropylene/graphene oxide nanocomposites prepared by in situ Ziegler−Natta polymerization. *Chemistry of Materials*, *22*(13), 4096-4102.

[42] Potts, J. R., Lee, S. H., Alam, T. M., An, J., Stoller, M. D., Piner, R. D., & Ruoff, R. S. (2011). Thermomechanical properties of chemically modified graphene/poly (methyl methacrylate) composites made by in situ polymerization. *Carbon*, *49*(8), 2615-2623.

[43] Ahir, S. V., Squires, A. M., Tajbakhsh, A. R., & Terentjev, E. M. (2006). Infrared actuation in aligned polymer-nanotube composites. *Physical review B*, *73*(8), 085420.

[44]   Diaconu, I., Dorohoi, D. O., & Topoliceanu, F. (2006). Electrostriction of a polyurethane elastomer-based polyester. *IEEE Sensors Journal*, *6*(4), 876-880.

[45]   Shahinpoor, M. (2003). Ionic polymer–conductor composites as biomimetic sensors, robotic actuators and artificial muscles—a review. *Electrochimica Acta*, *48*(14), 2343-2353.

[46]   Chen, T., Qiu, J., Zhu, K., He, X., Kang, X., & Dong, E. L. (2014). Poly (methyl methacrylate)-functionalized graphene/polyurethane dielectric elastomer composites with superior electric field induced strain. *Materials Letters*, *128*, 19-22.

[47]   Zhu, S. E., Shabani, R., Rho, J., Kim, Y., Hong, B. H., Ahn, J. H., & Cho, H. J. (2011). Graphene-based bimorph microactuators. *Nano letters*, *11*(3), 977-981.

[48]   Liang, J., Huang, L., Li, N., Huang, Y., Wu, Y., Fang, S., ... & Baughman, R. (2012). Electromechanical actuator with controllable motion, fast response rate, and high-frequency resonance based on graphene and polydiacetylene. *ACS nano*, *6*(5), 4508-4519.

[49]   Sen, I., Seki, Y., Sarikanat, M., Cetin, L., Gurses, B. O., Ozdemir, O., ... & Mermer, O. (2015). Electroactive behavior of graphene nanoplatelets loaded cellulose composite actuators. *Composites Part B: Engineering*, *69*, 369-377.

[50]   Jung, J. H., Jeon, J. H., Sridhar, V., & Oh, I. K. (2011). Electro-active graphene–Nafion actuators. *Carbon*, *49*(4), 1279-1289.

[51]   Surana, K., Singh, P. K., Bhattacharya, B., Verma, C. S., & Mehra, R. M. (2015). Synthesis of graphene oxide coated Nafion membrane for actuator application. *Ceramics International*, *41*(3), 5093-5099.

[52]   Loomis, J., King, B., Burkhead, T., Xu, P., Bessler, N., Terentjev, E., & Panchapakesan, B. (2012). Graphene-nanoplatelet-based photomechanical actuators. *Nanotechnology*, *23*(4), 045501.

[53] Loomis, J., King, B., & Panchapakesan, B. (2012). Layer dependent mechanical responses of graphene composites to near-infrared light. *Applied Physics Letters*, *100*(7), 073108.

[54] Ansari, S., Rahima, C., & Muralidharan, M. N. (2013). Photomechanical Characteristics of Thermally Reduced Graphene Oxide–Polydimethylsiloxane Nanocomposites. *Polymer-Plastics Technology and Engineering*, *52*(15), 1604-1610.

[55] Ansari, S., Muralidharan M. N., & Ushus, D. (2013). Graphene/poly (styrene-b-isoprene-b-styrene) nanocomposite optical actuators. *Journal of Applied Polymer Science*, *130*(6), 3902-3908.

[56] Deng, T., Yoon, C., Jin, Q., Li, M., Liu, Z., & Gracias, D. H. (2015). Self-folding graphene-polymer bilayers. *Applied Physics Letters*, *106*(20), 203108.

[57] Xu, R., Lu, Y., Jiang, C., Chen, J., Mao, P., Gao, G., ... & Wu, S. (2014). Facile fabrication of three-dimensional graphene foam/poly (dimethylsiloxane) composites and their potential application as strain sensor. *ACS applied materials & interfaces*, *6*(16), 13455-13460.

[58] Song, B., Wu, Z., Zhu, Y., Moon, K. S., & Wong, C. P. (2015, May). Three-dimensional graphene-based composite for flexible electronic applications. In *Electronic Components and Technology Conference (ECTC), 2015 IEEE 65th* (pp. 1803-1807). IEEE.

[59] Kochmann, S., Hirsch, T., & Wolfbeis, O. S. (2012). Graphenes in chemical sensors and biosensors. *TrAC Trends in Analytical Chemistry*, *39*, 87-113.

[60] Morales-Narváez, E., & Merkoçi, A. (2012). Graphene oxide as an optical biosensing platform. *Advanced Materials*, *24*(25), 3298-3308.

[61] Pumera, M. (2011). Graphene in biosensing. *Materials today*, *14*(7), 308-315.

[62] Kuila, T., Bose, S., Khanra, P., Mishra, A. K., Kim, N. H., & Lee, J. H. (2011). Recent advances in graphene-based biosensors. *Biosensors and Bioelectronics*, *26*(12), 4637-4648.

[63] Zhao, X. H., Kong, R. M., Zhang, X. B., Meng, H. M., Liu, W. N., Tan, W., ... & Yu, R. Q. (2011). Graphene–DNAzyme based biosensor for amplified fluorescence "turn-on" detection of Pb2+ with a high selectivity. *Analytical chemistry*, *83*(13), 5062-5066.

[64] Zhang, H., Feng, L., Liu, B., Tong, C., & Lü, C. (2014). Conjugation of PPV functionalized mesoporous silica nanoparticles with graphene oxide for facile and sensitive fluorescence detection of TNT in water through FRET. *Dyes and Pigments*, *101*, 122-129.

[65] Zhou, Y., Qu, Z. B., Zeng, Y., Zhou, T., & Shi, G. (2014). A novel composite of graphene quantum dots and molecularly imprinted polymer for fluorescent detection of paranitrophenol. *Biosensors and Bioelectronics*, *52*, 317-323.

[66] Huamin, Q., Lulu, F., Li, X., Li, L., Min, S., & Chuannan, L. (2013). Determination sulfamethoxazole based chemiluminescence and chitosan/ grapheme oxide-molecularly imprinted polymers. *Carbohydrate polymers*, *92*(1), 394-399.

[67] da Silva, H., Pacheco, J. G., Magalhães, J. M., Viswanathan, S., & Delerue-Matos, C. (2014). MIP-graphene-modified glassy carbon electrode for the determination of trimethoprim. *Biosensors and Bioelectronics*, *52*, 56-61.

[68] Wang, F., Zhu, L., & Zhang, J. (2014). Electrochemical sensor for levofloxacin based on molecularly imprinted polypyrrole–graphene–gold nanoparticles modified electrode. *Sensors and Actuators B: Chemical*, *192*, 642-647.

[69] Liu, Y., Zhu, L., Luo, Z., & Tang, H. (2013). Fabrication of molecular imprinted polymer sensor for chlortetracycline based on controlled electrochemical reduction of graphene oxide. *Sensors and Actuators B: Chemical*, *185*, 438-444.

[70] Yang, G., Zhao, F., & Zeng, B. (2014). Electrochemical determination of cefotaxime based on a three-dimensional molecularly imprinted film sensor. *Biosensors and Bioelectronics*, *53*, 447-452.

Development of Reduced Graphene Oxide/Polymer Nanocomposites for Optical Limiting, Optical Actuation and Electrical Applications

55

[71] Fu, X. W., Liao, Z. M., Zhou, J. X., Zhou, Y. B., Wu, H. C., Zhang, R., ... & Yu, D. (2011). Strain dependent resistance in chemical vapor deposition grown graphene. *Applied Physics Letters*, *99*(21), 213107.

[72] Wang, Y., Yang, R., Shi, Z., Zhang, L., Shi, D., Wang, E., & Zhang, G. (2011). Super-elastic graphene ripples for flexible strain sensors. *ACS nano*, *5*(5), 3645-3650.

[73] Li, X., Zhang, R., Yu, W., Wang, K., Wei, J., Wu, D., ... & Ruoff, R. S. (2012). Stretchable and highly sensitive graphene-on-polymer strain sensors. *Scientific reports*, *2*, 870.

[74] Eswaraiah, V., Balasubramaniam, K., & Ramaprabhu, S. (2012). One-pot synthesis of conducting graphene–polymer composites and their strain sensing application. *Nanoscale*, *4*(4), 1258-1262.

[75] Wu, Z., Chen, X., Zhu, S., Zhou, Z., Yao, Y., Quan, W., & Liu, B. (2013). Enhanced sensitivity of ammonia sensor using graphene/polyaniline nanocomposite. *Sensors and Actuators B: Chemical*, *178*, 485-493.

[76] Jang, W. K., Yun, J., Kim, H. I., & Lee, Y. S. (2013). Improvement of ammonia sensing properties of polypyrrole by nanocomposite with graphitic materials. *Colloid and Polymer Science*, *291*(5), 1095-1103.

[77] Hu, N., Yang, Z., Wang, Y., Zhang, L., Wang, Y., Huang, X., ... & Zhang, Y. (2013). Ultrafast and sensitive room temperature NH3 gas sensors based on chemically reduced graphene oxide. *Nanotechnology*, *25*(2), 025502.

[78] Bai, H., Sheng, K., Zhang, P., Li, C., & Shi, G. (2011). Graphene oxide/conducting polymer composite hydrogels. *Journal of Materials Chemistry*, *21*(46), 18653-18658.

[79] Al-Mashat, L., Shin, K., Kalantar-zadeh, K., Plessis, J. D., Han, S. H., Kojima, R. W., ... & Wlodarski, W. (2010). Graphene/polyaniline nanocomposite for hydrogen sensing. *The Journal of Physical Chemistry C*, *114*(39), 16168-16173.

[80] Tung, T. T., Castro, M., Kim, T. Y., Suh, K. S., & Feller, J. F. (2012). Graphene quantum resistive sensing skin for the detection of alteration biomarkers. *Journal of Materials Chemistry*, *22*(40), 21754-21766.

[81] Tung, T. T., Castro, M., Feller, J. F., Kim, T. Y., & Suh, K. S. (2013). Hybrid film of chemically modified graphene and vapor-phase-polymerized PEDOT for electronic nose applications. *Organic Electronics*, *14*(11), 2789-2794.

[82] Tung, T. T., Castro, M., Feller, J. F., Kim, T. Y., & Suh, K. S. (2013). Hybrid film of chemically modified graphene and vapor-phase-polymerized PEDOT for electronic nose applications. *Organic Electronics*, *14*(11), 2789-2794.

[83] Zhang, L., Li, C., Liu, A., & Shi, G. (2012). Electrosynthesis of graphene oxide/polypyrene composite films and their applications for sensing organic vapors. *Journal of Materials Chemistry*, *22*(17), 8438-8443.

[84] Wang, X., Sun, X., Hu, P. A., Zhang, J., Wang, L., Feng, W., ... & Cao, W. (2013). Colorimetric sensor based on self-assembled Polydiacetylene/ graphene-stacked composite film for vapor-phase volatile organic compounds. *Advanced Functional Materials*, *23*(48), 6044-6050.

[85] Chen, Z., Xu, C., Ma, C., Ren, W., & Cheng, H. M. (2013). Lightweight and flexible graphene foam composites for high-performance electromagnetic interference shielding. *Advanced materials*, *25*(9), 1296-1300.

[86] Hsiao, S. T., Ma, C. C. M., Tien, H. W., Liao, W. H., Wang, Y. S., Li, S. M., ... & Yang, R. B. (2015). Effect of covalent modification of graphene nanosheets on the electrical property and electromagnetic interference shielding performance of a water-borne polyurethane composite. *ACS applied materials & interfaces*, *7*(4), 2817-2826.

[87] Zhang, H. B., Yan, Q., Zheng, W. G., He, Z., & Yu, Z. Z. (2011). Tough graphene− polymer microcellular foams for electromagnetic interference shielding. *ACS applied materials & interfaces*, *3*(3), 918-924.

[88] Liang, J., Wang, Y., Huang, Y., Ma, Y., Liu, Z., Cai, J., ... & Chen, Y. (2009). Electromagnetic interference shielding of graphene/epoxy composites. *Carbon*, *47*(3), 922-925.

[89] Eswaraiah, V., Sankaranarayanan, V., & Ramaprabhu, S. (2011). Functionalized graphene–PVDF foam composites for EMI shielding. *Macromolecular Materials and Engineering*, *296*(10), 894-898.

[90] Liu, C., Qin, H., & Mather, P. T. (2007). Review of progress in shape-memory polymers. *Journal of Materials Chemistry*, *17*(16), 1543-1558.

[91] Jung, Y. C., Kim, J. H., Hayashi, T., Kim, Y. A., Endo, M., Terrones, M., & Dresselhaus, M. S. (2012). Fabrication of transparent, tough, and conductive shape-memory polyurethane films by incorporating a small amount of high-quality graphene. *Macromolecular rapid communications*, *33*(8), 628-634.

[92] Han, S., & Chun, B. C. (2014). Preparation of polyurethane nanocomposites via covalent incorporation of functionalized graphene and its shape memory effect. *Composites Part A: Applied Science and Manufacturing*, *58*, 65-72.

[93] Kim, Y. J., Park, H. C., & Kim, B. K. (2015). Triple shape-memory effect bysilanized polyurethane/silane-functionalized graphene oxide nanocomposites bilayer. *High Performance Polymers*, *27*(7), 886-897.

[94] Tan, L., Gan, L., Hu, J., Zhu, Y., & Han, J. (2015). Functional shape memory composite nanofibers with graphene oxide filler. *Composites Part A: Applied Science and Manufacturing*, *76*, 115-123.

[95] Ponnamma, D., Sadasivuni, K. K., Strankowski, M., Moldenaers, P., Thomas, S., & Grohens, Y. (2013). Interrelated shape memory and Payne effect in polyurethane/graphene oxide nanocomposites. *Rsc Advances*, *3*(36), 16068-16079.

[96] Wang, W., Liu, D., Liu, Y., Leng, J., & Bhattacharyya, D. (2015). Electrical actuation properties of reduced graphene oxide paper/epoxy-based shape memory composites. *Composites Science and Technology*, *106*, 20-24.

[97] Yoonessi, M., Shi, Y., Scheiman, D. A., Lebron-Colon, M., Tigelaar, D. M., Weiss, R. A., & Meador, M. A. (2012). Graphene polyimide nanocomposites; thermal, mechanical, and high-temperature shape memory effects. *Acs Nano*, *6*(9), 7644-7655.

[98] Tao, L., Zhou, B., Bai, G., Wang, Y., Yu, S. F., Lau, S. P., ... & Xu, D. (2013). Fabrication of covalently functionalized graphene oxide incorporated solid-state hybrid silica gel glasses and their improved nonlinear optical response. *The Journal of Physical Chemistry C*, *117*(44), 23108-23116.

[99] Du, Y., Dong, N., Zhang, M., Zhu, K., Na, R., Zhang, S., ... & Wang, J. (2017). Covalent functionalization of graphene oxide with porphyrin and porphyrin incorporated polymers for optical limiting. *Physical Chemistry Chemical Physics*, *19*(3), 2252-2260.

[100] Gan, Y., Feng, M., & Zhan, H. (2014). Enhanced optical limiting effects of graphene materials in polyimide. *Applied Physics Letters*, *104*(17), 171105.

[101] Husaini, S., Slagle, J. E., Murray, J. M., Guha, S., Gonzalez, L. P., & Bedford, R. G. (2013). Broadband saturable absorption and optical limiting in graphene-polymer composites. *Applied Physics Letters*, *102*(19), 191112

.....౸ఇ.....

Chapter **2**

EXPERIMENTAL METHODS

The details of materials used, experimental methods and the basic theory behind the experiments are discussed in this chapter.

2.1   Materials

2.1.1 Poly(vinyl alcohol)

Poly(vinyl alcohol) (PVA) was purchased from SD Fine Chemicals, India. The weight average molecular weight was 1,25,000 with degree of hydrolysis about 89%. The polymer was used as received.

2.1.2 Thermoplastic polyurethane

Thermoplastic polyurethane (TPU) used in this study was purchased from Bayer Material Science, India. This is a polyester based TPU (Desmopan 385S) specially meant for flexible engineering parts. The major properties as reported by the supplier are given in Table 2.1.

Development of Reduced Graphene Oxide/Polymer Nanocomposites for Optical Limiting, Optical Actuation and Electrical Applications

61

Table 2.1: Properties of TPU (Desmopan 385S)

No.	Property	Test condition	Test Standard	Value
1	Density	-	ISO 1183	1200 kg/m^3
2	Ultimate tensile strength	200 mm/min	i.A. ISO 527-1, -3	45 MPa
3	Elongation at break	200 mm/min	i.A. ISO 527-1, -3	550 %
4	Compression set	24h, 70 ^{o}C	ISO 815	48 %
5	Abrasion resistance	-	ISO 4649	23 mm^3
6	Impact resilience	-	ISO 4662	59 %
7	Melt temperature	-	-	160 – 200 ^{o}C

2.1.3 Reduced graphene oxide

Reduced graphene oxide (RGO) was synthesized in this work and the details are given in Chapter 3.

2.1.4 Other Chemicals

Graphite was obtained from Hind Minerals, India. Sulphuric acid (H_2SO_4, 98% GR), ortho phosphoric acid (H_3PO_4, 85% pure), potassium permanganate ($KMnO_4$, 99% GR), hydrogen peroxide (H_2O_2, 30% GR), N, N-Dimethyl formamide (DMF, GR) and hydrazine monohydrate were purchased from Merck, India. All the chemicals were used as received.

2.2   Experimental methods

2.2.1 Sample Preparation

Reduced graphene oxide (RGO) was synthesized from natural graphite flakes through graphene oxide (GO) intermediate. GO was synthesized through the chemical oxidation of graphite and the chemical or thermal reduction of GO yielded RGO. The synthesis of RGO is described

in Chapter 3. The RGO/polymer nanocomposites were prepared by a simple solvent blending and casting method. The details of nanocomposite preparation are given in Chapter 4.

2.2.2 Characterization techniques

2.2.2.1 X-ray Diffraction (XRD) analysis

XRD analysis is used to understand the crystalline nature of the material. When X-ray hits a crystalline phase, the atoms in the crystal scatter the incident rays. If the scattered rays from two adjacent planes have path difference which is equal to integer multiple of 2π, constructive interference takes place. The resultant intensity of diffracted waves in the angle of diffraction gives the XRD pattern. The Bragg's law is given by **$n\lambda = 2d \sin\theta$** where λ is the wavelength of the incident radiation, n is an integer, θ is the diffraction angle and d is the spacing of atomic planes of the crystal as described in figure 2.1. Diffraction can occur whenever the Bragg's law is satisfied [1]. For the XRD analysis we can either change the λ with a fixed θ or keep the λ constant and vary θ by rotating the sample.
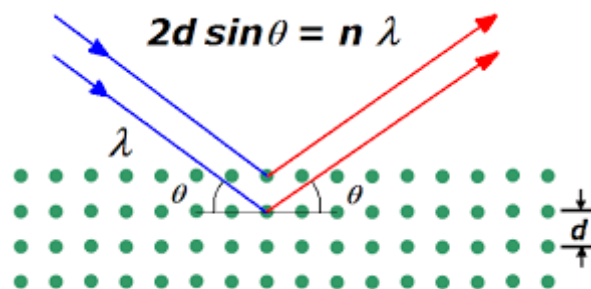

Figure 2.1: The Bragg's law of X-ray diffraction

Generally, in XRD instruments, a monochromatic X-ray beam with known λ is used. The sample will be kept stationary and the X-ray will be allowed to fall on the sample from different angles by rotating the X-ray source. The diffracted rays are captured using a detector. When the source moves θ, the detector moves 2θ to collect the diffracted rays. The XRD pattern is given with 2θ in the X-axis and intensity counts in the Y-axis. From the XRD pattern we can understand whether the material is crystalline or not. For amorphous materials, XRD cannot provide any characteristic peak.

In this work, XRD analysis of the samples were carried out using Ni filtered Cu Kα radiation ($\lambda = 0.154$ nm) using Bruker X-Ray diffractometer (Model D5005, Germany) at 40 kV and 30 mA. The samples were scanned in step mode with 2°min^{-1} scan rate.

2.2.2.2 Fourier Transform Infrared (FTIR) Spectroscopy

In spectroscopy, the spectral range in the infrared region, particularly in the frequency of 200 to 4000 cm^{-1} is of great importance in understanding the chemical structure of materials. The wavelengths corresponding to the energy required for the twisting, bending and vibrational motions of molecules fall under this region. When a material interacts with the infrared radiation, portions of the incident radiation are absorbed at particular wavelengths [2]. The multiplicity of vibrations occurring simultaneously produces a highly complex absorption spectrum which is uniquely characteristic of the functional groups comprising the molecule and of the overall configuration of the atoms.

In this work, the FTIR spectroscopic studies of the samples were carried out using a standard spectrophotometer (Avatar 370, Thermo Nicolet, Germany). For powder samples, KBr pellet method was used in which the powder was diluted with KBr and made in to pellets for measurements. Polymer film samples were measured in the ATR (Attenuated Total Reflection) mode. The measurements were generally made in the range 400 to 4000 cm^{-1}. A minimum of 60 scans were acquired with a resolution of 4 cm^{-1}. Back ground spectrum was captured before measurements and base line corrections were made using software.

2.2.2.3 Microscopic studies

The microscopic studies are generally used to understand the morphology of the materials. Microscopy using electron beams can produce images with significantly high resolution than light based microscopes due to the smaller de Broglie wave length of electrons. Electron microscopy is mainly employed to understand the microstructure of materials. The two types of electron microscopies generally used to study the morphology are Scanning Electron Microscopy (SEM) and Transmission Electron Microscopy (TEM).

In SEM, a focused beam of electrons is used to make the image of a sample by scanning the surface in a raster scan pattern. The electrons interact with the atoms on the sample surface producing signals which are combined with the beam's position to form the image. Various types of signals can be produced through the interaction of electron with atoms in the sample at various depths such as secondary electrons, reflected or back scattered electron, etc. Generally, the detection of secondary electrons

emitted by atoms excited by the electron beam is used to make the image [3]. SEM can achieve a resolution of better than 1 nm.

In TEM, the image is formed by the transmission of a beam of electrons through the sample. For TEM analysis, we have to use an ultra thin layer of sample (thickness in the order of 100 nm) or a suspension of particles on a grid. TEM can give better magnification and high resolution.

In this study, the SEM images of the samples were acquired using Hitachi SU 6600 field emission scanning electron microscope. The SEM images of the fractured surfaces of composite samples were taken by fracturing in liquid nitrogen.

The high resolution TEM images were taken using a transmission electron microscope (JEM 2100, JEOL, Japan). For RGO samples, the samples were dispersed in DMF and prepared on a carbon coated copper grid.

Energy dispersive spectroscopy (EDS) was used to understand the elemental compositions in the sample and Selected Area Electron Diffraction (SAED) was used to understand the crystallinity of RGO samples.

Another method used in this study to understand the topography of the composite films was Atomic Force Microscopy (AFM). In AFM, the equipment has a cantilever with a sharp tip on it as the probe. The reaction of the probe to the forces imposed by the sample is used for creating the image. There are mainly three modes of imaging: the contact mode, in which the probe comes in contact with the surface, the tapping mode in

which the image is created based on the intermittent contact of the probe tip on the surface and the non contact mode. In the non contact mode, the probe tip oscillates in its resonance frequency about a few nano meters above the surface. The van der Waals forces or any other long range forces on the surface which are strong typically about 1 to 10 nm above the surface affects the resonance frequency of the probe from which the topography can be created as an image. In this study, AFM images of the surface of the composites were taken using Park XE 100, in non contact mode.

2.2.2.4 Thermal analysis

Thermogravimetric analysis (TGA) is a method used to measure the changes in weight associated with thermal events [4]. The change in weight as a function of temperature can provide many valuable information about the material. By monitoring the weight change while heating with a controlled temperature program, one can understand various degradation temperatures and the thermal stability of the material. The differential thermal analysis (DTA) which is the derivative of the weight change with temperature can provide an easy understanding of the degradation temperatures of the material. In this work, TGA/DTA of the samples were carried out using TG/DSC analyzer (SDT Q600, TA Instruments, USA) at a heating rate of $10 \circ C$ min^{-1} under air or nitrogen atmosphere.

Differential Scanning Calorimetry (DSC) is another method used to understand the thermal behavior of a material as a function of temperature. During controlled heating/cooling, the materials undergo physical or chemical changes and they absorb (endothermic) or give out (exothermic)

heat energy with reference to a reference sample which can be measured as heat flow. The endothermic or exothermic heat flow at particular temperatures will be characteristic of various thermal transitions like phase changes, crystallisation, melting, glass transition, etc. DSC can be used to understand these thermal transitions and even crystallinity (χ_c) of the samples can be calculated from the heat flow data using the equation 2.1

$$\chi_c = \frac{\Delta H_m}{\Delta H_0}$$ ....(2.1)

where ΔH_m is the measured melting enthalpy and ΔH_0 is the enthalpy of pure crystal. In this study, the DSC analysis of the composite samples was carried out using an instrument of Mettler Toledo (DSC 822e, Hong Kong) with a heating rate of 10 ^{o}C min^{-1} in the range of -100 ^{o}C to 300 ^{o}C under nitrogen atmosphere.

2.2.2.5 UV-visible spectroscopy

UV-visible spectroscopy is a common characterization technique used to understand the transparency of the material in the UV and visible region. However, they can provide more information in the molecular level also which makes them an excellent tool for material characterization. The π-electrons or non-bonding electrons (n-electrons) in the molecules can absorb the energy in the form of ultraviolet or visible light and excite these electrons to higher energy levels. The more easy electronic transitions can occur by absorbing longer wavelengths. According to the energy required, the various electronic transitions can be arranged in the order of σ-σ*>n-σ*>π-π*>n-π*.

The UV-visible spectra of the samples in this study were recorded using a UV-visible spectrophotometer (JascoV-570, USA) in the 200-2000 nm wavelength region.

2.2.2.6 Mechanical properties

The mechanical properties of the polymer composites were measured using a universal testing machine (UTM, Autograph, Shimadzu, Japan). For RGO/PVA composite film samples, the testing was carried out as per ASDM D882 standard which describes the test method for determining the tensile properties of thin plastic sheeting (< 1mm thick) [5]. Strips of 5 mm width were cut from the sheet and subjected to tensile testing in the UTM with 10 kN force head with a displacement rate of 50 mm/min. For RGO/TPU composites, the specimens were cut in dumbbell shape as per ISO 37 (type 4) standard [6]. The samples were subjected to uniaxial tension at a displacement rate of 200 mm/min. All the measurements were recorded at room temperature. At least five specimens were tested from each sample.

2.2.2.7 Surface area measurements

The surface area of the RGO samples were measured by Brunauer–Emmett–Teller (BET) method using a surface area analyser (Quantachrome, USA). In BET method, the physical adsorption of gas molecules on solid surface is used to calculate the surface area.

According to BET theory, gas molecules adsorb to solid surface in layers infinitely [7]. There is no interaction between these layers and hence Langmuir theory can be applied to each layer. Hence the BET equation for monolayer adsorption is given by

$$\frac{1}{v[(p_0/p)-1]} = \frac{c-1}{v_m c}\left(\frac{p}{p_0}\right) + \frac{1}{v_m c}$$

where, p and p_0 are the equilibrium and the saturation pressure of adsorbates at the temperature of adsorption, v is the adsorbed gas quantity (for example, in volume units), and v_m is the monolayer adsorbed gas quantity. c is the BET constant, which is given by $c = \exp[(E_1-E_L)/RT]$ where E_1 is the heat of adsorption of first layer and E_L is the heat of liquefaction.

For surface area measurements, a gas, normally nitrogen, is allowed adsorb on the solid surface at liquid nitrogen temperature. A plot of p/p_0 in the X-axis and $1/v[(p/p_0)-1]$ in the Y- axis gives the BET plot. A linear relationship is maintained for this plot for monolayer adsorption. The slope of the curve A and the y-intercept I is used to calculate the monolayer adsorption gas volume v_m and BET constant c. From these values, the total surface area S_{total} can be calculated using the equation $S_{total} = (v_m NS)/V$ and specific surface area S_{BET} by $S_{BET} = S_{total}/a$ where, N is Avogadro number, S is the adsorption cross section of gas molecule, V is the molar volume of adsorbed gas and a is the mass of solid sample.

The properties of the pores in the solid material can be understood from the adsorption-desorption isotherm. By looking at the shape of the adsorption-desorption isotherm and the hysteresis pattern, we can have a general idea about the type of porous nature by comparison with standard patterns.

2.2.3 Nonlinear optical absorption and optical limiting studies
2.2.3.1 Non-linear optical properties

Non linear optical (NLO) materials have found wide spread applications in opto-electronic devices. The NLO properties of nano materials have been of great interest for the scientific community due to the fact that nano materials exhibit huge NLO behaviour compared to their bulk counter parts [8]. However, NLO behaviour of most of the nanoparticles was studied as dispersions in liquid medium. There has been an increasing demand for developing high performance NLO materials which can comply with specifications required for device fabrication. From a device perspective, in addition to good NLO properties, an ideal NLO material should possess good processability, flexibility in design, ease of fabrication, optical transparency, good environmental stability, nontoxicity and high mechanical and thermal stability [9].

When an intense light such as laser light comes into interaction with a material, the electric field of the intense light can modify the charge distributions in the material and polarize it. In an NLO material, the dielectric polarisation (P) of the material responds nonlinearly to the electric field (E) of light. For an instantaneous process in which the energy and momentum are conserved in the optical field, the polarisation density or the dipole moment per unit volume, P(t), at time t can be represented in terms of electric field E(t) as equation 2.2 (P(t) and E(t) are considered as scalar for simplicity).

$$P(t) = \varepsilon_0 (\chi^{(1)} E(t) + \chi^{(2)} E^2(t) + \chi^{(3)} E^3(t) + ...) \quad ....(2.2)$$

where $\chi^{(n)}$ represents the nth order susceptibility of the medium and presence of that term represents n^{th} order nonlinearity in that medium.

Materials with high third order nonlinearity have attracted much attention of the researches since they can find many potential applications in optical switching, optical limiting, optical data storage, etc. The NLO properties can be nonlinear optical absorption, nonlinear optical refraction, nonlinear optical scattering, etc. In the present work, nonlinear optical absorption of the developed RGO/polymer composites is studied. Hence it will be useful to look into various nonlinear absorption processes in detail.

2.2.3.2 Nonlinear absorption

In nonlinear absorption (NLA), change in absorption of a material behaves nonlinearly to the increasing intensity of light. At higher intensities, there is a possibility of absorbing more than one photon before relaxing to the ground state. The NLA behaviour can be of two types depending on the change in absorption as a function of input fluence. The first type of NLA is due to the Reverse Saturable Absorption (RSA) in which the absorption of the material increases with increasing laser intensity. In the second type, the absorption decreases with increasing light intensity which is due to Saturable Absorption (SA). When the excited state absorption is lower than the ground state absorption, SA is observed which increases the transmission through the material when intensity of light is increased. If the excited state absorption is higher than the ground state absorption, RSA is observed which decreases the transmission through the material once light intensity is increased. Generally, RSA may be due to excited state absorption (ESA) or two photon absorption (TPA) process.

2.2.3.2.1 Two photon absorption (TPA)

The TPA process involves the transition of electrons from ground state to an excited state by the simultaneous absorption of two photons from the incident radiation field. Figure 2.2 shows the schematic representation of the TPA process. The intermediate state is not real and two identical photons have to be absorbed simultaneously for the TPA process. Hence the TPA process is sensitive to instantaneous optical intensity.
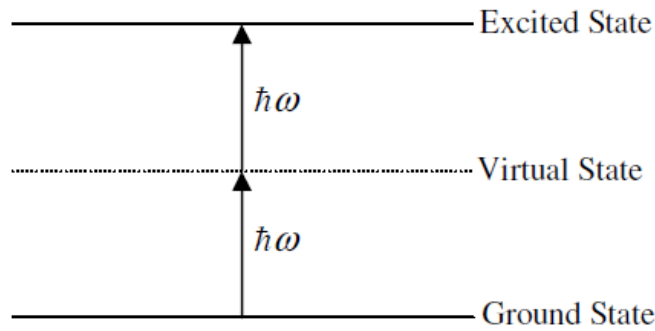
Figure 2.2: Schematic of TPA process

In a TPA process, the nonlinear absorption is directly proportional to the square of intensity of the incident radiation (I) and is given by equation 2.3 [10].

$$\frac{dI}{dz} = -\alpha I - \beta I^2 \qquad \dots\dots\dots\dots\dots\dots\dots\dots(2.3)$$

where α is the linear absorption coefficient and β is the TPA coefficient [10].

2.2.3.2.2 Multiphoton absorption

There can also be a process in which multiple photons are absorbed simultaneously. If (n+1) photons are absorbed simultaneously from a single beam, then the process can be represented by the equation 2.4 [10].

$$\frac{dI}{dz} = -(\alpha + \gamma^{(n+1)} I^n) I \quad \text{...}(2.4)$$

where $\gamma^{(n+1)}$ is the (n+1) photon absorption coefficient [10].

2.2.3.2.3 Excited state absorption (ESA)

In poly atomic molecules and semiconductors, there is always high density of states near the excited state. The excited electrons undergo rapid transitions into one of these states before coming back to ground state. Hence, before relaxation back to ground state, it undergoes further absorption and get promoted to a higher lying state. This process is generally termed as ESA [10].

2.2.3.3 Optical limiting

Optical limiters are material or devices which are transparent to light at low intensities and become opaque at higher intensities. Optical limiters can find applications in optical pulse compression, pulse shaping and protection of eyes and sensitive optical devices from powerful lasers. The intensity at which the optical limiter changes from transparent to opaque is generally called as the threshold intensity and a low threshold intensity is always preferred for practical applications. For an ideal optical limiter, the transmission is linear up to the threshold input intensity (I_{th}) and beyond the I_{th} the transmittance remains constant as shown in figure 2.3. The

most common process causing optical limiting is RSA due to ESA or TPA. Other processes such as free carrier absorption, nonlinear refraction, photo-refraction and induced scattering can also contribute to optical limiting [10].
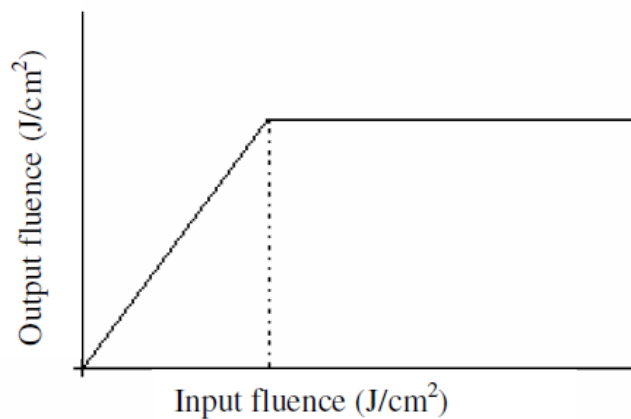
Figure 2.3: Behaviour of an ideal optical limiter

For a material to act as a promising optical limiter, it should have high linear transmittance in the required band width, low limiting threshold and excellent stability. The optical limiting threshold is mainly dependent on the nonlinear absorption coefficient of the material.

2.2.3.4 z-scan technique

Bahae et al. introduced a method in 1989, to determine the third order nonlinear coefficients of a material using a single beam technique which is generally known as z-scan technique [11, 12]. The technique can be used to measure both the sign and magnitude of the nonlinear absorption and nonlinear refraction. Spatial beam distortion is the major principle behind this technique. Compared to interferometric methods, it offers

simplicity and high sensitivity. When a high intensity laser beam propagates through a nonlinear material, due to the variations in photoinduced refractive index, the self focusing or defocusing of the beam occurs. This can be measured using z-scan technique which enables to determine the third order nonlinear properties of the material. Figure 2.4 represents the schematic of the experimental setup for the z-scan technique.
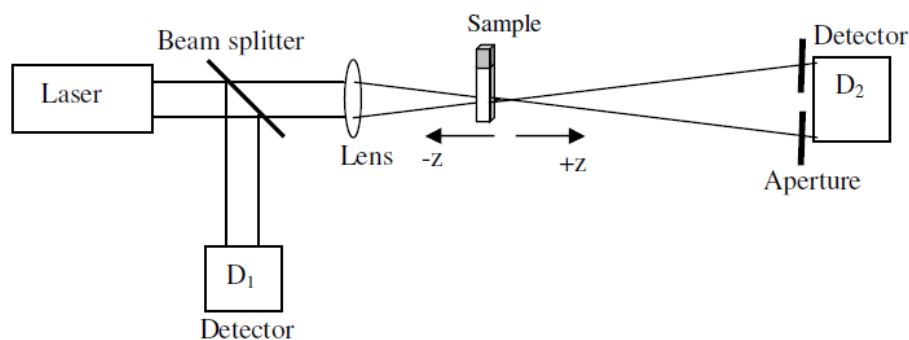
Figure 2.4: Schematic experimental setup for of z-scan technique

In the single beam configuration, the sample is moved along the propagation direction of a focused Gaussian beam and the transmittance is measured. While passing through the nonlinear medium, the laser beam will experience variations in both amplitude and phase. If the transmitted light is measured through an aperture kept before the detector as shown in figure 2.4, the technique is called closed aperture z-scan and if the transmitted light is measured without an aperture, it is called open aperture z-scan. In closed aperture z-scan, the phase distortion of the transmitted beam is converted into corresponding amplitude variation. This technique is sensitive to both nonlinear absorption and nonlinear refraction. In the case of open aperture z-scan, the throughput is sensitive only to the

nonlinear absorption. Closed aperture and open aperture z-scans give the real part and imaginary part of the third order nonlinear susceptibility ($\chi^{(3)}$) respectively [12].

The sample thickness in z-scan technique is assumed to be much less than Rayleigh's range z_0 (diffraction length of the beam) which is given by $z_0 = k\omega_0^2/2$ where k is the wave vector, ω_0 is the beam waist radius and is represented by $\omega_0 = f\lambda/D$. Here, f is the focal length of the lens, λ is the wavelength of the laser beam and D is the beam radius at the lens.

Open aperture z-scan method is generally used to measure the nonlinear absorption characteristics. The presence of nonlinear absorption like ESA or TPA can result in a transmission minimum at the focal point whereas a transmission maximum can be observed at the focal point if it is a saturable absorber. In an open aperture z-scan method, the transmitted light is sensitive only to the intensity variations. The intensity dependent nonlinear absorption coefficient $\alpha(I)$ can be expressed as a function of linear absorption coefficient α and TPA coefficient β by the equation 2.5 [12].

$$\alpha(I) = \alpha + \beta I \quad \text{...(2.5)}$$

The irradiance distribution is given by the equation 2.6

$$I_r(z,r,t) = \frac{I(z,r,t)e^{\alpha l}}{1 + q(z,r,t)} \quad \text{..(2.6)}$$

where $q(z,r,t) = \beta I(z,r,t)L_{eff}$ ....(2.6a)

L_{eff} is the effective length which is equal to $(1-e^{-\alpha l})/\alpha$ where l is the sample length.

By integrating equation 2.6 over r and t, we can get the total transmitted power as in equation 2.7

$$P(z,t) = P_I(t)e^{-\alpha l}\frac{\ln[1+q_o(z,t)]}{q_o(z,t)} \quad\text{..(2.7)}$$

where

$$P_I(t) = \frac{\pi\omega_0^2 I_0(t)}{2} \quad\text{..(2.8)}$$

and

$$q_o(z,t) = \frac{\beta I_0(t)L_{eff}\, z_0^2}{z_2 + z_0^2} \quad\text{..(2.9)}$$

For a Gaussian pulse, the integration of equation 2.7 gives the transmission as

$$T(z) = \frac{1}{q_o\sqrt{\pi}}\int_{-\infty}^{\infty}\ln(1+q_o e^{-t^2})dt \quad\text{......................................(2.10)}$$

If $|q_o| < 1$, equation 2.10 can be written as

$$T(z, S=1) = \sum_{m=0}^{\infty}\frac{[-q_o(z,0)]^m}{(m+1)^{3/2}} \quad\text{..(2.11)}$$

where m is an integer. The parameter q_0 can be obtained by fitting the equation 2.10 to the z-scan curve. Then the nonlinear absorption coefficient β can be deduced from the equation 2.6a.

The imaginary part of third order susceptibility $Im(\chi^{(3)})$ which determines the strength of nonlinear absorption is given by the equation 2.12 [12].

$$Im(\chi^{(3)}) = \frac{n_0^2 c^2 \beta}{240\pi^2 \omega} \quad (esu) \quad \text{.....................................} (2.12)$$

where n_0 is the linear refractive index, and c is the velocity of light in vacuum.

In this work, the open aperture z-scan technique was used to measure the nonlinear absorption. A *Q*-switched neodymium doped yttrium aluminum garnet laser (Spectra Physics LAB-1760) was used as the light source to generate 7ns pulses at 532 nm with a pulse repetition rate of 10Hz. The sample was moved in the direction of light incidence near the focal spot of the lens with a focal length of 200 mm. The transmitted beam energy and reference beam energy were measured simultaneously and their ratio was taken by an energy ratiometer (Rj7620, Laser Probe Corp.) having two identical pyroelectric detector heads (Rjp735, Laser Probe Corp.). Transmitted power is divided by the power obtained at the reference detector in order to eliminate the effect of fluctuations of laser power. The obtained data was analyzed as described by Bahae et al. [12]. The optical limiting property was measured in terms of non linear transmittance as a function of input fluence derived from z-scan data.

2.2.4 Optical actuation studies

The optical or photomechanical actuation properties of the composites were studied using an invitro muscle test system (1205A, 5.0 N, Aurora Scientific Inc., Canada) which consists of a dual mode system with lever arm (model 305 C) and 805A invitro test apparatus. The total system is

schematically shown in figure 2.5. An infrared (IR) lamp (Beurer GmbH, Germany) with red filter was used as the light source. Strips having a length of 20 mm and a width of 5 mm were cut from the nanocomposite films of thickness 0.05 to 0.1 mm. The actuation measurement was carried out at room temperature. The tips of the samples were placed between the grips of *in vitro* Muscle test system. Out of the two grips of the system one is stationary and the other is connected to a lever which can move. During photomechanical strain measurement, when IR light is irradiated, the free moving grip connected to the lever can move up or down depending on the expansion or contraction of the sample thereby measuring the displacement. The schematic of the photomechanical strain measurement is given in figure 2.6. During photomechanical stress measurement, the opposite force required to keep the moving grip at initial position is measured as the force generated. The stress and strain of the samples were measured at various pre-strains. For all measurements, the power density of the light source was kept constant at 16 mWcm^{-2}.
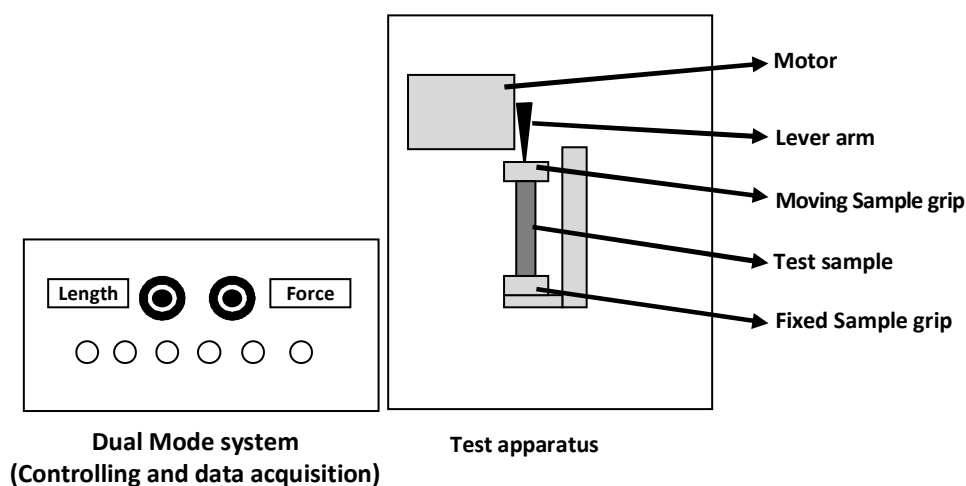
Figure 2.5: Schematic of the photomechanical measurement system
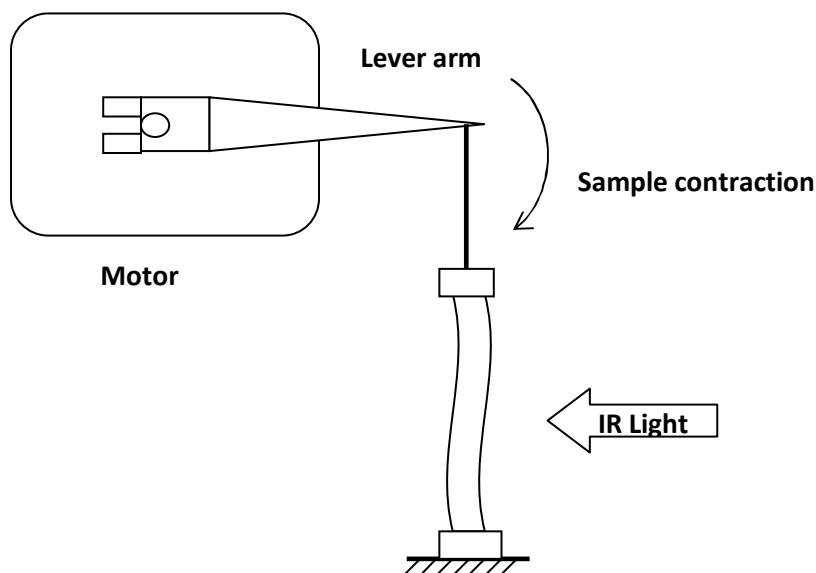
Figure 2.6: Schematic of the length change measurement on IR light illumination

2.2.5 Studies on the electrical properties

For the electrical measurements, the samples were prepared in the form of a parallel plate capacitor by applying silver conductive paste on both sides of the polymer film. The dc electrical measurements were taken using a two probe method in a Keithley 2400 source meter. The electrical properties in the frequency range 100 Hz to 1 MHz were measured using a precision impedance analyser (Agilent 4294A).

For obtaining the dc conductivity of the composites, the resistance of the sample was measured and the resistivity (ρ) was calculated by the equation, $\rho = RA/d$, where R is the resistance, A is the area and d is the thickness of the sample. The inverse of resistivity was taken as dc conductivity.

Development of Reduced Graphene Oxide/Polymer Nanocomposites for Optical Limiting, Optical Actuation and Electrical Applications

81

The dielectric properties in various frequencies were measured using the precision impedance analyser. The capacitance C of a dielectric is given by $C = (\varepsilon_0\varepsilon_r A)/d$ where ε_0 is the permittivity of free space, ε_r is the relative permittivity of the material, A is the cross sectional area and d is the thickness of the sample. From the measurement of capacitance, dielectric constant can be calculated.

AC conductivity of the sample can be calculated by the equation $\sigma_{ac} = \varepsilon_0\varepsilon\omega\tan\delta$, where ω is the angular frequency which is equal to $2\pi f$ where f is the frequency and $\tan\delta$ is the dissipation factor [13].

References

[1]   Waseda, Y., Matsubara, E., & Shinoda, K. (2011). *X-ray diffraction crystallography: introduction, examples and solved problems*. Springer Science & Business Media.

[2]   Banwell, C. N., & McCash, E. M. (1994) Fundamentals of molecular spectroscopy, McGraw-Hill.

[3]   Goodhew, P. J., Humphreys, J., & Beanland, R. (2000). *Electron microscopy and analysis*. CRC Press.

[4]   Gabbott, P. (Ed.). (2008). *Principles and applications of thermal analysis*. John Wiley & Sons.

[5]   ASTM, D. 882. (2002). *Standard test methods for tensile, properties of thin plastic sheeting*.

[6]   ISO 37 (2005) *Rubber, vulcanized or thermoplastic — Determination of tensile stress-strain properties*

[7]   Brunauer, S., Emmett, P. H., & Teller, E. (1938). Adsorption of gases in multimolecular layers. *Journal of the American chemical society*, *60*(2), 309-319.

[8]   Hari Singh Nalwa and Seizo Miyata (1997) *Nonlinear optics of organic molecules and polymers*, CRC press

[9]   Zhang, Y., Etxebarria, J. (2012) Ferroelectric Liquid Crystals for Nonlinear Optical Applications, in *Liquid Crystals Beyond Displays: Chemistry, Physics, and Applications* (ed Q. Li), John Wiley & Sons, Inc., Hoboken, NJ, USA.

[10]   Richard L Sutherland (2003) *Handbook of nonlinear optics,* CRC press.

[11]   Sheik-Bahae, M., Said, A. A., & Van Stryland, E. W. (1989). High-sensitivity, single-beam n 2 measurements. *Optics letters*, *14*(17), 955-957.

[12]   Sheik-Bahae, M., Said, A. A., Wei, T. H., Hagan, D. J., & Van Stryland, E. W. (1990). Sensitive measurement of optical nonlinearities using a single beam. *IEEE journal of quantum electronics*, *26*(4), 760-769.

[13]   Seema, A., Dayas, K. R., & Varghese, J. M. (2007). PVDF-PZT-5H composites prepared by hot press and tape casting techniques. *Journal of applied polymer science*, *106*(1), 146-151.

.....ॐ.....

Chapter **3**

SYNTHESIS AND CHARACTERIZATION OF GRAPHENE OXIDE AND REDUCED GRAPHENE OXIDE

3.1   Introduction

Since the ground breaking experiments on graphene by Geim and Novoselov in 2004, there was phenomenal growth in research for finding scalable and cost effective production methods for graphene. Even though processes like mechanical exfoliation, epitaxial growth and chemical vapour deposition can produce good quality graphene, they suffer from either lower scalability or higher cost. In this context, chemical synthesis methods have attracted enormous interest of researchers due to the simplicity of the process, scalability to industrial production and cost effectiveness. The synthesis of graphene through the graphene oxide route is the most widely used method in chemical synthesis of graphene [1]. In this method, graphite is converted in to graphite oxide which is an oxidized form of graphite with several stacked layers of graphene decorated with oxygen containing functional groups like hydroxy (–OH), epoxy (C_2O) and

carboxylic acid (–COOH) groups. This graphite oxide is completely exfoliated in a liquid medium to graphene oxide (GO) which is a single layer of graphene with oxygen containing functional groups attached to it. Due to the incorporation of functional groups to the graphene layers in GO, the two dimensional (2D) crystal lattice become highly defective and this makes GO entirely different in properties from pristine graphene; for instance, GO is an electrical insulator where as graphene is a highly conducting material. The second step of chemical production of graphene is the reduction of GO into graphene. The reduction of GO can be done through thermal or chemical reduction methods [2]. Thermal or chemical reduction results in removal of most of the oxygen containing groups yielding a graphene-like material, generally referred to as reduced graphene oxide (RGO). Even though RGO has extremely close resemblance to graphene in its properties, there can be still some oxygen residues and Stone-Wales defects (formation of five membered and seven membered rings) [3]. Hence for high quality electronic grade graphene for charge transport experiments, RGO is less preferred over graphene prepared from other methods like mechanical exfoliation [4]. However, RGO obtained from GO is considered as good as pristine graphene for many other practical applications including graphene/polymer composites. Moreover, RGO extends a more versatile possibility to fine tune its properties by controlling the extent of reduction. For polymer composite applications, the residual functional groups and defects make RGO more easily dispersible in polymer matrix. Taking these facts in to consideration, we have synthesized RGO for polymer composites by both chemical reduction and thermal reduction of GO.

3.1.1 Graphene oxide (GO)

Graphite oxide or graphitic acid is well known since its first preparation by Brodie in 1859 [5]. In his method, the repeated treatment of graphite with an oxidizing system consisting of potassium chlorate and fuming nitric acid resulted in a composition which consisted of carbon, oxygen and hydrogen which was dispersible in pure or basic water and hence he termed it as "graphic acid". Even though Brodie's intention was to study the structure of graphite, since this seminal discovery, various procedures were formulated by many researchers for the preparation of graphite oxide, most of them based on oxidizing mixtures containing one or more concentrated acids and oxidizing materials. Inspired from the Brodie's method, Staudenmaier in 1898 [6] and Hummers in 1958 [7] developed separate methodologies and got wide acceptance in the scientific community. After Hummers' method, many modifications were made to the synthesis routes to increase the yield and improve the oxidizing abilities. Some of these important methods for the preparation of graphite oxide are described briefly in the following section.

3.1.2 Different methods of graphite oxide synthesis

3.1.2.1 Brodie's method

In 1859, while exploring the structure of graphite by investigating the reactivity of flake graphite, a British chemist Benjamin Brodie found that by the addition of potassium chlorate ($KClO_3$) to a slurry of graphite in fuming nitric acid (HNO_3) a new material was obtained with an increase in overall mass of graphite. The resulting material was determined to be composed of carbon, hydrogen, and oxygen. He found that successive

reaction steps further increased the oxygen content reaching a limit after four oxidation reactions. He also noticed that the material was dispersible in pure or basic water but not in acid media. This observation prompted him to term this new material as "graphic acid". Later this became one of the first methods used for the synthesis of graphite oxide [5].

3.1.2.2 Staudenmaier's method

Almost after 40 years from Brodie's synthesis, in 1898, L. Staudenmaier improved Brodie's formulation by adding sulphuric acid (H_2SO_4) also in the system in order to increase the acidity of the medium [6]. Moreover, potassium chlorate ($KClO_3$) was added in multiple aliquots over the course of reaction to the slurry of graphite in fuming nitric acid (HNO_3)/ sulphuric acid (H_2SO_4) mixture. This small change of addition of potassium chlorate in multiple fractions rather than in a single addition as in Brodie's method resulted in same extent of oxidation in a single step compared to the multiple oxidation approach in Brodie's method.

3.1.2.3 Hummer's method and various modifications.

In both Brodie's method and Staudenmaier method, the use of potassium chlorate, which is highly explosive in nature, always raised a constant safety issue. Moreover, the process was very much time consuming and hazardous. This tempted Hummers and Offeman in 1958 to develop a totally different method. In Hummers' method, graphite was reacted with a mixture of potassium permanganate ($KMnO_4$), sodium nitrate ($NaNO_3$) and concentrated sulphuric acid (H_2SO_4) [7]. The level of oxidation achieved was similar to the levels of oxidation that obtained for other methods and the reaction could complete in lesser time. The

Hummers' method was also modified by increasing the amount of KMnO$_4$ in the reaction mixture to improve the oxidation.

In Hummers' method, it was later realized that, the complete oxidation of all the graphitic layers does not take place. In 1999, Kovtyukhova proposed a pre-expansion process for graphite to facilitate more oxidation [8]. He has pre treated graphite with a mixture of concentrated H$_2$SO$_4$, K$_2$S$_2$O$_8$ and P$_2$O$_5$ at 80 °C for several hours. After pre-expansion, it was subjected to oxidation by Hummers' method.

In 2010, Marcano et al., proposed an improved synthesis method in which, they modified the Hummers' method by eliminating NaNO$_3$ in the reaction mixture [9]. The amount of KMnO$_4$ was doubled and phosphoric acid (H$_3$PO$_4$) was added as a second acid in addition to H$_2$SO$_4$. The elimination of NaNO$_3$ helped to avoid hazards caused by toxic gases like NO$_2$ or N$_2$O$_4$. Moreover, this could also improve the degree of oxidation to a great extent with very high yield.

3.1.3 General reaction mechanism and structure of GO

Despite the ever increasing interest and a history of more than 150 years, the mechanism of graphene oxide formation still remains unclear. There has been a lot of efforts to understand the mechanism and structure of GO [10]. From our understanding of different chemical oxidation procedures for graphite, it is obvious that there are mainly two systems, (i) the potassium chlorate/nitric acid system and (ii) the potassium permanganate/sulfuric acid and optionally phosphoric acid system. Due to the high toxicity and explosive nature of the reaction system consisting of

potassium chlorate and nitric acid, the second system with potassium permanganate and sulfuric acid is preferred over the first one and is widely used.
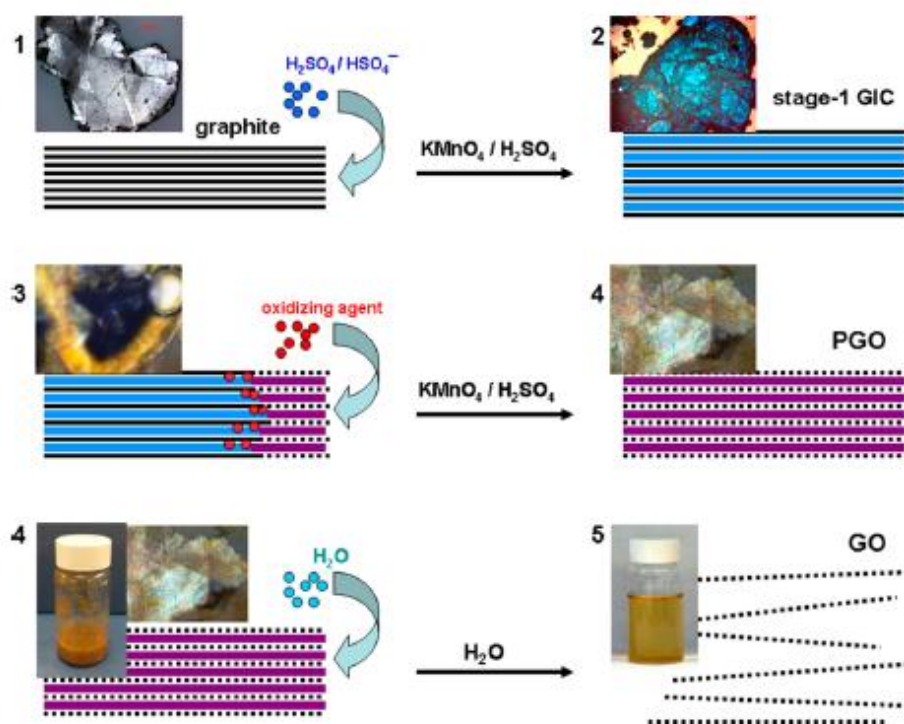
According to a recent study by Dimiev and Tour [11], the basic mechanism of oxidation of graphite can be divided into three steps. In the first step, graphite is converted into a graphite intercalation compound (GIC). In this step, H_2SO_4 creeps into the interlayer spacing of graphite layers and forms H_2SO_4-graphite intercalation compound. This is a relatively fast step and forms within 3 to 5 minutes of mixing of graphite with the acid. In the second step, the oxidation of graphite occurs to form pristine graphite oxide (PGO). This step involves the diffusion of oxidizing agents in to the preoccupied graphite galleries. This step is rather slow and is the rate determining step. It can take several hours to days depending upon the graphite source. The identity of the specific oxidizing species in $KMnO_4/H_2SO_4$ system is not yet exactly known. Manganese hepta oxide (Mn_2O_7) has been suggested as the major oxidizing agent in this system by many researchers. The suggested reaction for the formation of Mn_2O_7 is given in equation (3.1) [12].

$$KMnO_4 + 3H_2SO_4 \rightarrow K^+ + MnO_3^+ + H_3O^+ + 3HSO_4^-$$
$$MnO_3^+ + MnO_4^- \rightarrow Mn_2O_7$$
......(3.1)
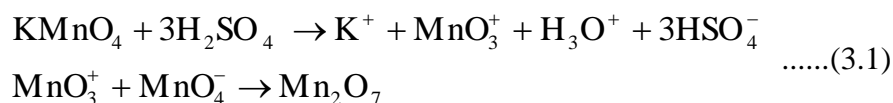
However, according to Dimiev and Tour, the Mn(VII) in H_2SO_4 is more likely to exist as planar permanganyl (MnO_3^+) cation which is closely associated with hydrogen sulphate (HSO_4^-) and sulphate ions (SO_4^{2-}). In highly concentrated acid, they remain in unionized form as MnO_3HSO_4, or

$(MnO_3)_2SO_4$ but on dilution ionization takes place [11]. Since the interlayer spacing of graphite is occupied by H_2SO_4 molecules and HSO_4^- during the first intercalation step, to diffuse between the graphene layers, oxidising agents need to replace the existing intercalants or need to get inserted between them. This makes the step more time consuming. As soon as the oxidizing agent diffuses between the graphene layers, they react with the carbon atoms. However the reaction mechanisms are not yet clear. In the final step, the PGO reacts with water under going reactions like hydrolysis of covalent sulfates and forming conventional GO with the loss of all inter layer registry. The general scheme of reaction is given in Figure 3.1.

Figure 3.1: General scheme of reaction to form GO from graphite [11]

Development of Reduced Graphene Oxide/Polymer Nanocomposites for Optical Limiting, Optical Actuation and Electrical Applications

91

The use of phosphoric acid as the second acid can help to control the post oxidation reaction. The formation of five membered phosphor rings helps to prevent further oxidation of diols and helps to keep intact the six membered carbon rings on the basal plane. Figure 3.2 explains a possible mechanism for the advantage of the addition of phosphoric acid as an additional component in the oxidizing mixture [13].
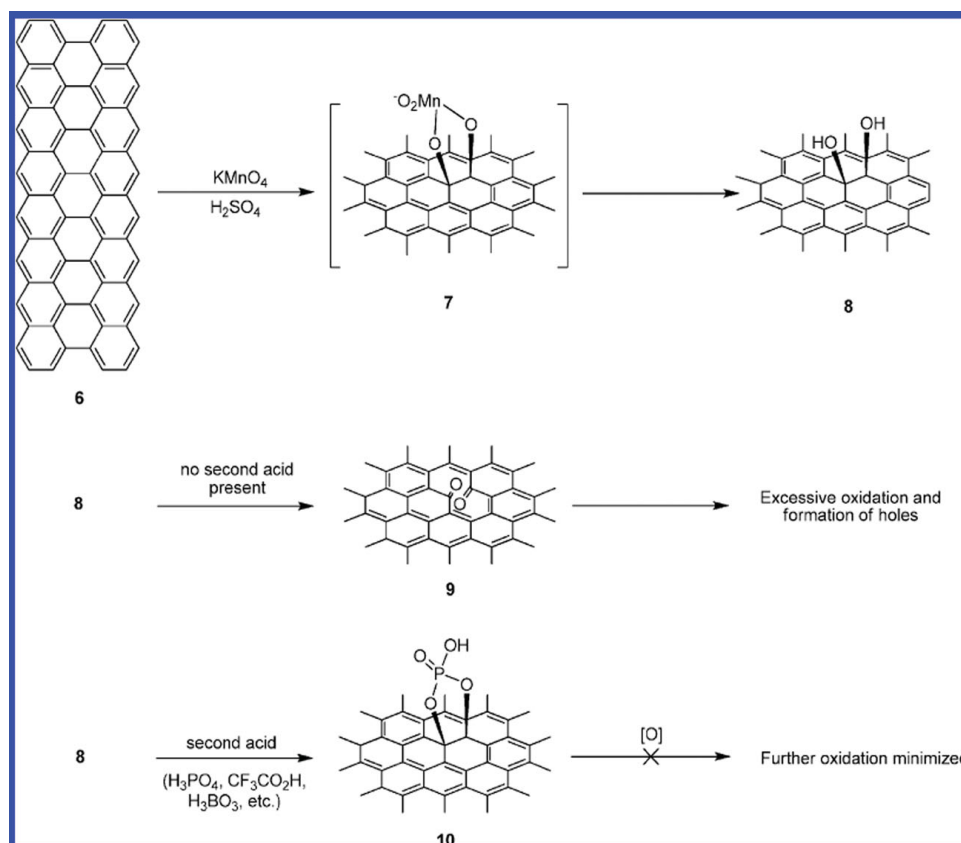
Figure 3.2: Effect of second acid in preventing over oxidation during GO synthesis [13]

As in the case of reaction mechanism, there were different proposals and continuous debate over the structure of GO and till now no unambiguous model exists. The main reason for this ambiguity is because of the complexity of the material due to its sample to sample variation and berthollide character (i.e., nonstoichiometric atomic composition)[14]. Many of the earlier models predicted regular lattices composed of discrete repeat units. Later, Hofmann and Holst's proposed a structure with epoxy groups spread across the basal planes of graphite, with a net molecular formula of C_2O [15]. In 1946, Ruess proposed a variation by incorporating hydroxyl groups in addition to the epoxy groups into the basal plane, accounting for the hydrogen content of GO [16]. In Ruess's model the basal plane structure was an sp^3 hybridized system whereas in Hofmann and Holsts model it was an sp^2 hybridized system. In 1969, Scholz and Boehm proposed a model without any epoxide and ether groups, but with regular quinoidal species in a corrugated backbone [17]. Nakajima and Matsuo model relied on the assumption of a lattice framework akin to poly(dicarbon monofluoride), $(C_2F)_n$, which forms a stage 2 graphite intercalation compound (GIC) [18]. Two of the most important models in the recent time are, one by Lerf and Klinowski and another by Decany. Lerf–Klinowski proposed a model in which the lattice based concept was substituted by a nonstoichiometric, amorphous alternative [19, 20]. The Decany model is another well-recognized structure with similarity to the Ruess and Scholz-Boehms model [21]. Figure 3.3 illustrates these different structures for GO.
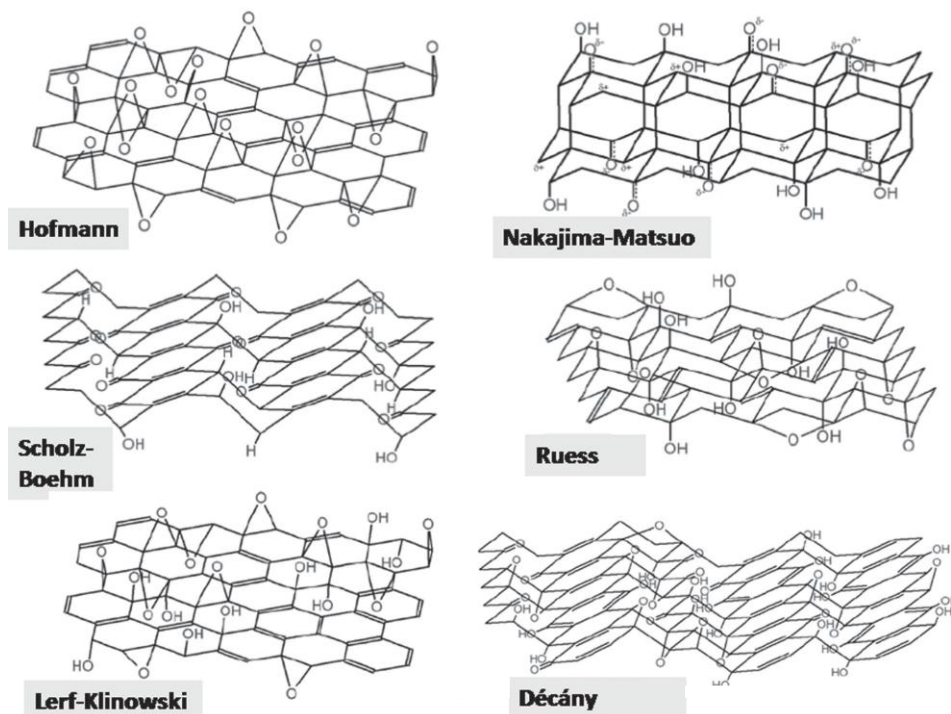
Figure 3.3: Different proposed models for GO [22]

A more generalized model can be of the form as given in Figure 3.4. The figure illustrates the presence of epoxy groups (A), hydroxyl groups (B) and carboxylic acid groups (C).
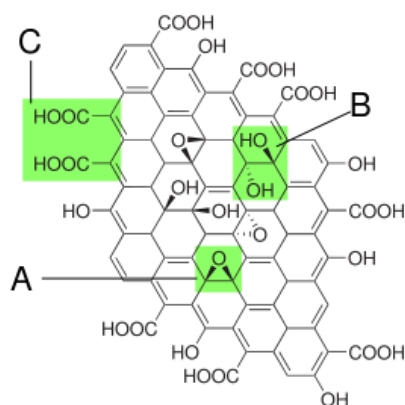

Figure 3.4: Generalized illustration of GO structure proposed by He et al. [23]

3.1.4 Reduced graphene oxide

Graphene synthesis methods like micro-mechanical exfoliation of highly ordered pyrolytic graphite, chemical vapour deposition or epitaxial growth can produce electronic grade graphene with relatively perfect structures suitable for most of the charge transport experiments. In comparison, through the reduction of GO, even though we will be able to obtain graphene like material similar to pristine graphene, the residual functional groups and defects can alter the structure of the carbon network and hence the properties. Many efforts have been made to improve the reduction protocol to achieve pristine graphene, but still the final goal is a dream. Thus, it is inappropriate to refer RGO as graphene since the properties can be different depending on the reduction method. However, there are mainly two reasons which make RGO still a hot topic in graphene research. The first and foremost advantage is that it can be prepared from inexpensive graphite as the raw material through cost effective and scalable chemical method with very high yield. Secondly, due to the presence of residual functional groups and defects, it can be easily dispersed in various liquids and polymers enabling the use of simple and cheap solution processes. Both these are very important advantages from an industrial perspective for the large scale application of graphene materials.

In this context, the reduction of GO is an extremely important aspect since the different reduction methodologies can affect the properties of RGO and in turn affect the final performance of the device made out of RGO.

3.2 Experimental

3.2.1 Synthesis of graphene oxide (GO)

In the present work, GO was synthesized in two different methods (1) modified Hummers' process and (2) A new modified protocol for the improved synthesis method developed in this work.

3.2.1.1 Modified Hummers method

In the modified Hummers' method, 16.25 moles of H_2SO_4 was added to a mixture of 1 mole of graphite and 0.099 moles of $NaNO_3$ with continuous stirring in an ice water bath. To this mixture, 0.324 moles of $KMnO_4$ was slowly added over about 1 hour in multiple aliquots. The addition of $KMnO_4$ resulted in a slight exothermic reaction, but the temperature of the reaction mixture was maintained below 35- 40 °C by continuous stirring in an ice water bath. The stirring was continued in ice water bath for 2 hours, and the mixture was allowed to stand for five days at room temperature with continuous stirring. In the course of reaction in these five days, the reaction mixture turns green, then dark brown, and then brick brown. After five days, about 350 mL of H_2O was added over about 1 hour with stirring. The temperature was kept at 98 °C during water addition, and the resultant mixture was further stirred for 2 h. After cooling down the mixture to room temperature, 3.691 moles of H_2O_2 (30 wt% solution) was added. The golden yellow coloured graphite oxide formed was separated from the reaction mixture by centrifuging, which removes the water soluble oxidants and other inorganic salts. The collected graphite oxide was washed with a mixture of 3% H_2SO_4 and 0.5% of H_2O_2 for several times followed by washing with 3% HCl solution. The washing

process continued for few more times using distilled water. For each washing, the mixture was sonicated for dispersing in the washing liquid and after washing the solid was separated by centrifugation. The resultant graphite oxide was then readily exfoliated to completely water dispersed graphene oxide (GO) by ultra-sonication.

3.2.1.2 New synthesis protocol for an improved GO synthesis

In this method, we have used orthophosphoric acid as the second acid in the oxidizing mixture of concentrated sulphuric acid and potassium permanganate as suggested by Marcano et al. [9] but with a new modified synthesis protocol. In the procedure explained by Marcano et al., graphite flakes and potassium permanganate were mixed and the acid mixture of sulphuric acid and phosphoric acid (9:1) was added to it. If we add acid altogether to potassium permanganate directly, due to the exothermic nature of the reaction, the heat generated will be too high and cannot be controlled which makes it highly unsafe. When the acid mixture is added to the mixture of graphite and potassium permanganate in small portions, the dissipation of heat generated in the solid will be less and hence due to localized heating, the reaction becomes unsafe. Hence we have modified the protocol by changing the addition sequence. Initially, 3g of graphite flakes were mixed with concentrated H_2SO_4 (360 ml) and H_3PO_4 (40 ml). 18g of $KMnO_4$ was added slowly in small portions, while keeping the reaction mixture in an ice bath and stirred for 2 h. Then the mixture was heated at 50 °C in a water bath for 45 minutes and stirring was continued at room temperature. After 24 h, the reaction mixture was added slowly to 400 ml of ice water which results in an increase of temperature of the

system to about 98 $^{\circ}$C. The stirring was continued for another 2 h and then, hydrogen peroxide (10 ml) was added. The solid collected from the reaction mixture was washed a few times with 5% HCl solution followed by distilled water. For each washing, solid was suspended by ultra-sonication and was collected by centrifugation. The synthesis protocol at this stage is also different from that of earlier report. The order of washing with acid and water was changed in order to remove remaining acids and the concentration of acid and number of times of washing was also modified. The resultant graphite oxide was then readily exfoliated to completely water dispersed graphene oxide (GO) by ultra-sonication.

3.2.2 Reduction of GO

In this work, reduction of GO were performed using two different methods: (i) Chemical reduction using hydrazine monohydrate and (ii) thermal reduction.

3.2.2.1 Chemical reduction

The chemical reduction of GO was done using hydrazine monohydrate as the reducing agent. To the GO dispersion in distilled water, aqueous solution of hydrazine monohydrate was added and heated at higher temperatures with continuous stirring. The concentration of hydrazine monohydrate, heating temperature and heating time were varied to optimize the reduction conditions. After several trials, an optimum concentration of 1μL of hydrazine monohydrate (35%) per 3 mg of GO at a temperature of 80 $^{\circ}$C for 8 hours yielded the best results. After reduction, RGO will precipitate as black particles since RGO is hydrophobic in nature. The RGO

is then filtered, washed with distilled water and dispersed in N,N-Dimethyl formamide (DMF) by ultrasonication.

3.2.2.2 Thermal reduction

In thermal reduction, the dried GO is subjected to a thermal shock to exfoliate and reduce the GO. The GO is taken in a quartz tube through which an inert gas like nitrogen is passed. The quartz tube with GO is directly introduced in to a muffle furnace kept at a high temperature of 700 to 1000 ^{o}C. The GO is allowed to stay in that higher temperature for less than a minute and then taken back. During the thermal shock, the GO will be converted in to fluffy flakes of RGO. The heating temperature and duration were varied and an optimum reduction condition of 900 ^{o}C for 30 seconds was arrived.

3.3   Results and discussion

3.3.1 Comparison of GO synthesized by the two methods

It was observed that the graphite oxide prepared by modified Hummers' method contained some black colored particles along with the golden yellow colored graphite oxide obtained after the reaction. These particles were under-oxidized graphite flakes and got settled later after a few hours. The presence of under oxidized graphite was confirmed from the X-ray diffraction analysis of graphite oxide obtained from modified Hummers' method. The yield was only between 60 to 70 %. The modified Hummers' process requires about 5 days for completing the oxidation reaction. These disadvantages of low yield and longer time required for modified Hummers' process was overcome by the new synthesis protocol.

In the new synthesis protocol for an improved GO synthesis, $NaNO_3$ was replaced with phosphoric acid and $KMnO_4$ was used in excess quantity. This resulted in improved yield (> 95%) and reduced the time required for completing the oxidation reaction. Moreover, due to the high yield of the reaction, the oxidation product obtained was completely free from under oxidized graphite flakes. This was further confirmed from the X-ray diffraction study. A comparison of the X-ray diffraction patterns of the as prepared GO obtained by the modified Hummers method designated as GO(MH) and by the new improved synthesis protocol designated as GO(NIS) is given in Figure 3.5.
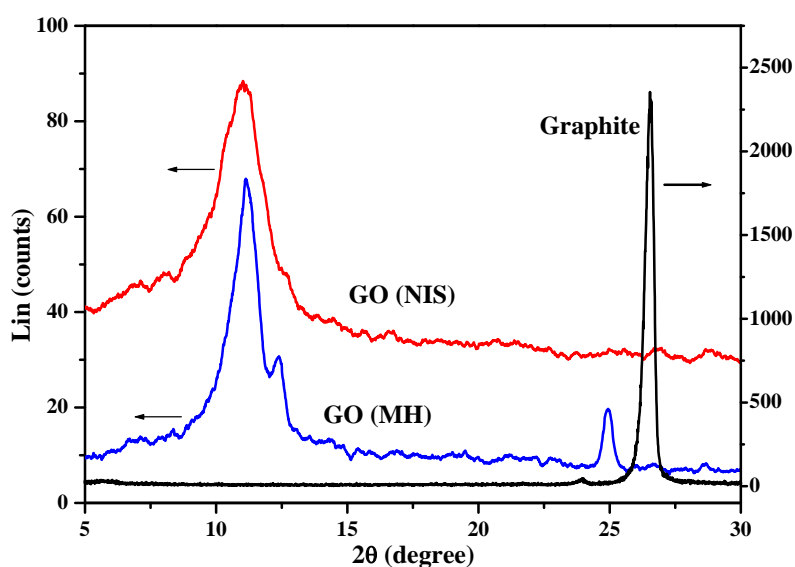
Figure 3.5: XRD patterns of GO synthesized by new modified improved synthesis protocol, GO (NIS) and modified Hummers' method, GO (MH)

It can be observed that the peak of graphite at $2\theta = 26.3^o$ corresponding to (002) plane with a d-spacing of 0.34 nm is completely

shifted to $2\theta = 11.2^{o}$ which corresponds to an increased d- spacing of 0.79 nm in the case of GO(NIS). The absence of any other peak of graphite in GO(NIS) confirms the complete conversion of graphite into GO. The increase in d spacing from 0.34 nm to 0.79 nm when graphite is converted to GO confirms the complete exfoliation of graphitic layers in GO(NIS). In the case of GO(MH), the peak at $2\theta = 11.2^{o}$ is more sharp with an additional shoulder peak at around $2\theta = 12.4^{o}$. Moreover an additional peak is observed at around $2\theta = 25^{o}$ which corresponds to unconverted graphite. This clearly brings out the fact that the new modified synthesis protocol completely oxidizes graphite whereas the modified Hummers' method results in under oxidized product. Hence it was found that the new modified synthesis protocol is more advantageous when compared to modified Hummer's process and this method of synthesis was employed for further studies in this work.
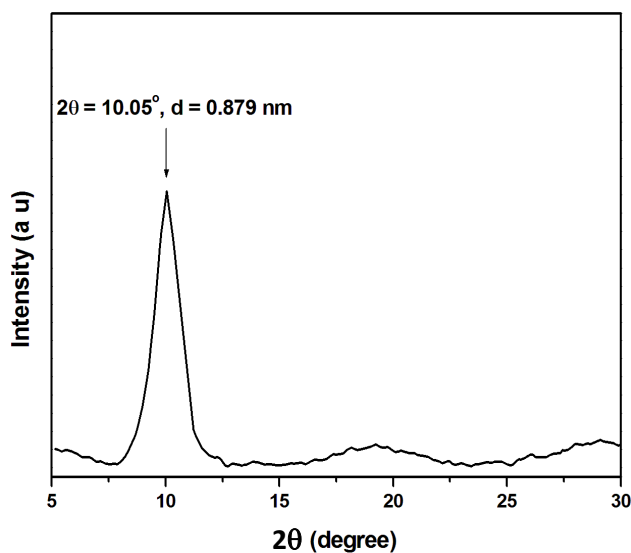
**Figure 3.6: XRD pattern of completely exfoliated GO**

For complete exfoliation, the GO (NIS) dispersion in distilled water was sonicated using a bath sonicator (140 W) for 8 hours. The XRD pattern of the completely exfoliated GO (NIS), hereinafter simply referred as GO, is given in Figure 3.6. It can be observed that the peak has further shifted to lower 2 theta values showing that the d-spacing has increased. A peak at 2 theta value of 10.05^o is observed which corresponds to an increased d-spacing of 0.879 nm.

3.3.2 Reduction of GO

Graphene oxide contains oxygen containing functional groups such as epoxy, carboxylic and hydroxyl groups. The reduction of graphene oxide removes these functional groups thereby retaining the disrupted sp^2 hybridized carbon network. The efficiency of the reduction method is of prime importance for the effective removal of these functional groups thereby obtaining RGO with maximum closeness in properties to that of pristine graphene. In the present study, chemical reduction using hydrazine monohydrate and thermal reduction were employed to prepare RGO.

Reduction using chemical reagent is one of the cheapest and simplest way of GO reduction and hence can be scaled up to mass production. Out of the two major functional groups in GO, epoxy groups are more stable than the hydroxyl groups. Many researchers have proved this through the density functional theory (DFT) calculations [24]. Due to the low binding energy, the hydroxyl groups attached to the interior of the aromatic domain of GO are less stable than the hydroxyl groups at the edges. Thus, the hydroxyl groups at the interiors of the aromatic domain either disintegrate or migrate to the edges. The mechanism of reduction of GO using

hydrazine and its derivatives is mainly through the epoxide ring opening reactions. The mechanism was first proposed by Stankovich et al. [25]. The reduction process is initiated by the ring opening of epoxy groups through the hydrogen transfer from hydrazine to form intermediates such as hydrazine alcohols. This intermediate reacts further to form aminoaziridine moiety which on further reaction eliminates a di-imide to re-establish the conjugated graphene network. Figure 3.7 (a) depicts the proposed reaction pathway for the epoxide reduction in GO using hydrazine.
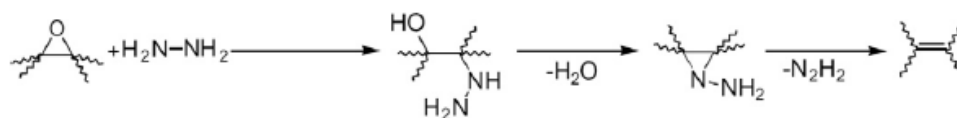
Figure 3.7(a): Proposed reaction pathway for the epoxide reduction in GO using hydrazine [25]

In thermal reduction, rapid heating (>2000 ^{o}C/min) is given to reduce GO and exfoliate the graphene layers. The sudden increase in temperature decomposes the oxygen containing functional groups in to gases. The sudden expansion of gases like CO or CO_2 evolved between the layers creates huge pressure between the stacked layers which helps to exfoliate the layers. The pressure generated between the layers depends on the heating temperature. For example, a pressure of 40 MPa is generated at 300 ^{o}C whereas 130 MPa is generated at 1000 ^{o}C [26]. However, in thermal reduction, during the decomposition of oxygen containing functional groups, carbon atoms are also removed from the carbon plane resulting in small size, wrinkled graphene sheets with more defects.

The mechanisms of reduction of various functional groups in GO through hydrazine and thermal treatment are given figure 3.7(b) [27].
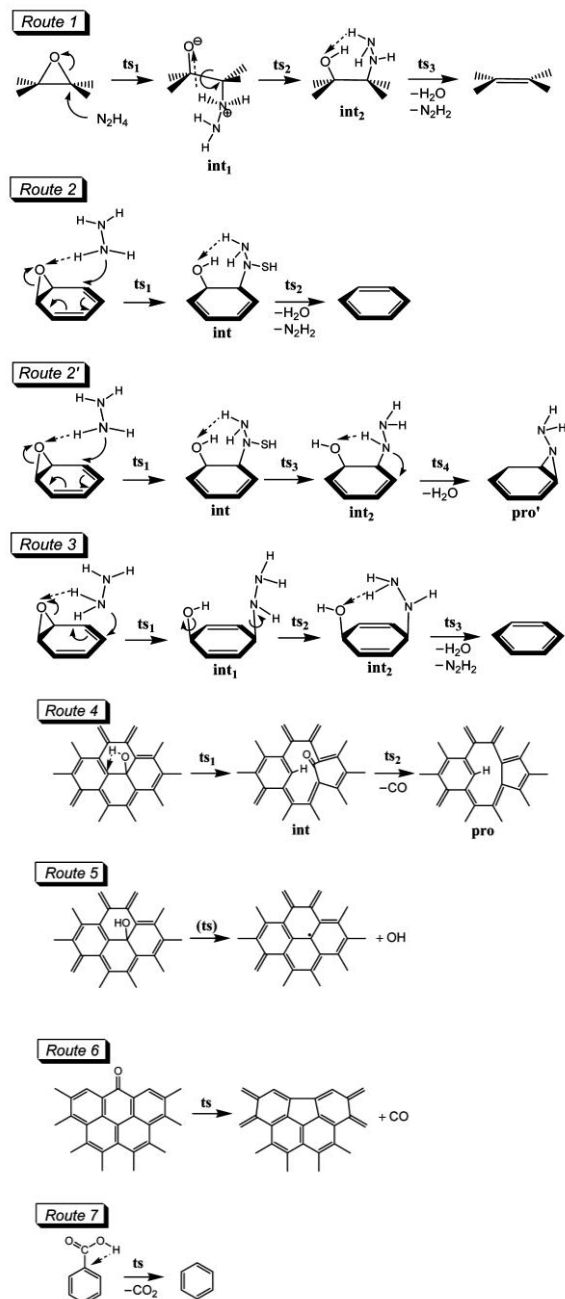
Figure 3.7(b): Various GO reduction mechanisms [27]. Routes 1-3 and 2' represent the mechanism for hydrazine de-epoxidation, routes 4 and 5 represent thermal de-hydroxylation and routes 6 and 7 represent thermal de-carbonylation and de-carboxylation of GO

3.3.3 Characterization of GO and RGO

3.3.3.1 Visual characteristics

Visual examination can be used as a direct tool to understand the conversion of graphite to GO and then the complete reduction of GO. Graphite turns to golden yellow graphite oxide which is exfoliated in water to form yellow dispersion of GO. On reduction, the dispersion changes from yellow to black in colour and due to the hydrophobic nature of reduced GO, it starts precipitating out. Figure 3.8 shows GO and RGO dispersed in water and DMF respectively.

Figure 3.8: (a) Graphene oxide dispersed in water,
(b) Reduced graphene oxide dispersed in DMF

3.3.3.2 Electrical conductivity

In graphene, the carbon atoms which are in sp^2 hybridized state, contains one free electron in the p orbital. These free electrons exist as a

Development of Reduced Graphene Oxide/Polymer Nanocomposites for Optical Limiting,
Optical Actuation and Electrical Applications

105

sea of electrons on both sides of the graphitic layer which imparts metal like conductivity to graphene. However, when graphite is converted in to GO, the carbon atoms get sp^3 hybridized and due to the anchoring of oxygen functional groups, the conductivity is completely lost. Thus GO is a completely insulating material. On reduction, the oxygen functional groups get removed and results in the regaining of sp^2 hybridization in carbon atoms which improves the conductivity. Thus measurement of electrical conductivity can be used as a tool for understanding the extent of reduction of GO.

The bulk resistivity of GO and RGO were measured using a two probe method. The conductivity increased with reduction temperature. After 80 ^{o}C, the conductivity almost levelled off. The reduction was also carried out for different durations with 80 ^{o}C as the reduction temperature. Finally, an optimized reduction condition of 80 ^{o}C for 8 hours was arrived at. A similar study was conducted for thermal reduction also. The optimized condition for thermal reduction was 900 ^{o}C for 30 sec. The conductivities of both hydrazine reduced GO (HRGO) and thermally reduced GO (TRGO) are given in table 3.1.

Table 3.1: Electrical properties of GO and RGO
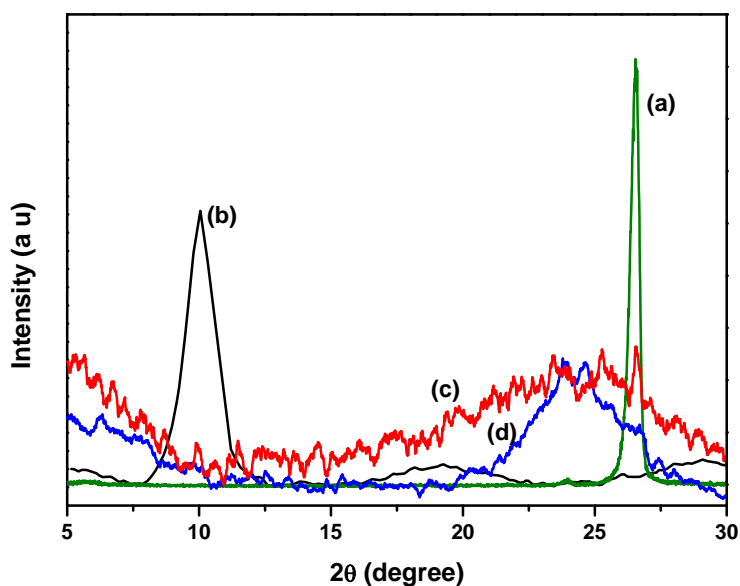
Sample	Conductivity (S.cm^{-1})
Graphene oxide (GO)	1.2×10^{-5}
Thermally reduced graphene oxide (TRGO)	6.4×10^{-2}
Hydrazine reduced graphene oxide (HRGO)	1.78×10^{-3}

3.3.3.3 X-ray Diffraction analysis

X-ray diffraction (XRD) analysis is an important tool which can give clear indication of conversion of graphite to graphene oxide and then back to graphene. In section 3.3.1, we have already discussed about the changes observed in the XRD pattern when graphite is converted to graphene oxide. However, figure 3.9 elucidate the XRD patterns of graphite, GO, TRGO and HRGO. As already discussed, the characteristic peak of graphite at $2\theta = 26.3^o$ (corresponding to (002) plane) get shifted to 10.05^o in GO due to increased interlayer spacing. On reduction the characteristic peak of GO is vanished and there is only a very broad peak around 25° due to the high degree of exfoliation of graphitic layer in reduced graphene oxide. The disappearance of peak corresponding to GO confirms the nearly complete reduction of GO into RGO.

Figure 3.9: XRD patterns of (a) graphite, (b) GO, (c) HRGO and (d) TRGO.

Development of Reduced Graphene Oxide/Polymer Nanocomposites for Optical Limiting, Optical Actuation and Electrical Applications

107

3.3.3.4 FTIR spectroscopy

The oxygen functional groups in GO are removed on reduction into RGO. This can be clearly understood from the FTIR analysis. FTIR spectra of graphene oxide, HRGO and TRGO are shown in figure 3.10. The FT-IR spectrum of GO confirms the introduction of oxygen functionalities like hydroxyl, epoxy and carboxylic groups on oxidation of graphite. The significant peaks in GO which confirms the conversion of graphite into GO are peaks at 3418 cm^{-1} (due to -O-H stretching vibration), 1720 cm^{-1} (stretching vibrations from C=O), 1600 cm^{-1} (skeletal vibrations from unoxidized graphitic domains), 1591 cm^{-1} (aromatic C=C), 1401 cm^{-1} (-O-H bending in tertiary alcohol), 1290 cm^{-1} (carboxyl O=C-O), 1168 cm^{-1} (epoxy group) and 1069 cm^{-1} (-C-O stretching).
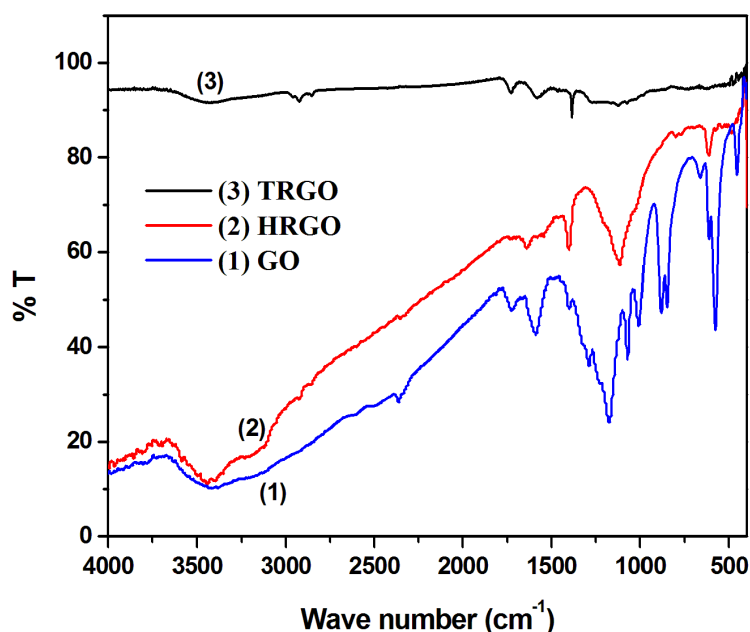

Figure 3.10: FTIR spectra of GO, HRGO and TRGO

When GO is thermally reduced, there is no significant peak observed in the FTIR spectrum of TRGO corresponding to the oxygen functional groups which indicates a nearly complete reduction. Similarly, in the case of hydrazine reduced GO (HRGO), after reduction, most of the peaks have either vanished or diminished to a great extent. In the case of HRGO, the peak corresponding to the presence of water was present near 3440 cm^{-1} (-O-H stretching). The peaks representing epoxy and carboxyl groups were absent which shows nearly complete reduction. However, as can be expected, still traces of some functional groups remained which will be helpful for the preparation of uniformly dispersed polymer composites.

3.3.3.5 Raman Spectroscopy

Raman spectroscopy is one of the most effective tools to study the structural changes during the chemical synthesis of GO and reduction of GO. Typically, the Raman spectrum of graphite exhibits a sharp G band at 1580 cm^{-1} and a very weak D band at 1350 cm^{-1} [28]. Figure 3.11(a) & (b) shows the Raman spectra of GO, HRGO and TRGO. Both the G and D bands arises from the vibrations of sp^2 carbon. The G band is due to the in plane bond stretching of sp^2 carbon pairs, whereas the D band is due to the breathing mode vibration of aromatic rings and requires defects for its activation. The Raman spectrum of graphene oxide displays peaks at 1357 and 1605 cm^{-1} that correspond to the D and G bands, respectively. In graphene oxide, the presence of large amounts of hydroxyl and epoxy groups decreases the amount of aromatic rings present, thereby diminishing the intensity of G band. Moreover, the decrease in sp^2 hybridized carbon in GO reduces the intensity of G band and presence of sp^3 hybridized carbon makes the G band to broaden.
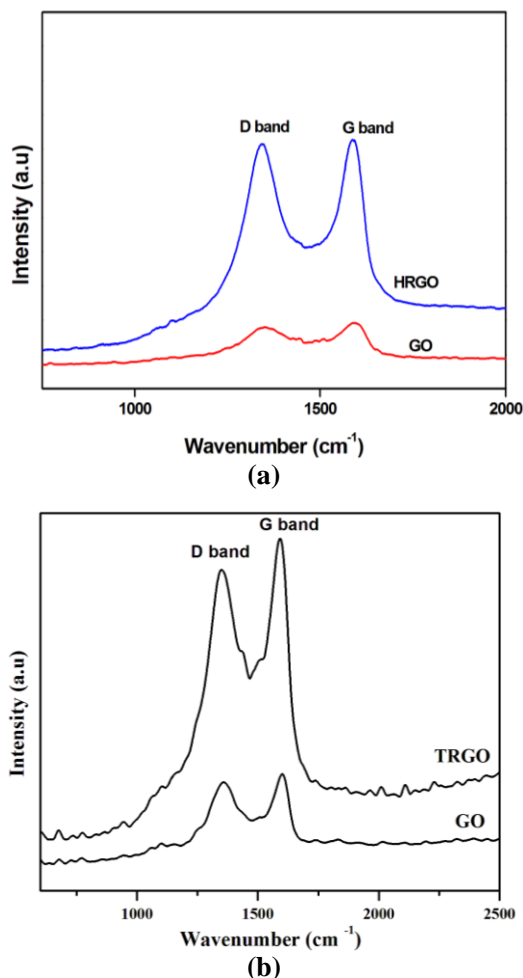
Figure 3.11: Raman spectra of (a) GO and HRGO (b) GO and TRGO showing the G and D bands.

Once graphene oxide is reduced either chemically or thermally; most of those oxygenated groups are eliminated, reintroducing aromaticity and electrical conductivity in the structure. In case of HRGO and TRGO, the strong G band intensity compared to that of graphene oxide could be explained by two factors. Firstly, the reduction process improves the aromaticity to a greater extend. Secondly, graphene produced by different

reduction methods possesses structural defects and these defects are more visible at the edge planes. In figure 3.11, the changes in Raman spectra of GO, TRGO and HRGO are clearly elucidated. When we consider the G band, it is located at a higher frequency in GO (1605 cm^{-1}) than that in pure graphite (1580 cm^{-1}). On reduction, there is shift of G band towards lower frequencies. In HRGO and TRGO, it is located almost near to the frequency of graphite. The table 3.2 shows the D band, G band and Intensity ratio of D and G bands (I_D/I_G ratio) of graphene oxide, TRGO and HRGO respectively.

Table 3.2 Raman spectra analysis of GO and RGO

	D band	**G band**	**I_D/I_G**
Graphene oxide	1357	1605	0.9908
HRGO	1347	1592	0.9651
TRGO	1343	1585	0.8621

From the table 3.2 we can see that the I_D/I_G ratio decreases on reduction that means the G band intensity increases which is a clear indication of effective reduction in both HRGO and TRGO. Moreover, the G band position of both RGO is shifted closely towards the actual G band position of pure graphite. This observation also supports the effective reduction of GO.

3.3.3.6 Scanning Electron Microscopy (SEM)

The SEM images of the GO are given in figure 3.12. The wrinkled sheet like structure, which is a characteristic feature of GO, can be clearly noticed in figure 3.12 (a) when observed from the surface and the graphitic layered structure can be understood from the cross sectional view given in figure 3.12(b).

Development of Reduced Graphene Oxide/Polymer Nanocomposites for Optical Limiting, Optical Actuation and Electrical Applications

111

(a) **(b)**
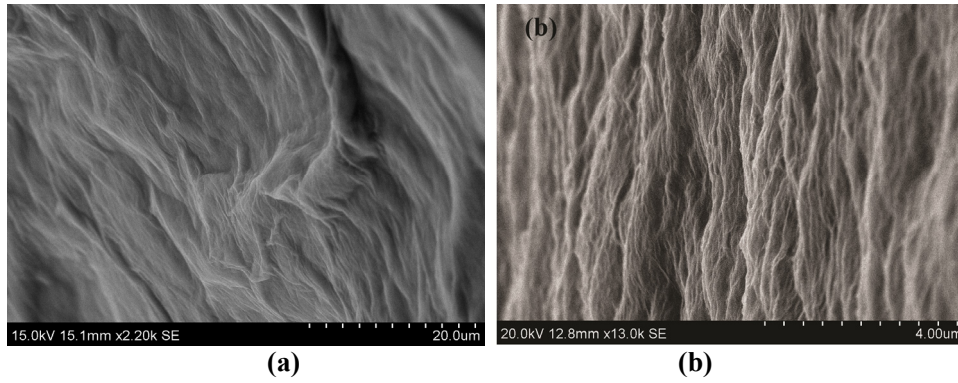
Figure 3.12: SEM image of GO (a) surface (b) cross section

(a) **(b)**

(c) **(d)**
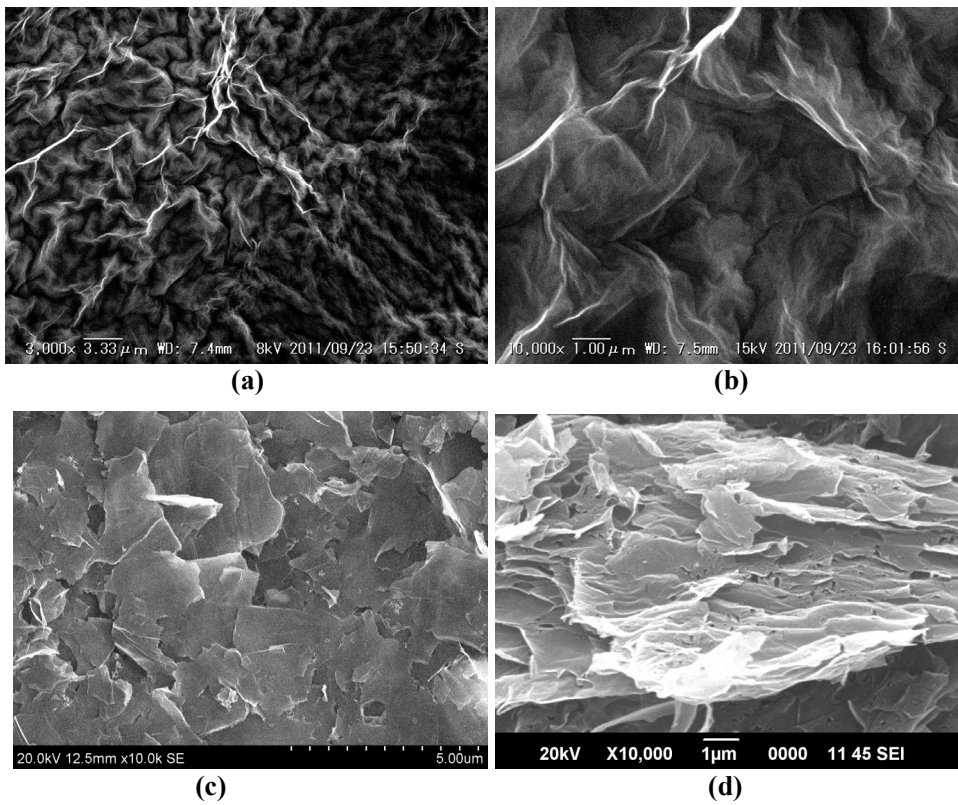
Figure 3.13: SEM images of (a) & (b) HRGO and (c) & (d) TRGO. The cross sectional view of TRGO is shown in (d).

The SEM images of HRGO at different magnifications are given in figure 3.13 (a) and (b). The wrinkled sheet like structure of the HRGO sheets is well evident from the SEM images. Similarly, from the SEM images of TRGO in Figures 3.13 (c) and (d), it can be observed that large RGO flakes with more than 1µm lateral dimension with highly exfoliated layer by layer structure are obtained.

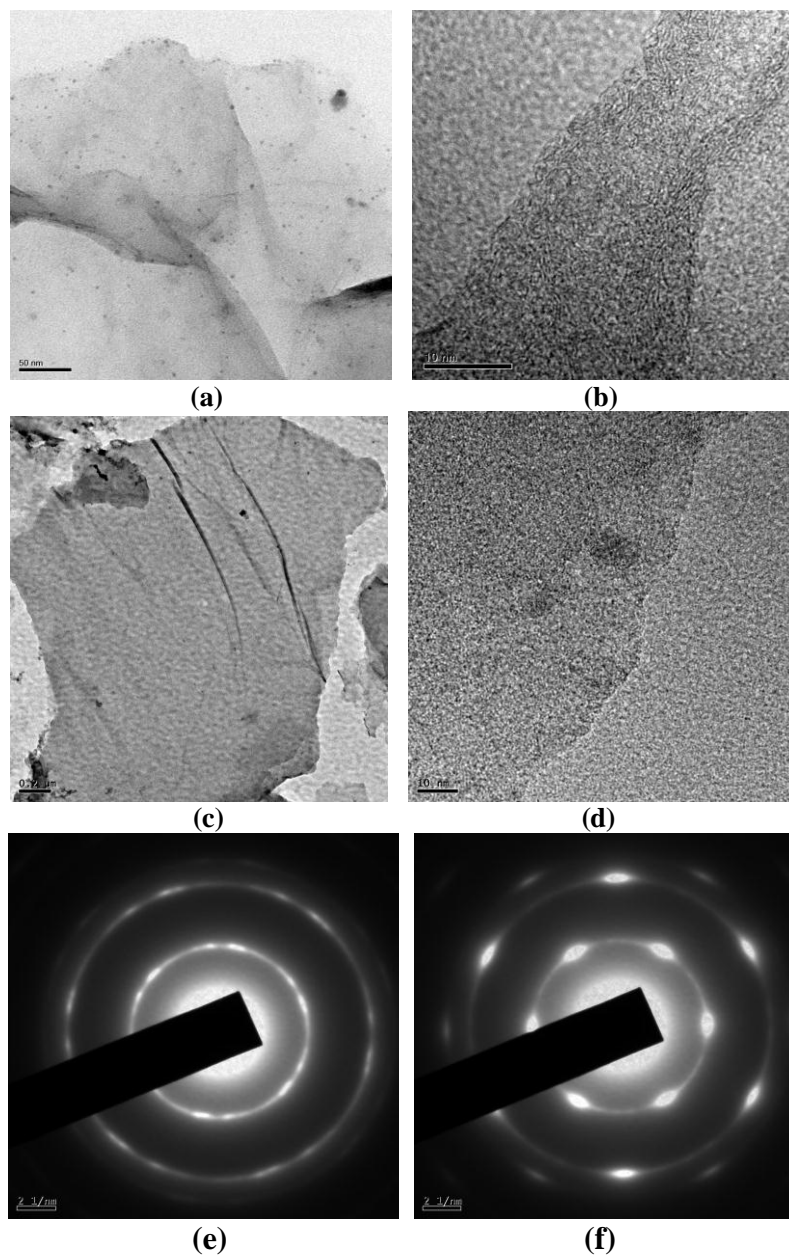### 3.3.3.7 Transmission Electron Microscopy (TEM)

HR-TEM images of reduced graphene oxide are given in figure 3.14. The HR-TEM image of HRGO and TRGO are almost transparent which indicates the presence of single layers. Moreover, the focused edges also show that both HRGO and TRGO contain some single layers, however, folding and restacking are also observed. The Selected Area Electron Diffraction (SAED) pattern of HRGO is shown in figure 3.14 (e). The crystalline structure of HRGO is evident from the presence of diffraction rings. However, the diffraction rings are weak and diffused which may be due to the curling and folding nature of HRGO. Strong diffraction spots present on the diffraction ring of TRGO (Figure 3.14 (f)) indicate a highly crystalline structure. The TEM analysis clearly confirms the synthesis of high quality RGO by both thermal and chemical reduction methods. It was also found from EDS analysis that HRGO contained about 87% carbon and TRGO contained about 93% carbon which clearly shows that reduction was effective.

Development of Reduced Graphene Oxide/Polymer Nanocomposites for Optical Limiting, Optical Actuation and Electrical Applications

113

Figure 3.14 HRTEM images of (a) surface of HRGO (b) focused edge of HRGO (c) surface of TRGO (d) focused edge of TRGO (e) SAED pattern of HRGO (f) SAED pattern of TRGO.
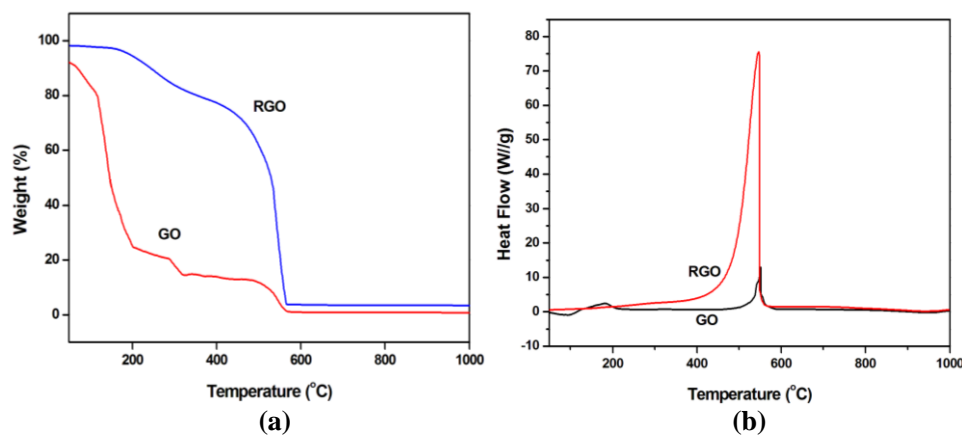
3.3.3.8 Thermal analysis

Thermal analysis of graphene oxide and RGO was carried out under air flow and the weight changes were noted as a function of temperature. Since TRGO was already heat treated near 900 ^oC during synthesis, HRGO was used to represent RGO. The samples were heated from 50 ^oC to 1000 ^oC at a heating rate of 10 ^oC/min. The figure 3.15 (a) and (b) shows the thermal gravimetric analysis (TGA) and differential Scanning Calorimetric (DSC) analysis results respectively.

The GO sample shows a major weight loss between 140 ^oC to 300 ^oC. The slow and continuous degradation in the above specified temperature range indicates that the exfoliation of graphene oxide sample could occur near this temperature range. Two major differential peaks were observed near 180 ^oC and 550 ^oC (Figure 3.15(b)). The peak near 180 ^oC corresponds to the decomposition of more volatile oxygen containing functional groups yielding CO, CO_2 and steam. The peak near 550 ^oC can be explained as the burning of carbon skeleton.

Once graphene oxide was reduced, the sample becomes less hydrophilic as the functional groups are removed to a greater extend. This is obvious from the broad degradation peak between 150 to 280 ^oC where negligible weight loss can be seen. For the RGO sample, only one characteristic differential peak was present near 550 ^oC, which indicates the burning of carbon skeleton. The high intensity of the peak at this temperature indicates the stability of the reduced graphene oxide sample.

Development of Reduced Graphene Oxide/Polymer Nanocomposites for Optical Limiting, Optical Actuation and Electrical Applications

115

Figure 3.15: (a) TGA of GO and RGO (b) DSC of GO and RGO

3.3.3.9 UV-visible spectroscopy

UV-visible spectra of GO and RGO are presented in figure 3.16. Graphene oxide sample was prepared by dispersing in distilled water (0.3 mg/mL) and the RGO sample was prepared by dispersing HRGO in DMF (0.3 mg/mL). The absorption peaks in the UV region correspond to the electronic transitions which are dependent on the number of sp^2 and sp^3 hybridized carbon atoms. In GO, due to the presence of functional groups, sp^3 carbon atoms will be more. When GO is reduced, the number of sp^2 carbon atoms increases in the expense of sp^3 carbons. It can be observed that, RGO shows a maximum absorption peak at higher wavelengths (~ 270nm) compared to that of GO. This absorption peak is due to the $\pi - \pi^*$ transition in C=C in the aromatic rings of RGO. This is an indication of the presence of almost completely reduced graphene oxide with regained π-conjugated network. As the number of sp^2 carbon atoms increases, there will be more conjugation and thus lesser energy is required for electronic transition and hence absorption at higher wavelength occurs.

Hence from the UV visible spectra, it can be confirmed that effective reduction has taken place in RGO.
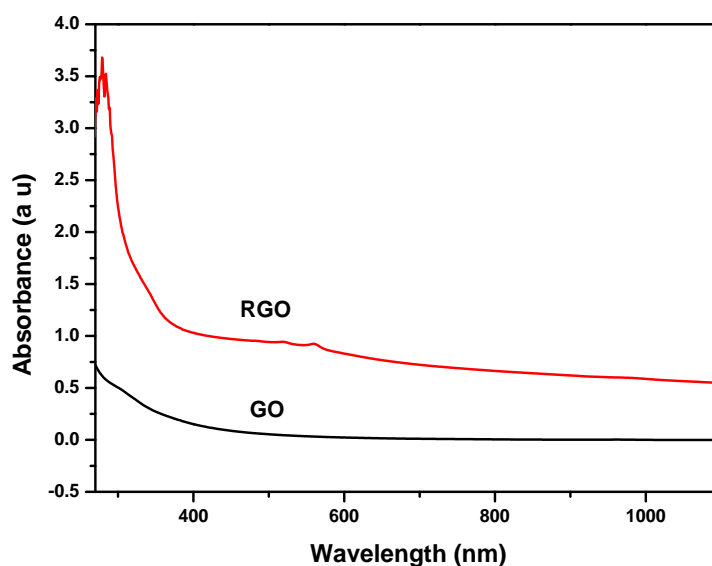
Figure 3.16: UV-visible spectra of GO and RGO

3.3.3.10 Surface area measurements

The surface area was measured using BET method by nitrogen gas adsorption and the BET plots are given in Figure 3.17. From the BET plots the surface area was calculated as described in Chapter 2. A BET surface area value of 390 m^2/g was yielded for HRGO. Despite the theoretically high specific surface area for completely exfoliated and isolated graphene sheets (up to 2675 m^2/g), this value has not yet been achieved in chemically synthesized graphene sheets due to re-stacking tendency of graphene layers during reduction.

(a)

(b)
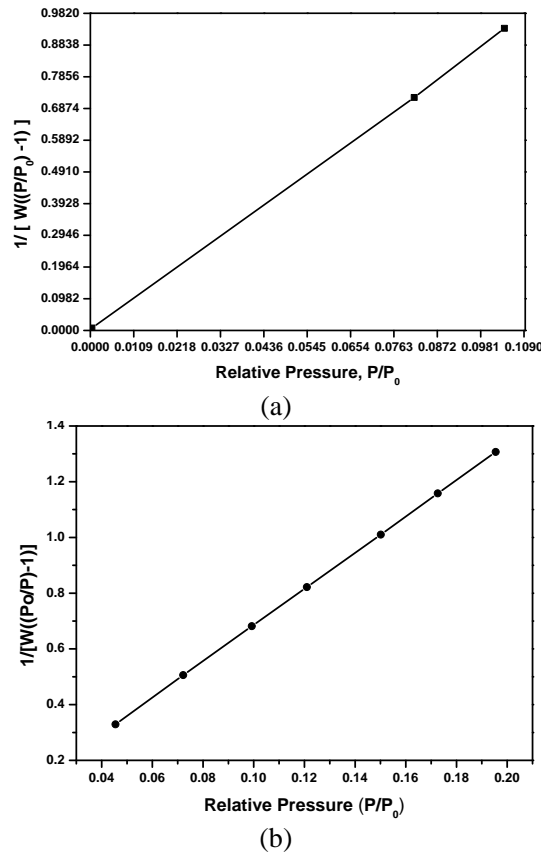
Figure 3.17: BET plots of (a) HRGO and (b) TRGO

In the case of HRGO, a major fraction of surface area is not available for nitrogen adsorption because of overlap, wrinkled nature and re-stacking of the exfoliated layers. Hence the measured surface area of the HRGO is therefore consistent with the folded, stacking structure and agglomerated morphology of the same as shown in SEM studies. TRGO could show a better BET surface area of 532 m^2/g because of the better exfoliated nature and lower tendency in folding and restacking. In order to understand the nature of porosity, adsorption-desorption isotherm of a representative HRGO sample was measured and given in Figure 3.18. It can be observed

that, there is a hysteresis during desorption. The hysteresis loop is of Type IV isotherm which corresponds to mesoporous structure. Hence it is clear that even after reduction, the RGO retains the exfoliated nature and consists of mesoporous voids between the layers.
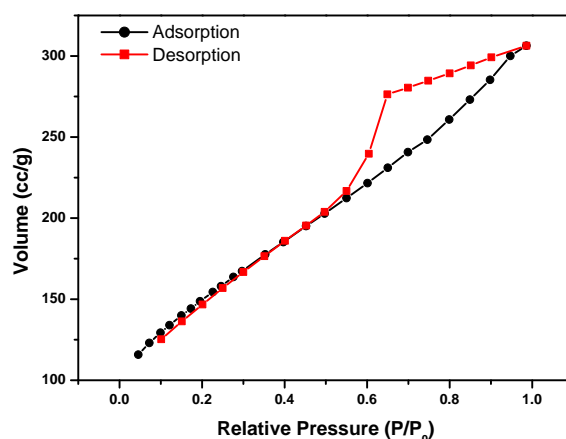
Figure 3.18: Adsorption—Desorption Isotherm of RGO

3.4   Conclusions

Graphene oxide (GO) was synthesised through a modified synthesis protocol using sulphuric acid, orthophosphoric acid and $KMnO_4$ as oxidising agents. The synthesised GO was reduced by both chemical and thermal methods. The characterisation of GO and RGO were carried out and it was found that graphene like material is obtained by the reduction of GO. Both chemically reduced GO and thermally reduced GO shows nearly complete reduction, however, there are still unreduced functional groups in both. Even though these can adversely affect some properties, the residual functional groups can facilitate good dispersion of RGO in polymer composites. Hence, the RGO can be utilized as an alternative to graphene in polymer nanocomposites for many potential applications.

References

[1] Segal, M. (2009). Selling graphene by the ton. *Nature nanotechnology*, *4*(10), 612-614.

[2] Pei, S., & Cheng, H. M. (2012). The reduction of graphene oxide. *Carbon*, *50*(9), 3210-3228.

[3] Galande, C., Gao, W., Mathkar, A., Dattelbaum, A. M., Narayanan, T. N., Mohite, A. D., & Ajayan, P. M. (2014). Science and engineering of graphene oxide. *Particle & Particle Systems Characterization*, *31*(6), 619-638.

[4] Novoselov, K. S., Geim, A. K., Morozov, S. V., Jiang, D., Zhang, Y., Dubonos, S. V., ... & Firsov, A. A. (2004). Electric field effect in atomically thin carbon films. *science*, *306*(5696), 666-669.

[5] Brodie, B. C. (1859). On the atomic weight of graphite. *Philosophical Transactions of the Royal Society of London*, *149*, 249-259.

[6] Staudenmaier, L. (1898). Verfahren zur darstellung der graphitsäure. *European Journal of Inorganic Chemistry*, *31*(2), 1481-1487.

[7] Hummers Jr, W. S., & Offeman, R. E. (1958). Preparation of graphitic oxide. *Journal of the American Chemical Society*, *80*(6), 1339-1339.

[8] Kovtyukhova, N. I., Ollivier, P. J., Martin, B. R., Mallouk, T. E., Chizhik, S. A., Buzaneva, E. V., & Gorchinskiy, A. D. (1999). Layer-by-layer assembly of ultrathin composite films from micron-sized graphite oxide sheets and polycations. *Chemistry of Materials*, *11*(3), 771-778.

[9] Marcano, D. C., Kosynkin, D. V., Berlin, J. M., Sinitskii, A., Sun, Z., Slesarev, A., ... & Tour, J. M. (2010). Improved synthesis of graphene oxide. *ACS nano*, *4*(8), 4806.

[10] Szabó, T., Berkesi, O., Forgó, P., Josepovits, K., Sanakis, Y., Petridis, D., & Dékány, I. (2006). Evolution of surface functional groups in a series of progressively oxidized graphite oxides. *Chemistry of materials*, *18*(11), 2740-2749.

[11] Dimiev, A. M., & Tour, J. M. (2014). Mechanism of graphene oxide formation. *ACS nano*, *8*(3), 3060-3068.

[12] Koch, K. R. (1982). Oxidation by Mn2O7: An impressive demonstration of the powerful oxidizing property of dimanganeseheptoxide. *J. Chem. Educ*, *59*(11), 973.

[13] Higginbotham, A. L., Kosynkin, D. V., Sinitskii, A., Sun, Z., & Tour, J. M. (2010). Lower-defect graphene oxide nanoribbons from multiwalled carbon nanotubes. *ACS nano*, *4*(4), 2059-2069.

[14] Dreyer, D. R., Park, S., Bielawski, C. W., & Ruoff, R. S. (2010). The chemistry of graphene oxide. *Chemical Society Reviews*, *39*(1), 228-240.

[15] Hofmann, U., & Holst, R. (1939). Über die Säurenatur und die Methylierung von Graphitoxyd. *European Journal of Inorganic Chemistry*, *72*(4), 754-771.

[16] Ruess, G. (1947). Über das graphitoxyhydroxyd (graphitoxyd). *Monatshefte für Chemie/Chemical Monthly*, *76*(3), 381-417.

[17] Scholz, W., & Boehm, H. P. (1969). Untersuchungen am graphitoxid. VI. Betrachtungen zur struktur des graphitoxids. *Zeitschrift für anorganische und allgemeine Chemie*, *369*(3-6), 327-340.

[18] Nakajima, T., Mabuchi, A., & Hagiwara, R. (1988). A new structure model of graphite oxide. *Carbon*, *26*(3), 357-361.

[19] He, H., Riedl, T., Lerf, A., & Klinowski, J. (1996). Solid-state NMR studies of the structure of graphite oxide. *The Journal of physical chemistry*, *100*(51), 19954-19958.

[20] Lerf, A., He, H., Forster, M., & Klinowski, J. (1998). Structure of graphite oxide revisited. *The Journal of Physical Chemistry B*, *102*(23), 4477-4482.

[21] Szabó, T., Berkesi, O., Forgó, P., Josepovits, K., Sanakis, Y., Petridis, D., & Dékány, I. (2006). Evolution of surface functional groups in a series of progressively oxidized graphite oxides. *Chemistry of materials*, *18*(11), 2740-2749.

Development of Reduced Graphene Oxide/Polymer Nanocomposites for Optical Limiting, Optical Actuation and Electrical Applications

121

[22] Gao, W. *Graphite Oxide: Struct. Reduction Appl.* (2012) Doctoral Thesis, Rice University. http://hdl.handle.net/1911/64614

[23] He, H., Klinowski, J., Forster, M., & Lerf, A. (1998). A new structural model for graphite oxide. *Chemical physics letters*, *287*(1), 53-56.

[24] Kim, M. C., Hwang, G. S., & Ruoff, R. S. (2009). Epoxide reduction with hydrazine on graphene: a first principles study. *The Journal of chemical physics*, *131*(6), 064704.

[25] Stankovich, S., Dikin, D. A., Piner, R. D., Kohlhaas, K. A., Kleinhammes, A., Jia, Y., ... & Ruoff, R. S. (2007). Synthesis of graphene-based nanosheets via chemical reduction of exfoliated graphite oxide. *carbon*, *45*(7), 1558-1565.

[26] McAllister, M. J., Li, J. L., Adamson, D. H., Schniepp, H. C., Abdala, A. A., Liu, J., ... & Aksay, I. A. (2007). Single sheet functionalized graphene by oxidation and thermal expansion of graphite. *Chemistry of materials*, *19*(18), 4396-4404.

[27] Gao, X., Jang, J., & Nagase, S. (2009). Hydrazine and thermal reduction of graphene oxide: reaction mechanisms, product structures, and reaction design. *The Journal of Physical Chemistry C*, *114*(2), 832-842.

[28] Ferrari, Andrea C., and Jf Robertson. "Interpretation of Raman spectra of disordered and amorphous carbon." *Physical review B* 61, no. 20 (2000): 14095.

.....ൟ.....

DEVELOPMENT OF REDUCED GRAPHENE OXIDE/POLYMER NANOCOMPOSITES

4.1 Introduction

Development of polymer nanocomposites has attracted enormous interest of the scientific community for the last few decades. Compared to conventional composites, in polymer nanocomposites, the nano filler can provide value-added properties to the system even when incorporated in very small quantities. Moreover, they can provide enhanced properties without affecting the processability of the polymer. Carbon nanotubes (CNTs) have been one of the most widely studied nano filler material for polymer nanocomposites for the past few years. CNTs were considered as one of the best filler materials for improving mechanical, electrical, thermal and optical properties. However, the intrinsic bundling nature of CNTs along with their high cost and limited availability of high quality CNTs prompted researchers to look for newer and better materials [1].

The past decade has witnessed the emergence of graphene as the most promising nano material which can cater to almost the entire spectrum of

technologies. There have been many efforts to develop graphene/polymer nanocomposites with excellent enhancement in properties compared to other filler materials [2-5]. Graphene has many advantages in terms of properties, cost and purity over CNTs and similar filler materials. However, the low dispersibility of graphene is the major challenge for many applications of polymer/graphene composites. Chemical functionalization of graphene has been the most common method employed by many researchers to overcome this challenge [6-9]. However, chemical functionalization can deteriorate many other important properties. The use of reduced graphene oxide (RGO) instead of pure graphene is now accepted as a better alternative to overcome the dispersibility issues. In RGO, the residual functional groups left out after the reduction of graphene oxide can help in uniform dispersion throughout the polymer matrix.

In this chapter, reduced graphene oxide/polymer nanocomposites have been developed through a simple solvent casting method. Two polymer systems have been used as the matrices: (1) Poy(vinyl alcohol) (PVA) and (2) Thermoplastic polyurethane (TPU). The motivation for selecting these polymers as the matrix for the composites has already been explained in Chapter 1 under "Scope of the work'' section. RGO/PVA composites have been developed by the *in situ* reduction of GO in polymer matrix. In the case of RGO/TPU composites, thermally reduced graphene oxide (TRGO) is used as the filler material. This chapter is divided in to two parts; Part – A deals with the preparation and characterisation of RGO/PVA nanocomposites and Part – B discusses the preparation and characterisation of RGO/TPU nanocomposites.

PREPARATION AND CHARACTERIZATION OF *IN SITU* REDUCED GRAPHENE OXIDE/POLY(VINYL ALCOHOL) NANOCOMPOSITES

4A.1 Introduction

Poly(vinyl alcohol) (PVA) is one of the most largely produced synthetic polymers which can find diverse applications in many fields including paper/textile industries, biomedical products and devices, ceramic industries, cosmetics, food packaging and so on [10]. The excellent film forming nature, good processability and biocompatibility has made this material a perfect choice for many optical and biomedical applications such as soft contact lenses [11]. The incorporation of graphene as a filler in to the PVA matrix can enhance its properties by many folds. However, graphene being extremely hydrophobic in nature, it is very difficult to form a uniform dispersion in hydrophilic PVA matrix [12]. Since the homogeneous distribution of the filler particles is the major criteria for the formation of a good composite material, finding out ways and methods to distribute graphene uniformly in the polymer matrix is the fore most challenge to be addressed.

In this context, reduced graphene oxide (RGO) is considered as a very good alternative to pure graphene for composite preparation due to the presence of residual functional groups in RGO which impart better dispersibility without compromising the properties to a great extend. In this work, for the development of RGO/PVA nanocomposites, we have utilized the hydrophilic nature of graphene oxide (GO) which was easily dispersed

in an aqueous solution of PVA and then reduced within the polymer matrix using a chemical reducing agent. The resulting RGO/PVA nanocomposites contained RGO platelets uniformly distributed in the PVA matrix. The composites were characterised in detail for evaluating their properties.

4A.2 Experimental

4A.2.1 Preparation of GO/PVA and RGO/PVA nanocomposites

GO was dispersed in 10 mL of distilled water by ultrasonication for 2 h to make a homogeneous brown dispersion. PVA powder was dissolved in distilled water at 90 ^{o}C and the solution was subsequently cooled to room temperature. The GO aqueous dispersion was gradually added to the PVA solution and sonicated at room temperature for 15 min and stirred to obtain homogeneous GO/PVA solutions which were cast in glass dishes and kept at 40 ^{o}C for film formation until its weight equilibrated. For preparing RGO/PVA nanocomposites, to the mixture of GO dispersion in PVA solution, 35% hydrazine monohydrate (1μL/3 mg GO) was added and heated at 80 ^{o}C for 3 h with stirring. Hydrazine, which is a strong reducing agent, removes the oxygen containing functional groups of the GO with in the polymer solution and results in a black coloured solution of RGO/PVA which was cast into composite film. RGO/PVA nanocomposite films with 0.1, 0.3, 0.5, 1 and 2 wt.% of RGO were prepared.

4A.2.2 Characterization

The crystallinity of the composite films was examined by X-ray diffraction (XRD) analysis (Bruker AXS D5005, Germany, with Cu Kα radiation, λ=0.154 nm). The morphology was studied using Scanning

Electron Microscopy (SEM SU 6600, Hitachi, Japan) and High Resolution Transmission Electron Microscopy (JEM 2100, JEOL, Japan). The surface morphology was also studied using Atomic Force microscopy (AFM, Park XE 100, non contact method). The absorption spectrum was taken in the wavelength range 200 to 2000 nm using a UV-Vis-NIR spectrophotometer (JascoV-570, USA). The chemical nature was studied using FTIR spectroscopy (Avatar 370, Thermo Nicolet, Germany) in the ATR mode. A minimum of 60 scans were obtained with a resolution of 4 cm^{-1}. Thermal analysis of the composites were carried out using TG/DSC analyzer (SDT Q600, TA Instruments, USA and Mettler Toledo DSC 822e, Hong Kong) with a heating rate of 10 ^{o}C min^{-1} under nitrogen atmosphere. The mechanical properties of the composites were studied using Universal Testing Machine (Autograph, Shimadzu, Japan) as per ASTM D882 standard.

The details of all the characterization techniques used are explained in Chapter 2.

4A.3 Results and discussions

4A.3.1 XRD analysis of GO/PVA and RGO/PVA nanocomposites

PVA is a well-known semi crystalline polymer, exhibiting an intense peak in the XRD at 2θ = 19.4^{o} [13]. Figure 4A.1(a) shows the XRD patterns of GO/PVA nanocomposites. It can be seen that the crystallinity of pure PVA increases with increasing GO content. The increase in intensity of the (101) diffraction peak at 19.4^{o} corresponds to the increase in the number of PVA chains packing together, resulting in more crystallinity in PVA during recrystallization from solution. The introduction of GO nanosheets into PVA, increases the intensity of the (101) diffraction peak.

It could be assumed that the fully exfoliated and well-dispersed graphene oxide nanosheets act as nucleating agents, and thus the crystallinity of the composites is improved [14]. It can be also noticed that, as the concentration of GO increases, the characteristic peak of GO at 11° starts to appear where as in Figure 4A.1(b), which shows the XRD pattern of RGO/PVA nanocomposites, there is no signature of GO even at higher concentrations which clearly indicate the almost complete reduction of GO in the RGO/PVA nanocomposites. In RGO/PVA composites also, the crystallinity is observed to be increasing with increasing RGO content. The RGO platelets in the PVA solution acts as nucleating sites and efficiently restrict and order the PVA chain arrangement due to its super-mechanical strength thereby increasing the crystallinity.
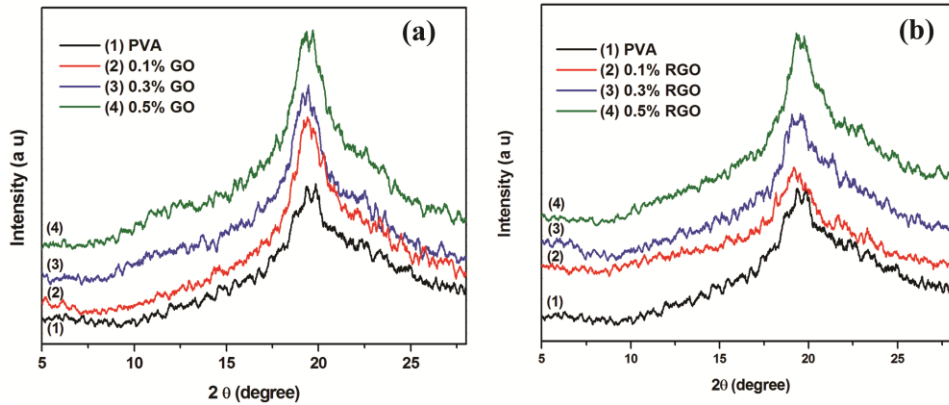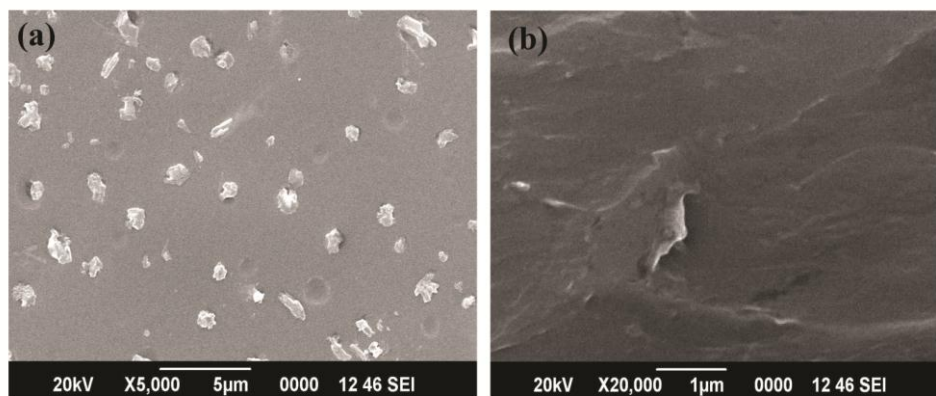

Figure 4A.1: XRD patterns of (a) GO/PVA and (b) RGO/PVA nanocomposites

4A.3.2 Morphology of the RGO/PVA nanocomposites

Figure 4A.2 shows the SEM images of RGO/PVA nanocomposites. The image of the surface of the composite shows a uniform and homogeneous distribution of RGO in the PVA matrix. The cross section

image clearly reveals the RGO nano sheet structure which is well exfoliated in the PVA matrix forming an excellent nanocomposite.

Figure 4A.2: SEM images of RGO/PVA nanocomposite (a) surface (b) cross section

Figure 4A.3 is another view of the SEM image of the cross section of RGO/PVA nanocomposite. It can be clearly seen that the uniform dispersion of RGO platelets with thickness in the nanometer regime were achieved in the RGO/PVA nanocomposites of this study. The platelet or sheet like morphology of the RGO is evident from the SEM images. Moreover, no agglomeration of the filler particles is observed. This clearly proves that the *in situ* reduction of GO within the polymer matrix is an excellent methodology to achieve nanocomposites with uniformly distributed RGO in the polymer matrix.

From the Energy dispersive Spectrum (EDS) analysis, it was found that the carbon content in the RGO in the PVA matrix is about 87%. This is a very good indication that the *in situ* reduction of GO was very effective.

Development of Reduced Graphene Oxide/Polymer Nanocomposites for Optical Limiting, Optical Actuation and Electrical Applications

129
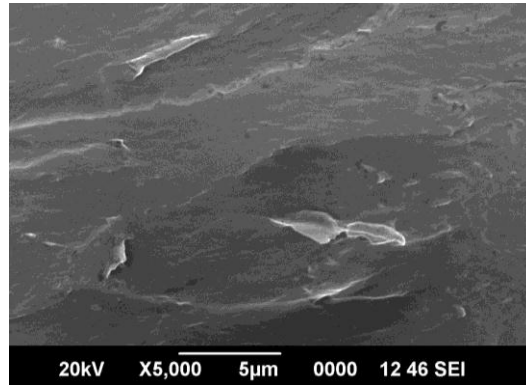
Figure 4A.3: SEM - cross section view of RGO/PVA nanocomposites

The AFM image of the surface of the RGO/PVA nanocomposite is given in Figure 4A.4. The topography clearly elucidates flat polymer surface with RGO platelets protruding outwards. The uniform distribution of RGO without any agglomeration in the PVA matrix is also clearly visible in the AFM image. The surface roughness is also found to be less than 40 nm which makes it suitable for optical applications also.
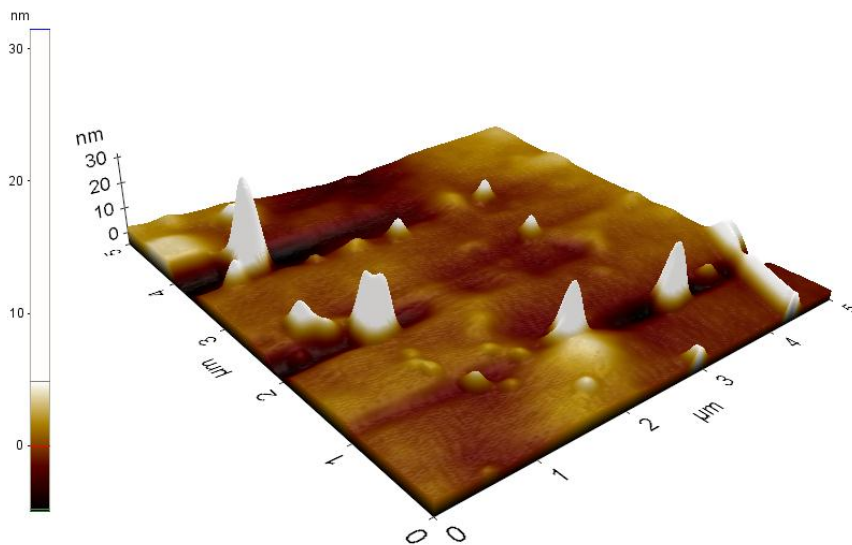
Figure 4A.4: AFM image of the RGO/PVA nanocomposite surface

4A.3.3 Thermal analysis

The thermogravimetric analysis (TGA) and its corresponding differential thermogravimetric analyses (DTA) of virgin PVA and 0.5% RGO/PVA composites are given in figure 4A.5 (a) and (b) respectively. It can be observed that there are mainly two degradation regions. The first weight loss region is upto around 150 $^{\circ}$C which is due to the loss of absorbed water molecules. The weight loss due to loss of water molecules in RGO/PVA composite is lower than that of virgin PVA which indicates that the moisture intake of the composite is reduced which is good for many practical applications. The onset of main degradation in virgin PVA is around 250 $^{\circ}$C where as it is considerably shifted to around 270 $^{\circ}$C in 0.5% RGO/PVA composite.
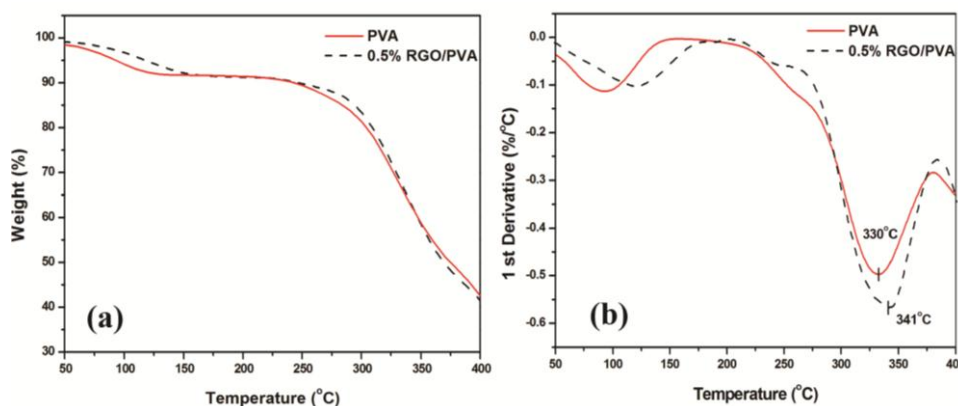
Figure 4A.5: Thermal characteristics of RGO/PVA composite (a) TGA (b) DTA

The temperature at which the rate of weight loss was maximum can be obtained from the peak temperature of the DTA curve. It can be observed that the peak temperature in DTA is shifted from 330 $^{\circ}$C of virgin PVA to 341 $^{\circ}$C in the composite. The molecular level interactions between PVA

and RGO such as hydrogen bonding between unreduced oxygen containing functional groups in RGO and hydroxyl groups in PVA may be the reason for an increased thermal stability [15]. Hence it is obvious that the addition of RGO even at a very low concentration can considerably improve the thermal stability of the virgin polymer which is very much desirable for practical applications.

The differential scanning calorimetry (DSC) of the virgin PVA and RGO/PVA composites in the temperature range –50 to 300 $^{\mathrm{o}}$C are given in Figure 4A.6. In pure PVA, we can observe a peak at around 85 $^{\mathrm{o}}$C which corresponds to the glass transition temperature (T_g) of PVA. The peak corresponding to T_g is a broad peak and the onset is from 38 $^{\mathrm{o}}$C. The peak corresponding to the melting point (T_m) is at 188 $^{\mathrm{o}}$C. With the incorporation of RGO, the T_g and T_m of the composite are dramatically improved. It can be observed that the T_g of pure PVA increases from 85 $^{\mathrm{o}}$C to 89 $^{\mathrm{o}}$C on addition of 1 wt.% RGO. The increase in T_m is more drastic in nature. With 1 wt.% RGO, the T_m was improved from 188 $^{\mathrm{o}}$C to 225 $^{\mathrm{o}}$C. As we have already observed in the XRD analysis, the crystallinity of PVA increases with RGO content. The DSC results also support this observation.

The thermal and mechanical properties of a semicrystalline polymer like PVA strongly depend on its crystallinity. Since we have seen from the XRD analysis that the crystallinity of PVA increases with increasing RGO content, we have calculated the crystallinity (χ_c) from the DSC data using the equation

$$\chi_c = \frac{\Delta H_m}{\Delta H_0}$$

Where ΔH_m is the measured melting enthalpy and ΔH_0 is the enthalpy of pure PVA crystal (138.6 Jg^{-1}) [16]. As clear from the Table 4.1, the crystallinity increases with RGO content. This clearly proves that RGO can nucleate and control the crystallisation of PVA.

Table 4.1: Crystallinity of RGO/PVA nanocomposites calculated from DSC data

Sample	ΔH_m (J g^{-1})	χ_c (%)	T_m (^{o}C)
Virgin PVA	29.38	21.19	188
0.5% RGO/PVA	44.51	32.11	223
1% RGO/PVA	50.59	36.50	225
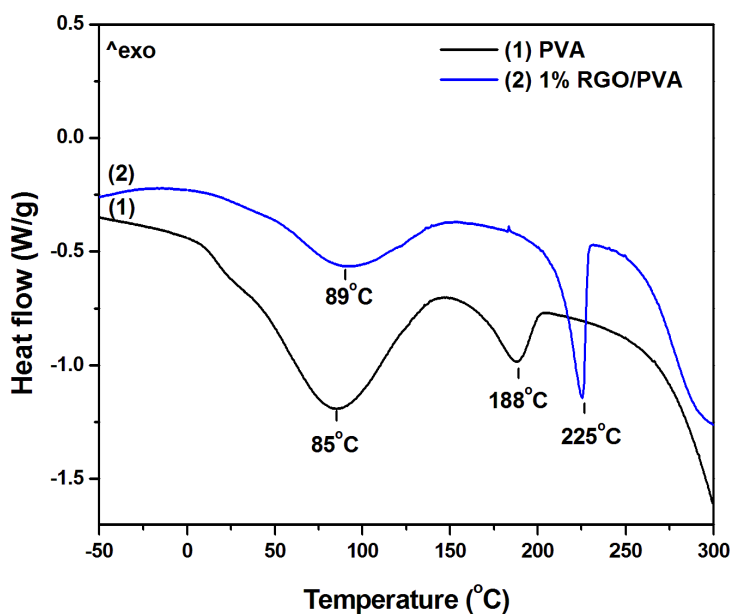
Figure 4A.6: DSC curve of pure PVA and RGO/PVA nanocomposite

The improvement in crystallinity of PVA with RGO content can help to achieve improved thermal and mechanical properties of the composites.

Development of Reduced Graphene Oxide/Polymer Nanocomposites for Optical Limiting, Optical Actuation and Electrical Applications

133

4A.3.4 Mechanical properties

Due to the large aspect ratio of RGO, it is expected to impart significant enhancement in mechanical properties [17-19]. The influence of RGO loading on the tensile strength of the composites is given in figure 4A.7. It can be observed that there is a huge enhancement of about 86% in the tensile strength of virgin PVA with an addition of 0.5 wt. % RGO as filler. However, with further addition of RGO, the enhancement in tensile strength is less. From 0.5 to 1 wt. % of RGO, the increase in tensile strength is only 11%. This is mainly due to the fact that, at lower filler loadings, the RGO is more uniformly dispersed and the residual hydroxyl groups in the RGO can interact with hydroxyl groups of PVA resulting in excellent reinforcing characteristics. On further increasing the RGO content, due to dilution effect, the enhancement is considerably less.
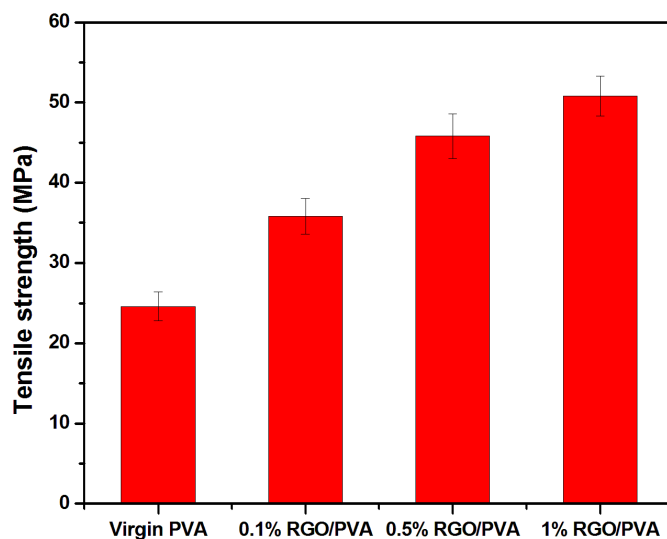
Figure 4A.7: **Tensile strength as a function of RGO wt % in RGO/PVA nanocomposite**

4A.3.5 Optical properties

The absorption spectra of RGO/PVA nanocomposites in the visible region are given in Figure 4A.8 (a). It can be observed that there is no significant absorption peaks in the visible wavelength region but the overall absorbance increases with RGO content. Hence it is possible to control the linear transmission properties by varying the RGO content in the PVA matrix. The absorption spectra of virgin PVA, GO/PVA and RGO/PVA composites in the lower wavelength region (ultraviolet region) are given in Figure 4A.8(b).
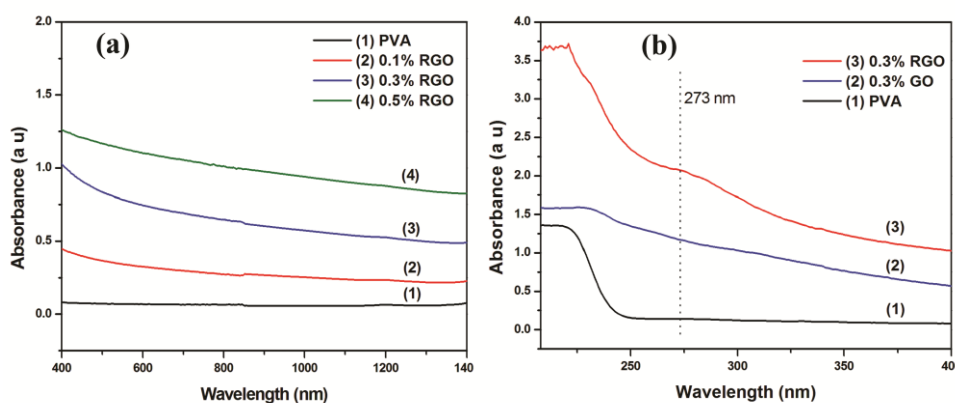
Figure 4A.8: **(a) Absorption spectra of RGO/PVA nanocomposites**
(b) absorption spectra of GO/PVA and RGO/PVA at lower wavelength region

The absorption peaks in the UV region give an indication of the electronic transitions which in turn depend on the number of sp^2 and sp^3 carbons. In GO, due to the presence of functional groups, sp^3 carbon atoms will be more. When GO is reduced, the number of sp^2 carbon atoms increases in the expense of sp^3 carbons. It can be observed that, other than the maximum absorption peak seen for both GO/PVA and RGO/PVA

composites at ~ 230 nm, the RGO/PVA composite shows an additional absorption peak at ~273 nm due to $\pi - \pi^*$ transition in C=C in the aromatic rings of RGO [20, 21]. This is an indication of the presence of almost completely reduced graphene oxide with regained π-conjugated network. As the number of sp^2 carbon atoms increases, there will be more conjugation and thus lesser energy is required for electronic transition and hence absorption at higher wavelength occurs.

4A.3.6 FTIR analysis

In order to understand the interaction of RGO with PVA, the FTIR analysis was performed in the range of 400 to 4000 cm^{-1} and the spectra are given in figure 4A.9. It can be observed that the broad peak between 3000 to 3600 cm^{-1} centred at around 3300 cm^{-1} in PVA corresponding to the O-H stretching vibrations is drastically diminished on addition of RGO.
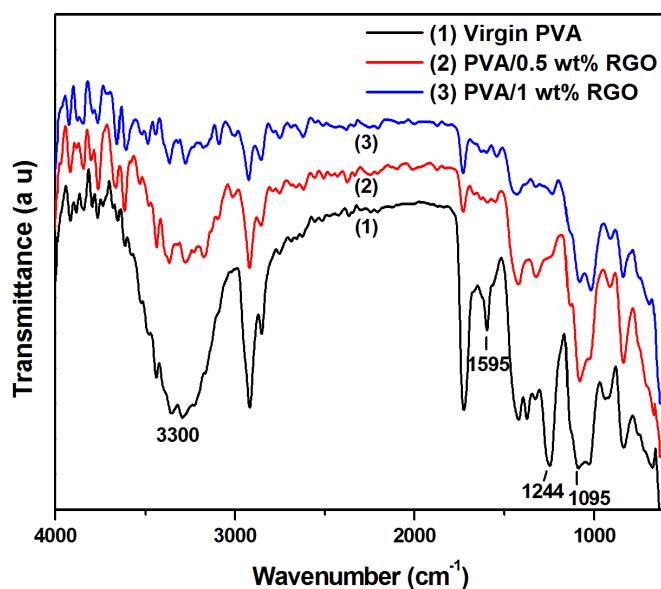
Figure 4A.9: FTIR spectra of RGO/PVA nanocomposites

It get further diminished with increasing RGO content. This is a clear indication that the hydrogen bonding and water absorption characteristics has been dramatically reduced with incorporation of RGO [15]. This makes the RGO/PVA composites more resistant to water absorption than pure PVA which is well preferred for many practical applications. This is also evident from the fact that the peak at around 1244 cm^{-1} corresponding to C-OH stretching vibration also diminishes with addition of RGO. The peak at 1595 cm^{-1} which is attributed to the scissoring vibrations of OH groups is also disappeared with the incorporation of RGO in to the PVA matrix. The peak at 1095 cm^{-1} corresponding to C-O vibrations also gets sharpened and shifts towards lower wavenumbers on addition of RGO indicating the interaction of RGO with PVA. From the FTIR analysis it is obvious that the incorporation of RGO in to PVA matrix results in the effective interaction of RGO with PVA thereby reducing the affinity of composite towards water which is a preferred modification for many practical device applications.

The interaction between the unreduced functional groups in RGO and hydroxyl groups in PVA is the major reason for improved thermal and mechanical stability and reduced water affinity in RGO/PVA nanocomposites. The schematic of the hydrogen bonding between hydroxyl and carboxylic acid groups in RGO and hydroxyl groups in PVA is given in figure 4A.10.
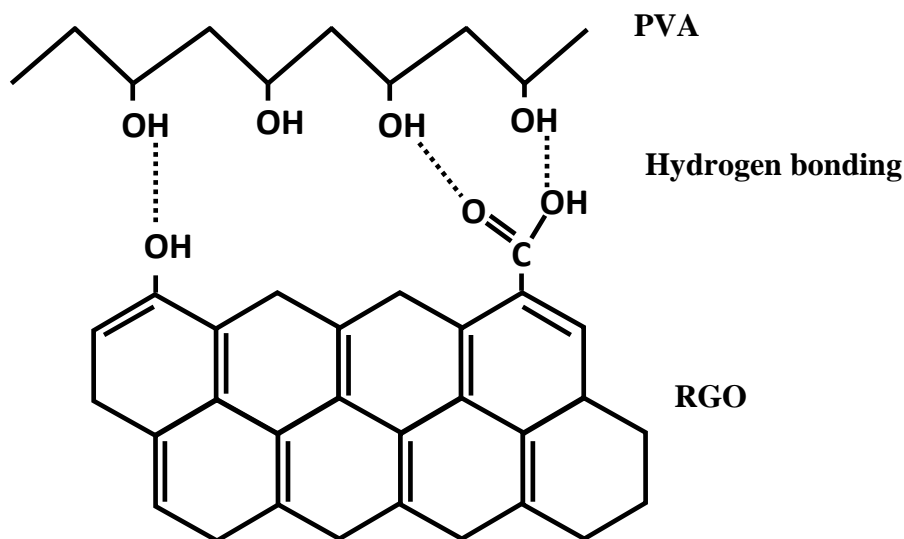
Figure 4A.10: Schematic of hydrogen bonding interactions between residual functional groups in RGO and hydroxyl groups of PVA

4A.4 Conclusions

RGO/PVA nanocomposites were prepared by the *in situ* reduction of GO with in the polymer. Uniform dispersion of filler particles enhanced the thermal and mechanical properties of the composite. Due to the nano scale distribution of RGO in the polymer matrix, enhancement in properties were achieved even with very low loading. PVA's affinity towards water was also significantly reduced with the incorporation of RGO making the composite more useful in practical applications.

PREPARATION AND CHARACTERIZATION OF THERMALLY REDUCED GRAPHENE OXIDE/THERMOPLASTIC POLYURETHANE NANOCOMPOSITES

4B.1 Introduction

Polyurethanes (PU) are widely used high-performance materials with unique properties including excellent elongation and high impact strength, good elasticity, excellent low temperature resistance, biocompatibility, etc. [22-24]. They have applications ranging from rigid foam as insulation in walls, roofs and appliances to flexible foam in upholstered furniture, as sealants, adhesives and coatings, as medical devices and in foot wears [25]. PU are thermoplastic or thermoset polymers formed from polyisocyanates with at least one other species containing active hydrogen such as polyols, polyamines, hydroxyl-terminated polyesters, polyethers or polycarbonates. Various filler materials including carbon black, carbon nanotubes, clays, etc. have been used to prepare PU composites which exhibit enhanced properties for many applications. PU composites and blends have wide applications in electronics and optoelectronics which include sensors, actuators, EMI shielding, electrolytes for supercapacitors, electrostatic dissipation and shape memory applications.

This part of the chapter discusses about the development and characterization of polyurethane based nanocomposite with RGO as the filler material. A poly ester based thermoplastic polyurethane is used as the matrix and thermally reduced graphene oxide (TRGO) has been used as the filler material.

4B.2 Experimental

4B.2.1 Preparation of thermally reduced graphene oxide - polymer composite

The preparation of thermally reduced graphene oxide (TRGO) is explained in detail in Chapter 3. The TRGO powder was uniformly dispersed in N,N-Dimethyl formamide (DMF) by ultrasonication. A polyester based Thermoplastic polyurethane (TPU) (Desmopan 385 S) was dissolved in DMF. To the polymer solution, TRGO dispersion in DMF was added and uniformly mixed using a mechanical stirrer followed by ultrasonication. The resultant slurry was then cast on a stainless steel mould preheated at 100 ^{o}C and dried at 120 ^{o}C for 2 h. The TRGO/TPU nanocomposite films were then peeled off from the mould. Composite films with varying weight percentage of filler loading were prepared under same conditions.

4B.2.2 Characterization

Fourier transform infra red spectroscopy (FT-IR, Avatar 370, Thermo Nicolet, Germany) were carried out in the ATR mode. A minimum of 60 scans were acquired with a resolution of 4 cm^{-1}. Back ground spectrum was captured before measurements and base line corrections were made using software.

The morphology of the composite films was studied using scanning electron microscopy (SEM, SU 6600, Hitachi, Japan). The TRGO/TPU composite film was fractured in liquid nitrogen and the SEM image of the fractured surface was recorded. High Resolution Transmission Electron Micrographs (HR TEM) of the thin slice of the composite film was also taken using a transmission electron microscope (JEM 2100, JEOL, Japan). The AFM image was recorded using Park XE 100, in non contact mode.

The mechanical properties of the composites were studied using Universal Testing Machine (Autograph, Shimadzu, Japan). The specimens were cut in dumbbell shape as per ISO 37 (type 4) standard. The samples were subjected to uniaxial tension at a displacement rate of 200 mm/min with a gauge length of 12 mm. All the measurements were recorded at room temperature.

4B.3 Results and Discussion

4B.3.1 Morphological analysis of TRGO/TPU nanocomposites

AFM analysis was carried out to understand the surface morphology of the composites. The surface topography of the TRGO/TPU nanocomposite is given in figure 4B.1. The RGO platelets protruding from the surface of the composites can be observed from the figure. The surface seems to be uniform and with a roughness of less than 30 nm which is quite acceptable even for optical applications.
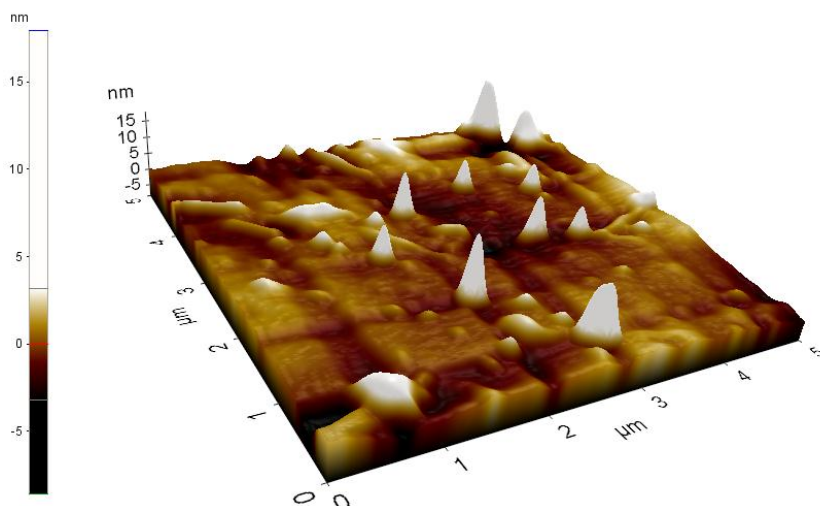
Figure 4B.1: AFM image of TRGO/TPU nanocomposite film

Development of Reduced Graphene Oxide/Polymer Nanocomposites for Optical Limiting, Optical Actuation and Electrical Applications

141

The uniform dispersion of TRGO in the TPU matrix is also evident from the SEM images of TRGO/TPU composite (Figure 4B.2). The uniformity of the filler particles in the polymer matrix ensures the improved properties as a composite material. Even though pure graphene is difficult to disperse uniformly in a polymer matrix, the residual functional groups present in the TRGO is responsible for the uniform dispersion in the polymer matrix. This clearly depicts that thermal reduction of GO is an effective method for synthesizing dispersible RGO for polymer composite preparation.
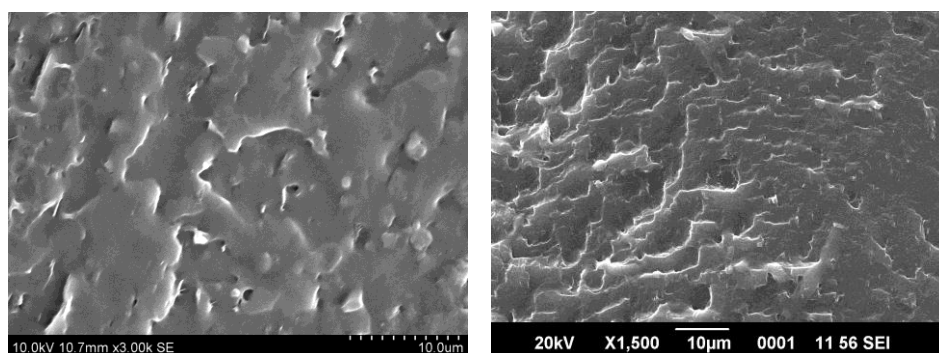
Figure 4B.2: SEM images of TRGO/TPU nanocomposites

4B.3.2 Mechanical properties of TRGO/TPU nanocomposites

The TRGO/TPU composites exhibit better mechanical properties when compared to virgin TPU (Table 4B.1). The stress-strain curves of TRGO/TPU composites are presented in figure 4B.3. The tensile strength and the elongation are improved at lower filler loading but decreases at higher filler loading. Since TRGO has very high surface to volume ratio, they can impart reinforcement to the polymer matrix at very low concentrations

itself [26]. At high concentrations of TRGO, due to the high volume fraction of TRGO, the polymer matrix gets diluted and hence the mechanical properties are decreased [27]. However, in all concentrations, the modulus is not affected very much which is a well desired property for many applications including actuators.

Table 4B. 1: Mechanical properties of TRGO/TPU nanocomposites

TRGO loading (wt.%)	Tensile strength (N/mm^2)	Elongation at break (%)	Tensile Modulus (N/mm^2)
0	46.68	808	5.77
0.5	54.83	1029	5.32
1.0	47.72	894	5.34
2.5	45.81	745	6.16
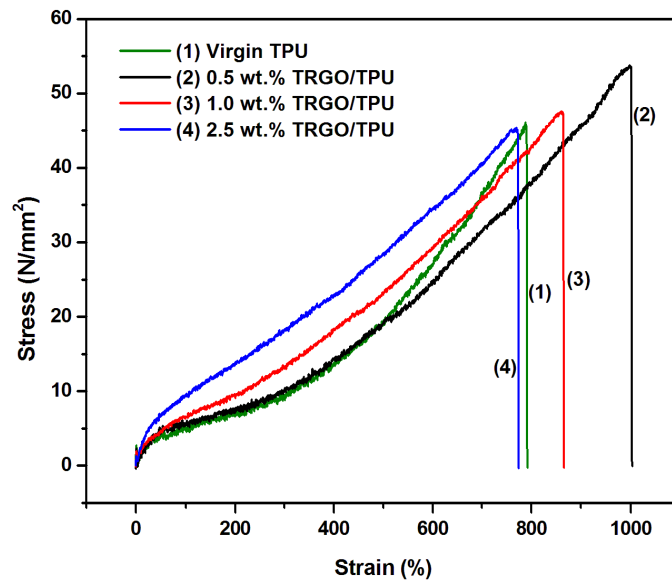
Figure 4B.3: stress-strain curves of TRGO/TPU nanocomposites

Development of Reduced Graphene Oxide/Polymer Nanocomposites for Optical Limiting, Optical Actuation and Electrical Applications

143

4B.3.3 Thermal properties of TRGO/TPU nanocomposites

The incorporation of TRGO has dramatically improved the thermal properties of the composite. The TGA and DTA curves of pure TPU and the 2 wt.% TRGO/TPU composite are given in figure 4B.4. It can be clearly observed that the thermal stability has increased with addition of TRGO and the peak in DTA for maximum weight loss has shifted from 382 ^{o}C in the case of pure TPU to 404 ^{o}C for 2 wt.% RGO/TPU composite. Similar increases in thermal stability with filler content were reported for other types of polyurethane/graphene composites also [28, 29]. The TPU used in this work is a linear ester-based polyurethane with hydrogen bonded urethane linkages (hard segments) and the ester (-COO-) groups of polyol soft segments. The curve also has a weight loss peak at lower temperatures (at around 310 ^{o}C for TPU) which may be due to the presence of soft segments in TPU.
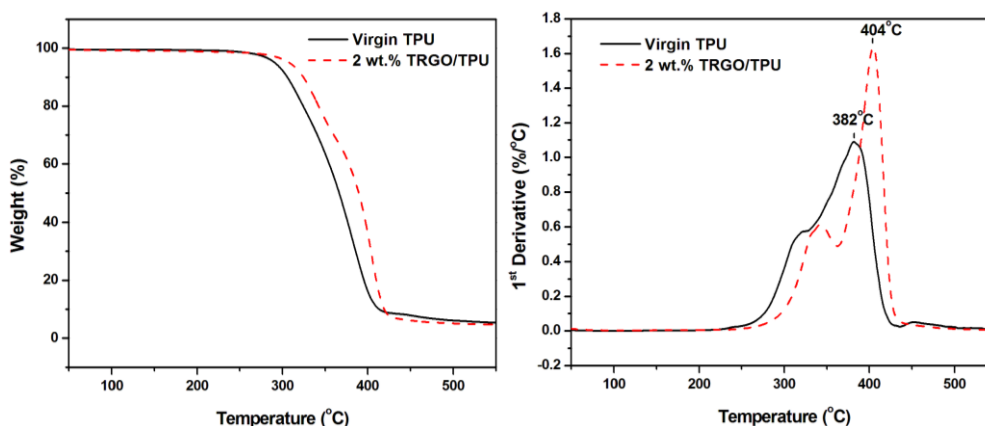
Figure 4B.4: TGA/DTA curves of TRGO/TPU composites

The differential scanning calorimetry (DSC) analysis was carried out to further understand the effect of RGO in the composite. The DSC curve is given in figure 4B.5. Since there is soft and hard segments in the TPU, there are multiple transition temperatures in the DSC curve of TPU. The T_g of virgin TPU was found to be around -39 ^{o}C which was slightly increased with addition of TRGO in to the matrix. This is well expected as the fillers can restrict the motion of polymer chains. However, there is no significant crystalline melting peak in the DSC of virgin TPU in the range 160 to 200 ^{o}C indicating that TPU is mostly amorphous in nature. There is only a very slight endothermic peak at 165 ^{o}C for pure TPU but in the case TRGO/PVA composites, the crystalline melting peak is more prominent.
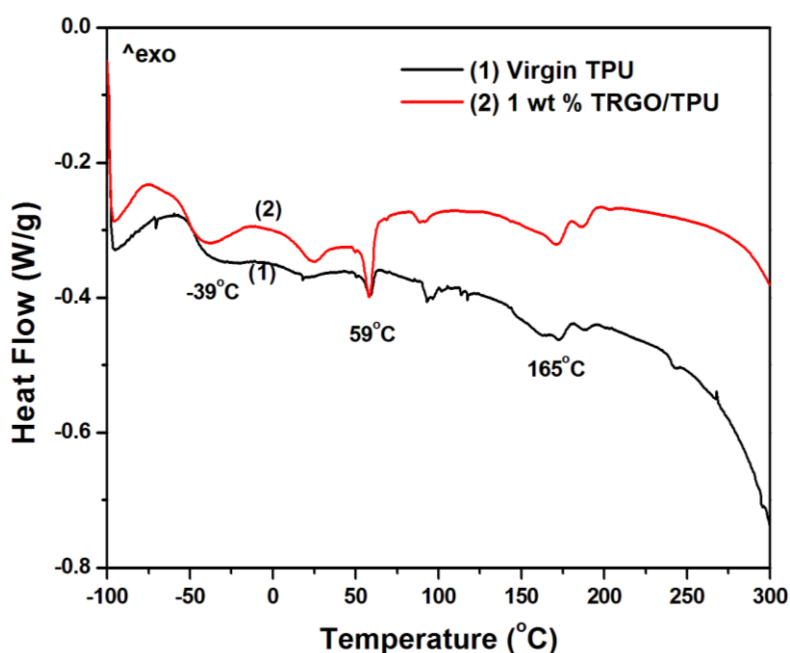
Figure 4B.5: DSC curves of TPU and TRGO/TPU nanocomposite

Development of Reduced Graphene Oxide/Polymer Nanocomposites for Optical Limiting, Optical Actuation and Electrical Applications

145

4B.3.4 FTIR analysis

The interaction between TRGO and TPU is very important for obtaining a very good composite material. The FTIR analysis was carried out to understand the existence of any interaction between the filler and the matrix (Figure 4B.6). The peak at 3618 cm^{-1} corresponding to the hydrogen bonding of N-H groups slowly get evolved after the addition of TRGO.
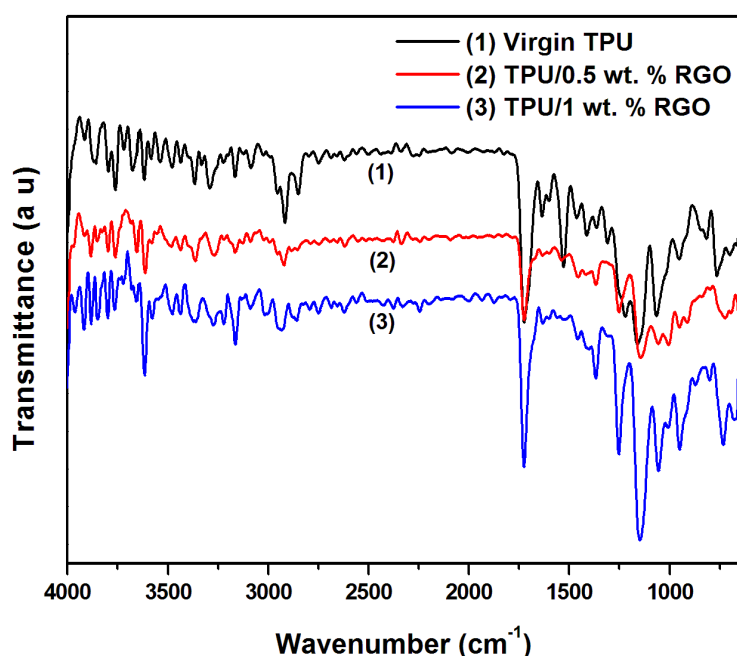
Figure 4B.6: FTIR spectra of TRGO/TPU nanocomposites

This clearly indicates that there is an interaction of RGO with TPU through hydrogen bonding between N-H groups of TPU and residual functional groups of TRGO. The -CH$_2$ stretching vibration peak at 2915 cm^{-1} and C-H stretching peak at 1525 cm^{-1} disappears with addition of TRGO. The peak at 1726 cm^{-1} is attributed to hydrogen-bonded carbonyl

groups in the urethane linkage (−H−N−COO−). The stretching of C−O and C−O−C peaks are present at 1145 and 1058 cm^{-1}, respectively [30]. The FTIR spectrum clearly shows that there is an effective interaction between TRGO and TPU which helps in better distribution of the filler material and enhancement in thermal and mechanical properties.

4B.3.5 Optical properties

The UV-visible spectra of pure TPU and TRGO/TPU composites are given in figure 4B.7. It can be observed that pure TPU is almost transparent in the entire visible region whereas the addition RGO even in small quantities decreases the transparency significantly which is well expected.
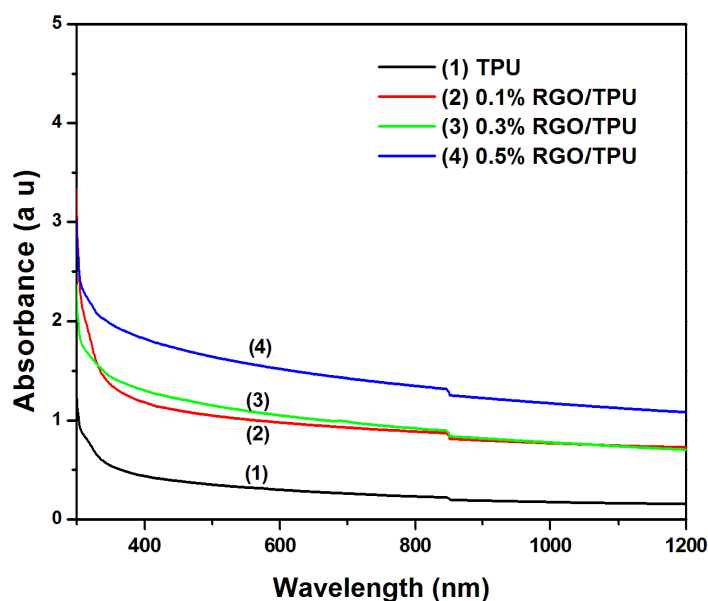
Figure 4B.7: UV- visible spectra of TRGO/TPU nanocomposites

4B.4 Conclusions

Thermally reduced graphene oxide/thermoplastic polyurethane composites were developed through a simple solvent casting method. The thermal and mechanical properties were found to improve with the incorporation of RGO. The unreduced functional groups in RGO were found to interact with the TPU polymer chains which helped to improve the properties. Flexible nanocomposites of RGO/TPU were developed which can find many functional engineering applications such as in stretchable and flexible wearable devices.

References

[1]   Verdejo, R., Bernal, M. M., Romasanta, L. J., & Lopez-Manchado, M. A. (2011). Graphene filled polymer nanocomposites. *Journal of Materials Chemistry*, *21*(10), 3301-3310.

[2]   Kumar, P., Yu, S., Shahzad, F., Hong, S. M., Kim, Y. H., & Koo, C. M. (2016). Ultrahigh electrically and thermally conductive self-aligned graphene/polymer composites using large-area reduced graphene oxides. *Carbon*, *101*, 120-128.

[3]   O'Masta, M. R., Russell, B. P., & Deshpande, V. S. (2017). An exploration of the ballistic resistance of multilayer graphene polymer composites. *Extreme Mechanics Letters*, *11*, 49-58.

[4]   Alam, A., Meng, Q., Shi, G., Arabi, S., Ma, J., Zhao, N., & Kuan, H. C. (2016). Electrically conductive, mechanically robust, pH-sensitive graphene/polymer composite hydrogels. *Composites Science and Technology*, *127*, 119-126.

[5]   Singh, B. P., Nayak, S., Nanda, K. K., Singh, A., Takai, C., Takashi, S., & Fuji, M. (2016). Transparent, flexible, and conducting films based on graphene–polymer composites. *Polymer Composites*.

[6]   Wan, Y. J., Yang, W. H., Yu, S. H., Sun, R., Wong, C. P., & Liao, W. H. (2016). Covalent polymer functionalization of graphene for improved dielectric properties and thermal stability of epoxy composites. *Composites Science and Technology*, *122*, 27-35.

[7]   Li, Y., Wang, S., & Wang, Q. (2017). Enhancement of tribological properties of polymer composites reinforced by functionalized graphene. *Composites Part B: Engineering*, *120*, 83-91.

[8]   Xue, Q., Lv, C., Shan, M., Zhang, H., Ling, C., Zhou, X., & Jiao, Z. (2013). Glass transition temperature of functionalized graphene–polymer composites. *Computational Materials Science*, *71*, 66-71.

[9]   Hu, K., Kulkarni, D. D., Choi, I., & Tsukruk, V. V. (2014). Graphene-polymer nanocomposites for structural and functional applications. *Progress in Polymer Science*, *39*(11), 1934-1972.

[10]   Roohani, M., Habibi, Y., Belgacem, N. M., Ebrahim, G., Karimi, A. N., & Dufresne, A. (2008). Cellulose whiskers reinforced polyvinyl alcohol copolymers nanocomposites. *European polymer journal*, *44*(8), 2489-2498.

[11]   Yusong, P., Jie, D., Yan, C., & Qianqian, S. (2016). Study on mechanical and optical properties of poly (vinyl alcohol) hydrogel used as soft contact lens. *Materials Technology*, *31*(5), 266-273.

[12]   Xu, S., Yu, W., Yao, X., Zhang, Q., & Fu, Q. (2016). Nanocellulose-assisted dispersion of graphene to fabricate poly (vinyl alcohol)/graphene nanocomposite for humidity sensing. *Composites Science and Technology*, *131*, 67-76.

[13]   Qian, X. F., Yin, J., Yang, Y. F., Lu, Q. H., Zhu, Z. K., & Lu, J. (2001). Polymer–inorganic nanocomposites prepared by hydrothermal method: Preparation and characterization of PVA–transition-metal sulfides. *Journal of applied polymer science*, *82*(11), 2744-2749.

[14]   Zhao, X., Zhang, Q., Chen, D., & Lu, P. (2010). Enhanced mechanical properties of graphene-based poly (vinyl alcohol) composites. *Macromolecules*, *43*(5), 2357-2363.

[15] Yang, X., Li, L., Shang, S., & Tao, X. M. (2010). Synthesis and characterization of layer-aligned poly (vinyl alcohol)/graphene nanocomposites. *Polymer*, *51*(15), 3431-3435.

[16] Liu, Y., Geever, L. M., Kennedy, J. E., Higginbotham, C. L., Cahill, P. A., & McGuinness, G. B. (2010). Thermal behavior and mechanical properties of physically crosslinked PVA/Gelatin hydrogels. *Journal of the mechanical behavior of biomedical materials*, *3*(2), 203-209.

[17] Li, J., Shao, L., Zhou, X., & Wang, Y. (2014). Fabrication of high strength PVA/rGO composite fibers by gel spinning. *Rsc Advances*, *4*(82), 43612-43618.

[18] Ma, H. L., Zhang, Y., Hu, Q. H., He, S., Li, X., Zhai, M., & Yu, Z. Z. (2013). Enhanced mechanical properties of poly (vinyl alcohol) nanocomposites with glucose-reduced graphene oxide. *Materials Letters*, *102*, 15-18.

[19] Bao, C., Guo, Y., Song, L., & Hu, Y. (2011). Poly (vinyl alcohol) nanocomposites based on graphene and graphite oxide: a comparative investigation of property and mechanism. *Journal of Materials Chemistry*, *21*(36), 13942-13950.

[20] Husaini, S., Slagle, J. E., Murray, J. M., Guha, S., Gonzalez, L. P., & Bedford, R. G. (2013). Broadband saturable absorption and optical limiting in graphene-polymer composites. *Applied Physics Letters*, *102*(19), 191112.

[21] Anand, B., Kaniyoor, A., Sai, S. S. S., Philip, R., & Ramaprabhu, S. (2013). Enhanced optical limiting in functionalized hydrogen exfoliated graphene and its metal hybrids. *Journal of Materials Chemistry C*, *1*(15), 2773-2780.

[22] Li, Y. J., Hanada, T., & Nakaya, T. (1999). Surface modification of segmented polyurethanes by grafting methacrylates and phosphatidylcholine polar headgroups to improve hemocompatibility. *Chemistry of materials*, *11*(3), 763-770.

[23] Shirasaka, H., Inoue, S. I., Asai, K., & Okamoto, H. (2000). Polyurethane urea elastomer having monodisperse poly (oxytetramethylene) as a soft segment with a uniform hard segment. *Macromolecules*, *33*(7), 2776-2778.

[24] Liu, Z., Bai, G., Huang, Y., Ma, Y., Du, F., Li, F., ... & Chen, Y. (2007). Reflection and absorption contributions to the electromagnetic interference shielding of single-walled carbon nanotube/polyurethane composites. *Carbon*, *45*(4), 821-827.

[25] Gurunathan, T., Rao, C. R., Narayan, R., & Raju, K. V. S. N. (2013). Polyurethane conductive blends and composites: synthesis and applications perspective. *Journal of Materials Science*, *48*(1), 67-80.

[26] Gao, J., Hu, M., Dong, Y., & Li, R. K. (2013). Graphite-nanoplatelet-decorated polymer nanofiber with improved thermal, electrical, and mechanical properties. *ACS applied materials & interfaces*, *5*(16), 7758-7764.

[27] Choi, J. T., Kim, D. H., Ryu, K. S., Lee, H. I., Jeong, H. M., Shin, C. M., ... & Kim, B. K. (2011). Functionalized graphene sheet/polyurethane nanocomposites: effect of particle size on physical properties. *Macromolecular Research*, *19*(8), 809-814.

[28] Liu, H., Dong, M., Huang, W., Gao, J., Dai, K., Guo, J., ... & Guo, Z. (2017). Lightweight conductive graphene/thermoplastic polyurethane foams with ultrahigh compressibility for piezoresistive sensing. *Journal of Materials Chemistry C*, *5*(1), 73-83.

[29] Bera, M., & Maji, P. K. (2017). Effect of structural disparity of graphene-based materials on thermo-mechanical and surface properties of thermoplastic polyurethane nanocomposites. *Polymer*, *119*, 118-133.

[30] Liu, S., Tian, M., Yan, B., Yao, Y., Zhang, L., Nishi, T., & Ning, N. (2015). High performance dielectric elastomers by partially reduced graphene oxide and disruption of hydrogen bonding of polyurethanes. *Polymer*, *56*, 375-384.

.....ৰু৹ঔ.....

OPTICAL LIMITING PROPERTIES OF REDUCED GRAPHENE OXIDE/POLYMER NANOCOMPOSITES

Contents

Part A
Nonlinear absorption and optical limiting properties of in situ reduced graphene oxide/poly(vinyl alcohol) nanocomposites.

Part B
Non linear absorption and optical limiting properties of thermally reduced graphene oxide/thermoplastic polyurethane nanocomposites.

5.1 Introduction

The last few decades have witnessed many revolutionary developments in the areas of photonics and optoelectronics. As a result, lasers and laser based devices are finding more and more applications every day. Protection from powerful lasers is one of the greatest concerns in the modern optoelectronic era and this makes the development of optical limiting materials extremely important. Human eyes and delicate optical sensors can be protected from powerful lasers by the use of optical limiting materials which transmit light at low intensities and limit the transmission above certain threshold input intensity [1]. In most of the materials, optical limiting is caused by various nonlinear light-matter interactions, especially nonlinear absorption, nonlinear refraction and nonlinear scattering [2]. In the recent past, enormous work has gone into the study of optical limiting behaviour of various materials such as carbon black suspensions,

Development of Reduced Graphene Oxide/Polymer Nanocomposites for Optical Limiting, Optical Actuation and Electrical Applications

153

semiconductor nanoparticles, organic nanocrystals, fullerenes, carbon nanotubes, organic chromophores and metal nanostructures [3-9]. However, for practical device applications, use of a single material or limiting mechanism cannot meet all the stringent application requirements and hence investigations on new material systems for optical limiting applications would be a noteworthy attempt.

Graphene, a single atom thick layer of sp^2 hybridized carbon atoms in a two dimensional structure, has emerged as one of the most promising material for optoelectronics [10]. Graphene exhibits extraordinary thermal, mechanical, electrical and optical properties owing to its unique structure. Recently, the nonlinear optical properties of materials in the graphene family including graphene oxide, graphene nanosheets and graphene nanoribbons have been studied extensively by many researchers [1,11-14]. Most of the studies reported excellent optical limiting properties of graphene materials when dispersed in a liquid medium. However, graphene materials dispersed in liquids always suffer agglomeration over a period of time restricting its use in practical device applications. From a device integration perspective, finding a suitable solid matrix for uniformly dispersing the graphene material is very significant. In this context, graphene/polymer composites, which combine the optical properties of graphene and structural properties of polymers, have the potential to emerge as a new class of optical limiters. Works in this direction had already been initiated by a few researchers [15-21]. However, the solubility and processability are the major issues for many prospective applications of graphene/polymer composites. In many cases, chemical functionalization of graphene is required to improve the solubility and processability to make polymer composites [15-21].

Nevertheless, the chemical functionalization can definitely alter the optical properties of graphene.

In this context, reduced graphene oxide has many advantages over pure graphene in polymer composites [22]. In graphene synthesis using chemical methods, graphene oxide is first synthesized from graphite using a strong oxidizing medium. After the separation of graphitic layers due to the incorporation of oxygen functional groups in graphene oxide, it is then reduced back to regain the sp^2 hybridised conjugated structure of graphene. At this stage, the complete reduction of graphene oxide resulting in a perfect crystalline graphene with no defects is practically very difficult. Invariably, there will be some defects or unreduced functional groups. Reduced graphene oxide (RGO) possesses almost similar properties to that of pure graphene and has better dispersibility in different solvents than graphene. Hence for polymer nanocomposite preparation, the RGO is well preferred.

For optical limiting applications, we have used two different polymer systems and accordingly two different methods for the preparation of RGO. In the first system, RGO/poly(vinyl alcohol) (PVA) nanocomposites were prepared by the *in situ* reduction of graphene oxide (GO) within the PVA solution and in the second system, a thermally reduced graphene oxide (TRGO) was used to prepare nanocomposites using a polyester based thermoplastic polyurethane (TPU). The nonlinear absorption (NLA) and optical limiting behaviour were studied using z-scan method as described in Chapter 2. This chapter is subdivided into two parts. The NLA and optical limiting properties of RGO/PVA are discussed in Part A and that of RGO/TPU is discussed in Part B.

Development of Reduced Graphene Oxide/Polymer Nanocomposites for Optical Limiting,
Optical Actuation and Electrical Applications

155

NONLINEAR ABSORPTION AND OPTICAL LIMITING PROPERTIES OF
IN SITU **REDUCED GRAPHENE OXIDE/POLY(VINYL ALCOHOL)**
NANOCOMPOSITES.

5A.1 Introduction

Unlike pure graphene, graphene oxide (GO), obtained through the chemical oxidation of graphite, is strongly hydrophilic and highly dispersible in water due to the presence of oxygen containing functional groups. GO is also a proven optical limiting material. The optical limiting properties of GO can be significantly improved by the partial reduction of GO [23, 24]. The composites of GO with water soluble polymers can be easily processed using simple solution processes like spin coating or drop casting. Hence, the *in situ* reduction of GO dispersed in the polymer solution, prepared through a simple processing technique, combines the advantages of a uniformly dispersed composite with improved optical limiting properties.

In this work, reduced graphene oxide (RGO)/Polyvinyl alcohol (PVA) nanocomposites were prepared through the *in situ* reduction of GO dispersed in PVA solution. Uniformly dispersed RGO/PVA composite films were formed by simple solution casting method. PVA was selected as the polymer matrix because of its good mechanical properties, excellent film forming nature and very good solubility in water. Moreover, the use of water alone as the solvent makes the whole process environmentally friendly. The non linear absorption properties and the optical limiting behaviour of RGO/PVA nanocomposites were studied using z-scan

technique. The effect of laser power density and the RGO content on the nonlinear absorption and optical limiting properties were also investigated.

5A.2 Experimental

The preparation of RGO/PVA nanocomposites is described in detail in Chapter 4. The nonlinear absorption and optical limiting characteristics were studied using a laser emitting 532 nm radiation (7 ns) by employing z-scan technique. The detailed description of the z-scan technique for the measurement of nonlinear absorption and optical limiting is given in Chapter 2.

5A.3 Results and discussion

5A.3.1 UV-Vis spectroscopy

The absorbance spectra of virgin PVA, GO/PVA and RGO/PVA nanocomposites in the lower wavelength region (ultraviolet region) are given in Figure 5A.1. The absorption peaks in the UV region give an indication of the electronic transitions which in turn depend on the number of sp^2 and sp^3 carbons. In GO, due to the presence of functional groups, sp^3 carbon atoms will be more. When GO is reduced, the number of sp^2 carbon atoms increases at the expense of sp^3 carbons. It can be observed that, other than the maximum absorption peak seen for both GO/PVA and RGO/PVA nanocomposites at ~ 230nm, the RGO/PVA composite shows an additional absorption peak at 273 nm due to $\pi - \pi^*$ transition in C=C in the aromatic rings of RGO [25, 26]. This is an indication of the presence of almost completely reduced graphene oxide with regained π-conjugated network. As the number of sp^2 carbon atoms

Development of Reduced Graphene Oxide/Polymer Nanocomposites for Optical Limiting, Optical Actuation and Electrical Applications

157

increases, there will be more conjugation and thus lesser energy is required for electronic transition and hence absorption at higher wavelength occurs.
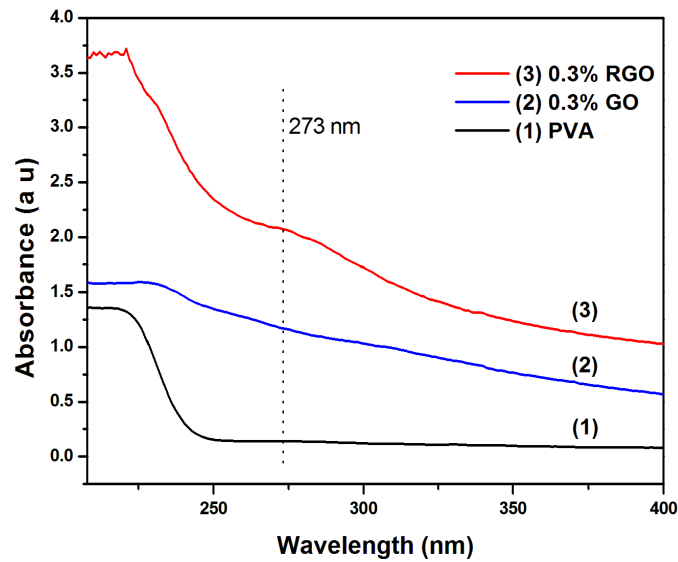

Figure 5A.1: **Absorption spectra of PVA, GO/PVA and RGO/PVA at lower wavelength region.**
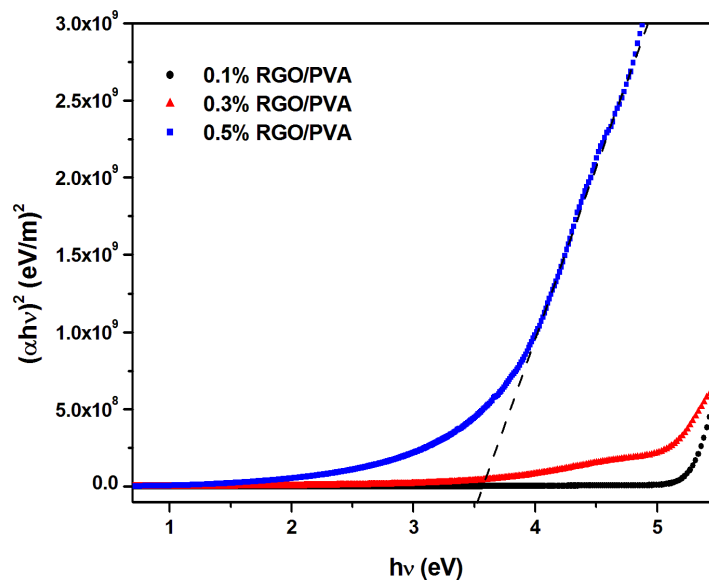

Figure 5A.2: **The tauc plot of RGO/PVA nanocomposites showing optical bandgap**

Figure 5A.2 depicts the tauc plot for the RGO/PVA nanocomposites. It can be noticed that the composites have a definite optical band gap particularly providing them semiconductor behaviour which essentially affects the optical properties.

5A.3.2 Non Linear absorption and Optical limiting Properties

The nonlinear absorption characteristics of the composites as obtained by open aperture z-scan technique for an irradiation wavelength of 532 nm is given in Figure 5A.3. The open-aperture curve exhibits a reduction in transmittance (valley) near the laser beam focus (z = 0). The presence of a normalized transmittance valley with symmetrical curves on both sides with respect to the focal point indicates typical nonlinear absorption (NLA) behaviour and occurrence of optical limiting in the composites [26].

Even though there are many mechanisms responsible for NLA in different materials, the normalized transmittance valley in graphene and graphene oxide materials can be mainly due to two mechanisms, reverse saturable absorption (RSA) and two photon absorption (TPA). RSA is a kind of excited state absorption (ESA) which originates due to inter band electron transition [27]. In TPA, two photons of identical frequencies are simultaneously absorbed. The optical limiting in RSA is due to the greater absorption of excited state than the ground. In TPA, at high intensities, various processes associated with TPA, including free carrier generation and absorption and defocusing due to induced change in refractive index, limit the throughput of light [28]. In graphene nanostructures, extent of π conjugation and defects can also affect the limiting mechanism. In

chemically reduced graphene oxide, it is certain to have some unreduced functional groups and defects. The presence of sp^3 hybridized domains in RGO can give rise to a finite band gap [29]. The tauc plot in figure 5A.2 clearly reveals that the RGO/PVA nanocomposites have a finite band gap. TPA normally occurs in semiconductors with band gap energy greater than the photon energy. Moreover, considering the absorbance in RGO/PVA composite at ~270 nm (in Figure 5A.1) it is reasonable to deduce that TPA plays an important role in the optical limiting of RGO/PVA nanocomposites at this wavelength (532 nm) [16]. In order to identify the NLA mechanism, the experimental z-scan data were numerically fitted with the transmission equation for TPA process as described in equation (5.1) [30]. The data were found to fit well with the TPA process confirming that TPA is the major mechanism for NLA and optical limiting in RGO/PVA nanocomposites of the present study.

$$T(z) = \frac{1}{q_0 \sqrt{\pi}} \int_{-\alpha}^{\alpha} \ln(1 + q_o e^{-t^2}) \, dt \quad \text{..(5.1)}$$

where

$$q_0(z, r, t) = \beta I_0(t) L_{eff}$$

Here, $L_{eff} = \dfrac{1 - e^{-\alpha l}}{\alpha}$ is the effective thickness with linear absorption coefficient α, nonlinear absorption coefficient β and I_0 is the irradiance at focus.

Figure 5A.3(a) shows the nonlinear absorption of RGO/PVA nanocomposites with different RGO loading at a laser intensity of 121 MW/cm^2. The solid curve in the figure is the theoretical fit to the experimental data which closely fits to a two photon absorption process. The depth of the valley in the z-scan curve is a direct indication of the NLA behaviour. The increase in depth of the valley in the z-scan curve with increase in RGO concentration indicates that the NLA increases with increasing RGO content. Moreover, the broadening of curves with increasing RGO content proves that optical limiting occurs at lower power for higher RGO concentration. This dependence of RGO concentration on nonlinear optical properties provides an opportunity to tune the nonlinear optical properties of the composites to our desired values by tuning the concentration of RGO in the polymer matrix which is very important for practical device applications.

The nonlinear absorption coefficient β for all the composites were calculated and is given in Table 5A.1. In an earlier report by Husaini et al., nonlinear absorption coefficient β_{eff} obtained for 50% functionalized graphene/PVA composites using a 785 nm laser (3.63 ns) was 5.4 cm/GW where as in this work, we have obtained 680 cm/GW for 0.5 wt. % RGO/PVA composite film with a low laser intensity of 121 MW/cm^2 (532 nm, 7 ns) [25]. Thus it is obvious that we could achieve very high non linear absorbance at extremely low RGO loading and very low laser intensity.

Development of Reduced Graphene Oxide/Polymer Nanocomposites for Optical Limiting,
Optical Actuation and Electrical Applications

161

The nonlinear absorption of the 0.3 wt. % RGO/PVA composite at various laser intensities is given in Figure 5A.3(b). It can be observed that as the laser intensity increases, the open aperture curve also gets broadened. This also proves that the RGO/PVA composite is an excellent optical limiter.
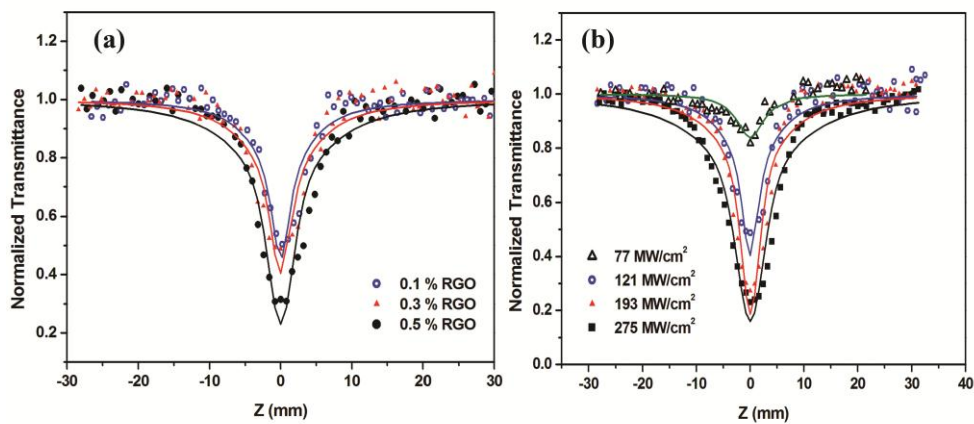
Figure 5A.3: Non linear absorption of (a) RGO/PVA nanocomposites with different filler loading at a laser intensity of 121 MW/cm² (b) 0.3% RGO/PVA composite at different laser intensities. Solid lines are theoretical fit to a TPA process.

The parameter q in equation 5.1 is a measure of the depth of the NLA curve. Figure 5A.4 gives the relation between q and input intensity. It can be observed that there is almost a linear relation between the input power density and depth of the NLA curve. This clearly depicts that the absorption increases steadily with increasing input power density which is the preferred property for an optical limiting material.
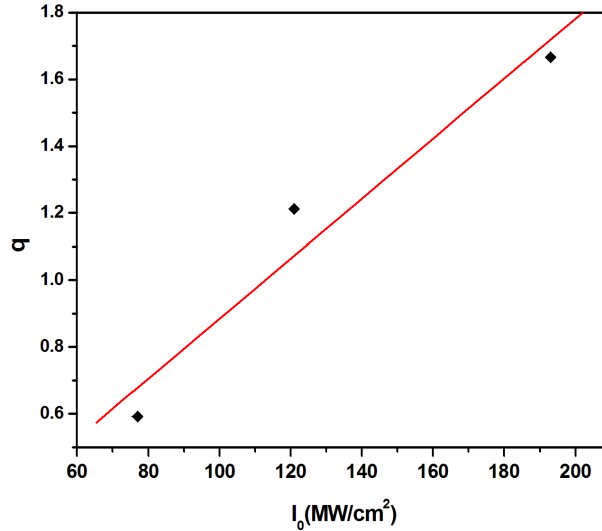
Figure 5A.4: Input power density (I₀) Vs depth of the NLA curve

The imaginary part of the third order susceptibility (χ^3) determines the strength of non linear absorption. Im (χ^3) can be calculated from the non linear absorption coefficient β using equation 5.2 [4].

$$\text{Im}(\chi^3) = \frac{n_0^2 c^2 \beta}{240\pi^2 \omega} \quad\text{...(5.2)}$$

where n_0 is the linear refractive index, c is the velocity of light in vacuum and ω is the angular frequency of the radiation.

The relation between Im (χ^3) and RGO concentration in PVA matrix is illustrated in figure 5A.5. It can be observed that the Im (χ^3) value increases with increase in RGO content and shows a tendency to level off at higher concentration of RGO which may be due to increase in linear absorption. It clearly shows that the nonlinear absorption of RGO/PVA composite films can be controlled by varying the RGO concentration.
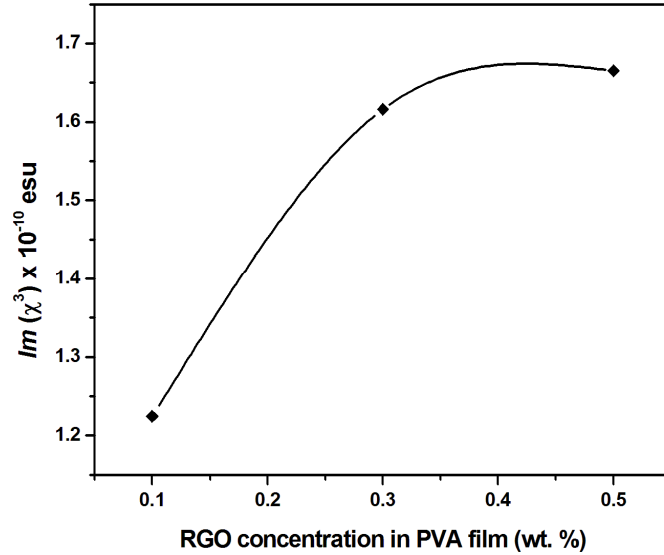
Figure 5A.5: Relation between Im (χ^3) and RGO concentration in PVA matrix

The non linear absorption of 0.3% GO/PVA and 0.3% RGO/PVA at a laser intensity of 275 MW/cm^2 is compared in Figure 5A.6. As expected the nonlinear absorption was more in RGO/PVA composite than in GO/PVA composite. It has already been reported that reduced graphene oxide has better NLA than GO by other research groups also [1, 31].

Table 5A.1: Nonlinear optical parameters of RGO/PVA nanocomposites

Composite	Nonlinear optical parameters at 532 nm			
	I_0 (x 10^{12} W/m^2)	β (x 10^{-9} m/W)	Im (χ^3) (x 10^{-10} esu)	P_{th} (MW/cm^2)
0.1% RGO/PVA	1.21	5.0	1.22	100
0.3% RGO/PVA	1.21	6.6	1.61	90
0.5% RGO/PVA	1.21	6.8	1.66	70
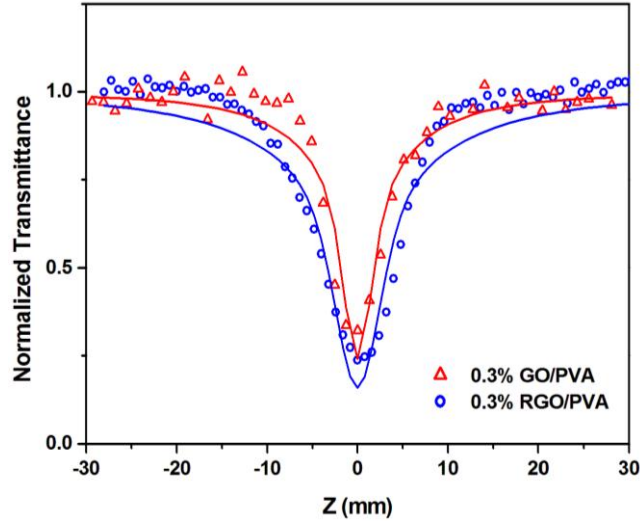
Figure 5A.6: Nonlinear absorption of 0.3% GO/PVA and 0.3% RGO/PVA at a laser intensity of 275 MW/cm^2. Solid lines are theoretical fit to a TPA process.

The optical limiting properties, derived from the z-scan data, are given in figure 5A.7. The RGO/PVA nanocomposites show excellent optical limiting properties. At higher intensities of light, the transmittance steadily decreases. For evaluating the optical limiting performance, one has to look into the optical limiting threshold power density (P_{th}). P_{th} is the input power density at which the onset of optical limiting starts. It is obvious that, lower the P_{th} better the optical limiting material. From the figure 5A.7(a), it can be observed that the composite films are transparent up to certain input power and there after it becomes opaque. Figure 5A.7(b) illustrates RGO concentration dependent output fluence as a function of input fluence. It can be observed that at higher intensities, all the three composites deviate from the linear transmission (solid line). The onset of deviation from the linear transmission is taken as P_{th} and is included in Table 5A.1. It is observed that, the P_{th} decreases with

Development of Reduced Graphene Oxide/Polymer Nanocomposites for Optical Limiting, Optical Actuation and Electrical Applications

165

increasing RGO content making better optical limiters at higher RGO concentration. This is very important from a practical device point of view. We can fine tune the threshold power of an optical limiting device by simply adjusting the concentration of the RGO in the polymer matrix.
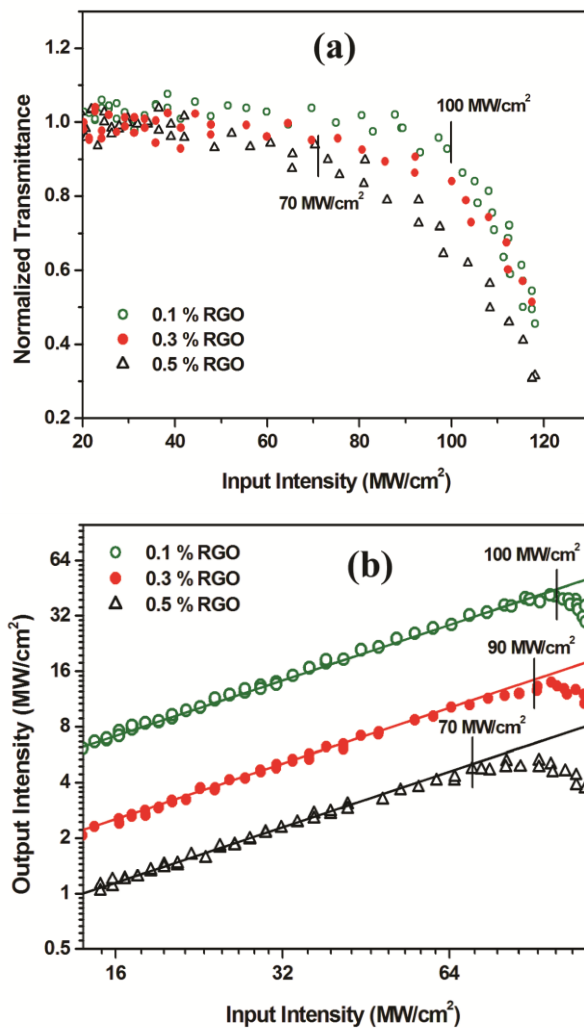
Figure 5A.7: Optical limiting properties of RGO/PVA nanocomposites (a) Normalized transmittance as a function of input laser intensity (b) Output laser intensity as a function of input laser intensity
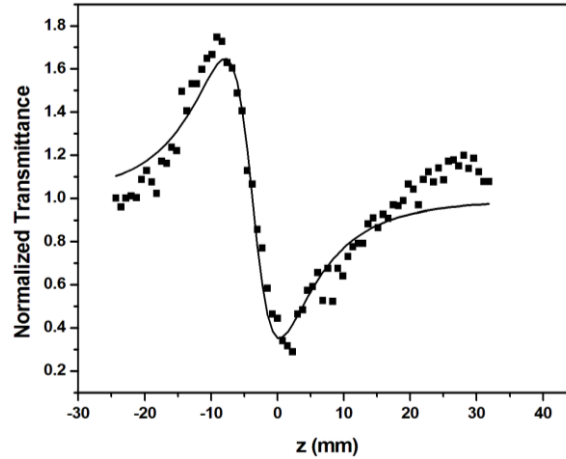
Figure 5A.8: Closed aperture z-scan traces of 0.3% RGO/PVA nanocomposites

Inorder to understand the sign of non-linear refraction closed aperture z-scan studies were also conducted. Figure 5A.8 represents the closed aperture z-scan traces of 0.3% RGO/PVA nanocomposites. It can be observed that the composite film shows a negative nonlinear refraction i.e., a peak followed by valley in the transmittance curve. The closed aperture z-scan can be used to understand the self refraction and self phase modulation effects. In this technique, the transmittance of the nonlinear medium is measured through an aperture placed in the far field as a function of sample position z. As the intensity varies with z position, the refractive index also varies ($n = n_0+n_2I$). Hence the sample can be considered as a thin lens with variable refractive index. When the sample is away from the focus (-z), the irradiance is low and hence there is negligible nonlinear refraction. As the sample moves towards focus, the irradiance increases and it results in self lensing in the sample. A negative self lens prior to focus will result in beam collimation and the beam gets narrowed at the aperture which in turn makes the transmittance to increase. As the sample

moves again, due to negative lensing, defocusing increases which results in beam broadening at the aperture and the transmittance decreases. Thus there is a minimum transmittance at focus (z_0). When sample is moved away from the focus (+z), irradiance is again reduced and transmittance increases. Thus the whole measurement results in a prefocal transmittance maxima (peak) followed by a post focal transmittance minima (valley) which is a typical signature of negative refraction nonlinearity.

5A.4 Conclusions

Poly(vinyl alcohol)/Reduced Graphene Oxide nanocomposites were successfully prepared by the in situ reduction of graphene oxide within the polymer matrix. The nonlinear optical properties of the composites were investigated using z-scan technique. The composites were having very good nonlinear absorption. We have obtained a very high nonlinear absorption coefficient 680 cm/GW for 0.5 wt. % RGO/PVA composite film with a low laser intensity of 121 MW/cm^2 (532 nm, 7 ns). The reduction of GO within the polymer matrix helped to form uniformly distributed RGO/PVA nanocomposites and hence very high non linear absorbance was achieved at extremely low RGO loading and very low laser intensity. The studies on optical limiting properties proved that these composites can be effectively used as very good optical limiters in practical applications. The nonlinear absorption and the optical limiting properties increased with increasing RGO content. The optical limiting properties can be tuned by adjusting the RGO concentration which is of paramount importance from an optical limiting application perspective. This low cost, nontoxic RGO/polymer composite can be a potential candidate for optical limiting applications.

NON LINEAR ABSORPTION AND OPTICAL LIMITING PROPERTIES OF THERMALLY REDUCED GRAPHENE OXIDE/THERMOPLASTIC POLYURETHANE NANOCOMPOSITES

5B.1 Introduction

The ease of processability along with stretchability and transparency has made thermoplastic polyurethanes (TPU) one of the most promising polymer materials for many consumable gadgets including wearable devices. The ability to form thin films and coatings has enabled TPU to find many potential applications in electronic and optoelectronic industries. In this section, the possibility of developing an optical power limiter using TRGO/TPU nanocomposites has been explored. The members of graphene family including graphene oxide, reduced graphene oxide, graphene ribbons, etc. were reported to exhibit nonlinear optical properties when irradiated with lasers. However, most of these studies were carried out by dispersing the active material in a suitable solvent. From a practical perspective, it is very much important to find out various suitable solid matrices to fabricate solid state devices. There have been a few reports on utilizing glass, plastic materials, gels, etc. as solid matrices for optical limiters. Elastomeric optical limiters can be of great interest for soft contact lenses and many smart devices. There have been a few reports on polyurethane based composites with fullerenes and carbon nanotubes (CNTs) for optical limiters [32-34]. However, to the best of our knowledge, not much work has gone into utilizing graphene/thermoplastic

polyurethane based composites for optical limiting application. Hence it is a noteworthy attempt to study the optical limiting applications of RGO dispersed in an elastomeric matrix like TPU.

5B.2 Experimental

The preparation of TRGO/TPU composite is explained in detail in Chapter 4. Thin films were prepared by solvent casting method. Samples with uniform surface were prepared for analysing the optical properties. The smooth surface morphology was confirmed by AFM analysis (Chapter 4). The nonlinear optical properties were studied using z-scan technique as described in Chapter 2.   A Q-switched Nd-YAG laser (532 nm, 7 ns) was used as the light source. The theoretical curve fitting for the deduction of optical parameters was done using Matlab software.

5B.3 Results and Discussion

5B.3.1 Linear optical properties

We have observed that the absorption in the UV-visible region increases with increasing RGO content which is well expected (Chapter 4). Moreover, as can be observed from figure 5B.1, the maximum absorption wavelength has shifted to higher wavelength with the addition of RGO into TPU. Due to the presence of conjugated carbon atoms in RGO, electronic transitions require lesser energy and hence absorption occurs at higher wavelengths. From the tauc plot in figure 5B.2, it can also be observed that, on addition of RGO, there is a finite band gap for the composite films which have profound effect on the optical properties.
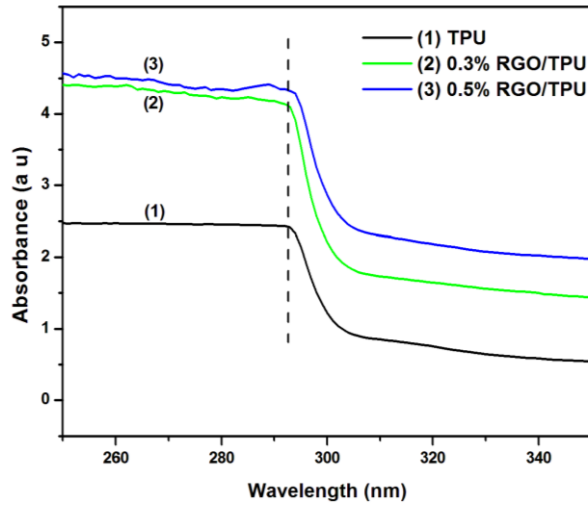
Figure 5B.1: Absorption spectra of RGO//TPU nanocomposites
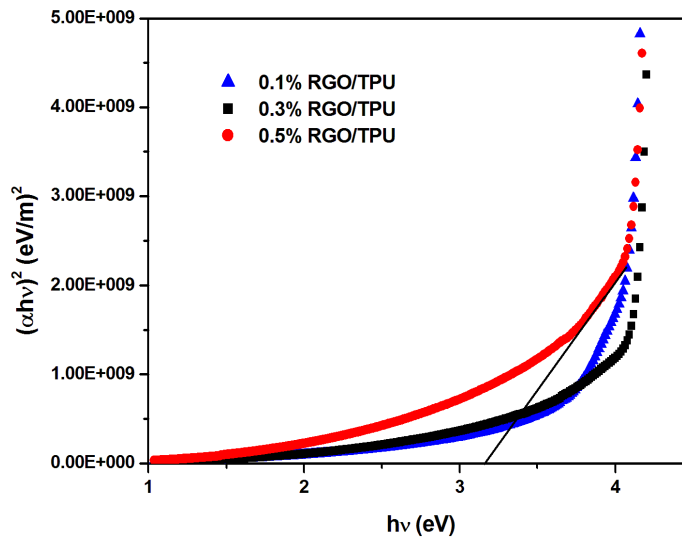
Figure 5B.2: The tauc plot of RGO/TPU nanocomposites showing optical bandgap

Development of Reduced Graphene Oxide/Polymer Nanocomposites for Optical Limiting, Optical Actuation and Electrical Applications

171

5A.3.2 Non Linear absorption and Optical limiting Properties

The nonlinear absorption characteristics of the RGO/TPU nanocomposites obtained through open aperture z-scan method is given in Figure 5B.3. It can be observed that, similar to the RGO/PVA nanocomposites, RGO/TPU nanocomposites also exhibit more absorption near to the focus creating a normalized transmittance with symmetrical curves on both sides of the laser beam focus (z=0). In order to understand the mechanism of non linear absorption, the curves were fitted with the standard equation for two photon absorption (TPA) process and the theoretical model gave a reasonable fit to the experimental curve confirming that TPA is the major mechanism for the NLA behaviour. However, there can be contributions from ESA also.
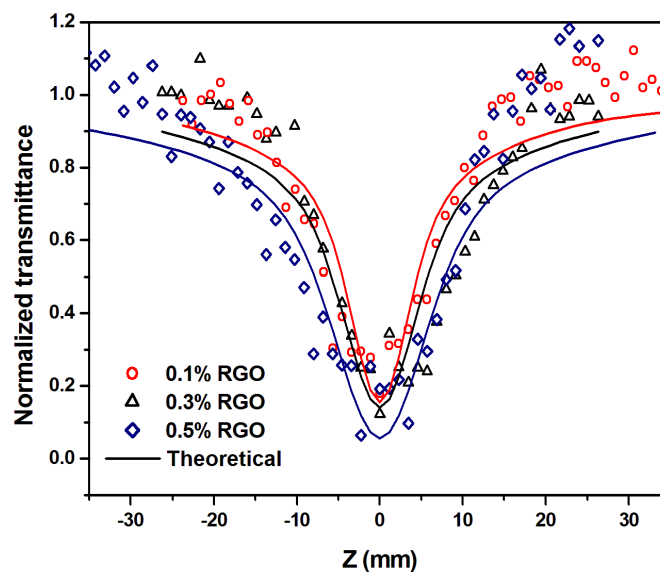
Figure 5B.3: **Non linear absorption in RGO/TPU nanocomposites - open aperture z-scan data at 87.6 MW/cm^2**

The depth of the absorption increases with increasing RGO content. Hence, the effective nonlinear absorption increases with RGO content. The NLA curve was also found to broaden with increasing RGO content which implies that as the RGO content increases, the sudden absorption of light occurs at a lower laser power. This is the property exactly required for an optical limiter. In order to further confirm this behaviour, 0.3% RGO/TPU composite was exposed to different laser powers and the NLA curve was recorded using open aperture z-scan method. The effect of laser power on NLA behaviour is represented in figure 5B.4. It can be observed that the depth and broadness of the curve increases with increasing laser intensity.
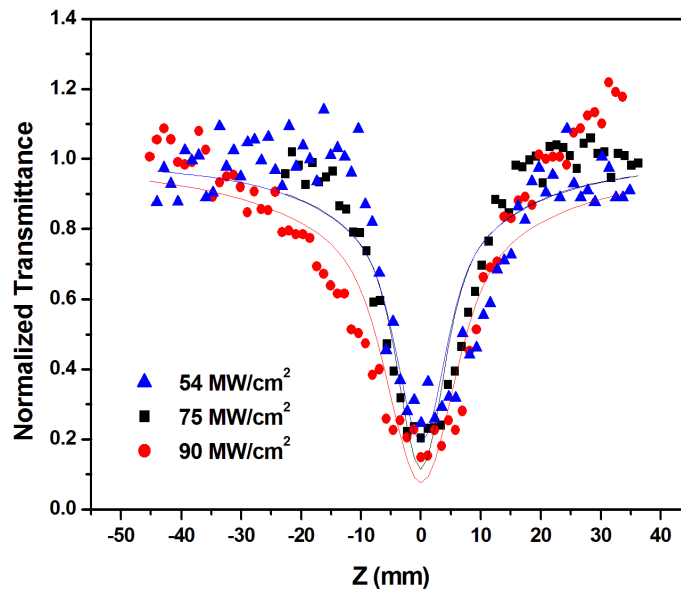
Figure 5B.4: **Nonlinear absorption of 0.3% RGO/TPU nanocomposites at different laser intensities**

Development of Reduced Graphene Oxide/Polymer Nanocomposites for Optical Limiting, Optical Actuation and Electrical Applications

173

The nonlinear optical parameters were calculated and summarised in table 5B.1. The values of Im (χ^3) were also calculated from the non linear absorption coefficient β using equation 5.2 and included in Table 5B.1. The variation of Im (χ^3) with RGO concentration is given in figure 5B.5. It can be noticed that the Im (χ^3) increases with RGO content. It proves that the NLA properties can be fine tuned by adjusting the RGO content. The q parameter which is a measure of depth of the NLA absorption curve also shows a linear increase with increasing intensity (Figure 5B.6).
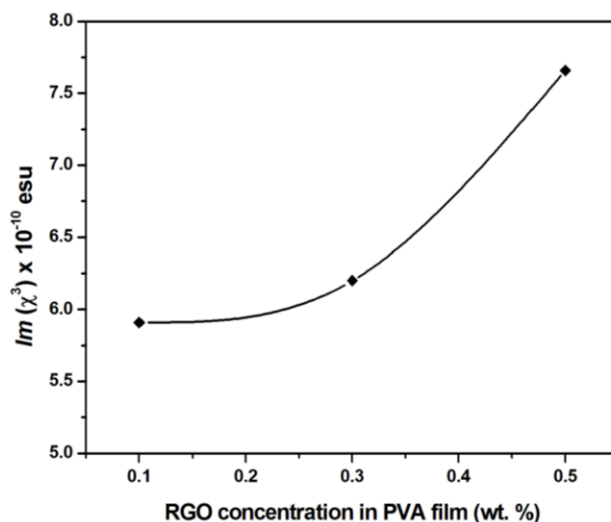
Figure 5B.5: Relation between RGO concentration and Im (χ^3)

The optical limiting behaviour of the RGO/TPU composite was derived from the z-scan data and are represented in figure 5B.7. It is clear from the figure that the composites exhibit excellent optical limiting behaviour and the optical limiting threshold decreases from about 50 MW/cm^2 to 15 MW/cm^2 up on increasing the RGO content to 0.5%.
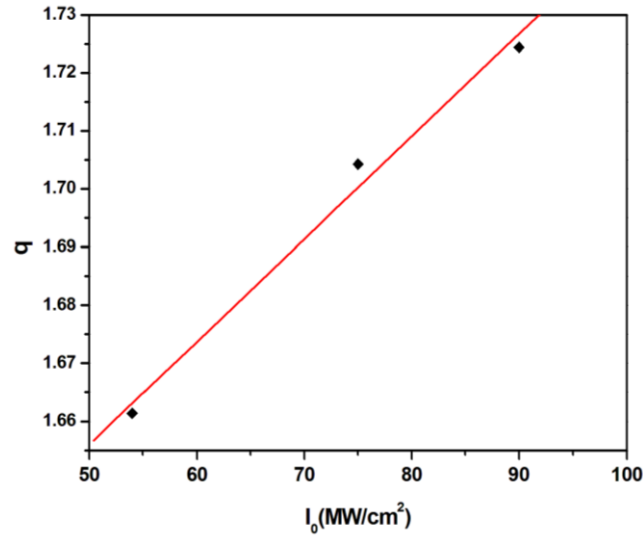
Figure 5B.6: Relation between q parameter and I₀
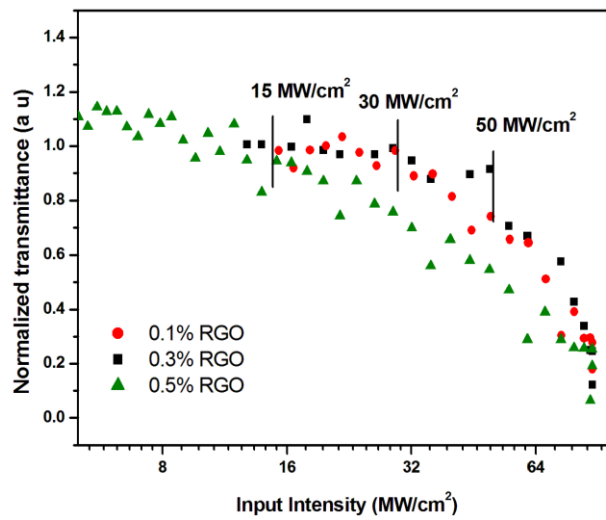
Figure 5B.7: Optical limiting in RGO/TPU nanocomposites

Development of Reduced Graphene Oxide/Polymer Nanocomposites for Optical Limiting, Optical Actuation and Electrical Applications

175

Table 5B.1: Nonlinear optical parameters RGO/TPU nanocomposites

Composite	Nonlinear optical parameters at 532 nm			
	I_0 (x 10^{11} W/m^2)	β (x 10^{-9} m/W)	Im (χ^3) (x 10^{-10} esu)	P_{th} (MW/cm^2)
0.1% RGO/TPU	8.76	23.5	5.91	50
0.3% RGO/TPU	8.76	24.7	6.20	30
0.5% RGO/TPU	8.76	30.5	7.66	15

5B.4 Conclusions

The z-scan measurements of RGO/TPU composite films revealed that they exhibit excellent nonlinear optical properties. The non linear absorption characteristics were found to increase with increase in RGO content. The major mechanism for the NLA behaviour in RGO/TPU nanocomposites is two photon absorption process. The composites also show excellent optical limiting behaviour. The optical limiting threshold was reduced by around 70% when the RGO content was increased from 0.1 to 0.5 wt%. This clearly indicates that the optical limiting properties can be controlled by adjusting the RGO content which is very much important from a practical device perspective.

References

[1]   Zhao, B., Cao, B., Zhou, W., Li, D., & Zhao, W. (2010). Nonlinear optical transmission of nanographene and its composites. *The Journal of Physical Chemistry C*, *114*(29), 12517-12523.

[2]   Xue-Qiong, Q., Hui-Xia, W. U., Rui, T. O. N. G., Shi-Xiong, Q. I. A. N., Yang-Hui, L., & Rui-Fang, C. (2008). Optical limiting properties of two soluble polymer/multi-walled carbon nanotube composites. *Chinese Physics Letters*, *25*(2), 536.

[3]   Vincent, D., Petit, S., & Chin, S. L. (2002). Optical limiting studies in a carbon-black suspension for subnanosecond and subpicosecond laser pulses. *Applied optics*, *41*(15), 2944-2946.

[4]   Irimpan, L., Nampoori, V. P. N., & Radhakrishnan, P. (2008). Spectral and nonlinear optical characteristics of nanocomposites of ZnO–CdS. *Journal of Applied Physics*, *103*(9), 094914.

[5]   Patra, A., Venkatram, N., Rao, D. N., & Radhakrishnan, T. P. (2008). Optical limiting in organic molecular nano/microcrystals: nonlinear optical effects dependent on size distribution. *The Journal of Physical Chemistry C*, *112*(42), 16269-16274.

[6]   Tutt, L. W., & Kost, A. (1992). Optical limiting performance of C60 and C70 solutions. *Nature*, *356*(6366), 225-226.

[7]   Chen, P., Wu, X., Sun, X., Lin, J., Ji, W., & Tan, K. L. (1999). Electronic structure and optical limiting behavior of carbon nanotubes. *Physical review letters*, *82*(12), 2548.

[8]   Zheng, Q., Gupta, S. K., He, G. S., Tan, L. S., & Prasad, P. N. (2008). Synthesis, Characterization, Two-Photon Absorption, and Optical Limiting Properties of Ladder-Type Oligo-p-phenylene-Cored Chromophores. *Advanced Functional Materials*, *18*(18), 2770-2779.

[9]   Han, Y. P., Luo, M. H., Wang, Q. W., Wang, J. X., & Gao, X. L. (2011). Synthesis of silver nanowires and investigation of their optical limiting properties. In *Advanced Materials Research* (Vol. 295, pp. 152-155). Trans Tech Publications.

[10]   Correa, D. S., De Boni, L., Nowacki, B., Grova, I., Fontes, B. D., Rodrigues, P. C., ... & Mendonça, C. R. (2012). Two-photon excitation and optical limiting in polyfluorene derivatives. *Journal of Polymer Science Part B: Polymer Physics*, *50*(2), 148-153.

[11]   Jiang, Y., Wang, Y., Yang, J., Hua, J., Wang, B., Qian, S., & Tian, H. (2011). Synthesis, two-photon absorption, and optical power limiting of new linear and hyperbranched conjugated polyynes based on bithiazole and triphenylamine. *Journal of Polymer Science Part A: Polymer Chemistry*, *49*(8), 1830-1839.

[12]   Sivasubramanian, D., Ponnusamy, R., & Gandhiraj, V. (2015). Low power optical limiting and thermal lensing in Mn doped ZnO nanoparticles. *Materials Chemistry and Physics*, *159*, 93-100.

[13]   Boni, L., Fonseca, R. D., Cardoso, K. R., Grova, I., Akcelrud, L., Correa, D. S., & Mendonca, C. R. (2014). Characterization of two-and three-photon absorption of polyfluorene derivatives. *Journal of Polymer Science Part B: Polymer Physics*, *52*(11), 747-754.

[14]   Saravanan, M., & Girisun, T. S. (2015). Nonlinear optical absorption and optical limiting properties of cadmium ferrite. *Materials Chemistry and Physics*, *160*, 413-419.

[15]   Bonaccorso, F., Sun, Z., Hasan, T., & Ferrari, A. C. (2010). Graphene photonics and optoelectronics. *Nature photonics*, *4*(9), 611-622.

[16]   Feng, M., Zhan, H., & Chen, Y. (2010). Nonlinear optical and optical limiting properties of graphene families. *Applied Physics Letters*, *96*(3), 033107.

[17]   Liu, Z., Wang, Y., Zhang, X., Xu, Y., Chen, Y., & Tian, J. (2009). Nonlinear optical properties of graphene oxide in nanosecond and picosecond regimes. *Applied physics letters*, *94*(2), 021902.

[18]   Liaros, N., Iliopoulos, K., Stylianakis, M. M., Koudoumas, E., & Couris, S. (2013). Optical limiting action of few layered graphene oxide dispersed in different solvents. *Optical Materials*, *36*(1), 112-117.

[19]   Wang, A., Yu, W., Huang, Z., Zhou, F., Song, J., Song, Y., ... & Shao, J. (2016). Covalent functionalization of reduced graphene oxide with porphyrin by means of diazonium chemistry for nonlinear optical performance. *Scientific reports*, *6*, 23325.

[20] Du, Y., Dong, N., Zhang, M., Zhu, K., Na, R., Zhang, S., ... & Wang, J. (2017). Covalent functionalization of graphene oxide with porphyrin and porphyrin incorporated polymers for optical limiting. *Physical Chemistry Chemical Physics*, *19*(3), 2252-2260.

[21] Zhu, G. A., Dong, Y. M., & Li, J. X. (2016). Preparation and Nonlinear Optical Properties of Poly (2, 3-Dimethylaniline) Grafted Reduced Graphene Oxide. In *Materials Science Forum* (Vol. 852, pp. 754-759). Trans Tech Publications.

[22] Sabira, K., Saheeda, P., Divyasree, M. C., & Jayalekshmi, S. (2017). Impressive nonlinear optical response exhibited by Poly (vinylidene fluoride)(PVDF)/reduced graphene oxide (RGO) nanocomposite films. *Optics & Laser Technology*, *97*, 77-83.

[23] Gan, Y., Feng, M., & Zhan, H. (2014). Enhanced optical limiting effects of graphene materials in polyimide. *Applied Physics Letters*, *104*(17), 171105.

[24] Wang, J., Feng, M., & Zhan, H. (2014). Preparation, characterization, and nonlinear optical properties of graphene oxide-carboxymethyl cellulose composite films. *Optics & Laser Technology*, *57*, 84-89.

[25] Husaini, S., Slagle, J. E., Murray, J. M., Guha, S., Gonzalez, L. P., & Bedford, R. G. (2013). Broadband saturable absorption and optical limiting in graphene-polymer composites. *Applied Physics Letters*, *102*(19), 191112.

[26] Anand, B., Kaniyoor, A., Sai, S. S. S., Philip, R., & Ramaprabhu, S. (2013). Enhanced optical limiting in functionalized hydrogen exfoliated graphene and its metal hybrids. *Journal of Materials Chemistry C*, *1*(15), 2773-2780.

[27] Zheng, X., Feng, M., & Zhan, H. (2013). Giant optical limiting effect in Ormosil gel glasses doped with graphene oxide materials. *Journal of Materials Chemistry C*, *1*(41), 6759-6766.

[28] Tutt, L. W., & Boggess, T. F. (1993). A review of optical limiting mechanisms and devices using organics, fullerenes, semiconductors and other materials. *Progress in quantum electronics*, *17*(4), 299-338.

[29] Zhou, Y., Bao, Q., Tang, L. A. L., Zhong, Y., & Loh, K. P. (2009). Hydrothermal dehydration for the "green" reduction of exfoliated graphene oxide to graphene and demonstration of tunable optical limiting properties. *Chemistry of Materials*, *21*(13), 2950-2956.

[30] Sheik-Bahae, M., Said, A. A., Wei, T. H., Hagan, D. J., & Van Stryland, E. W. (1990). Sensitive measurement of optical nonlinearities using a single beam. *IEEE journal of quantum electronics*, *26*(4), 760-769.

[31] Zheng, X., Jia, B., Chen, X., & Gu, M. (2014). In Situ Third-Order Non-linear Responses During Laser Reduction of Graphene Oxide Thin Films Towards On-Chip Non-linear Photonic Devices. *Advanced Materials*, *26*(17), 2699-2703.

[32] Zhang, T., Xi, K., Yu, X., Gu, M., Guo, S., Gu, B., & Wang, H. (2003). Synthesis, properties of fullerene-containing polyurethane–urea and its optical limiting absorption. *Polymer*, *44*(9), 2647-2654.

[33] Chen, Y., Muthukumar, V. S., Wang, Y., Li, C., Krishnan, S. S., Sai, S. S. S., ... & Mitra, S. (2009). Microwave-assisted solid-state grafting of multi-walled carbon nanotubes on polyurethane for the synthesis of a composite with optical limiting properties. *Journal of Materials Chemistry*, *19*(36), 6568-6572.

[34] Guo, S. L., Gu, B., & Zhang, T. (2004). Third-Order Nonlinearities and Optical Limiting of C60 Polyurethane–Urea Films. *Journal of Nonlinear Optical Physics & Materials*, *13*(01), 45-54.

.....ೞᓂ.....

OPTICAL ACTUATORS USING REDUCED GRAPHENE OXIDE/POLYMER NANOCOMPOSITES

Contents	*Part A* *Optical actuation of in situ reduced graphene oxide/poly(vinyl alcohol) nanocomposites*
	Part B *Thermally reduced graphene oxide/thermoplastic polyurethane nanocomposites as photomechanical actuators*

6.1 Introduction

Actuators are materials or devices which can undergo shape or mechanical change in response to an appropriate external stimulus [1]. In an actuator, the energy received from an external source triggers changes in the internal state of the system which can result in a much larger mechanical response than the initial input. There are different types of actuators depending on their properties and triggering mechanisms. Selection of a particular type of actuator depends on how best it can fulfil the technological requirements of a particular application. The most common materials used for actuation are piezoelectrics, ferroelectrics, shape memory alloys, electrostrictive materials and conducting polymers or polymer composites. Among the various actuator materials, polymers and their composites with unique advantages like low cost, light weight and good processability, have generated enormous interest in many technological fields such as micro robotics and artificial muscles [2, 3]. Moreover, they have stroke, force and

---

Part of this chapter was published as "Thermally reduced graphene oxide/thermoplastic polyurethane nanocomposites as photomechanical actuators", **M. N. Muralidharan** et al., *Advanced Materials Letters* 4 (2013) 927-932

efficiency similar to that of human muscles which make them the most preferred actuator systems for bio mimicking applications. Unlike conventional ceramic actuators, polymer actuators can give larger displacements even though the generative force is comparatively less.

Depending on the type of stimulus, actuators can be classified into electrical, thermal, chemical or optical actuators. In the present scenario, electrically triggered actuators hold the major share of actuator industry. In most of the actuator devices, an external power source like a battery or even a voltage generator is required to drive the actuators. The use of power devices can create problems when an actuator needs to be operated in or near the human body or other biological systems. Moreover, even with the latest technological advancements, batteries are still the most spacious and heavy parts in an electrical assembly. Additionally, toxicity of materials, requirement of constant recharge and frequent replacements poses disadvantages for these kind of systems. In some specialized areas like biomedical field, where actuators are directly dealing with living tissues, any stimulus other than electricity is much preferred. In this context, optically triggered polymer actuators are extremely useful. In addition to this, the unique advantages like wireless actuation and remote control makes optically triggered polymer actuators an attractive choice for many other applications [4]. Moreover, photo-induced actuation technologies offer additional advantages like low electromagnetic noise, easy construction, better scalability and capability of working in harsh environments.

Light triggered polymer actuators can be either pure polymers or polymer composites. In both the cases, actuator material system should have

an 'energy transfer' unit and a 'molecular switch' unit [5]. The energy transfer unit absorbs the light energy and transfers to the molecular switch unit which undergoes the mechanical change. The molecular switch unit is the polymer network itself whereas the energy transfer unit can either be a functional group as in the case of pure polymers or a filler material as in composites [6]. When compared to a pure polymer actuator material, polymer composite actuators have the advantage of improved mechanical and thermal properties and tunable actuator properties. In the last few years, many polymer composite systems were reported for optical actuator applications [7-14]. Carbon nanotubes (CNT) are the most widely studied energy transfer units for optical actuators. Many researchers have reported the use of CNT/polydimethyl siloxanes (PDMS) [1,4,9], CNT/liquid crystal elastomers (LCE) [1,11] and CNT/TPU [12] composites as optically triggered actuators. However, the inherent bundling nature of CNTs, high cost, poor dispersibility and intrinsic impurities have made them less attractive for practical applications.

Graphene, a single atom thick layer of graphite, is one of the most promising alternatives for CNTs due to their unique electrical, thermal and optical properties [15-17]. Graphene can be effectively utilized as a nanofiller for improving the mechanical, thermal, optical and electrical properties of composites even at very low loadings [18-23]. Graphene could also find a variety of applications in different types of actuators [24-29]. Due to the sp^2 carbon network of graphene, it possesses excellent thermal conductivity and IR absorption. Recently, a few research groups have utilized the unique properties of graphene as an energy transfer unit in light triggered polymer composite actuators [30-33]. Even though graphene have many advantages in terms of properties, cost and purity over CNTs and similar filler materials, the

Development of Reduced Graphene Oxide/Polymer Nanocomposites for Optical Limiting, Optical Actuation and Electrical Applications

183

low dispersibility of graphene is the major challenge for many applications of polymer/graphene composites. In most of the cases, this challenge is overcome by the chemical functionalization of graphene [34-37]. However, chemical functionalization can deteriorate many other important properties. Another alternative is the use of reduced graphene oxide. Graphene oxide (GO) is an intermediate obtained during the chemical synthesis of graphene. Thermal or chemical reduction results in removal of most of the oxygen containing groups yielding a graphene-like material, generally referred to as reduced graphene oxide (RGO). Even though RGO is less preferred in place of high quality electronic grade graphene for charge transport experiments due to the presence of oxygen residues and defects, RGO obtained from GO is considered as good as pristine graphene for many other practical applications including graphene/polymer composites. Moreover, RGO extends a more versatile possibility to fine tune its properties by controlling the extent of reduction. For polymer composite applications, the residual functional groups and defects make RGO more easily dispersible in polymer matrix.

In this chapter, optical actuation or the photomechanical actuation in RGO/polymer composites is studied using infrared (IR) light as the stimulus. RGO is used as the energy transfer unit which has excellent IR absorption characteristics and two different polymers, poly(vinyl alcohol) (PVA) and a thermoplastic polyurethane (TPU) are studied as the polymer matrices which act as the molecular switch unit. Part – A of this chapter discusses about the photomechanical actuation of RGO/PVA optical actuators which were prepared by the *in situ* chemical reduction of GO in PVA solution. In Part-B, optical actuation in RGO/TPU composites with thermally reduced graphene oxide (TRGO) as the filler, is discussed.

OPTICAL ACTUATION OF *IN SITU* REDUCED GRAPHENE OXIDE/POLY(VINYL ALCOHOL) NANOCOMPOSITES

6A.1 Introduction

Compared to graphene, graphene oxide (GO), an intermediate product obtained during chemical synthesis of graphene, is highly dispersible in water due to the presence of oxygen containing hydrophilic functional groups. GO can be easily dispersed in a water soluble polymer solution and the *in situ* reduction of GO within the polymer matrix results in homogeneous dispersion of reduced graphene oxide (RGO) in the polymer matrix. In this method, the composite films can be easily formed by simple processes like spin coating or drop casting.

In the present work, polyvinyl alcohol (PVA) was selected as the polymer matrix due to its biocompatibility, good mechanical properties, excellent film forming nature, and very good solubility in water. RGO/PVA nanocomposites were prepared through the *in situ* reduction of GO dispersed in PVA solution. Homogeneously dispersed RGO/PVA composite films were prepared by a simple solution casting process. In the whole process, water alone was used as the solvent and this makes the process environment friendly. The optical actuation of RGO/PVA photomechanical actuators under IR illumination was studied under various filler concentration and applied pre-strains.

6A.2 Experimental

The synthesis of RGO, prepration of composites and their characteristics have been explained in detail in chapters 3 and 4. The photomechanical actuation measurement procedure is explained in Chapter 2. A schematic of the optical actuation measurement process is given in figure 6A.1.
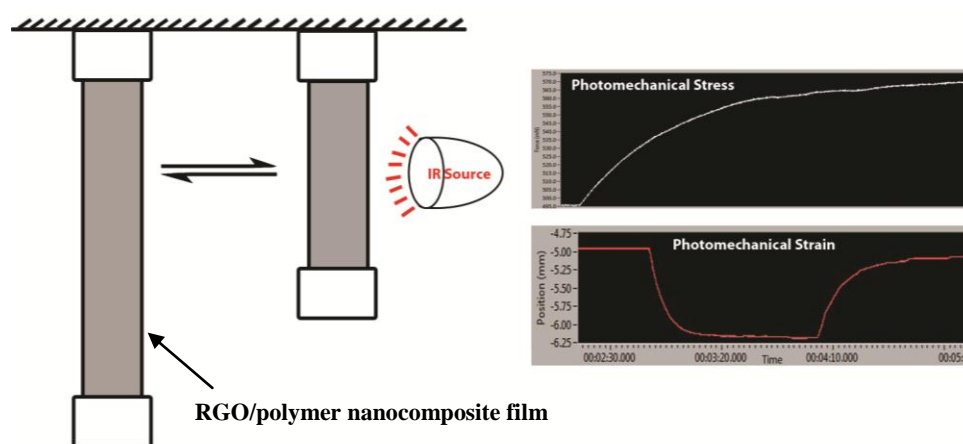
Figure 6A.1: Schematic of optical actuation measurement

6A.3 Results and discussions

6A.3.1 Effect of filler loading in photomechanical actuation

When illuminated with IR light, virgin PVA did not show any significant response. In the case of RGO/PVA composites, at lower concentrations, an expansion was observed initially which on continued irradiation showed a tendency of changing to contraction mode. As the concentration of RGO was increased, the time in expansion mode decreased and the contraction increased. At higher RGO loading, the

contraction mode was significantly larger both in time and magnitude than the expansion mode. The photomechanical response for different RGO loading under IR illumination is given in figure 6A.2 (a) and (b). The initial expansion is due to the thermal expansion of the material. PVA, being a semicrystalline polymer, has amorphous regions and crystalline regions in the matrix. As the IR irradiation continues, the crystalline regions in the polymer 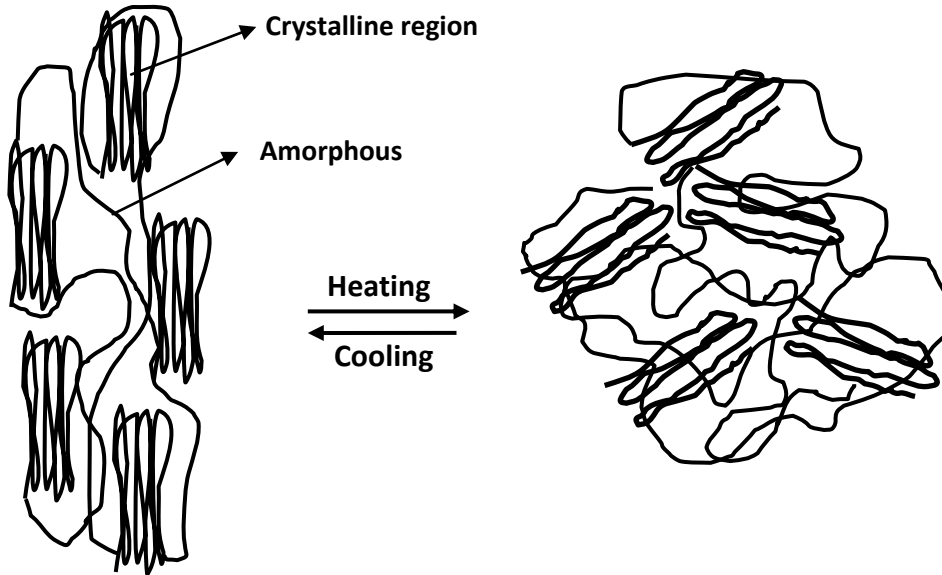get enough energy to relax resulting in coiling and entanglement of polymer chains. This leads to contraction. RGO acts as an IR absorber which transfers the energy to the polymer matrix where the amorphous regions expand whereas the crystalline regions contract. The contraction increases with increasing RGO content. This is well expected, as we have already discussed in Chapter 4 that the crystallinity increases with increasing RGO content. As the crystallinity increases, more crystalline domains undergo relaxation resulting in more coiling and entanglement of polymer chains which finally results in more contraction. The schematic of the process resulting in contraction of PVA with more crystalline regions is given in figure 6A.2 (c).
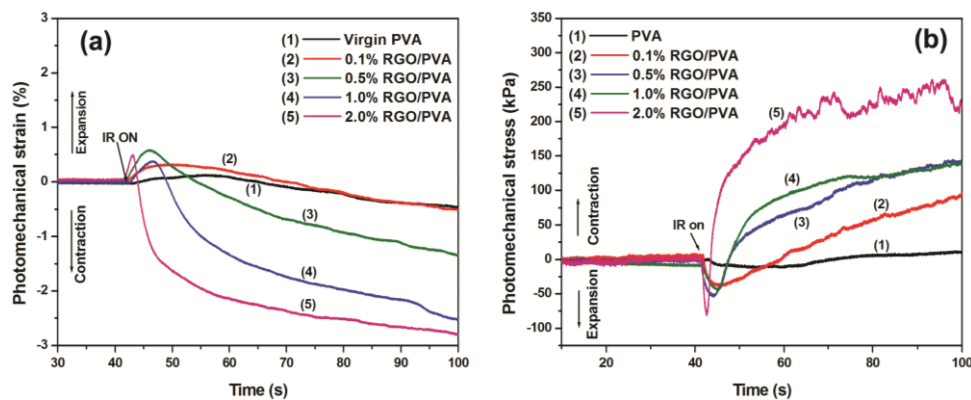
Figure 6A.2: **Photomechanical response of RGO/PVA nanocomposites with different filler loading (a) in strain mode (b) in stress mode**

Development of Reduced Graphene Oxide/Polymer Nanocomposites for Optical Limiting, Optical Actuation and Electrical Applications

187

Figure 6A.2 (c): Schematic of contraction in PVA with crystalline regions when exposed to IR light
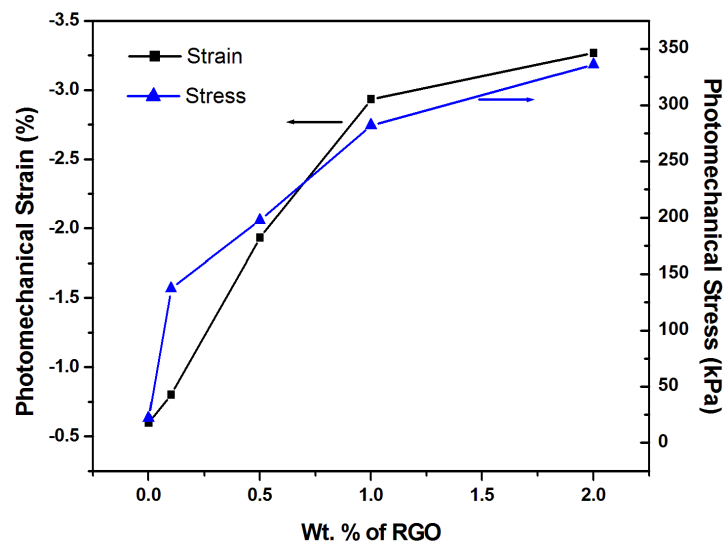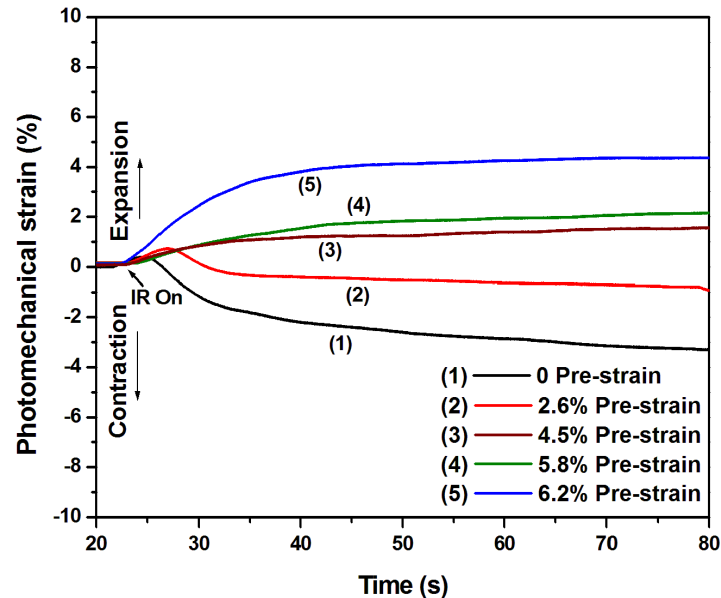

Figure 6A.3: Photomechanical actuation properties as a function of RGO loading.

The photomechanical strain and stress as a function of RGO loading is given in Figure 6A.3. It can be noted from figure 6A.3 that a

photomechanical strain of ~3.25% (contraction) with a stress of ~335 kPa was obtained for 2 wt.% RGO/PVA composite under an IR illumination intensity of only 16 mW/cm^2. The results give a promising indication that the optical actuation properties of RGO/PVA nanocomposites can be tuned by varying the RGO loading.

6A.3.2 Effect of pre-strain in photomechanical actuation

The optical actuation properties of RGO/PVA composites are greatly dependent on the structural properties of the polymer matrix. Inducing a pre-strain in the polymer composite before optical excitation can drastically affect the optical actuation properties. Optical actuation properties of the RGO/PVA nanocomposites were studied at different extents of pre-strain. Pre-strain was given by uniaxial stretching of the samples. It was observed that, on giving pre-strain, the contraction mode was changing to expansion mode. Figure 6A.4 shows the effect of pre-strain on photomechanical response of 1 wt. % RGO/PVA composite. The change from contraction to expansion mode is obvious from the figure 6A.4. Without any pre-strain, 1wt.% RGO/PVA composite shows a contraction of ~3%. As the pre-strain increases, the contraction decreases. On giving pre-strain, the expansion mode competes with contraction mode and at lower pre-strains, the net effect is observed as a decrease in stress (contraction mode). Above 4.5% pre-strain, the actuation mode is completely changed to expansion mode. At around 6.2% pre-strain, ~3% photomechanical strain in expansion mode, which is exactly opposite to the no pre-strain effect, is obtained. This clearly shows the possibility of tuning the optical actuation behaviour by judiciously selecting the required pre-strain.

Development of Reduced Graphene Oxide/Polymer Nanocomposites for Optical Limiting, Optical Actuation and Electrical Applications

189

Figure 6A.4: Photomechanical response of 1 wt. % RGO/PVA nanocomposite actuator at various applied pre-strain

The change in mode of actuation on applied pre-strain can be explained based on the change in crystallinity of the polymer. Since PVA is a soft polymer, when stretched, instead of strain induced crystallization, the crystalline regions get disrupted and the crystallinity is lost. This is evident from the XRD patterns of un-stretched and stretched polymer films as given in Figure 6A.5. It can be seen that the intensity of the characteristic peak of PVA at $2\theta=19^{o}$ is diminished and more broadened. At higher filler loading, it is easier to disrupt the crystallinity due to dilution effect. Hence only a low applied pre-strain is required for changing the actuation mode from contraction to expansion. This is evident from the photomechanical response of 2 wt.% RGO/PVA composite actuator at various applied pre-strain as given in Figure 6A.6. For 2 wt.%

RGO/PVA composite, only 3.3% pre-strain was required for the complete conversion of the contraction mode to expansion mode.
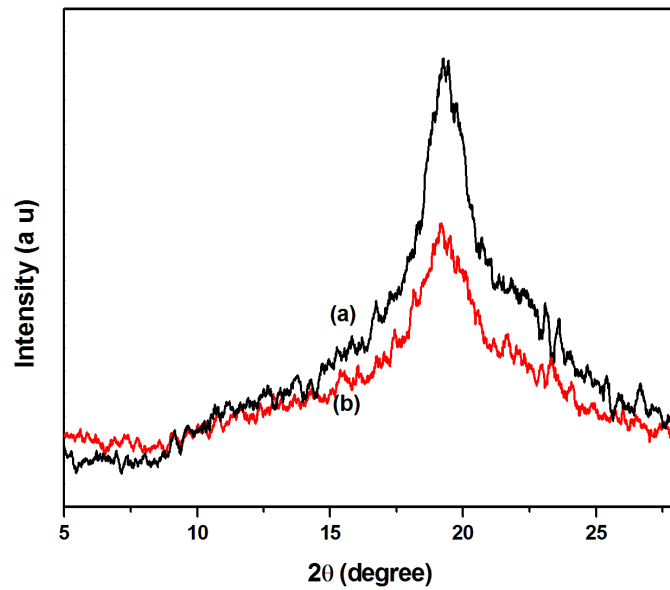
Figure 6A.5: XRD pattern of 1 wt.% RGO/PVA composite
(a) un-stretched and (b) after giving pre-strain
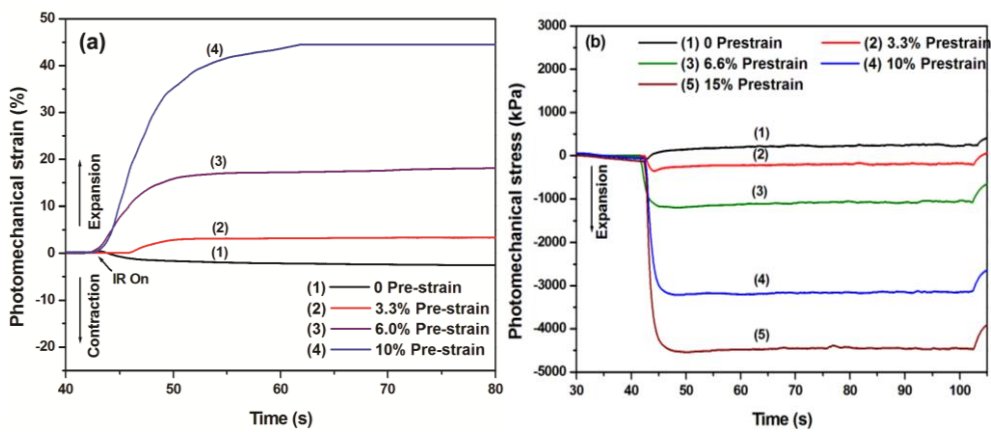
Figure 6A.6: Photomechanical response of 2 wt. % RGO/PVA composite actuator at various applied pre-strain
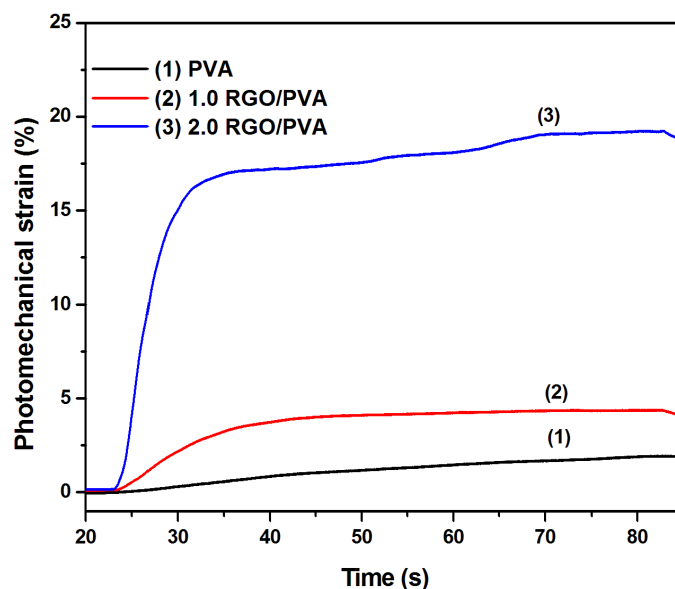
Figure 6A.7: Photomechanical response of RGO/PVA composites at 6.0% applied pre-strain

The increase in photomechanical strain of virgin PVA to 2 wt. % RGO/PVA composite was almost 5 times (contraction mode) when no pre-strain was applied (Figure 6A.3). However, when a 6% pre-strain was given, the increase in photomechanical strain was almost 9 times (expansion mode) from virgin PVA to 2 wt.% RGO/PVA nanocomposite. The photomechanical stress was also found to increase with increasing pre-strain (Figure 6A.7).

The photomechanical properties of 2 wt.% RGO/PVA nanocomposite at various applied pre-strain is given in Figure 6A.8. It can be observed that a photomechanical strain as high as 44% and a stress of 4.5 MPa was obtained for the RGO/PVA composites. This clearly establishes this

composite as a very useful optical actuator material for practical device application including robotics and artificial muscles.
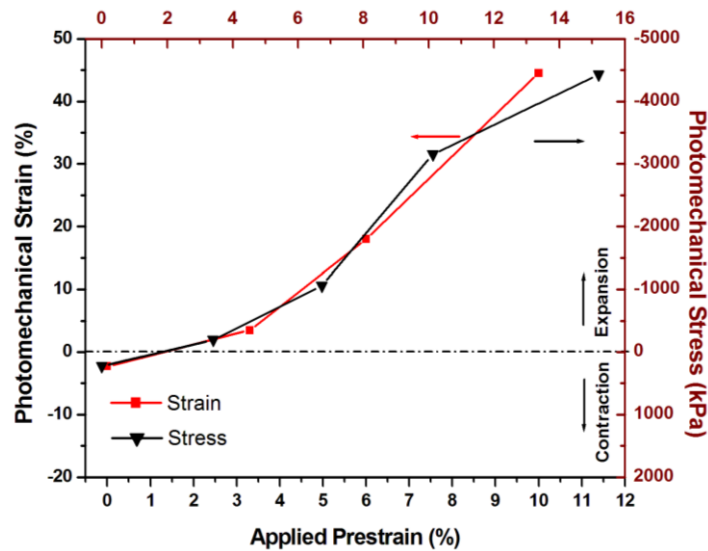
Figure 6A.8: Photomechanical actuation properties of 2 wt. % RGO/PVA composite as a function of applied pre-strain.

6A.3.3 Reversibility of actuation

The reversibility of actuation is very important for many practical applications like optically triggered switches or valves. RGO/PVA composites exhibited good reversibility in optically triggered actuation. Figure 6A.9 shows the reversibility of 1 wt. % RGO/PVA composite actuators on optical actuation. The reversibility continues to be intact even after several cycles. It can be also noted that almost 80 % of the actuation is completed within 10 seconds which shows that the optical actuation is fast enough for practical applications.

Development of Reduced Graphene Oxide/Polymer Nanocomposites for Optical Limiting,
Optical Actuation and Electrical Applications

193
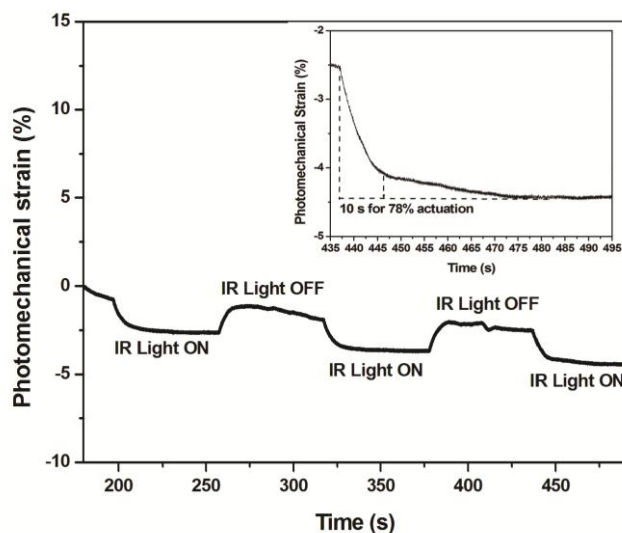
**Figure 6A.9: Reversibility of optical actuation of 1 wt. %
RGO/PVA composite under IR illumination.**

6A.4 Conclusions

The photomechanical actuation behaviour of RGO/PVA nanocomposites were studied and found to exhibit excellent actuation behaviour. The photomechanical actuation properties were found to increase with increasing RGO content. Without any pre-strain, the composite actuators exhibited contraction in response to IR light. When a pre-strain was applied, the contraction mode was changed to expansion mode. The study provides promising possibility of tuning the actuation behaviour either by tuning the filler content or by giving a suitable applied pre-strain. It is obvious that RGO/PVA composites prepared in this work can be effectively used as optically triggered actuators for many potential applications. The fact that the optical actuation properties can be fine tuned by tuning the RGO composition and the applied pre-strain makes these optical actuators more attractive from a device fabrication perspective.

THERMALLY REDUCED GRAPHENE OXIDE/THERMOPLASTIC POLYURETHANE NANOCOMPOSITES AS PHOTOMECHANICAL ACTUATORS

6B.1 Introduction

Even though many polymer systems including ionomers [8], polysiloxanes [9,10] and Liquid crystal elastomers (LCE) [11] were studied as the matrix for composite based actuators, thermoplastic polyurethanes (TPU) have many advantages over other polymers. TPU has two-phases: hard segments (net points) and soft segments (switches). The soft segment which is a thermally reversible phase, can store large strains by fixing a transient shape. The original shape can be recovered due to the presence of a hard segment [12]. Thus TPU is an ideal candidate for actuator application.

Generally in polyurethanes, netpoints can be formed either by physical cross-links or by chemical cross-links through covalent bonds [38]. Chemically cross-linked polyurethanes (thermosets) exhibit less creep when compared to physically cross-linked polyurethanes (thermoplastics) and hence the irreversible deformation during shape recovery is less. TPU has many advantages over other available thermoplastic shape memory polymers, including higher shape recoverability (maximum recoverable strain >400%), a wider range of shape recovery temperature (from -30 to 70°C), better biocompatibility and better processability [39-41]. In TPU, the hard segments are formed either from a long chain macro diol with a higher thermal transition temperature, or from diisocyanates and chain

extenders. The soft segment is formed from the polyols [42]. A schematic representation of PU structure is given in figure 6B.1.

—R'—NHCOO—R''—OOCHN—R'—NHCOO————R—O—[—CO—(CH$_2$)$_5$—O]$_n$—H
(Hard segment, Diisocyanate + extender)   (Soft segment, Polyol)
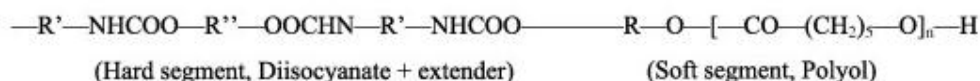
Figure 6B.1: Polyurethane with micro-phase separation structure [43]

The IR absorption characteristics of graphene materials and the unique properties of TPU can be combined to develop an IR triggered actuator with significantly enhanced actuator performance. However, not much work was carried out in this direction. Recently, one work was reported on the photomechanical properties of sulfonated graphene/TPU and isocyanate-graphene/TPU composites by a research group [33]. They had to chemically functionalize graphene in order to get a reasonably good performance. Nevertheless, a more quantitative and detailed study of the optical actuation characteristics of graphene/TPU composites are not yet carried out. Thermal reduction of graphene oxide has an added advantage of better dispersibility in addition to the high IR absorption characteristics. Hence, in the present work, thermally reduced graphene oxide (TRGO) without any additional functionalization is used as the energy transfer unit. Uniformly dispersed TRGO/TPU composites were prepared without any chemical functionalization through a simple solvent casting route. We have studied the photomechanical actuation properties of TRGO/TPU composites at various pre-strains and different filler loadings.
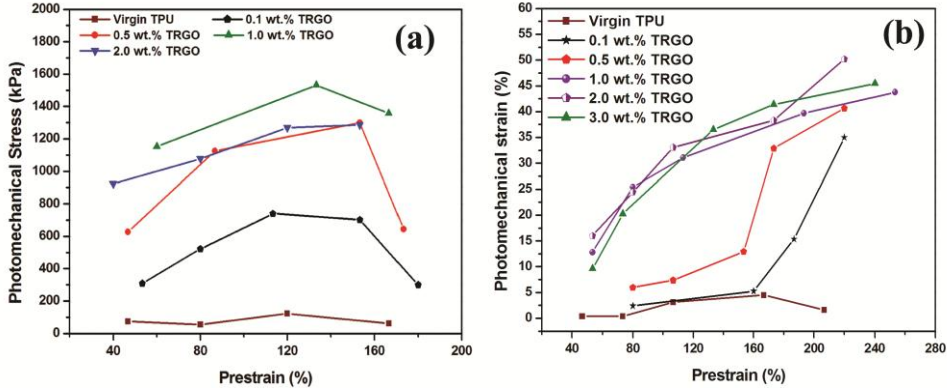
6B.2 Experimental

For the photomechanical actuation measurements of the composites, an invitro muscle test system (1205A, 5.0 N, Aurora Scientific Inc., Canada) was used as described earlier. An infrared (IR) lamp (Beurer GmbH, Germany) with red filter was used as the light source. 20 mm length and 5 mm width strips were cut from the TRGO/TPU nanocomposite sheets. The thickness of the samples was about 0.1 mm. The samples were given pre-strain at 100 ^{o}C for 4 h. Pre-strain was given by uniaxial stretching of the samples. The actuation measurement was carried out after keeping the pre-strained samples at room temperature for 8 h. The tips of the samples were placed between the grips of *in vitro* muscle test system. The stress and strain of the samples were measured at various pre-strains. For all measurements, the power density of the light source was kept constant at 16 mWcm^{-2}.

6B.3 Results and discussion

6B.3.1 Photomechanical properties of TRGO/TPU composites under IR light

The TRGO/TPU composite films were found to show fast photomechanical response under IR illumination when a pre-strain was given. The actuation was much less without any pre-strain, but exhibited large displacement and high generative force at higher pre-strains. The photomechanical stress and strain of the composites at different pre-strains are shown in the Figure 6B.2 (a) & (b).

Development of Reduced Graphene Oxide/Polymer Nanocomposites for Optical Limiting, Optical Actuation and Electrical Applications

197

Figure 6B.2: **The photomechanical (a) stress and (b) strain of TRGO/TPU composites at different pre-strains**

The effect of TRGO loading at a given pre-strain of ~ 220% is given in Figure 6B.3.
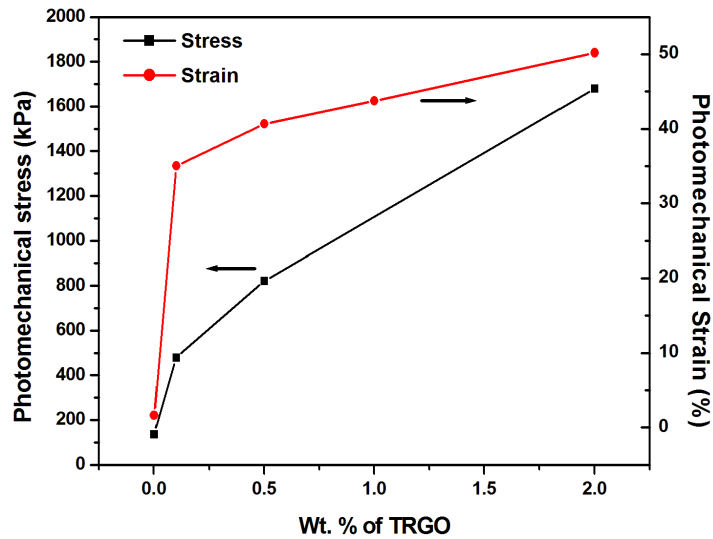
Figure 6B.3: **Photomechanical stress and strain of TRGO/TPU composites with different filler loading at a pre-strain of 220%**

For all pre-strains, samples show contraction in response to IR light. Photomechanical strain increases with pre-strain but there is an optimum pre-strain for maximum photomechanical stress. When compared to virgin TPU, the photomechanical actuation remarkably increases with TRGO as filler. Virgin TPU is transparent to IR light and hence shows negligible photomechanical response. Thermally reduced graphene oxide acts as an energy transfer unit. It can absorb IR light due to the resonant induction by edge oxygen motion of mobile electrons localized in the vicinity of the oxygen. The absorbed energy is effectively transferred into the polymer matri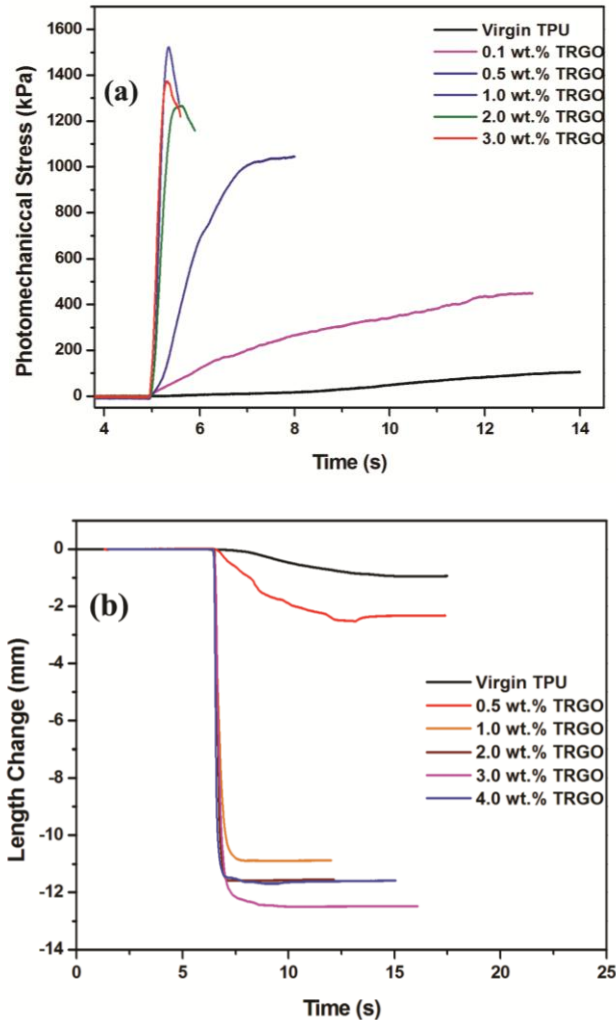x, which makes a large difference in the photomechanical responses of the composite. The IR absorption of TRGO/TPU composites mainly depends on two factors: the restoration of sp^2 carbon network in TRGO and the homogeneous distribution of TRGO in the polymer matrix. The restoration of sp^2 carbon network is achieved by the thermal reduction of graphene oxide. Maximum IR absorption of the composite is ensured by the homogeneous distribution of the TRGO platelets in the polymer matrix. TPU has hard segments and soft segments. On giving a pre-strain, the soft segments can undergo strain induced crystallization and the mechanical energy can be stored. On IR irradiation, TRGO absorbs the energy and transfers to the polymer matrix. This results in actuation by the triggering and subsequent release of stored mechanical energy in the material when in deformed state. Both the photomechanical stress and strain increase at lower filler loading but decrease as the filler loading is further increased which is complementary to the observations in mechanical properties as discussed in Chapter 4.

Development of Reduced Graphene Oxide/Polymer Nanocomposites for Optical Limiting, Optical Actuation and Electrical Applications

199

Figure 6B.4: The photomechanical response of the TRGO/TPU composites with time (a) stress (b) length change (at a pre-strain of ~120%)

From figure 6B.2, it can be observed that TRGO/TPU composites give very high photomechanical response. For instance, at ~120% pre-strain, 1.0 wt.% TRGO/TPU composite gives a photomechanical force as high as 0.383 N with a stress of 1532 kPa and can contract about 31% of its length i.e., it can lift a weight of 39.08 g to a height of 10.8 mm.

Previously, 1 wt.% sulfonated graphene–TPU composites were reported to give a force of 0.21 N (for a sample of dimension ~30 mm $\times$ 5 mm $\times$ 0.05 mm) at a pre-strain of 200 %, which corresponds to a photomechanical stress of 840 kPa [33]. The intensity of IR light used was 30 mWcm^{-2}. However in the present work, 1 wt.% TRGO/TPU composite exhibits much better photomechanical response. We could obtain a photomechanical stress of 1357 kPa (0.475 N) at 166 % pre-strain even at a lower light intensity of 16 mWcm^{-2}. Similarly a photomechanical strain as high as 50.2 % is obtained for 2 wt.% TRGO/TPU composites at 220 % pre-strain with a stress of 1680 kPa. This indicates that at a pre-strain of 220 %, under IR irradiation, it can lift 42.85g to a height of 25 mm. The photomechanical response of the composites with time is given in Figure 6B.4 (a) and (b). The time required for photomechanical response is also reduced when TRGO loading is increased. At higher loading the composites show very fast photomechanical response of less than 1s.
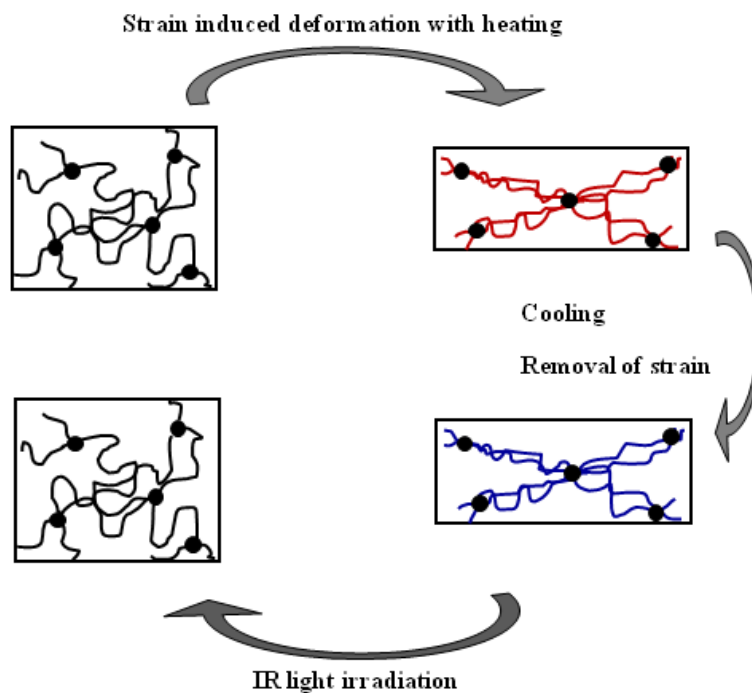
The mechanism of optical actuation in RGO/TPU nanocomposites was more like that of a shape memory effect. Giving a pre-strain by stretching at higher temperature resulted in strain induced crystallisation of the soft segments in TPU as evident from the XRD pattern given in figure 6B.5. The deformed state is maintained by cooling the sample to room temperature under the applied strain. Once cooled, the strain is removed. On IR irradiation, the RGO absorbs the IR radiation and act as nano heaters in the polymer matrix. This again helps the polymer chains to relax and the stored mechanical energy is released as the sample contracts to its initial state. The schematic representation of the mechanism is given in figure 6B.6.

Development of Reduced Graphene Oxide/Polymer Nanocomposites for Optical Limiting, Optical Actuation and Electrical Applications

201
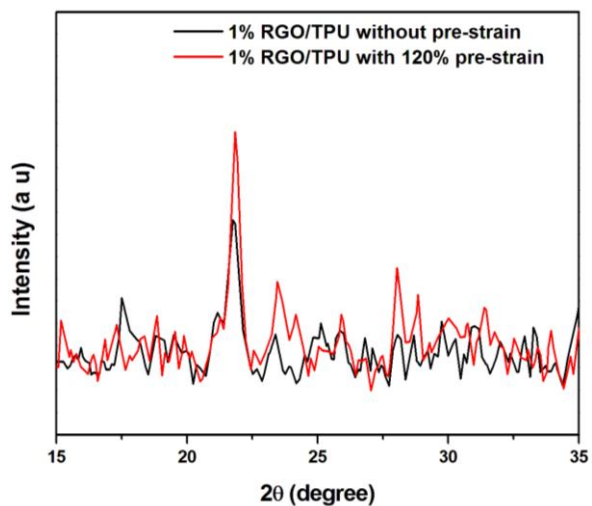
Figure 6B.5: **XRD patterns of RGO/TPU nanocomposite with and without pre-strain**

Figure 6B.6: Mechanism of optical actuation in RGO/TPU nanocomposites

6B.4 Conclusions

The photomechanical actuation properties of Thermally Reduced Graphene Oxide (TRGO)/Thermoplastic Polyurethane (TPU) composites were studied using IR light source. The composites were found to exhibit fast photomechanical response. All the samples show contraction on IR irradiation at a given pre-strain. The photomechanical stress and strain increased with pre-strain. At lower filler loading, the photomechanical response was found to increase with TRGO loading. However, at higher loading, it is slightly decreased. The response time was also improved as the TRGO content was increased. 1 wt.% TRGO/TPU nanocomposite exhibited photomechanical stress and strain as high as 1532 kPa and 31 % respectively. Similarly a photomechanical strain as high as 50.2 % is obtained for 2 wt.% TRGO/TPU nanocomposites at 220 % pre-strain with a stress of 1680 kPa. Hence this can find potential application as light triggered actuators in many fields including robotics.

References

[1]   Ahir, S. V., Squires, A. M., Tajbakhsh, A. R., & Terentjev, E. M. (2006). Infrared actuation in aligned polymer-nanotube composites. *Physical review B*, *73*(8), 085420

[2]   Gerratt, A. P., & Bergbreiter, S. (2012). Incorporating compliant elastomers for jumping locomotion in microrobots. *Smart Materials and Structures*, *22*(1), 014010.

[3]   Brochu, P., Stoyanov, H., Niu, X., & Pei, Q. (2013). All-silicone pre-strain-locked interpenetrating polymer network elastomers: free-standing silicone artificial muscles with improved performance and robustness. *Smart Materials and Structures*, *22*(5), 055022.

[4] Lu, S., & Panchapakesan, B. (2007). Photomechanical responses of carbon nanotube/polymer actuators. *Nanotechnology*, *18*(30), 305502.

[5] Lendlein, A., Jiang, H., Jünger, O., & Langer, R. (2005). Light-induced shape-memory polymers. *Nature*, *434*(7035), 879-882.

[6] Jiang, H. Y., Kelch, S., & Lendlein, A. (2006). Polymers move in response to light. *Advanced Materials*, *18*(11), 1471-1475.

[7] Ahir, S. V., Huang, Y. Y., & Terentjev, E. M. (2008). Polymers with aligned carbon nanotubes: Active composite materials. *Polymer*, *49*(18), 3841-3854.

[8] Levitsky, I. A., Kanelos, P. T., Woodbury, D. S., & Euler, W. B. (2006). Photoactuation from a carbon nanotube− nafion bilayer composite. *The Journal of Physical Chemistry B*, *110*(19), 9421-9425.

[9] Ahir, S. V., & Terentjev, E. M. (2006). Fast relaxation of carbon nanotubes in polymer composite actuators. *Physical review letters*, *96*(13), 133902.

[10] Ahir, S. V., & Terentjev, E. M. (2005). Photomechanical actuation in polymer–nanotube composites. *Nature materials*, *4*(6), 491-495.

[11] Yang, L., Setyowati, K., Li, A., Gong, S., & Chen, J. (2008). Reversible infrared actuation of carbon nanotube–liquid crystalline elastomer nanocomposites. *Advanced Materials*, *20*(12), 2271-2275.

[12] Koerner, H., Price, G., Pearce, N. A., Alexander, M., & Vaia, R. A. (2004). Remotely actuated polymer nanocomposites—stress-recovery of carbon-nanotube-filled thermoplastic elastomers. *Nature materials*, *3*(2), 115-120.

[13] Ge, F., Lu, X., Xiang, J., Tong, X., & Zhao, Y. (2017). An Optical Actuator Based on Gold-Nanoparticle-Containing Temperature-Memory Semicrystalline Polymers. *Angewandte Chemie International Edition*, *56*(22), 6126-6130.

[14] Kularatne, R. S., Kim, H., Boothby, J. M., & Ware, T. H. (2017). Liquid crystal elastomer actuators: Synthesis, alignment, and applications. *Journal of Polymer Science Part B: Polymer Physics*, *55*(5), 395-411.

[15] Geim, A. K. (2009). Graphene: status and prospects. *science*, *324*(5934), 1530-1534.

[16] Stankovich, S., Dikin, D. A., Dommett, G. H., Kohlhaas, K. M., Zimney, E. J., Stach, E. A., ... & Ruoff, R. S. (2006). Graphene-based composite materials. *nature*, *442*(7100), 282-286.

[17] Naumis, G. G., Barraza-Lopez, S., Oliva-Leyva, M., & Terrones, H. (2017). Electronic and optical properties of strained graphene and other strained 2D materials: a review. *Reports on Progress in Physics*.

[18] Kumar, P., Yu, S., Shahzad, F., Hong, S. M., Kim, Y. H., & Koo, C. M. (2016). Ultrahigh electrically and thermally conductive self-aligned graphene/polymer composites using large-area reduced graphene oxides. *Carbon*, *101*, 120-128.

[19] Wang, M., Duan, X., Xu, Y., & Duan, X. (2016). Functional three-dimensional graphene/polymer composites.

[20] Kuilla, T., Bhadra, S., Yao, D., Kim, N. H., Bose, S., & Lee, J. H. (2010). Recent advances in graphene based polymer composites. *Progress in polymer science*, *35*(11), 1350-1375.

[21] Ji, X., Xu, Y., Zhang, W., Cui, L., & Liu, J. (2016). Review of functionalization, structure and properties of graphene/polymer composite fibers. *Composites Part A: Applied Science and Manufacturing*, *87*, 29-45.

[22] Gao, Y. (2017). Graphene and Polymer Composites for Supercapacitor Applications: a Review. *Nanoscale Research Letters*, *12*(1), 387.

[23] Niu, Y., Zhang, X., Fang, Q., & Li, Y. (2017). Fabrication, optical and electrical properties of solvethermal reduced graphene oxide/polyimide composites by in situ polymerization. *Synthetic Metals*, *224*, 86-91.

[24] Selvakumar, D., Alsalme, A., Alghamdi, A., & Jayavel, R. (2017). Reduced graphene oxide paper as bimorphic electrical actuators. *Materials Letters*, *191*, 182-185.

[25] Li, W., Li, F., Li, H., Su, M., Gao, M., Li, Y., ... & Song, Y. (2016). Flexible circuits and soft actuators by printing assembly of graphene. *ACS applied materials & interfaces*, *8*(19), 12369-12376.

[26] Han, D. D., Zhang, Y. L., Liu, Y., Liu, Y. Q., Jiang, H. B., Han, B., ... & Sun, H. B. (2015). Bioinspired graphene actuators prepared by unilateral UV irradiation of graphene oxide papers. *Advanced Functional Materials*, *25*(28), 4548-4557.

[27] Kong, L., & Chen, W. (2014). Carbon Nanotube and Graphene-based Bioinspired Electrochemical Actuators. *Advanced materials*, *26*(7), 1025-1043.

[28] Inamuddin, Khan, A., Jain, R. K., & Naushad, M. (2016). Study and preparation of highly water-stable polyacrylonitrile–kraton–graphene composite membrane for bending actuator toward robotic application. *Journal of Intelligent Material Systems and Structures*, *27*(11), 1534-1546.

[29] He, J., Xiao, P., Zhang, J., Liu, Z., Wang, W., Qu, L., ... & Chen, T. (2016). Highly Efficient Actuator of Graphene/Polydopamine Uniform Composite Thin Film Driven by Moisture Gradients. *Advanced Materials Interfaces*, *3*(14).

[30] Wu, C., Feng, J., Peng, L., Ni, Y., Liang, H., He, L., & Xie, Y. (2011). Large-area graphene realizing ultrasensitive photothermal actuator with high transparency: new prototype robotic motions under infrared-light stimuli. *Journal of Materials Chemistry*, *21*(46), 18584-18591.

[31] Loomis, J., King, B., & Panchapakesan, B. (2012). Layer dependent mechanical responses of graphene composites to near-infrared light. *Applied Physics Letters*, *100*(7), 073108.

[32] Kurapati, R., & Raichur, A. M. (2013). Near-infrared light-responsive graphene oxide composite multilayer capsules: a novel route for remote controlled drug delivery. *Chemical Communications*, *49*(7), 734-736.

[33] Liang, J., Xu, Y., Huang, Y., Zhang, L., Wang, Y., Ma, Y., ... & Chen, Y. (2009). Infrared-triggered actuators from graphene-based nanocomposites. *The Journal of Physical Chemistry C*, *113*(22), 9921-9927.

[34] Wan, Y. J., Yang, W. H., Yu, S. H., Sun, R., Wong, C. P., & Liao, W. H. (2016). Covalent polymer functionalization of graphene for improved dielectric properties and thermal stability of epoxy composites. *Composites Science and Technology*, *122*, 27-35.

[35] Li, Y., Wang, S., & Wang, Q. (2017). Enhancement of tribological properties of polymer composites reinforced by functionalized graphene. *Composites Part B: Engineering*, *120*, 83-91.

[36] Xue, Q., Lv, C., Shan, M., Zhang, H., Ling, C., Zhou, X., & Jiao, Z. (2013). Glass transition temperature of functionalized graphene–polymer composites. *Computational Materials Science*, *71*, 66-71.

[37] Hu, K., Kulkarni, D. D., Choi, I., & Tsukruk, V. V. (2014). Graphene-polymer nanocomposites for structural and functional applications. *Progress in Polymer Science*, *39*(11), 1934-1972.

[38] Hu, J.L. (2007) Shape memory polymers and textiles. In: Characterization of shape memory properties in polymers. CRC Press, Boca Raton, pp 197–225.

[39] Ratna, D., Karger-Kocsis, J. (2008) Recent advances in shape memory polymers and composites: a review. *Journal of Material Science*, 43, 254–269.

[40] Yakacki, C. M., Willis, S., Luders, C., Gall, K. (2008) Deformation limits in shape-memory polymers. *Advanced Engineering Materials*, 10, 112–119.

[41] Kim, B. K., Lee, S. Y., Lee, J. S., Baek, S. H., Choi, Y. J., Lee, J. O., Xu, M. (1998) Polyurethane ionomers having shape memory effects. *Polymer,* 39, 2803–2808.

[42] Leng, J. S., Du, S. Y. (2010) Shape memory polymer and multifunctional composite. In: Jiang HY, Schmidt A (eds) The structural variety of shape memory polymers. CRC Press, Boca Raton, pp 21–64.

[43] Leng, J., Lan, X., Liu, Y., Du, S. (2011) Shape-memory polymers and their composites: stimulus methods and applications. *Progress in Material Science,* 56, 1077–1135.

.....ॐ.....

REDUCED GRAPHENE OXIDE/POLYMER NANOCOMPOSITES FOR ELECTRICAL APPLICATIONS

Contents	*Part A* *Electrical properties of reduced graphene oxide/poly(vinyl alcohol) nanocomposites*
	Part B *Electrical properties of thermally reduced graphene oxide/thermoplastic polyurethane nanocomposites*

7.1 Introduction

Conductive polymer nanocomposites can find many potential technological applications such as antistatic materials, sensors, microwave absorbers, EMI shields and conductive coatings. Even though there are many types of conductive fillers, the inclusion of graphitic nano structures into the polymer matrix has always been the most preferred method for improving the electrical properties of the polymer composites. Conductive fillers with their size in the nano regime can form percolative network in the polymer matrix at a relatively low weight fraction. Incorporation of these conductive nano-inclusions can alter the permittivity of the composite system thereby enhancing the energy storing capacity [1]. The conductive nano particles can be considered as a network of nano

capacitors distributed in the polymer matrix which can form an energy storing system at nanoscale level [2]. The electrical property of the polymer composite is directly related to the conductivity, diepersibility and the interaction of the nano particle with the polymer matrix. Conductive fillers with larger aspect ratio are often preferred to get a low percolation threshold. Out of the various forms of graphitic materials, graphene, the two dimensional monolayer of sp^2 carbons, has been considered as the most ideal material for preparing conductive polymer composites due to its high conductivity and large aspect ratio [3]. However, the re-stacking nature of graphene sheets due to their strong π-π interactions, makes it extremely difficult to uniformly disperse graphene in polymer systems. If graphene is not homogenously dispersed, it is difficult to form the continuous conductive pathways within the composites at low filler loading. The use of reduced graphene oxide (RGO) instead of pristine graphene is an alternative solution to overcome the dispersibility issue. The oxygen functional groups left behind after reduction of graphene oxide can help to disperse RGO in the polymer matrix in a better way. However, one has to strike a balance between the conductivity and dispersibility of RGO by controlling the extent of reduction.

In this chapter, RGO is used as conducting filler in two polymer systems and their electrical properties are studied to understand the suitability of these composites for electrical applications. Part A deals with the electrical properties of composites made using *in situ* reduced graphene oxide in PVA matrix and Part B discusses the electrical properties of thermally reduced graphene oxide/TPU nanocomposites.

ELECTRICAL PROPERTIES OF REDUCED GRAPHENE OXIDE/POLY(VINYL ALCOHOL) NANOCOMPOSITES

7A.1 Introduction

Poly(vinyl alcohol) has always been a polymer of prime importance in many practical applications mainly because of the ease of processing and ability to form thin films and coatings. The affinity towards water has always been a challenge for their practical applications. However, making a composite with a hydrophilic filler like graphene has improved its water resistance many folds. Hence graphene/PVA composites are even finding applications in electrical fields like antistatic coatings, EMI shields and so on.

In this work, in order to get a homogeneous dispersion of RGO in the PVA matrix, we have used GO as the starting material. GO which is a water dispersible system was uniformly dispersed in PVA solution and then reduced to form RGO within the polymer solution. The electrical properties of the composite films were studied in detail and the results are discussed in this section.

7A.2 Experimental

The preparation of RGO/PVA composites with varying filler content is detailed in Chapter 4. Samples from the composite film were made into the form of a parallel plate capacitor by applying silver paste on both sides. The dc electrical measurements were taken using a two probe method in a

Keithley 2400 source meter. The electrical properties in the frequency range 100 Hz to 10 MHz were measured using a precision impedance analyser (Agilent 4294A).

7A.3 Results and discussion

7A.3.1 DC Electrical conductivity

The dc electrical conductivity as a function of RGO loading for the RGO/PVA composites is given in figure 7A.1. It can be observed that there is an increase in dc conductivity with increasing RGO content. As we know, the sharp increase in conductivity occurs only at the percolation threshold where a continuous conductive path is established. It can be either through direct contact between conductive filler particles or through the tunneling between the two filler particles surrounded by thin layer of polymer [4]. The conductivity of a conductor-insulator composite near the percolation threshold can be described by a power law in the form $\sigma \propto (p-p_c)^\beta$, where σ is the conductivity of the composite, p is the volume fraction of the filler, p_c is the percolation threshold and β is the critical exponent [5]. The weight fraction of RGO in the composite was converted in to volume fraction by the equation 7.1.

$$v = \frac{w\rho_p}{w\rho_p + (1-w)\rho_g} \qquad \dots\dots\dots\dots\dots\dots\dots(7.1)$$

where, v and w are the volume fraction and mass fraction of graphene nanosheets, respectively. ρ_p and ρ_g represent the density of PVA matrix and graphene nanosheets, which are 1.3 g/cc and 2.2 g/cc respectively. The straight line graph for the log-log plot of σ vs (p-p_c) for the volume

fractions near the percolation threshold is shown in figure 7A.2. The percolation threshold was 0.3714 vol% (i.e., 0.5 wt.%) and the β value was 2.8 which is similar to those reported earlier by other groups [6].
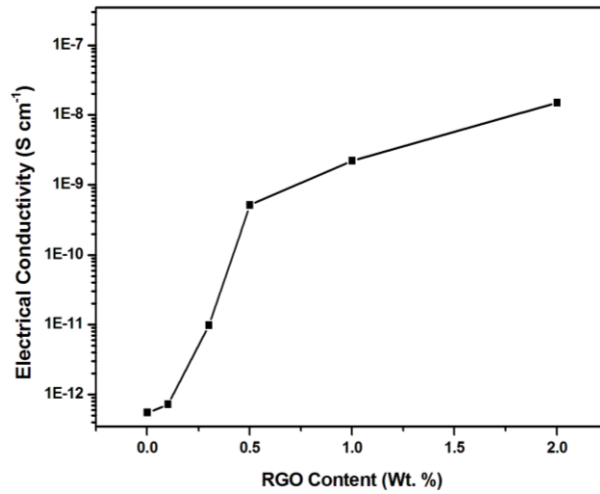
Figure 7A.1: Electrical conductivity (dc) as a function of RGO loading
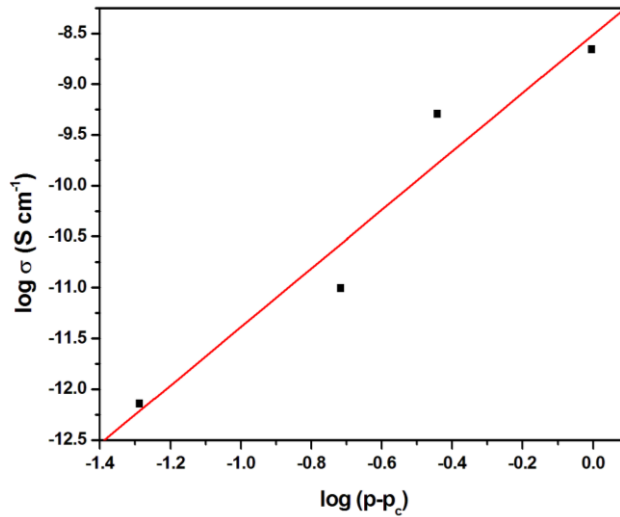
Figure 7A.2: log-log plot of σ and p-p$_c$

7A.3.2 Dielectric properties

7A.3.2.1 AC Electrical conductivity

The ac conductivity of the composites were studied in the frequency range 100 Hz to 1MHz and is given in figure 7A.3. Similar to the dc conductivity, the ac conductivity also increases with increasing RGO content. The conductivity also increases with increasing frequency which is a common observation for conducting composites.
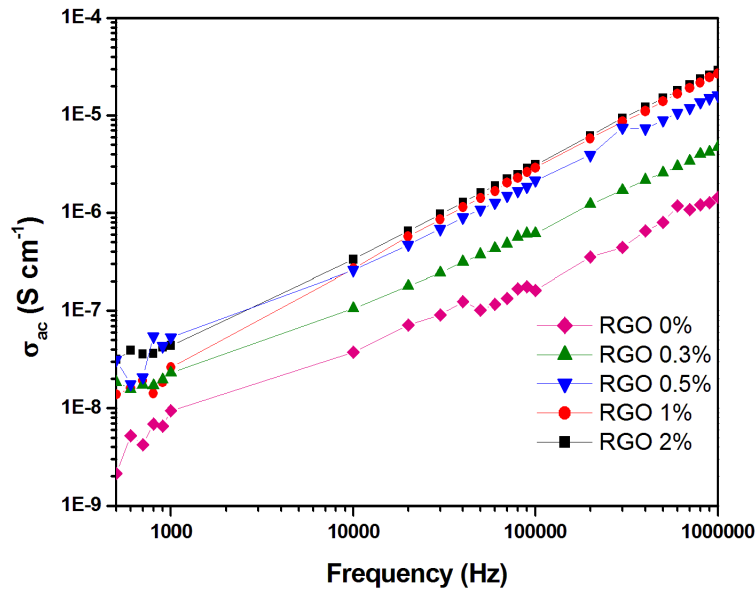

Figure 7A.3: AC conductivity of the RGO/PVA composites as a function of frequency

7A.3.2.2 Dielectric constant and dissipation factor

The measurement of dielectric properties can help to understand the charge transport mechanism in conducting composites. The dielectric constant of the RGO/PVA nanocomposites at 1 MHz as a function of RGO

content is given in figure 7A.4. The dielectric constant of the composite was found to increase with increasing RGO content. This clearly indicates that the energy storage capacity increases with increasing RGO content.
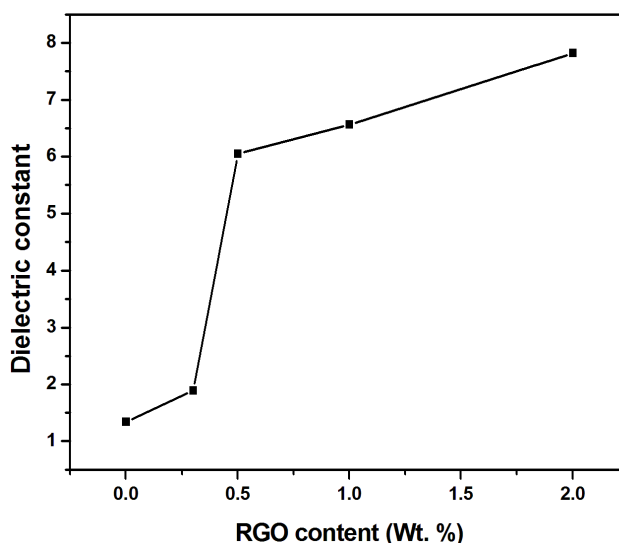
Figure 7A.4: Dielectric constant of RGO/PVA composites at 1 MHz

In order to have a better understanding of the dielectric properties, we have delineated the real part and imaginary part of the dielectric constant. The real part of the dielectric constant (ε_r') represents the capacity of a material to store energy where as the imaginary part (ε_r'') represents how lossy the material is. The dissipation factor is given by $\varepsilon_r''/\varepsilon_r'$.

The dependence of ε_r' on RGO content as a function of frequency is given in figure 7A.5. The dielectric performance is found to increase with RGO content. The increase is prominent up to 0.5 wt. % and thereafter it is nominal. All the compositions exhibited relatively large value of ε_r' at lower frequencies. However, ε_r' decreased with increasing frequency. At

Development of Reduced Graphene Oxide/Polymer Nanocomposites for Optical Limiting, Optical Actuation and Electrical Applications

215

lower frequencies, the dipole moments and charge carriers are free to move within the nanocomposites and follow the variation in applied electric field. Whereas at higher frequencies, the charge carriers or diploes are not able to follow the electromagnetic field varying at higher rates and hence the ε_r' decreases at higher frequencies. Interfacial polarization is the major reason for the high dielectric performance at low frequencies.
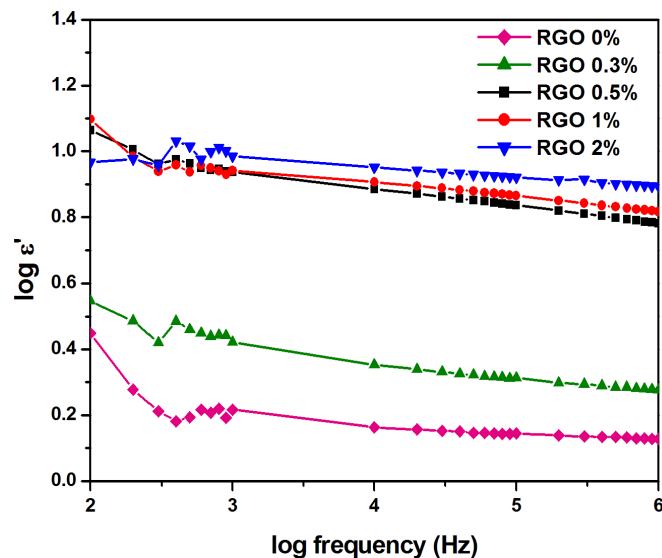
Figure 7A.5: Variation of real part of dielectric constant with frequency

In RGO/PVA nanocomposites, the charges in RGO nanoparticles get delocalized by the applied electric field and accumulate at the RGO/PVA interface resulting in large scale polarization. This has resulted in the significant improvement of dielectric properties of the polymer with the addition of RGO. The imaginary part of dielectric constant (ε_r'') also shows similar behaviour (Figure 7A.6).
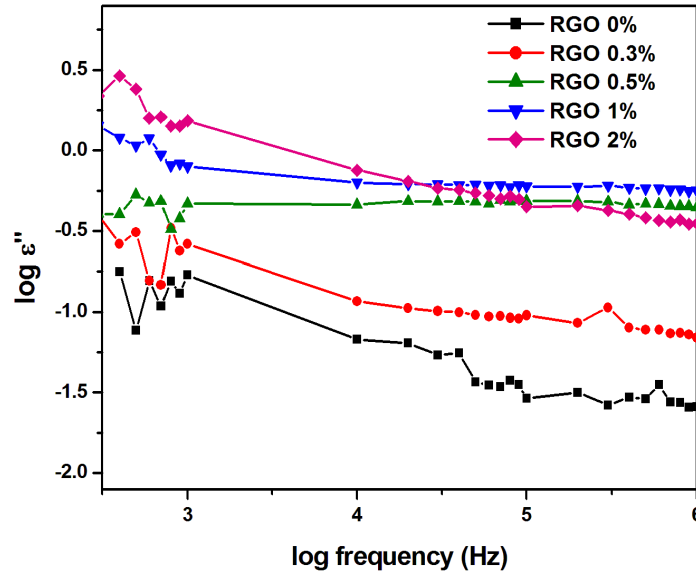
Figure 7A.6: Variation of imaginary part of dielectric constant with frequency

The variation of dielectric loss as a function of frequency is given in figure 7A.7. It can be observed that the composite system becomes more lossy as the RGO content increases which is well expected due to the increase in conductivity. The loss slightly decreases with increasing frequency at lower frequency region due to dielectric relaxation and then becomes almost constant at higher frequencies. However, the ac conductivity values and the loss values clearly prove these composites as a potential candidate for many electrical applications like antistatic coatings. Normally antistatic coatings are made on walls or enclosures of equipments, devices or rooms where static electricity buildup needs to be avoided. A slightly conductive pathway can restrict the accumulation of static electricity. For such applications, the processability to form thin

Development of Reduced Graphene Oxide/Polymer Nanocomposites for Optical Limiting, Optical Actuation and Electrical Applications

217

films or coatings is very important. The solution processable RGO/PVA nanocomposites can be readily employed for such applications.
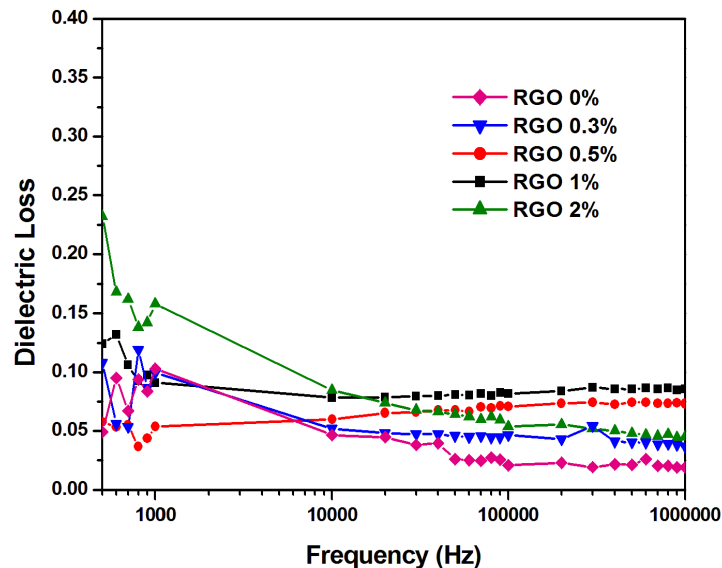
Figure 7A.7: Dielectric loss as a function of frequency

7A.3.3 RGO/PVA based thermally sensitive resistors

The change in resistance of a material with temperature is of great importance from both material aspects and a device perspective. Temperature monitoring and control are of paramount importance in many electrical devices especially in the consumer sector including air conditioners, washing machines, refrigerators, etc. Most of the thermal sensors utilize the change in resistance with temperature as the parameter for sensing and controlling temperatures. There are two types of thermal sensors based on the nature of their change in resistance with temperature. In PTC (positive temperature coefficient of resistance) thermal sensors, the

resistance increases with temperature whereas in NTC (negative temperature coefficient of resistance) thermal sensors the resistance decreases with temperature. Most of the polymer based thermal sensors exhibit PTC behaviour.

The resistance change in RGO/PVA nanocomposites as a function of temperature was studied in a calibration temperature bath (Fluke 7340) with silicon oil as the bath fluid. The variation in resistance with temperature for RGO/PVA composites is given in figure 7A.8. It can be observed that the composites show NTC behaviour i.e., the resistance decreases with temperature. The decrease in resistance with temperature is an exponential change. The general behaviour of an NTC thermal sensor is explained by the equation 7.2.

$$\rho = \rho_0 \exp(\frac{\phi}{K_B T}) \quad \dots\dots\dots\dots\dots\dots\dots\dots\dots\dots\dots\dots\dots\dots\dots\dots\dots(7.2)$$

Where ρ is the resistivity, K_B is the boltzman constant, ϕ is the activation energy and T is the temperature [7]. To confirm this relation, log Resistivity is plotted against $1/T$ in figure 7A.9 for the temperature region showing NTC behaviour. It can be noted that the curve gives a linear relation which means that the actual change in resistance with temperature is an exponential change. This decrease in resistance or increase in conductivity can be due to the thermally activated tunneling effect between the neighboring RGO platelets in the polymer matrix. Similar observation was also reported by Mitra et al. [7, 8].

Development of Reduced Graphene Oxide/Polymer Nanocomposites for Optical Limiting, Optical Actuation and Electrical Applications
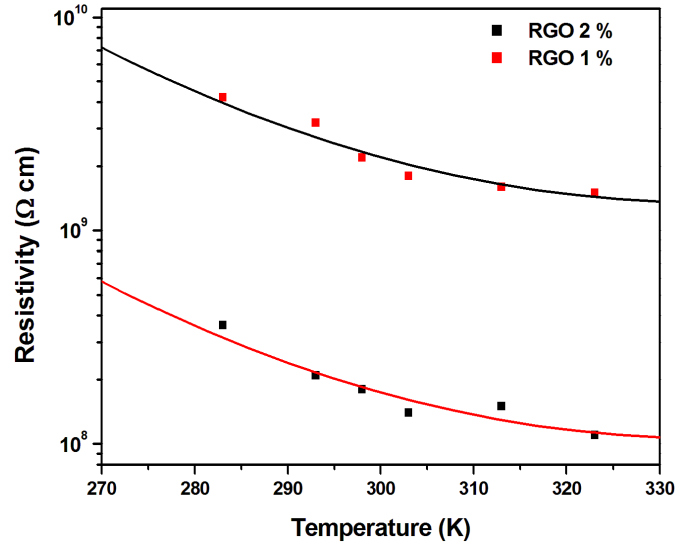
219

Figure 7A.8: Change in resistivity with temperature for RGO/PVA composites

The NTC behavior can be utilized for many practical applications including thermal sensor applications.
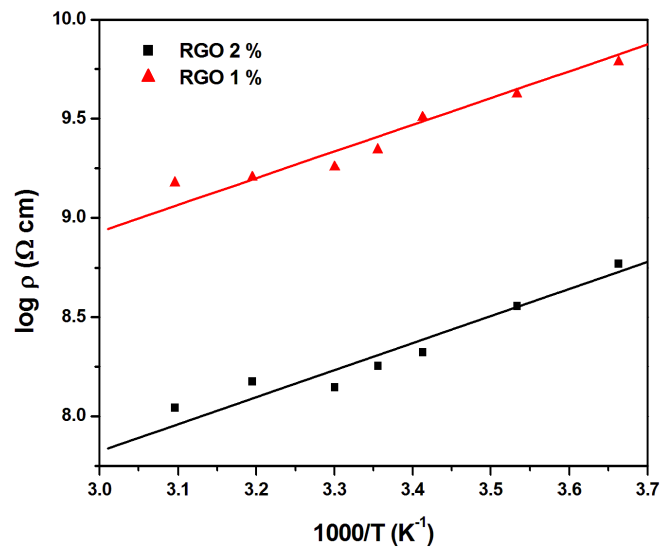
Figure 7A.9: Linear relation of log ρ with 1/T for RGO/PVA composites

7A.4 Conclusions

The incorporation of RGO in to PVA matrix has dramatically improved the conductivity of the composites. A low percolation threshold of 0.37 vol % was achieved. Even though the RGO used contained residual functional groups which affect the conductivity, homogeneous dispersion was possible which in turn helped in a fivefold improvement of conductivity with as low as 1% filler loading. The dielectric properties were also improved with RGO content. The enhancement in the real part of dielectric constant with increasing RGO content proves that charge storage capacity of the composites has improved which will make them suitable for capacitor applications especially in passive integrated circuits. The conductivity of the material is suitable for applications such as antistatic coatings. The RGO/PVA composites exhibited an NTC behavior with temperature. The decrease in resistance with increasing temperature can be utilized for applications like temperature sensors.

Development of Reduced Graphene Oxide/Polymer Nanocomposites for Optical Limiting, Optical Actuation and Electrical Applications

221

ELECTRICAL PROPERTIES OF THERMALLY REDUCED GRAPHENE
OXIDE/THERMOPLASTIC POLYURETHANE NANOCOMPOSITES

7B.1 Introduction

Conducting elastomeric composites have attracted enormous interest in the recent past due to the evolution of flexible and stretchable electronics. Electrically conductive elastomeric composites are generally made by dispersing conductive filler into the elastomeric matrix. Graphene has been considered as one of the most suitable conductive filler for composite preparation. Thermoplastic polyurethanes (TPU) hold the advantages of processability of thermoplastics and flexible and stretchable properties of elastomers. Thus, graphene/TPU composites shall be good choice of composite system for conductive elastomers. Electrically conductive graphene/TPU composites can find a variety of applications including strain sensors [9], EMI shielding [10], pressure sensors [11], etc.

In order to facilitate better dispersibility in the polymer matrix, thermally reduced graphene oxide was used as the filler material in TPU matrix. The electrical properties of the composites were studied at various frequencies.

7B.2 Experimental

The preparation of RGO/TPU composites was described in detail in the chapter 4. The composite films prepared by solvent casting were subjected to electrical studies as described in chapter 2. The conductivity

and other dielectric properties were studied in the frequency range of 100 Hz to 1 MHz.

7B.3 Results and discussion

7B.3.1 DC Conductivity

The DC conductivity of the composite films as a function of RGO loading is given in figure 7B.1. The conductivity was found to increase with increasing RGO content. As evident from the figure 7B.1, the percolation threshold was achieved at 1 wt. %. In some earlier works, with a similar kind of RGO (thermally exfoliated GO referred to as FGS) in PVDF matrix, a percolation threshold of 2 wt.% was reported [12]. Thus we were able to achieve the percolation threshold at a lower filler loading despite the RGO containing residual oxygen functional groups.
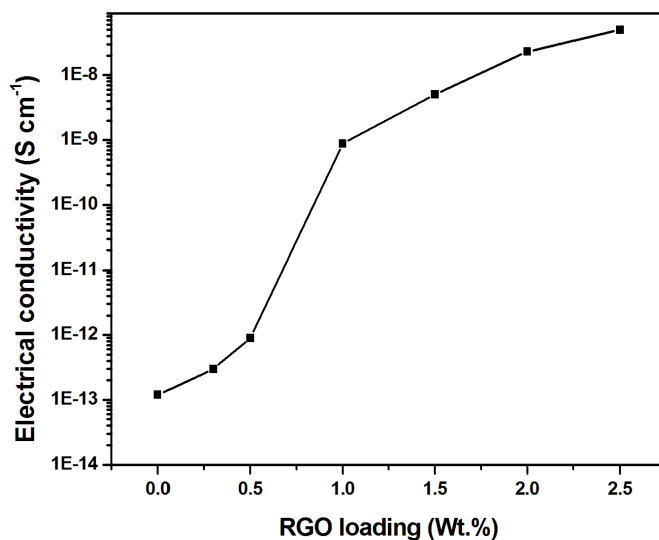
Figure 7B.1: DC conductivity of the composites as a function of RGO loading

Development of Reduced Graphene Oxide/Polymer Nanocomposites for Optical Limiting, Optical Actuation and Electrical Applications

223

In order to verify the power law regarding percolation $\sigma \, \alpha \, (p{-}p_c)^{\beta}$, log(p-pc) was plotted against log σ and is shown in figure 7B.2. It gives almost a linear fit with Pc of 1 vol% and critical exponent β of 1.76. This means that the system is fairly holding the percolation theory.
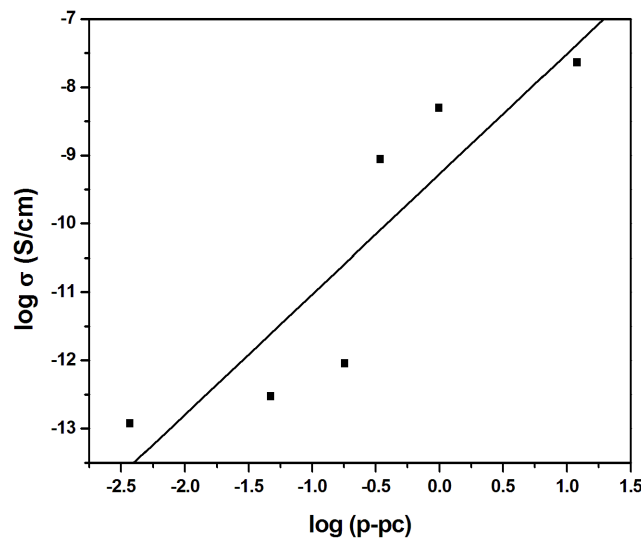
Figure 7B.2: Relation between log(p-pc) and log σ

7B.3.2 Dielectric properties

7B.3.2.1 AC conductivity

The frequency dependence of ac conductivity of the RGO/TPU composites with various RGO content is given in figure 7B.3. The ac conductivity is also found to increase with increasing RGO content. All the composites irrespective of the RGO content exhibited an increase in conductivity with increasing frequency. This is a common behaviour observed in disordered solids and seems to be in accordance with the 'ac universality law'. This can be considered as a strong indication for charge migration via the hopping mechanism [13, 14].
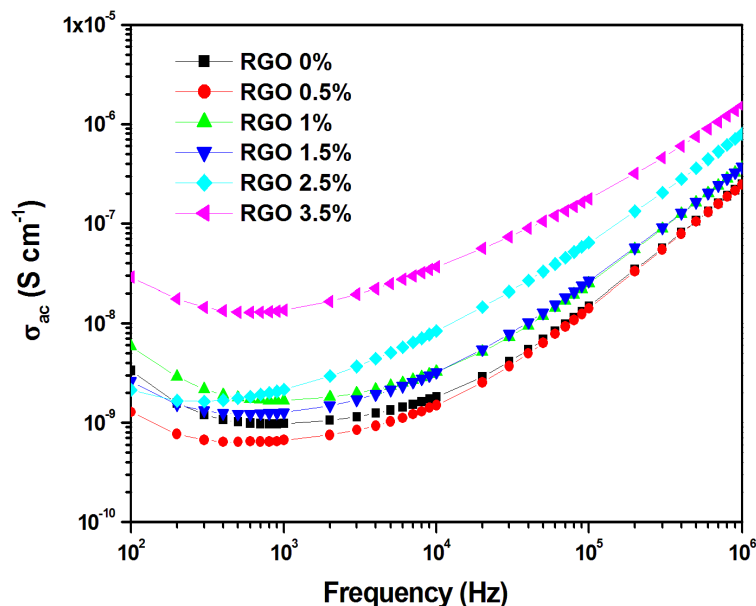
Figure 7B.3: The frequency dependence of ac conductivity of the RGO/TPU composites

7B.3.2.2 Dielectric constant

The variation of the dielectric constant with frequency for RGO/TPU composites with varying RGO content is depicted in figure 7B.4. The dielectric constant is found to be enhanced dramatically at higher filler loading. There is almost 5 times increase in the dielectric constant for 3.5% RGO/TPU in the lower frequency region. The high dielectric constant in the lower region can be mainly attributed to the interfacial polarization. However, as the frequency increases, the dielectric constant decreases. This is mainly because, at higher frequencies, the charge carriers cannot follow the variation in electric field and this results in less polarization and hence low dielectric constant. However, the increase in dielectric constant with RGO content improves the charge storage capability.

Development of Reduced Graphene Oxide/Polymer Nanocomposites for Optical Limiting,
Optical Actuation and Electrical Applications

225
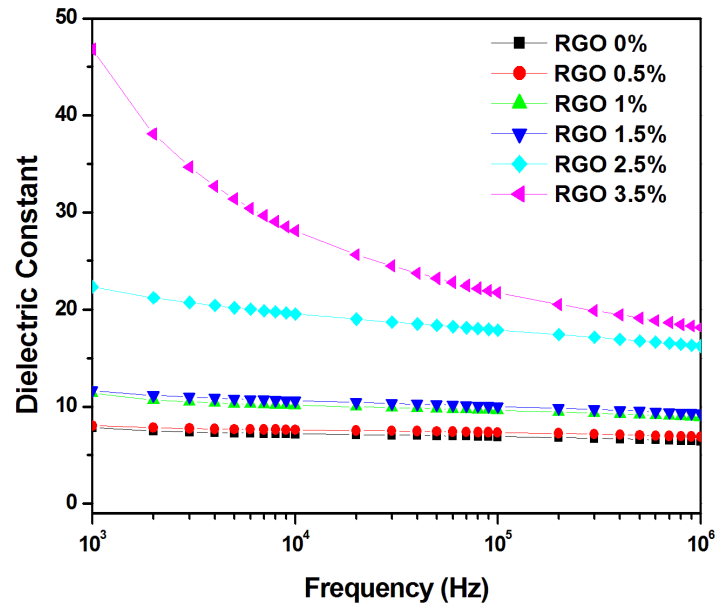
Figure 7B.4: Dielectric constant of RGO/TPU composites as a function of frequency

7B.3.2.3 Dielectric Loss

Dielectric loss or dissipation factor is a measure of the energy dissipated in the material. Normally for conducting composites, it will be high. The dissipation factor of RGO/TPU composites as a function of frequency is given in figure 7B.5. It can be observed that the loss increases with increasing RGO content which is well expected as the conductivity increases. As the frequency increases the loss decreases initially in the low frequency domain. However, the dielectric loss is slightly increased at higher frequencies. The interfacial polarization is the major phenomenon at low frequencies and hence as the frequency increases, the interfacial polarization decreases and loss decreases

initially. In the higher frequency region, the dielectric relaxation dominates which results in the increase of dielectric loss.
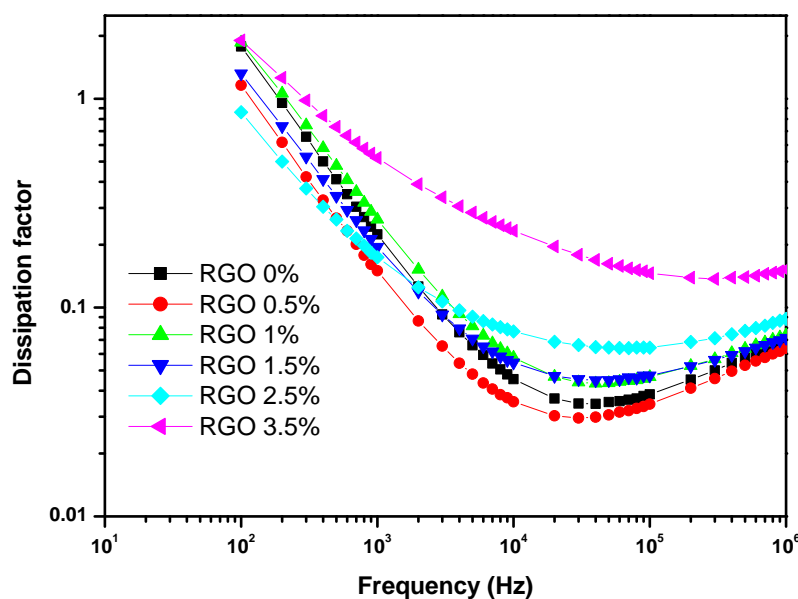
Figure 7B.5: Dissipation factor as a function of frequency for the RGO/TPU composites

7B.3.3 Temperature dependence of resistance

The changes in resistance as a function of temperature for RGO/TPU composites were studied and the results are depicted in figure 7B.6. It can be observed that there is an increase in resistance with temperature. Unlike in RGO/PVA composites, we have observed a PTC behavior throughout the temperature range. There can be two reasons for this observation. Firstly, being an elastomer, the thermal expansion in TPU is more and hence the RGO sheets get separated on increasing the temperature. Another reason can be the formation of small agglomerates of RGO in TPU matrix which can increase the resistance. As we can see in the DSC

Development of Reduced Graphene Oxide/Polymer Nanocomposites for Optical Limiting, Optical Actuation and Electrical Applications

227

of TPU (in Chapter 4), there is a transition temperature near 60 ^{o}C. It is clear from the Resistance − Temperature curve that the rate of increase in resistance is higher after 60 ^{o}C. The PTC behavior can be utilized for both sensor and resettable fuse applications.
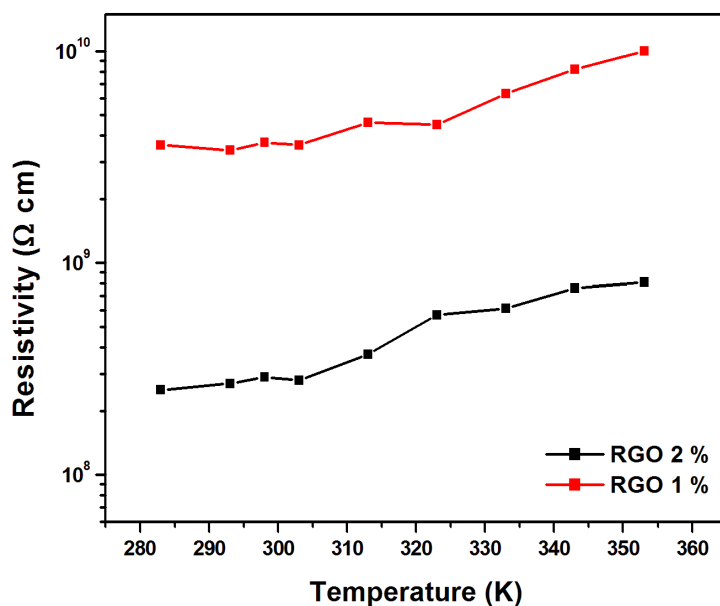
Figure 7B.6: R-T curve of RGO/TPU composites

The current − voltage (I-V) characteristics of 1 wt. % RGO/TPU composite is shown in figure 7B.7. The I-V characteristics shows a linear relation confirming that the resistance remains almost constant with varying current. However, at higher current, there is a tendency to deviate from the linearity, which may be due to heating up of the composite which can increase the resistance. This result indicates that these can be used for inrush current limiters which can restrict the high current flow by increasing the resistance.
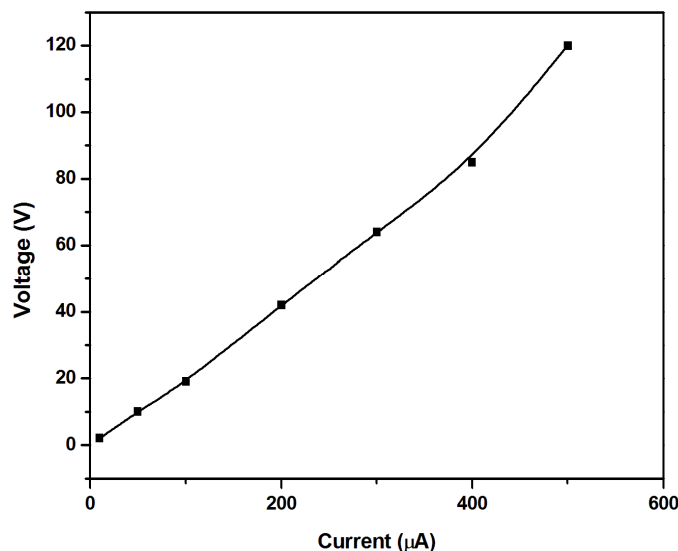
Figure 7B.7: I-V curve of RGO/TPU composites

7B.4 Conclusions

The conductivity of the RGO/TPU composites were found to be improved by the incorporation of RGO in to TPU matrix. The percolation threshold achieved was about 1 vol.%. There was almost a six fold improvement of conductivity with 2.5% filler loading. The dielectric properties were also found to be improved with RGO content. The enhancement in dielectric constant with increasing RGO content proves that charge storage capacity of the composites has improved which will make them suitable for capacitor applications especially in passive integrated circuits. The conductivity of the material is suitable for applications such as antistatic coatings. The RGO/TPU composites exhibited a PTC behavior with temperature. The PTC behaviour can be utilized for thermal sensor and resettable fuse applications.

Development of Reduced Graphene Oxide/Polymer Nanocomposites for Optical Limiting, Optical Actuation and Electrical Applications

229

References

[1]   Zhang L. L., Zhao S., Tian X. N., Zhao X. S. (2010) Layered graphene oxide nanostructures with sandwiched conducting polymers as supercapacitor electrodes. *Langmuir*, 26, 17624–17628

[2]   Psarras G. C. (2008) Nanodielectrics: An emerging sector of polymer nanocomposites. *Express Polymer Letters*, 2, 460.

[3]   Novoselov K. S., Geim A. K., Morozov S. V., Jiang D., Zhang Y., Dubonos S. V., Grigorieva I. V., Firsov A. A. (2004) Electric field effect in atomically thin carbon films. *Science*, 306, 666–669

[4]   Potts JR, Dreyer DR, Bielawski CW, Ruoff RS. (2011) Graphene-based polymer nanocomposites. *Polymer*, 52, 5 – 25

[5]   Bindu Sharmila T.K.,   Ajalesh B. Nair,   Beena T. Abraham,. Sabura Beegum P.M and Eby Thomas Thachil (2014) Microwave exfoliated reduced graphene oxide epoxy nanocomposites for high performance applications. Polymer, 55, 3614 – 3627

[6]   Stankovich, S., Dikin, D. A., Dommett, G. H., Kohlhaas, K. M., Zimney, E. J., Stach, E. A., ... & Ruoff, R. S. (2006). Graphene-based composite materials. *Nature*, *442*(7100), 282-286.

[7]   Sreemanta Mitra, Sourish Banerjee, and Dipankar Chakravorty. (2013) Tunneling conduction in graphene/(poly)vinyl alcohol composite. *Journal of Applied Physics,* 113, 154314

[8]   Sreemanta Mitra, Oindrila Mondal, Dhriti Ranjan Saha, Anindya Datta, Sourish Banerjee and Dipankar Chakravorty. (2011) Magnetodielectric Effect in Graphene-PVA Nanocomposites. *Journal of Physical Chemistry C*, 115, 14285–14289

[9]   Liu, H., Li, Y., Dai, K., Zheng, G., Liu, C., Shen, C., ... & Guo, Z. (2016). Electrically conductive thermoplastic elastomer nanocomposites at ultralow graphene loading levels for strain sensor applications. *Journal of Materials Chemistry C*, *4*(1), 157-166.

[10]   Bansala, T., Joshi, M., Mukhopadhyay, S., Doong, R. A., & Chaudhary, M. (2017). Electrically conducting graphene-based polyurethane nanocomposites for microwave shielding applications in the Ku band. *Journal of Materials Science*, *52*(3), 1546-1560.

[11]   Tung, T. T., Robert, C., Castro, M., Feller, J. F., Kim, T. Y., & Suh, K. S. (2016). Enhancing the sensitivity of graphene/polyurethane nanocomposite flexible piezo-resistive pressure sensors with magnetite nano-spacers. *Carbon*, *108*, 450-460.

[12]   Seema Ansari, Emmanuel P. Giannelis (2009) Functionalized Graphene Sheet—Poly(vinylidene fluoride) Conductive Nanocomposites. Journal of Polymer Science Part B: Polymer Physics, 47, 888–897

[13]   Psarras G. C.: Conductivity and dielectric characterization of polymer nanocomposites. in 'Physical properties of polymer nanocomposites' (eds.: Tjong S. C., Mai Y. W.) Woodhead, Cambridge, (2010) 31–69

[14]   Psarras G. C.: Hopping conductivity in polymer matrix– metal particles composites. (2006) *Composites Part A: Applied Science and Manufacturing*, 37, 1545–1553

.....୨୦ଓଷ.....

Chapter 8

CONCLUSIONS AND FUTURE OUTLOOKS

The present work was an effort to develop a simple and cost effective method for the preparation of reduced graphene oxide/polymer nanocomposites. The work also emphasized on finding out the suitability of the materials developed for practical applications and demonstrated the applications at laboratory level.

In this work, graphene oxide (GO) was synthesised through a modified synthesis protocol. The synthesised GO was reduced by both chemical and thermal methods. It was found that graphene-like material is obtained by the reduction of GO. Both chemically reduced GO and thermally reduced GO shows nearly complete reduction. The traces of residual functional groups can facilitate good dispersion of RGO in polymer composites.

Two polymer systems were used for developing RGO/polymer nanocomposite. One of the polymers selected was a low cost, biocompatible poly(vinyl alcohol) (PVA) and another polymer was a thermoplastic polyurethane (TPU). The first polymer represents the plastic family of polymers whereas the second polymer is a thermoplastic elastomer.

Development of Reduced Graphene Oxide/Polymer Nanocomposites for Optical Limiting,
Optical Actuation and Electrical Applications

233

RGO/PVA nanocomposites were prepared by the *in situ* reduction of GO with in the polymer. Uniform dispersion of filler particles enhanced the thermal and mechanical properties of the composite even with very low loading. PVA's affinity towards water was also significantly reduced with the incorporation of RGO making the composite more useful in practical applications. Similarly, thermally reduced graphene oxide/thermoplastic polyurethane composites were developed through a simple solvent casting method. The thermal and mechanical properties were found to improve with the incorporation of RGO.

The developed nanocomposites were studied for Optical limiting applications. The nonlinear optical properties and optical limiting behaviour of the composites were investigated using z-scan technique. In the case of RGO/PVA composites, we could obtain a very high nonlinear absorption coefficient of 680 cm/GW for 0.5 wt. % RGO/PVA composite film with a low laser intensity of 121 MW/cm^2 (532 nm, 7 ns). It was also observed that these composites can be effectively used as very good optical limiters in practical applications. The nonlinear absorption and the optical limiting properties increased with increasing RGO content. The optical limiting properties can be tuned by adjusting the RGO concentration which is of paramount importance from an optical limiter application perspective. Similar results were observed in RGO/TPU composites also. These composites exhibited excellent optical limiting behaviour. The optical limiting threshold was reduced by around 70% when the RGO content was increased from 0.1 to 0.5 wt%. This clearly indicates that the optical limiting properties can be controlled by adjusting the RGO content.

Another area of application explored for the developed nanocomposites was optically triggered actuators. The photomechanical actuation behaviour of RGO/PVA nanocomposites were studied and found to exhibit excellent actuation behaviour. The photomechanical actuation properties were found to increase with increasing RGO content. Without any pre-strain, the composite actuators exhibited contraction in response to IR light. When a pre-strain was applied, the contraction mode was changed to expansion mode. The study provided promising possibility of tuning the actuation behaviour either by tuning the filler content or by giving a suitable applied pre-strain. Contrary to the results obtained for RGO/PVA composites, the RGO/TPU composites exhibited contraction in length in response to IR light when a pre-strain was applied. This difference in properties was mainly due to the strain induced crystallisation effect in TPU. The RGO/TPU composites exhibited faster photomechanical response. The photomechanical stress and strain increased with pre-strain and filler loading up to a certain limit. Photomechanical strain as high as 50.2% is obtained for 2 wt% TRGO/TPU composites at 220% pre-strain with a stress of 1680 kPa. Hence this can find potential application as light triggered actuators in many fields including robotics.

The incorporation of RGO into PVA matrix has dramatically improved the conductivity of the composites. A low percolation threshold of 0.37 vol % was achieved. Even though the RGO used contained residual functional groups which affect the conductivity, homogeneous dispersion was possible which in turn helped in a fivefold improvement of conductivity with as low as 1% filler loading and these composites can find applications in antistatic coatings. The dielectric properties were also improved with

Development of Reduced Graphene Oxide/Polymer Nanocomposites for Optical Limiting,
Optical Actuation and Electrical Applications

235

RGO content. The RGO/PVA composites exhibited a NTC behavior with temperature which can be utilized for temperature sensor applications. Similarly, the conductivity of the RGO/TPU composites was also found to improve by the incorporation of RGO. However, the percolation threshold achieved was about 1 vol.% which is higher than that obtained for RGO/PVA composites. This clearly shows that the *in situ* reduced RGO/polymer composites have better uniformity in filler dispersion. The dielectric properties of RGO/TPU composites were also found to be improved with RGO content. The enhancement in dielectric constant with increasing RGO content proves that charge storage capacity of the composites has improved which will make them suitable for capacitor applications especially in passive integrals. The conductivity of the material is suitable for applications such as antistatic coatings. The RGO/TPU composites exhibited a PTC behavior with temperature. The PTC behaviour can be utilized for thermal sensor and resettable fuse applications.

In summary, RGO/polymer nanocomposites were developed and their applications in optical limiting and optical actuation were demonstrated. The electrical properties were investigated and it was found that the composites can find applications as conductive polymer composites in various fields including antistatic coatings, EMI shielding, thermal sensors, re-settable fuses, etc.

Future prospects

In the present work, the RGO/polymer composites were demonstrated as optical limiters at laboratory level. A real device such as a soft contact lens which can protect from powerful lasers in the real scenario will help to

upscale the technology to a commercialization stage. RGO based IR sensors on contact lenses for enabling night vision is a possibility which needs to be explored. RGO coated soft contact lenses to protect eyes from electromagnetic radiations can also be considered for study. Similarly, other optical applications such as optical switching could be explored. Utilizing the optical actuation behaviour, robotic arms or devices can be planned which can be remotely controlled using a laser source. These kinds of actuators will be extremely useful in areas such as biomedical field where electricity and wired connections are less preferred. Optical actuators can be used to fabricate high performance devices such as micro positioning stages and smart Braille displays for visually challenged people.

.....ॐ.....

⫼⫼ List of Publications ⫼⫼

From Thesis

In refereed journals

[1] Optical limiting properties of in situ reduced graphene oxide/polymer nanocomposites, **M. N. Muralidharan** et al., *Materials Chemistry and Physics* 171 (2016) 367-373

[2] Thermally reduced graphene oxide/thermoplastic polyurethane nanocomposites as photomechanical actuators , **M. N. Muralidharan** et al., *Advanced Materials Letters* 4 (2013) 927-932

[3] Optical actuation in reduced graphene oxide/polyvinyl alcohol nanocomposites, **M. N. Muralidharan** et al., (Communicated)

[4] Nonlinear absorption and optical limiting behaviour of thermally reduced graphene oxide/thermoplastic polyurethane nanocomposites, **M. N. Muralidharan** et al., (Communicated)

[5] Electrical properties of situ reduced graphene oxide/polymer nanocomposites, M. N. Muralidharan et al., (Communicated)

[6] Electrical properties of thermally reduced graphene oxide/thermoplastic polyurethane nanocomposites, **M. N. Muralidharan** et al., (Communicated)

In Conferences

[1] "Electrical Characteristics of *in-situ* Reduced Graphene Oxide/Polymer Nanocomposites'', **M. N. Muralidharan**, A. Seema, P. Radhakrishnan, Thomas Kurian, International Conference on Science and Technology; Future Challenges and Solutions (STFCS -2016) held at Mysuru, Karnataka during 8th and 9th August 2016.

[2] "Nonlinear optical characteristics of reduced graphene oxide/thermoplastic polyurethane nanocomposites", **M. N. Muralidharan**, S. Mathew, A. Seema, P. Radhakrishnan, Thomas Kurian, International Conference on Advances in Polymer Technology (APT'16) held at Kochi, Kerala during February 25- 26, 2016

Development of Reduced Graphene Oxide/Polymer Nanocomposites for Optical Limiting, Optical Actuation and Electrical Applications

239

[3]   "Photomechanical actuation in reduced graphene oxide/poly(vinyl alcohol) nanocomposites", **M. N. Muralidharan**, A. Seema, P. Radhakrishnan, Thomas Kurian, Prof. K. V. Thomas Endowment National Seminar 2015 on Molecular Approach to Current Advances in Chemistry held at Thevara, Kochi, Kerala during December 7-8, 2015

[4]   "Optical actuators using in situ reduced graphene oxide/polymer nanocomposites", **M. N. Muralidharan**, A. Seema, Thomas Kurian, National Seminar on Analytical Techniques for Synthesis and Characterization of Materials (ATSCM-2015) held at Kottayam, Kerala during February 26-27, 2015

[5]   "Nonlinear Absorption and Optical Limiting Behaviour of Reduced Graphene Oxide/Polymer Nanocomposites", **M. N. Muralidharan**, S. Mathews, A. Seema, P. Radhakrishnan, Thomas Kurian, National Seminar on Nanostructured Materials (NSM2014) Held at Changanachery, Kerala during August 12-13, 2014

From Works Related To Thesis

In refereed journals

[1]   "Optically triggered actuation in chitosan/reduced grapheme oxide nanocomposites", M. N. Muralidharan, et al., *Carbohydrate Polymers* 114 (2016) 115-121.

[2]   "Graphene/poly(styrene-*b*-isoprene-*b*-styrene) nanocomposite optical actuators". M. N. Muralidharan, et al., *Journal of Applied Polymer Science* 130 (2013) 3902-3908.

[3]   "Photomechanical characteristics of thermally reduced graphene oxide - Polydimethylsiloxane nanocomposites". M. N. Muralidharan, et al., *Polymer-Plastics Technology and Engineering* 52 (2013) 1604-1610.

[4]   Tween80 Modified Graphene with Improved Processability for the Fabrication of Supercapacitors". M. N. Muralidharan, et al., *Materials and Manufacturing Processes* 28 (2013) 1253-1259.

Book Chapters

[1]   "Electronic Applications of Polyurethane and Its Composites", in the book   "Flexible and Stretchable Electronic Composites", Springer International Publishing Switzerland, 2016

[2]   "Polymer-Graphene Composites: Electronic Applications" in the book "Encyclopedia of Polymeric Applications", Taylor & Francis Group, USA, 2017 (In Press)

Patent (Filed)

[1]   "Graphene-Polymer Nanocomposites and Photomechanical Actuators With High Actuation Properties Thereof", Indian Patent Application No. 526/ DEL/2013.

.....೪ೞ.....

▌▌▌▌ **Curriculum Vitae** ▌▌▌▌

Muralidharan M.N
"Komalalayam",
Vadassery (P.O),
Keralassery,
Palakkad-678641,
Kerala, India

Mob: +91(0) 9446503954
E-Mail: muralidharan@cmet.gov.in
mnmuralidharan@gmail.com

Educational Qualification

- **PhD** in pursuit at Department of Polymer Science and Rubber Technology, Cochin University of Science and Technology, Kerala, India (Part time)

- **MSc Polymer Chemistry**, University of Calicut , Kerala, India. (2002 - 2004)
  First Class

- **BSc Industrial Chemistry**, University of Calicut, Kerala, India (1998-2001)
  First Class

- **Pre-Degree Course (Physics, Chemistry, Biology)**, University of Calicut, Kerala, India (1996-1998)
  First Class

- **All India Secondary School Examination (AISSE – Xth Std.)**, Central Board of Secondary Education (CBSE), New Delhi, India (1996)
  First Class

Current Position

Scientist - A at **Centre for Materials for Electronics Technology (C-MET)**, [Ministry of Electronics & Information Technology, Government of India], Athani P.O, M.G Kavu, Thrissur-680581, Kerala (October 2015 - Till date)

Area of Research: Graphene, Polymer nanocomposites, Thermal sensors, actuators, supercapacitors

Part time **PhD Student** at the Department of Polymer Science and Rubber Technology, Cochin University of Science and Technology, Kerala

Area of Research : Reduced graphene oxide/polymer nanocomposites for optical limiting, optical actuation and electrical applications

Development of Reduced Graphene Oxide/Polymer Nanocomposites for Optical Limiting,
Optical Actuation and Electrical Applications

243

Technical Skills

Computer Awareness: MS Office tools, Microcal Origin, Programming with Visual Basic 5.0 (Diploma in System and Software Management from Aptech Computer Education, India)

Equipment Awareness: Supercapacitor testing system, Gas Sorption Analyzer (BET surface area analyzer), Impedence Analyzer, Universal Testing Machine (UTM), UV-Visible-NIR Spectrophotometer, Fluorimeter, Optical Microscope, High temperature high pressure Autoclaves for Super Critical Drying of polymeric gels, Fiber drawing station, Microprocessor controlled furnaces, Dicing Machine, Cold Isostatic Press, Thermal Cycling Equipment.

Experience

1) **Staff Technical IV** at **Centre for Materials for Electronics Technology (C-MET)**, [Ministry of Electronics & Information Technology, Government of India], Athani P.O, M.G Kavu, Thrissur-680581, Kerala (Nov. 2008 – Oct. 2015)
   Area of Research: Graphene, Polymer nanocomposites, Thermal sensors, actuators, supercapacitors

2) **Project Fellow** at International School of Photonics, Cochin University of Science and Technology, Kochi – 682 022, Kerala, India (in an industrial project) (July2007 – November 2008)
   Area of Research : Polymer Optical Fibers

3) **Project Staff** at **Centre for Materials for Electronics Technology (C-MET)**, Athani P.O, M.G Kavu, Thrissur-680581, Kerala, India, in a project supported by VSSC, *Indian Space Research Organization*, Government of India. (December 2005 – July 2007)
   Area of Research – Sol-gel Synthesis, Aerogels, Pre-ceramic polymers

4) **Research Assistant** to Dr.S Anil Kumar, Lecturer, Department of Chemistry, NSS College, Ottapalam, Kerala, India in a UGC sponsored project. (March 2005 - December 2005)
   Area of Research – Polymer Membranes

5) **Quality controller** in Maliyakkal Roller Flour Mills Pvt. Ltd. (ISO 9001-2000 certified),
   Kanjikkode, Palakkad, Kerala, India (May 2002-December 2002)

6) **Trainee Chemist** in NEM Laboratories Pvt. Ltd., Vasai Road, Mumbai, India (October 2001-April 2002)

Research Publication

Patents (Filed)

[1] "Composition, Thermistor and methods thereof". Seema Ansari, **Muralidharan Malamal Neelanchery**, Sunny Erukulam Kochappan and Dayas Kalaparamban Rapai, Indian Patent Application No. 1343/DEL/2015

[2] "An Energy Storage Device and a System Thereof". Seema Ansari, **Muralidharan Malamal Neelanchery**, Suraj Subramanian, Mejo Akkaraparambil Johny, Dayas Kalaparamban Rappai, Indian Patent Application No. 265/DEL/2015

[3] "Composition comprising reduced graphene oxide, supercapacitor and process of preparation thereof". Seema Ansari, **Muralidharan Malamal Neelanchery**, Divya Maniyara, Manikandan Padinhare Meleppat, Dayas Kalaparamban Rapai and Sunny Erukulam Kochappan, Indian Patent Application No. 293/CHE/2015

[4] "Graphene-Polymer Nanocomposites and Photomechanical Actuators With High Actuation Properties Thereof", Seema Ansari, **Muralidharan Malamal Neelanchery**, Rahima Cheerokkara, Sunny Erukulam Kochappan and Dayas Kalaparamban Rapai, Indian Patent Application No. 526/DEL/2013.

Book Chapters

[1] "Electronic Applications of Polyurethane and Its Composites", S Ansari, **M. N. Muralidharan,** in the book "Flexible and Stretchable Electronic Composites", Springer International Publishing Switzerland, 2016

[2] "Polymer-Graphene Composites: Electronic Applications" S Ansari, **M. N. Muralidharan,** in the book "Encyclopedia of Polymeric Applications", Taylor & Francis Group, USA, 2017 (In Press)

In Refereed Journals

[1] "Optically triggered actuation in chitosan/reduced graphene oxide nanocomposites", **M. N. Muralidharan**, K.P. Shinu, A. Seema, *Carbohydrate Polymers* **114** (2016) 115-121

[2] "Optical limiting properties of in situ reduced graphene oxide/polymer nanocomposites", **M. N. Muralidharan**, S. Mathew, A Seema, P Radhakrishnan, T Kurian, *Materials Chemistry and Physics* **171** (2016) 367-373

[3] "Tween80 Modified Graphene with Improved Processability for the Fabrication of Supercapacitors". **M. N. Muralidharan**, A. Seema, M. M. Saj Mohan, K. R. Dayas and E. K. Sunny, *Materials and Manufacturing Processes* **28** (2013) 1253-1259

[4] "Thermally reduced graphene oxide/thermoplastic polyurethane nanocomposites as photomechanical actuators". **M. N. Muralidharan** and Seema Ansari, *Advanced Materials Letters* **4** (2013) 927-932

[5] "Graphene/poly(styrene-*b*-isoprene-*b*-styrene) nanocomposite optical actuators". Seema Ansari, **Muralidharan Malamal Neelanchery** and Deepthi Ushus, *Journal of Applied Polymer Science* **130** (2013) 3902-3908

[6] "Photomechanical characteristics of thermally reduced graphene oxide - Polydimethylsiloxane nanocomposites". Seema Ansari, C. Rahima and **M. N. Muralidharan**, *Polymer-Plastics Technology and Engineering* **52** (2013) 1604-1610

[7] "Effect of Cu and Fe on the electrical properties of Ni-Mn-Co-O NTC thermistor compositions", **M. N. Muralidharan**, P. R. Rohini, E. K. Sunny, K. R. Dayas and A. Seema, *Ceramics International* **38** (2012) 6481-6486

[8] "Design, Fabrication and Electrical characterization of high material constant Chip-in-Glass Thermal sensors", **M. N. Muralidharan**, A Seema, E. K. Sunny and K. R. Dayas, *Proceedings of the 2012 1st International Symposium on Physics and Technology of Sensors*, March 8-10, 2012, Pune, India

IEEE Xplore http://dx.doi.org/10.1109/ISPTS.2012.6260925

[9] "Optimization of process parameters for the production of Ni-Mn-Co-Fe based NTC chip thermisotrs through tape casting route", **M. N. Muralidharan**, E.K. Sunny, K. R. Dayas, A. Seema and K.R. Resmi, *Journal of alloys and compounds* **509** (2011) 9363-9371

[10] "Photoluminescence and FTIR studies of pure and rare earth doped silica xerogels and aerogels", **M. N. Muralidharan**, C A Rasmitha, R Ratheesh, *Journal of Porous Materials* **16** (2009) 635-640

[11] "Pervaporation of alcohol-aromatic hydrocarbon mixtures through poly (ethylene-co-vinyl acetate) membranes" **M. N. Muralidharan**, S. Anil Kumar and Sabu Thomas, *Journal of Macromolecular Science Part A* **46** (2009) 274-281

[12] "Morphology and transport characteristics of poly(ethylene-*co*-vinyl acetate)/clay nanocomposites", **M. N. Muralidharan**, S. Anil Kumar and Sabu Thomas, *Journal of Membrane Science* **315** (2008) 147-154

[13] "Crystallization and Oxidation resistance properties of boron modified Silicon Oxycarbides derived from polymeric precursors by sol-gel method", **M. N. Muralidharan**, N C Pramanik, P A Abraham, K Stanly Jacob and N Rani Panicker, *Materials Letters* **62** (2008) 2547-2550

[14] "Pervaporation of Chloroform-Acetone mixtures through DCP crosslinked Poly(ethylene-*co*-vinylacetate) membranes", **M. N. Muralidharan** and S. Anil Kumar, *Indian Journal of Chemical Technology,* **12** (2005) 441-446

[15] "Permeation of chlorinated hydrocarbon vapors through poly(ethylene-*co*-vinyl acetate) membranes", S. Anil Kumar, **M. N. Muralidharan**, M. G. Kumaran and Sabu Thomas, *Polymers and Polymer Composites* **16** (2008) 283-290

[16] "Microwave oven for rapid determination of total solids content of natural rubber latex", Z.P. Hamza, K.F. Anna Dilfi, **M. N. Muralidharan** and T. Kurian, *International Journal of Polymeric Materials* **57** (2008) 918-923

[17] "Permeation of oxygen and nitrogen gases through poly(ethylene-*co*-vinyl acetate) membranes", S. Anil Kumar, **M. N. Muralidharan**, M. G. Kumaran, Abi S. Aprem and Sabu Thomas, *International Journal of Polymeric Materials* **57** (2008) 1104 – 1118

Awards and Achievements

- Senior Research Fellowship (SRF) - Council of Scientific & Industrial Research (CSIR), Govt. of India
- Visited Yamagata University, Japan, under "JSPS Invitation Programme for East Asian Young Researchers", supported by Japan Society for the Promotion of Science (JSPS)

Personal Details

Sex	:	Male
Date of Birth	:	2nd January, 1981
Nationality	:	Indian
Marital status	:	Married
Father's Name	:	Mr. P. Govindankutty Nair
Languages Known	:	English, Malayalam (Mother Tongue), Hindi, Tamil

…..ॐ…..

Annexure I

Based on the suggestions of the Examiners

1. **Chapter 3, P-113, section 3.3.3.7 '…. Which clearly shows that reduction was effective' why? How? Please explain.**

   In graphene oxide, due to the presence of oxygen containing functional groups, the relative carbon content will be less. The increase in carbon content of the reduced graphene oxide is an indication of the effective reduction of graphene oxide.

2. **Chapter 4, P-129, section 4A.3.2, Fig.4A.2 panel 'a' and 'b' should be in same magnification. Moreover, in the cross-sectional image, none of the RGO clusters/platelets is visible which suspects that clusters of RGO only in the surface interns raise the question about the dispersibility. Please consider it seriously. On the other hand, magnification should be high enough to support the claim.**

   Cross sectional image with same magnification as that of Fig.4A.2(a) was given in figure 4A.3 in the thesis. However for better understanding, figures with similar magnification are now given in Fig. 1 below. The RGO platelets are clearly visible in this figure showing good dispersion. Higher magnification of the cross section was provided at Fig. 4A.2 (b) of the thesis. It is now provided as Fig. 2 below. It is obvious from this figure that the thickness of the RGO platelet in the composite is in nanometer regime.
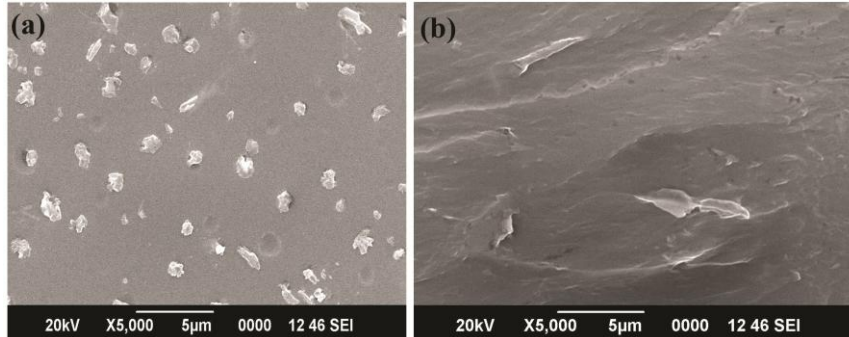
Development of Reduced Graphene Oxide/Polymer Nanocomposites for Optical Limiting, Optical Actuation and Electrical Applications

i

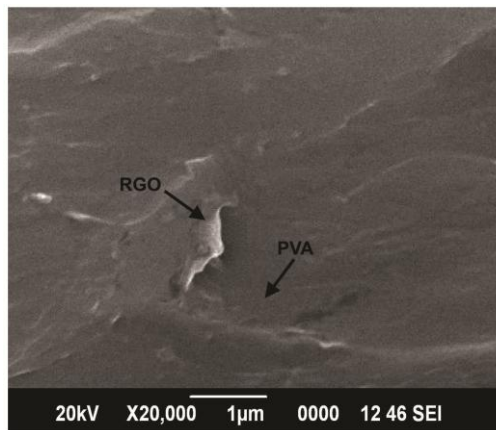**Figure 1 SEM images of RGO/PVA composite (a) surface (b) cross section**

Figure 2: Higher magnification of the SEM image of RGO/PVA composite (cross section)

3.   Chapter 4, P-128, 10th line. How micro order RGO platelets (as clearly visible in Fig.4A, panel 'a' show discrete distributions) act as nucleating sites in PVA solution (percentage of PVA not mentioned!?)…. Due to having super-mechanical strength…. Not clear.

The concentration of PVA solution used was 5 wt. %. While forming films from such a low concentration solution, the GO platelets act as nucleating agents and the polymer crystallites are built around the GO platelets and hence the crystallinity increases. Since RGO have high mechanical strength, they can restrict the random coiling of

polymer chains and induce ordered alignment which results in higher crystallinity.

4. **None of the composites attained the conductivity level which can be called as the conductive composite. Please compare with the conventional level scale. (such as superconductor, conductor, semiconductor, insulator etc.)**

The composites in this study can be considered in the conventional level scale as semiconductors.

5. **Page 129, 'Energy dispersive spectrum analysis showed 87% carbon content in RGO/PVA indicating in situ reduction'….Here carbon content in GO/PVA also needs to be given for comparison to support this statement and confirm in-situ reduction.**

In GO/PVA composites, GO showed a carbon content of 70% and since the carbon content of RGO in RGO/PVA composites has increased significantly, it is clear that reduction was effective.

6. **Page 129 & 141, AFM pictures of RGO and TRGO show submicron size platelets which tend to protrude out of surface where as SEM shows much bigger (micron size) flat plates.**

The lateral dimensions of RGO are in micrometers, as obvious from SEM. The thickness is in nanometer level. However, in AFM, only a portion of the edges protruding out from the surface is seen which is in sub micron level.

7. **Page no. 158 & 171, Tauc plots for the RGO/PVA and RGO/TPU are shown. Decrease in band gap is very high for RGO/PVA compared to RGO/TPU. Why? Band gap values may be calculated from these plots and put as a table.**

Virgin TPU or PVA are generally insulators and addition of conductive filler is required to bring down their band gap to the

Development of Reduced Graphene Oxide/Polymer Nanocomposites for Optical Limiting,
Optical Actuation and Electrical Applications

iii

range of semiconductors. In RGO/TPU, the RGO used is thermally reduced which has better conductivity compared to that of chemically reduced GO which is used in RGO/PVA, due to more effective reduction. Hence, in RGO/TPU even a low RGO content helped to decrease the band gap of RGO/TPU to the range of semiconductors. On addition of RGO, the band gap of RGO/TPU decreases slowly but steadily. Whereas in RGO/PVA, an RGO content of 0.5 wt.% was required to bring down the band gap to the semiconductor regime. At lower concentrations of RGO in PVA, the band gap was high. The band gap of the composites is given in Table 1 below. It can be observed that RGO/TPU has lower band gap values as expected.

**Table 1: Calculated band gaps of RGO/Polymer composites**

Sl No.	RGO content	Calculated band gap (eV)	
		For RGO/TPU	**For RGO/PVA**
1	0.1 wt. %	3.5	5.2
2	0.3 wt.%	3.35	4.8
3	0.5 wt.%	3.15	3.5

8. **Page 164 & 174, Composites with RGO content from 0.1 to 0.5 wt% were studied. For RGO/TPU, the strength of non linear absorption, Im(χ^3) is found to increase with RGO content. Higher concentrations would have given better non linear absorption. What is the basis for optimization of RGO concentration for this study in the range 0.1 to max. of 0.5 wt%**

For most of the practical applications, an optical limiter should be reasonably transparent to normal light. However, above 0.5 wt%, the transparency of the RGO/polymer composites is significantly low and hence the study was limited to a max. of 0.5 wt% RGO content.
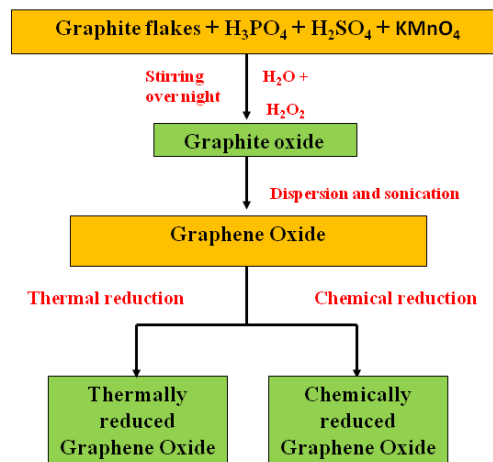
9. **Clarity of Figure 1.3 should be improved.**

A clearer schematic showing the chemical synthesis of graphene is given in Fig. 3 below.
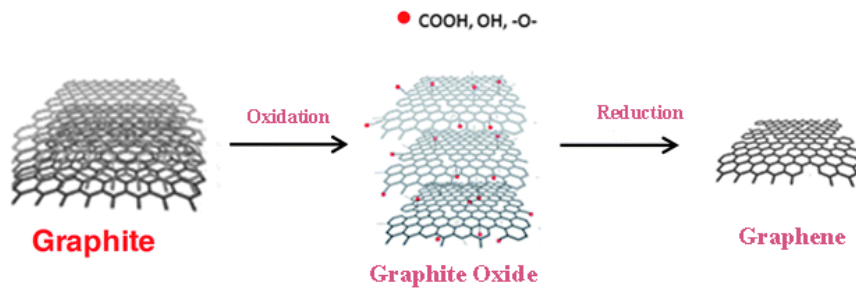
**Figure 3: Chemical synthesis of grapheme**

10. Section 3.2.1.2 Show flow chart for synthesis process.

Figure 4: Flow chart for the synthesis of reduced graphene oxide

**11.** **Section 4A.3.1 Explanation of Fig. 4A.1(a) is not clearly described. Characteristic peaks of GO**

Characteristic peak of GO at around 11° is observable in the XRD patterns of GO/PVA composites as marked in Fig.5 below.
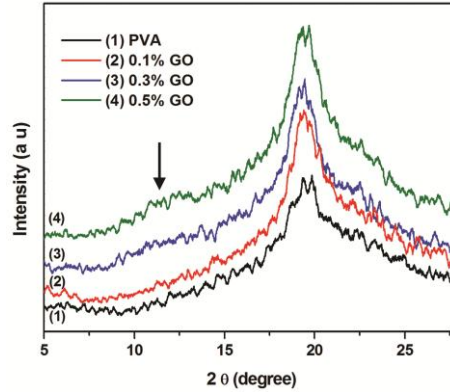
Figure 5: XRD patterns of GO/PVA composites with position of characteristic peak of GO marked by arrow.

12. **Figure 4B.2: From SEM photograph it is not clear whether TRGO is dispersed uniformly**

A new SEM with some of the TRGO platelets marked by arrows is given as Fig.6 which shows uniform dispersion.
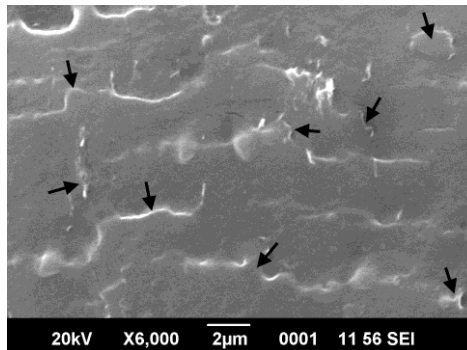
Figure 6: SEM of TRGO/TPU composites (cross section) with some of the TRGO platelets marked by arrows

13. **Figure 4B.4: Based on mechanical characterization 0.5 wt% of TRGO/TPU shows better mechanical properties. Hence if possible, TGA of such samples may be included.**

Figure 4B.4 has been re-plotted with TGA of 0.5 wt% of TRGO/TPU and given below as Fig. 7.
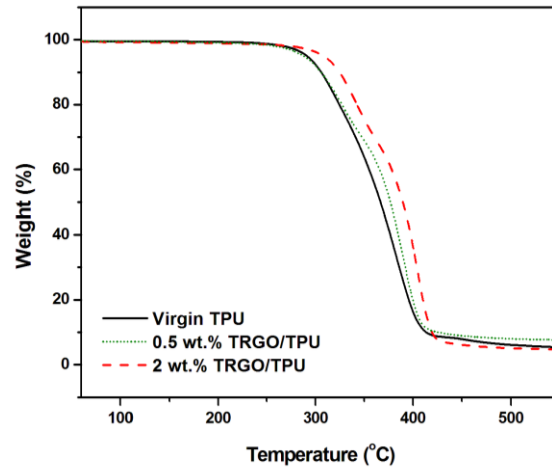
Figure 7: TGA of TRGO/TPU composites

14. **Figure 5A.3: Absorption characteristics of PVA with 0% RGO may also be included.**

Figure 5A.3 has been re-plotted by including absorption of 0% RGO also and is given below as Fig.8.
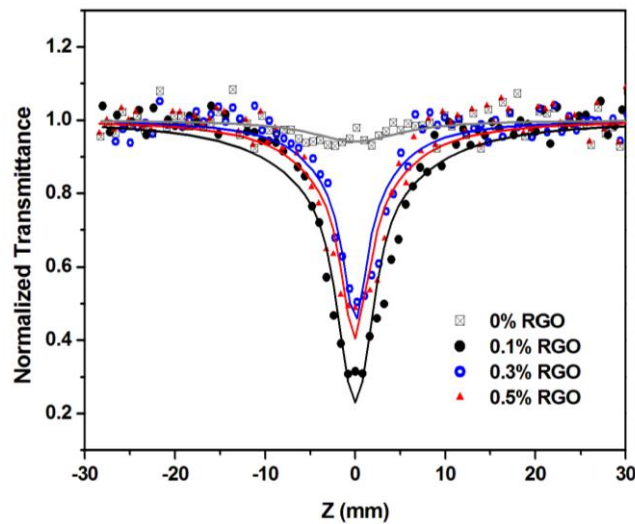

Figure 8: Nonlinear absorption of RGO/PVA composites

Development of Reduced Graphene Oxide/Polymer Nanocomposites for Optical Limiting, Optical Actuation and Electrical Applications

vii

15. **Section 7A.3.3 Short description of thermally activated tunneling effect may be included.**

    In a composite where two graphene platelets are separated by a thin layer of polymer, the conduction of electrons from one graphene platelet to the other is hindered by the layer. However, when heated, if the polymer film between the graphene platelets is thin enough, the electrons absorb the thermal energy and forms a tunneling path between the conduction barrier through which flow of electrons occur and the conductivity of the composite increases at higher temperature.

    .....ജാര.....